



UNIVERSITY OF
BATH

**Hygrothermal performance of Moso bamboo-based
building material**

Puxi Huang

A thesis submitted for the degree of Doctor of Philosophy (PhD)

University of Bath

Department of Architecture and Civil Engineering

March 2017

COPYRIGHT

Attention is drawn to the fact that copyright of this thesis rests with its author. This copy of the thesis has been supplied on condition that anyone who consults it is understood to recognise that its copyright rests with the author and they must not copy it or use material from it except as permitted by law or with the consent of the author.

This thesis may be made available for consultation within the University Library and may be photocopied or lent to other libraries for the purpose of consultation.

Signature:.....

Date:.....

Content

Abstract	I
List of abbreviations.....	II
List of symbols	III
List of figures	VI
List of tables	X
Chapter 1 Introduction.....	1
1.1 Background	1
1.2 Research gaps	3
1.3 Current bamboo products and field study in China.....	4
1.4 Challenges	6
1.5 Motivation	7
1.6 Research objectives	7
1.7 Thesis Layout	8
Chapter 2 Literature review.....	10
2.1 From heat transfer to coupled heat and moisture transfer	10
2.2 Density research	14
2.3 Specific heat capacity research.....	15
2.4 Thermal diffusivity and thermal conductivity research.....	17
2.5 Water vapour diffusion resistance factor research	18
2.6 Sorption isotherm research.....	20
2.7 Liquid water diffusivity research.....	22
2.8 Thermal and hygroscopic expansion	23
2.9 Simulation and experiment research.....	24
2.10 Summary of literature review	25
Chapter 3 Anatomical features, density and porosity of Moso bamboo.....	26
3.1 Anatomical features of Moso bamboo.....	26
3.2 Density profile of Moso bamboo.....	29
3.2.1 Research objectives	29

3.2.2 Methodology.....	29
3.2.3 Results and discussion.....	32
3.2.4 Summary	36
3.3 Porosity of Moso bamboo	37
3.3.1 Research objectives	37
3.3.2 Specimen preparation and methods.....	40
3.3.3 Results and discussions	46
3.3.4 Summary	53
Chapter 4 Specific heat capacity of Moso bamboo	54
4.1 Research objectives	54
4.2. Methodology	54
4.2.1 Specimen preparation	54
4.2.2 Specific heat capacity measurement by DSC	56
4.3 Results and discussions	56
4.3.1 Results from three directions.....	56
4.3.2 Typical results summery.....	63
4.3.3 Discussion	64
Chapter 5 Thermal diffusivity of Moso bamboo	70
5.1 Research objectives	70
5.2 Methodology	71
5.2.1 Specimen preparation	71
5.2.2 Thermal diffusivity measurement by flash tube method	72
5.3 Results and discussions	73
5.3.1 Thermal diffusivity results	73
5.3.2 Discussion	79
5.4. Summary	82
Chapter 6 Water vapour diffusion resistance factor of Moso bamboo.....	83
6.1 Research objectives	83
6.2 Methodology	83

6.2.1 Specimen preparation and water vapour diffusion resistance factor measurement	83
6.2.2 Water vapour permeability calculation.....	86
6.3 Results and discussion.....	87
6.4 Summary	92
Chapter 7 Sorption isotherm and liquid transport coefficient of Moso bamboo	93
7.1 Sorption isotherm of Moso bamboo	93
7.1.1 Research objectives	93
7.1.2 Methodology.....	93
7.1.3 Results and discussion.....	97
7.1.4 Summary	104
7.2 Liquid water diffusivity assumption.....	105
7.2.1 Research objective.....	105
7.2.2 Methods	105
7.2.3 Summary	107
Chapter 8 Thermal and hygroscopic expansion characteristics of Moso bamboo	108
8.1 Research objectives	108
8.2 Methodology	108
8.3 Results and discussion.....	111
8.3.1 Thermal expansion results and discussion.....	111
8.3.2 Hygroexpansion results and discussion	115
8.4 Summary	119
Chapter 9 Heat and moisture transfer behaviour of Moso bamboo based panels.....	120
9.1 Research objectives	120
9.2 Methodology	121
9.2.1 Heat and moisture transfer experiment design	121
9.2.2 Heat and moisture transfer simulation.....	124
9.2.3 Boundary conditions.....	128
9.2.4 Assumptions	130
9.2.5 Model validation.....	130

9.3. Results and discussion.....	131
9.3.1 Simulation and experimental results.....	131
9.3.2 Parametric studies.....	136
9.4 Conclusions	151
Chapter 10 Conclusions and future work	152
10.1 Conclusions	152
10.2 Future work	156
References	158
Self bibliography and published work.....	171

Acknowledgements

This thesis crystallises considerable efforts from many people. It is my honour to record their names here:

Dr. Chang Wen-shao: My lead supervisor lets me understand the true meaning of scientific research. His noble morality and creative thinking style can illuminate my life.

Dr. Martin P Ansell: My supervisor is always kind to me and strict to my academic works. Any word is pale to describe my respect for him.

Dr. Andy Shea: My supervisor provides basic knowledge of thermal properties of building materials and assistance for field experiments.

Dr. John Chew: My supervisor makes great efforts to disseminate the expertise of hygro-thermal transfer simulation. Without him, effective simulation works cannot be finished in this thesis. He is a legend.

Dr. Mike Lawrence and Dr. Eshrar Latif: Without their help, the dynamic hygrothermal transfer experiments, water vapour permeability experiments, and sorption isotherm experiments cannot be presented in this thesis. They deserve special thanks.

Dr. Anita Zeidler: She spends large amount of time and provides considerable support on the DSC experiment in this thesis.

Dr. Simon Pickering: He is a talented expert of the non-destructive test on the materials. Precious support on diffusivity experiments and MATLAB programming suggestions are provided by him.

Prof. Chris Rhys Bowen and Dr. Vana Adamaki: Their helps on the thermal expansion experiments are grateful. I still remember the day when Prof. Chris came to kneel on the ground to adjust the dilatometer for my experiment.

Mrs Clare Ball and Dr. Andrew Rhead: They contributed many important support and provide much insight into the CT visualisation suite to this thesis.

Mr. Glen Stewart, Mr. Walker Guy, Mr. Alan Carver, Mr. Neil price, Mr. Graham Mott, Mr. David Williams and Mr. Mathew Ball: Their help of teaching me the basics of carpentry and preparing the bamboo specimens and experiment equipments are extremely meaningful to this thesis.

Dr. Graham Ormondroyd and Dr.Simon Curling: They provide effective supports on my DVS experiments from Wales.

Mr. Zhiqiang Xue, Mr. Zhong Xue, Mr. Chen Chen and Mr. Pujin Weng: They provided kindly help on my field study in China.

Dr. John Mitchels and Ms. Ursula Potter: They bring me into a beautiful 'Micro-world' in Microscopy and Analysis Suite (MAS).

Dr. Alistair Calum Bradley, Dr. Hector Archila, Dr. Neal Holcroft, and Dr. Dragos Naicu: My colleagues hold torches for me to brighten the way to the PhD.

Mr. Cheng Wang, Mr.Xu Liu, Mr. Yang Liu, Mr. Qiushi Peng, and Dr. Boyang Mao: My friends always support and encourage me to overcome difficulties.

Mrs. Li Siqu: My deeply loved wife. She came to stay with me from China when I was doing my PhD programme. Then, she awarded a MBA in University of Bath, started her own business in UK, and brought baby for me. What a fantastic wife.

Mrs. Chu Xiaoxia and Mr. Huang Jianzhong: My deeply loved mother and father. They are my life supervisors. Their love means everything to me.

Abstract

This study focuses on the hygrothermal performance of Moso bamboo. The knowledge in this aspect is remarkable important for the research of building energy saving and the low carbon building design. However, the detailed hygrothermal properties of Moso bamboo are fairly rare. To obtain these data, a series of experimental works have been done for measurement of density, porosity, thermal conductivity, specific heat capacity, water vapour permeability, hygrothermal expansion and sorption isotherm of Moso bamboo.

To obtain further understanding on the hygrothermal performance of Moso bamboo, a number of dynamic heat and moisture transfer experiments were conducted. These experiments simulated two extreme outdoor environments and one indoor environment. The temperature and RH responses of Moso bamboo panels were monitored. Then a coupled transient heat and moisture transfer numerical simulation at the material level was conducted to predict and validate the hygrothermal performance of Moso bamboo. A sensitivity study of the hygrothermal properties of bamboo was also presented to indentify the influence of each hygrothermal property of Moso bamboo.

Major findings include the following aspects. Both experiment and simulation results appear to be consistent with the results of measurements of the basic hygrothermal parameters. The parametric study found that density can be regarded as the most sensible parameter to influence the temperature simulation results at the transient state, while the thermal conductivity dominated the temperature variation at the steady state. The water vapour diffusion resistance factor can be regarded as the most critical parameter to influence the RH simulation results. The influence of liquid water diffusivity is negligible in this study. The parametric study results indicated that the simulation with moisture is more accurate than the simulation without moisture in both equilibrium and transient state. The results also imply that the existence of moisture could increase the heat capacity and reduce the thermal conductivity. The results of this study recommend that the external part of the bamboo culm wall can be utilised to minimise the RH variation of the panel while the internal part of the bamboo culm wall is suitable to increase the thermal insulation performance of the panel. To avoid hygroexpansion, the implementation of external part of bamboo culm wall needs to be minimised.

Keywords: Hygrothermal performance of Moso bamboo; Dynamic heat and moisture transfer experiments and simulations; Sensitivity study.

List of abbreviations

ACU	Air-coupled ultrasound
ANOVA	Analysis of variance
BRE CICM	Building Research Establishment Centre for Innovative Construction Materials
BSE	Backscattered electron
CaCl ₂	Calcium Chloride
CFD	Computational fluid dynamics
COV	Coefficient of Variation
CT	Computed tomography
DCLG	Department for Communities and Local Government
DPI	Dots per inch
DSC	Differential Scanning Calorimetry
DVS	Dynamic water Vapour Sorption
FE-SEM	Field-emission scanning electron microscopy
GP	Gas pycnometry
HM	Her Majesty's
KCl	Potassium Chloride
KNO ₃	Potassium Nitrate
KOH	Potassium Hydroxide
kV	Kilo Volt
LM	Light Microscopy
MFA	Microfibril angle
MgCl ₂ 6H ₂ O	Magnesium Chloride Hexahydrate
MIP	Mercury intrusion porosimetry
MWIR	Mid-Wave Infrared
NaBr	Sodium Bromide
NaCl	Sodium Chloride
PC	Personal Computer
PDEs	Partial Differential Equations
PP	Polypropylene
PPMCC	Pearson Product-Moment Correlation Coefficient
RH	Relative Humidity
SD	Standard Deviation
SE	Secondary Electron
SEM	Scanning Electron Microscopy
TWI	Thermal Waving Imaging
UK	United Kingdom
UNEP	United Nations Environment Programme
X- μ CT	X-ray microtomography

List of symbols

α	Thermal diffusivity (m^2/s)
δ_{air}	Water vapour permeability of air ($\text{kg}/\text{m s Pa}$)
δ_p	Water vapour permeability ($\text{kg}/\text{m s Pa}$)
Δm	Mass change in 24 hours (kg)
Δt	Time interval in 24 hours
Δp	The water vapour pressure difference=1400 (Pa)
λ	Total or the equivalent thermal conductivity of a bamboo ($\text{W}/\text{m K}$)
λ_s	Thermal conductivity of bamboo solid phase ($\text{W}/\text{m K}$)
λ_w	Thermal conductivity of water phase ($\text{W}/\text{m K}$)
μ	Water vapour diffusion resistance factor, dimensionless
μA	Microampere
ξ	Moisture capacity
ρ	Density (kg/m^3)
ρ_a	Density of the water vapour in the ambient air (kg/m^3)
ρ_b	Density of the water vapour in the bamboo surface (kg/m^3)
ρ_{air}	Density of air (kg/m^3)
ρ_{bulk}	Bulk density (kg/m^3)
ρ_s	Skeletal density (kg/m^3)
ρ_{sat}	Saturated density of the water vapour (kg/m^3)
v_a	The absolute humidity of air (kg/m^3)
φ	Relative humidity
ϕ	Porosity
∇	Gradient operator
∇^2	Laplace operator

A	The water adsorption coefficient ($\text{kg/m}^2\text{s}^{0.5}$)
A_{ex}	Exposed area (m^2)
C	Total molar concentration (kmol/m^3)
C_p	Specific heat capacity (kJ/kg K)
C_{pb}	Specific heat capacity of the bamboo solid phase (kJ/kg K)
C_{pl}	Specific heat capacity of the liquid phase, e.g. water. (kJ/kg K)
C_{pa}	Specific heat capacity of the gas phase, e.g. water vapour and air. (kJ/kg K)
C_s	Specific heat capacity of skeleton phase (kJ/kg K)
C_w	Specific heat capacity of water (J/kg K)
d	Thickness of the specimen (m)
D_{AB}	Mass diffusivity (m^2/s)
D_l	Liquid water diffusivity (m^2/s)
D_{wcap}	Capillary saturation liquid water diffusivity (m^2/s)
\dot{E}_g	Energy generation rate in the system
\dot{E}_{in}	Heat flow rate in the system
\dot{E}_{out}	Heat flow rate out the system
\dot{E}_s	Energy storage rate
F	Steepness of the moisture front, is usually in the range of 5 to 10
g	Acceleration due to gravity (m/s^2)
g_i	Internal heat generation (W/m^3)
g_l	Liquid water flow ($\text{kg/m}^2\text{s}$)
g_m	Moisture flow ($\text{kg/m}^2\text{s}$)
g_v	Vapour flow ($\text{kg/m}^2\text{s}$)
G_s	Greyscale
h	Heat transfer coefficient ($\text{W/m}^2\text{K}$)
h_m	Water vapour transfer coefficient drove by the difference of water vapour density (m/s)
h_{mRH}	Water vapour transfer coefficient drove by the difference of RH ($\text{kg/m}^2 \text{ s}$)
h_v	Evaporation enthalpy of water (J/kg)
J_{As}^*	Constant species flux ($\text{kmol/m}^3\text{s}$)
kJ	Kilo joules
kg	Kilo gram
K	Coefficient of liquid permeability (kg/m s Pa)
K_a	Air permeance (s)
l	Length of the specimen in equilibrium state (mm)
l_0	Length of the specimen in oven dry state (mm)
\dot{m}	Water vapour flux density ($\text{kg/m}^2 \text{ s}$)
p	Pressure (Pa)

p_0	Standard atmospheric pressure (101325 Pa)
p_a	Ambient air pressure (Pa)
p_{suc}	Capillary suction stress (Pa)
q	Heat flux density (W/m^2)
q_s	Surface heat flux (W/m^2)
r_a	Density of air flow rate (m^3/m^2s)
R_v	Gas constant for water (461.5 J/K kg)
S	Moisture content in equilibrium state (%)
t	Time (s)
T	The temperature (K)
T_a	Temperature of the ambient air (K)
T_b	Temperature of the bamboo surface (K)
T_s	Constant temperature (°C)
T_∞	Ambient temperature (°C)
u''	The ratio of water substance to dry wood substance, dimensionless
U_z	The unit vector in the vertical direction
W	Moisture content (kg/m^3)
W_{cap}	Capillary saturation moisture content (kg/m^3)
X,Y,Z	Distance in three dimensional Cartesian co-ordinate system (m)
X_{As}	Constant species concentration
z	Height above a datum level (m)

List of figures

Figure 1.1 (a): Recombination bamboo panel front view (b): section view	5
Figure 1.2 (a): Recombination bamboo panel front view (b): section view	5
Figure 1.3 (a): Laminated bamboo panel front view (b): section view	5
Figure 1.4 (a): Laminated bamboo panel front view (b): section view	5
Figure 1.5 (a): Laminated bamboo panel front view (b): section view	6
Figure 1.6 (a): Laminated bamboo panel front view (b): section view	6
Figure 1.7 The thesis layout	8
Figure 2.1 The non-homogenous section view of Moso bamboo	15
Figure 2.2 Differential scanning calorimeter (DSC)	16
Figure 2.3 Peak temperature test image of the specimen in flash tube experiment.....	18
Figure 2.4 Water vapour diffusion resistance factor measurements by dry cup method.....	19
Figure 2.5 Sorption isotherm curves of Moso bamboo specimen	20
Figure 2.6 Dynamic vapour sorption (DVS) equipment	21
Figure 2.7 Water absorption coefficient measurement (BS 15148: 2002 +A1:2016).....	23
Figure 2.8 Dilatometer for thermal expansion measurement	24
Figure 3.1.1 Terminology for a bamboo culm.....	26
Figure 3.1.2 Anatomical features of Moso bamboo in the radial direction.....	27
Figure 3.1.3 CT-scanned images of the morphological features of the Moso bamboo	28
Figure 3.2.1 (a) Orientation of culm section showing a part cut for CT scanning. (b) Definition of radial elements in culm section. (c) Tangential elements in culm section. (d). Longitudinal elements in culm section.....	31
Figure 3.2.2 Density distribution in the radial direction of internode specimen	32
Figure 3.2.3 Density distribution in the radial direction of node specimen	32
Figure 3.2.4 Density distribution in the longitudinal direction of internode specimen	34
Figure 3.2.5 Density distribution in the longitudinal direction of node specimen	34
Figure 3.2.6 Density distribution in the tangential direction of internode specimen.....	35
Figure 3.2.7 Density distribution in the tangential direction of node specimen	36
Figure 3.3.1 Group number and cutting position of Moso bamboo	41
Figure 3.3.2 CT scanning measurement area of a Moso bamboo specimen	42
Figure 3.3.3 Comparison between the BSE image and secondary electron (SEM) image.....	44
Figure 3.3.4 The transfer procedure from BSE image to porosity values	45
Figure 3.3.5 Typical porosity results of a specimen from CT scanning and BSE.....	48
Figure 3.3.6 Porosity results of internode specimens from BSE and CT results by group comparison	49

Figure 3.3.7 Porosity results of node specimens from BSE and CT results by group comparison	50
Figure 3.3.8 Porosity results of internode portions from BSE and CT results by portion comparison	51
Figure 3.3.9 Porosity results of nodes portions from BSE and CT results comparison by portions	52
Figure 4.2.1 The dimension of the bamboo specimen.....	54
Figure 4.2.2 Nomenclature of the directions of specific heat capacity measurements.....	55
Figure 4.2.3 The cutting positions and numbers of bamboo specimens.....	56
Figure 4.3.1 Specific heat capacity of internode bamboo specimens in the radial direction...	57
Figure 4.3.2 Specific heat capacity of node bamboo specimens in the radial direction.....	58
Figure 4.3.3 Specific heat capacity of internode bamboo specimens in the tangential direction.	59
Figure 4.3.4 Specific heat capacity of node bamboo specimens in the tangential direction. ..	60
Figure 4.3.5 Specific heat capacity of internode bamboo specimens in the longitudinal direction	61
Figure 4.3.6 Specific heat capacity of node bamboo specimens in the longitudinal direction	62
Figure 4.3.7 Average specific heat capacity comparison at 25 °C.	63
Figure 4.3.8 (a) The radial-tangential section view of the Moso bamboo BSE image. (b) The tangential-longitudinal section view of the Moso bamboo BSE image. (c) The radial -longitudinal section view of the Moso bamboo BSE image. (d) The radial -longitudinal section view of the Moso bamboo BSE image at a high magnification.	68
Figure 5.2.1 The dimension and fixation of Moso specimens.....	71
Figure 5.2.2 The cutting position of Moso bamboo specimens.....	72
Figure 5.2.3 Flash tube system for thermal diffusivity measurement	73
Figure 5.3.1 Thermal diffusivity of internode bamboo specimens in the radial direction	74
Figure 5.3.2 Thermal diffusivity of node bamboo specimens in the radial direction.....	75
Figure 5.3.3 Thermal diffusivity of node bamboo specimens in the tangential direction	76
Figure 5.3.4 Thermal diffusivity of node bamboo specimens in the tangential direction	77
Figure 5.3.5 Thermal diffusivity of internode bamboo specimens in the longitudinal direction	78
Figure 5.3.6 Thermal diffusivity of node bamboo specimens in the longitudinal direction....	79
Figure 5.3.7 Thermal diffusivity of materials.....	80
Figure 5.3.8 CT and BSE pictures of Moso bamboo specimens	81
Figure 6.2.1 Nomenclature for a bamboo culm and orientation of specimens.....	84
Figure 6.2.2 The cutting position of bamboo specimens in the radial direction.....	84
Figure 6.2.3 The cutting position of bamboo specimens in the tangential direction.....	85

Figure 6.2.4 The cutting position of bamboo specimens in the longitudinal direction	85
Figure 6.2.5 Assemblies for water vapour diffusion resistance factor measurement	86
Figure 6.3.1 Water vapour diffusion resistance factor (μ).....	87
Figure 6.3.2 The SEM image of a bamboo specimen ($\times 60$).....	89
Figure 6.3.3 A BSE image of a bamboo cross-section ($\times 100$).....	89
Figures 6.3.4 A BSE image of a bamboo radial-longitudinal section ($\times 100$)	90
Figure 6.3.5 The BSE image of a radial-longitudinal section ($\times 600$)	90
Figure 6.3.6 A computed tomography image of a bamboo cross-section	90
Figure 6.3.7 A BSE image of a section through a node. ($\times 60$)	91
Figure 7.1.1 Nomenclature for a bamboo culm.....	94
Figure 7.1.2 The cutting position of bamboo specimens in the radial direction.....	94
Figure 7.1.3 The cutting position of bamboo specimens in the tangential direction.....	95
Figure 7.1.4 The cutting position of bamboo specimens in the longitudinal direction	95
Figure 7.1.5 The size of specimens	96
Figure 7.1.6 The desiccator assembly	96
Figure 7.1.7 Sorption isotherm curves in the radial direction	98
Figure 7.1.8 Sorption isotherm curves in the tangential direction.....	99
Figure 7.1.9 Sorption isotherm curves in the longitudinal direction	100
Figure 7.1.10 The moisture content of all specimens in sorption process.....	101
Figure 7.1.11 The moisture content of all specimens in desorption process.....	101
Figure 7.1.12 The moisture content difference between sorption curve and desorption curve of all specimens	102
Figure 7.1.13 Computed tomography picture of a Moso bamboo culm.....	103
Figure 7.1.14 A backscattered electron image of the cross-section (RT plane) of Moso bamboo	104
Figure 7.2.1 Cutting position of Moso bamboo specimens for water adsorption coefficient measurement.....	106
Figure 7.2.2 Testing apparatus for water adsorption coefficient measurement.....	107
Figure 8.2.1 Cutting position and directions of bamboo specimens.....	109
Figure 8.2.2 The desiccator assemblies.....	110
Figure 8.3.1 The thermal expansion of internode specimens in the radial direction.....	112
Figure 8.3.2 The thermal expansion of node specimens in the radial direction	112
Figure 8.3.3 The thermal expansion of internode specimens in the tangential direction	113
Figure 8.3.4 The thermal expansion of node specimens in the tangential direction.....	113
Figure 8.3.5 The thermal expansion of internode specimens in the longitudinal direction...	114
Figure 8.3.6 The thermal expansion of node specimens in the longitudinal direction	114
Figure 8.3.7 The hygroexpansion of internode specimens in the radial direction.....	115

Figure 8.3.8 The hygroexpansion of node specimens in the radial direction	116
Figure 8.3.9 The hygroexpansion of internode specimens in the tangential direction	116
Figure 8.3.10 The hygroexpansion of node specimens in the tangential direction	117
Figure 8.3.11 The hygroexpansion of internode specimens in the longitudinal direction.....	117
Figure 8.3.12 The hygroexpansion of node specimens in the longitudinal direction.....	118
Figure 9.1.1 Section view of a Moso bamboo culm wall	120
Figure 9.2.1 Four laminate types of bamboo panels.....	121
Figure 9.2.2 The assembling of the bamboo panel with the temperature and RH sensor	122
Figure 9.2.3 The assembling of the bamboo panel with the temperature and RH sensor	122
Figure 9.2.4. Bamboo panels in a special designed polypropylene foam panel.....	123
Figure 9.2.5 Twin climate chambers for heat and moisture transfer study	123
Figure 9.2.6 The average specific heat capacity results of bamboo specimens.....	126
Figure 9.2.7 Sorption isotherm curves of the Moso bamboo in the radial direction	127
Figure 9.2.8 The benchmark validation results of the temperature	131
Figure 9.2.9 The benchmark validation results of the moisture content	131
Figure 9.3.1 Temperature results of four panels.....	133
Figure 9.3.2 The RH results of four panels	135
Figure 9.3.3 Parametric study results of temperature of four panels.....	137
Figure 9.3.4 Parametric study results at a temperature change period	138
Figure 9.3.5 Parametric study results of enlarged density values at a temperature change period.....	140
Figure 9.3.6 Parametric study results of RH of four panels	142
Figure 9.3.7 Parametric study results of the RH by increasing the μ	143
Figure 9.3.8 Parametric study results of the RH by increasing the moisture content of sorption isotherm.....	144
Figure 9.3.9 The RH results of individual layer μ adjustment	146
Figure 9.3.10 The RH results of individual layer μ adjustment and sorption isotherm adjustment	147
Figure 9.3.11 The liquid water diffusivity adjustment results.....	148
Figure 9.3.12 The results of the simulation with and without moisture content	150

List of tables

Table 1.1 Limiting fabric thermal parameters in L1A (HM Government, 2010).....	1
Table 2.1 Boundary conditions for heat transfer (Luikov 1966, Incropera 1981).....	13
Table 2.2 Boundary conditions for moisture transfer (Luikov 1966, Incropera 1981)	13
Table 3.3.1 Summary of current techniques on the porosity measurement.....	40
Table 3.3.2 Nomenclature of each specimen by external diameter sequence	41
Table 3.3.3 Macro data statistics of BSE and CT scanning	46
Table 4.3.1 Specific heat capacity results at 25 °C.....	63
Table 4.3.2 T-test of the specific heat capacity of bamboo specimens	65
Table 4.3.3 ANOVA of the specific heat capacity of bamboo specimens	67
Table 5.3.1 Thermal diffusivity results	73
Table 7.1.1 Relative humidities in desiccators	97
Table 8.2.1 Relative humidities in desiccators	111
Table 9.2.1 The temperature condition plan of two climate chambers	123
Table 9.2.2 The essential parameters for heat and moisture transfer PDEs	125
Table 9.3.1 The adjustment of water vapour diffusion resistance factors for individual layer	145

Chapter 1 Introduction

1.1 Background

In this century, global developments have taken human civilization into new heights. Meanwhile, human beings also have triggered a number of disasters and paid a painful price in the process of global developments. For example, depletion of fossil fuels, air pollution and climate change have caused considerable negative impacts on the global environment. Learning from these mistakes, the importance of improving energy efficiency has been well recognised by global organisations, governments and scientists (Ritzen *et al.* 2016).

The building industry has great potential to improve energy efficiency. According to statistical analysis from UNEP (2014), at least one third of global energy use and 30 to 40% of global greenhouse gas emissions are attributable to buildings e.g. materials, constructions and maintenance.

To mitigate these impacts, the Energy Performance in Building Directive (EPBD) of European Union (EU) required all new buildings to be nearly zero energy consumption by the end of 2020. For existing buildings, the deadline is 2050 (EPBD 2010 and Kavgić *et al.* 2010). The government of the United Kingdom (UK) required local planned authorities to ensure the energy efficiency of new development. Furthermore, all new homes are planned to be zero carbon from 2016. This scheme is expected to extend to include all other buildings from 2019 (DCLG and Ellison 2015).

Energy efficiency can be improved by decreasing the building energy consumption and the embodied energy of building materials. The implementation of the building materials with high insulation performance can minimise the building energy consumption (Castleton *et al.* 2010). Using biological materials can reduce the embodied energy of building materials (Hammond and Jones 2008).

In the UK, at building regulation level, L1A (HM Government, 2010) mentioned that the lowest U-value of the fabric items should not exceed the relevant values listed in Table 1.1.

Table 1.1 Limiting fabric thermal parameters in L1A (HM Government, 2010)

Limiting fabric parameters	
Roof	0.20 W/m ² K
Wall	0.30 W/m ² K
Floor	0.25 W/m ² K
Windows, roof windows, glazed rooflights, curtain walling and pedestrian doors	2.00 W/m ² K

Commercialized insulation materials have been reviewed by Schiavoni *et al.* (2016). In this research, cork, stone wool, glass wool, expanded polystyrene, phenolic foam, cellulose and wood fibres are regarded as conventional insulation building materials. Hemp, flax, sheep's wool and cardboard-based panels are alternative insulation materials. Vacuum insulation panels, gas filled panels (GFP) and Aerogels are classified as advanced insulation materials. All advanced insulation materials can provide extremely low thermal conductivity. However, higher price, cutting difficulty and condensation problems are disadvantages (Baetens *et al.* 2010, Jelle 2011 and Griffith *et al.* 1993). For conventional and alternative insulation building materials, the difference of thermal conductivity among these materials is not significant. Natural materials demonstrated better performance in terms of carbon neutrality, recyclability, low toxicity and ease of manufacturing (Shamaeva *et al.* 1987, Kymäläinen and Sjöberg 2008, Figueiro 2011, Zach *et al.* 2013 and Hurtado *et al.* 2016).

Using natural material to minimise environmental impact has proved to be an effective strategy in the building industry (Bribián 2011). Especially for building envelope components, the application of natural materials not only focuses on neutralising the embodied energy during the construction period but also aims to reduce the operational energy consumption during the building service period. Therefore, seeking a natural material with high hygrothermal performance can make a significant contribution to minimise the energy consumption and environmental impact of the building industry.

The Building Research Establishment Centre for Innovative Construction Materials (BRE CICM) at the University of Bath has investigated a number of natural materials including timber, straw bale, and bamboo (Lawrence *et al.* 2009, Trujillo *et al.* 2013 and Ansell 2015). Among a large number of natural plants, bamboo has considerable potential to be utilised as a sustainable building material due to its fast reproductive capacity, competitive mechanical properties and ease of manufacturing bamboo structures. For example, the wood forests are harvested after twenty to fifty years. Bamboo forests can be harvest after four to five years. (Lobovikov 2003, Van Der Lugt *et al.* 2006 and Flander and Rovers 2009).

Building envelope components are not only the boundary but also the medium between the indoor and outdoor environment. Their hygrothermal performance is the crucial factor to impact the capability of energy saving for a building. To evaluate the applicability of bamboo as a material for building envelope utilisation, the understanding of hygrothermal performance of bamboo is essential. This research examines the hygrothermal performance of *Phyllostachys edulis* (Moso bamboo) which is commonly used as a construction material in Far East.

1.2 Research gaps

The heat and moisture transfer theory has been developed systematically. Delgado *et al.* (2012) reviewed 14 hygrothermal modelling tools. All these models were based on the partial differential equations (PDEs). The accuracy of the models can be validated by a British standard (BS EN 15026 2007). A representative numerical model is shown in Eq.1.1 (Portal 2011 and Nusser and Teibinger 2012).

$$\begin{aligned}\frac{\partial H}{\partial T} \frac{\partial T}{\partial t} &= \nabla(\lambda \nabla T) + h_v \nabla[\delta_p \nabla(\varphi P_{sat})] \\ \frac{\partial w}{\partial \varphi} \frac{\partial \varphi}{\partial t} &= \nabla[(D_l \nabla \varphi + \delta_p \nabla(\varphi P_{sat})]\end{aligned}\quad (1.1)$$

$\frac{\partial H}{\partial T}$: Heat storage capacity (J/m³ K)

T: Temperature (K)

t: Time (s)

λ : Thermal conductivity (W/m K)

h_v : Evaporation enthalpy of water (J/kg)

δ_p : Water vapour permeability (kg/m s Pa)

φ : Relative humidity

P_{sat} : Saturated pressure of water vapour (Pa)

W: water content of the bamboo substance (kg/m³)

$\frac{\partial w}{\partial \varphi}$: Moisture capacity $\frac{\partial w}{\partial \varphi} = \xi$

D_l : Liquid water diffusivity (m²/s)

∇ : Gradient operator $\nabla T = \frac{\partial T}{\partial x}$ in one dimension

This numerical model can provide the temperature and relative humidity results of the material if initial conditions, boundary conditions and six basic hygrothermal properties are known. The six basic hygrothermal properties are density, specific heat capacity, thermal conductivity or thermal diffusivity, water vapour permeability or water vapour resistance factor, liquid diffusion coefficient and sorption isotherm.

For Moso bamboo, the data of basic hygrothermal properties of bamboo are fairly rare in the current literature:

- The density of Moso bamboo is often an average value or in a narrow range which is between 600 and 800 kg/m³ in literature (Wu *et al.* 2004 and CES EduPack, 2013). However, Moso bamboo is a biological material with non-homogenous features in different positions and directions. Previous study indicated that the density variation of Moso bamboo is much higher than the literature data (Huang *et al.* 2014).
- Temperature is an important factor to influence the specific heat capacity data of Moso bamboo. Beside the non-homogenous features caused variation, the published data did not provide the specific heat capacity variation as the function of temperature in common indoor and outdoor temperature range (Wu *et al.* 2004 and Huang *et al.* 2014).
- Non-homogenous features caused variation is also not considered in the thermal diffusivity data of Moso bamboo (Wu *et al.* 2004 and Huang *et al.* 2014).
- The water vapour diffusion resistance factor or the water vapour permeability of Moso bamboo cannot be found in the literature.
- The sorption isotherm of Moso bamboo has been investigated in the longitudinal direction by a saturated solution method (Ohmae and Nakano 2009). Data from other directions are still insufficient.
- The liquid water diffusivity of Moso bamboo still remains under development in the literature.

Due to the lack of data, heat and moisture simulation work on bamboo is still at an initial stage. Thermal expansion, shrinking and swelling of bamboo are difficult to evaluate. The experimental work often focuses on the measurement of one of the basic hygrothermal properties in the steady state rather than coupled heat and moisture transfer in the transient state. A detailed review of the literature is presented in the Chapter 2.

1.3 Current bamboo products and field study in China

Two original birthplaces of Moso bamboo in China were visited for investigating current bamboo products. Field study in China indicated that the hygrothermal performance of Moso bamboo products is not specifically controlled.

The manufacturing companies have no awareness about hygrothermal properties, such as the thermal conductivity and water vapour permeability. Manufacturing convenience, mechanical

properties, artistic effects and indoor air quality (harmful gas release) are the primary manufacturing considerations. Several common forms of bamboo panels are displayed in Figures 1.1-1.6.



Figure 1.1 (a): Recombination bamboo panel front view (b): section view



Figure 1.2 (a): Recombination bamboo panel front view (b): section view



Figure 1.3 (a): Laminated bamboo panel front view (b): section view



Figure 1.4 (a): Laminated bamboo panel front view (b): section view



Figure 1.5 (a): Laminated bamboo panel front view (b): section view



Figure 1.6 (a): Laminated bamboo panel front view (b): section view

The recombination (scrimber) bamboo panels (Figure 1.1 and 1.2) are made from crushed bamboo stripe with adhesive. The bamboo strips are oriented randomly and not sorted according to any hygrothermal performance consideration. The forms of laminated bamboo panels (Figure 1.3 to 1.6) are made from raw bamboo strips with adhesive. None of these panels are manufactured to satisfy any hygrothermal requirement. The contact surfaces of bamboo strips are random without designated orientation.

The field study found that the manufacturers still lack the awareness of the hygrothermal properties of their products. Moso bamboo panels still have considerable potential to be further optimised for the purpose of serving as a building envelope component.

1.4 Challenges

Based on a review of published literature, the main factor to cause the aforementioned research gaps is the non-homogeneous characteristics of Moso bamboo in different directions. This fact leads to a series of challenges for this study.

Firstly, wide range of hygrothermal properties of Moso bamboo indicated that the average value or median cannot be considered as the representative data. Moreover, the existing data of Moso bamboo are already very rare. Therefore, it is extremely difficult to find the acceptable hygrothermal properties data of Moso bamboo for numerical simulation.

Secondly, a bamboo culm can be approximated as a hollow tube with relatively small thickness. Direct measurement of the hygrothermal properties, for example, density, porosity, thermal conductivity, specific heat capacity and vapour permeability, is restricted by the curved shape of bamboo.

Thirdly, the heat and moisture transfer experiments need specially designed equipment. In addition, the time consumed in making moisture related experiments, such as sorption isotherm or vapour permeability measurement, is fairly long. The scarce experimental resources restrict the quantity of specimens, the cycle number of the experiment conditions, and the time of the experiments.

Lastly, the measured hygrothermal property data and boundary conditions are variables or the function of other factors rather than constants. This fact can significantly increase the complexity of the numerical model. A number of exist software cannot be utilised to process the numerical model.

1.5 Motivation

The motivation for this thesis is to address the gaps in existing knowledge, evaluate the applicability of bamboo as a building envelop component from a hygrothermal performance perspective, and promote the wide implementation of bamboo in the building industries.

1.6 Research objectives

To respond to the aforementioned research gaps, challenges, and motivation, this thesis aims to investigate the hygrothermal properties of Moso bamboo, indentify heat and moisture transfer processes, and provide suggestions for manufacturing the bamboo-based building envelope component with superior hygrothermal performance.

To approach these targets, the following objectives need to be accomplished:

- Investigation of the density and porosity of Moso bamboo;
- Investigation of the thermal diffusivity of Moso bamboo;
- Investigation of the specific heat capacity of Moso bamboo;
- Investigation of the water vapour diffusion resistance factor and liquid water diffusion coefficient of Moso bamboo;
- Investigation of the sorption isotherm of Moso bamboo;

- Investigation of the hygrothermal expansion of Moso bamboo
- Evaluation of non-steady state heat and moisture transfer of Moso bamboo panels;
- Numerical study of non-steady state heat and moisture transfer of Moso bamboo panels;

1.7 Thesis Layout

The thesis layout is illustrated by figure 1.7.

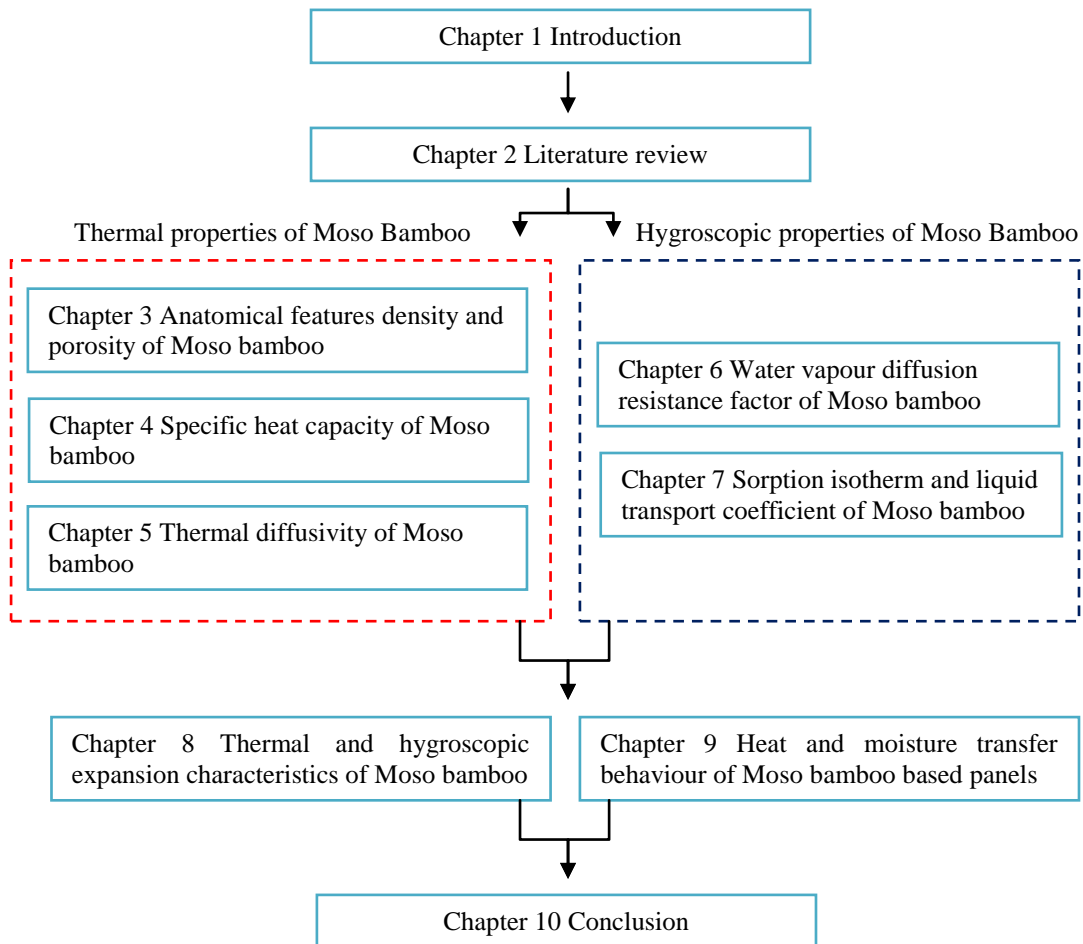


Figure 1.7 The thesis layout

Chapter 2 reviews the basic theory of heat and moisture transfer, current research status of the hygrothermal properties of Moso bamboo, and the status of heat and moisture transfer models.

Chapter 3 studies anatomical features of Moso bamboo. The density distribution is investigated between the internodes and the nodes parts of *Phyllostachys edulis* (Moso Bamboo) in the radial, tangential and longitudinal directions. The porosity of Moso bamboo from different height is also quantified in this chapter.

Chapter 4 measures the specific heat capacity of the Moso Bamboo in three directions of the cylindrical coordinate system. Due to the lack of knowledge of the specific heat capacity and

requirements of the heat and moisture simulation on Moso bamboo, this study measured the specific heat capacity of Moso bamboo using Differential scanning calorimetry (DSC). To investigate the variation of the specific heat capacity in different directions in bamboo culms, the measurements are conducted in the radial, longitudinal and tangential directions. The results of this study will be utilised as a physical property database for the future work on the heat and moisture transfer simulation of Moso bamboo.

Chapter 5 measures the thermal diffusivity of Moso bamboo using the flash method. The measurements are conducted in the radial, longitudinal and tangential directions for the purpose of understanding the effect of anisotropy on thermal diffusivity.

Chapter 6 investigates the water vapour permeability or water vapour diffusion resistance factor of Moso bamboo in both internode and node specimens. As a result moisture movement mechanisms within bamboo panels may be elucidated when the spatial arrangement of the raw materials is considered.

Chapter 7 measures sorption isotherm curves for the moisture sorption and desorption of Moso bamboo specimens in the radial, tangential and longitudinal directions. Sorption and desorption experiments are conducted by the use of desiccators containing six saturated solutions. This chapter also tries to quantify the liquid water diffusivity in the cross section of Moso bamboo culm wall. However, due to the size restriction of Moso bamboo, this chapter attempts to provide some assumed values of liquid water diffusivity.

Chapter 8 investigates the linear thermal and hygroscopic expansion characteristics of Moso bamboo in three directions with respect to the cylindrical coordinate system. Temperature and humidity are two common driving potentials for the expansion or contraction of bamboo. Thermal expansion is utilised to characterise the deformation by temperature variation while the hygroscopic expansion, namely shrinking and swelling, are used to understand deformation caused by relative humidity changes.

Chapter 9 focused on the heat and moisture transfer behaviours of the Moso bamboo panels in various temperature and relative humidity conditions. To quantify the influence of the non-homogeneous hygrothermal properties on the temperature and relative humidity results, both experimental studies and simulation prediction works are included in this chapter.

Chapter 10 draws the conclusions for the whole thesis. Finally, suggestions for future work are stated.

Chapter 2 Literature review

2.1 From heat transfer to coupled heat and moisture transfer

Heat transfer is the main form of energy transfer in building. The theory of heat transfer has been explained by Fourier (Fourier 1878).

The first law of thermodynamics can be stated as shown in Equation 2.1.

$$\dot{E}_{in} + \dot{E}_g = \dot{E}_{out} + \dot{E}_s \quad (2.1)$$

\dot{E}_{in} : heat flow rate in the system.

\dot{E}_{out} : heat flow rate out the system.

\dot{E}_g : energy generation rate in the system.

\dot{E}_s : energy storage rate

For the three dimensional Cartesian co-ordinate system, equation 2.1 can be transferred into the differential form by 2.2.

$$\lambda \left(\frac{\partial^2 T}{\partial X^2} + \frac{\partial^2 T}{\partial Y^2} + \frac{\partial^2 T}{\partial Z^2} \right) + g_i = \rho C_p \frac{\partial T}{\partial t} \quad (2.2)$$

λ : Thermal Conductivity (W/m K)

X, Y, Z : Distance in three dimensional Cartesian co-ordinate system (m)

T : Temperature (K)

g_i : Internal heat generation (W/m³)

ρ : Density (kg/m³)

C_p : Specific heat capacity (J/kg K)

t : Time (s)

Energy generation is often caused by chemical reactions. Combustion and ageing are two common situations for chemical reactions which are rarely evaluated in building physics. Therefore, the internal generated heat will not be discussed in this study.

In the steady state, the temperature difference is not changing with time. If the internal generated heat is not considered, the equation 2.2 can be expressed by equation 2.3.

$$\frac{\partial^2 T}{\partial x^2} + \frac{\partial^2 T}{\partial y^2} + \frac{\partial^2 T}{\partial z^2} = 0 \quad (2.3)$$

However, the actual heat transfer is often not in steady state. Equation 2.2 is more frequently utilised to describe the actual heat transfer situations for building envelop components. Moreover, actual heat transfer is also combined with moisture transfer and air transfer.

Moisture transfer can be described by equation 2.4.

$$g_m = g_v + g_l \quad (2.4)$$

g_m : Moisture flow (kg/m²s)

g_v : Vapour flow (kg/m²s)

g_l : Liquid water flow (kg/m²s)

The vapour flow can be expressed by equation 2.5.

$$g_v = (-\delta_p) \nabla p + r_a v_a \quad (2.5)$$

g_v : Vapour flow (kg/m²s)

δ_p : Water vapour permeability (kg/m s Pa)

p : Pressure (Pa)

r_a : Volume airflow rate vector (m³/m²s)

v_a : The absolute humidity of air (kg/m³)

∇ : Gradient operator $\nabla T = \frac{\partial T}{\partial x}$ in one dimension

The liquid flow can be expressed by equation 2.6.

$$g_l = K \nabla P_{suc} \quad (2.6)$$

g_l : Liquid water flow (kg/m²s)

K : Coefficient of liquid permeability (kg/m s Pa)

P_{suc} : Capillary suction stress (Pa)

∇ : Gradient operator $\nabla T = \frac{\partial T}{\partial x}$ in one dimension

Equation 2.5 expresses the existence of the air phase in building materials. The density of air flow rate can be calculated by equation 2.7. The air flow can be neglected under small pressure differences (Luikov 1966, Incropera 1981, Chapman 1987, Hagentoft *et al.* 2004 and Hens 2007).

$$r_a = -K_a \nabla (P_a - \rho_a \cdot g \cdot z \cdot U_z) \quad (2.7)$$

r_a : Volume airflow rate vector ($\text{m}^3/\text{m}^2\text{s}$)

K_a : Air permeance ($\mu\text{m}/\text{Pa s}$)

P_a : Overall air pressure (Pa)

ρ_a : Density of air (kg/m^3)

g : Acceleration due to gravity (m/s^2)

z : Height above a datum level (m)

U_z : The unit vector in the vertical direction

∇ : Gradient operator $\nabla T = \frac{\partial T}{\partial x}$ in one dimension

The heat transfer, moisture, and air transfer can be described by integrating the aforementioned equations. The coupled equations are written by 2.8 (Kunzel and Kiessl 1996, Delgado *et al.* 2012 and Nusser and Teibinger 2012).

$$\begin{aligned} \frac{\partial H}{\partial T} \frac{\partial T}{\partial t} &= \nabla(\lambda \nabla T) + h_v \nabla[\delta_p \nabla(\varphi P_{sat})] \\ \frac{\partial w}{\partial \varphi} \frac{\partial \varphi}{\partial t} &= \nabla[(D_l \nabla \varphi + \delta_p \nabla(\varphi P_{sat})] \end{aligned} \quad (2.8)$$

$\frac{\partial H}{\partial T}$: Heat storage capacity ($\text{J}/\text{m}^3 \text{K}$)

T: Temperature (K)

t: Time (s)

λ : Thermal conductivity ($\text{W}/\text{m K}$)

h_v : Evaporation enthalpy of water (J/kg)

δ_p : Water vapour permeability ($\text{kg}/\text{m s Pa}$)

φ : Relative humidity

P_{sat} : Saturated pressure of water vapour (Pa)

W : water content of the bamboo substance (kg/m^3)

$\frac{\partial w}{\partial \varphi}$: Moisture capacity $\frac{\partial w}{\partial \varphi} = \xi$

D_l : Liquid water diffusivity (m^2/s)

∇ : Gradient operator $\nabla T = \frac{\partial T}{\partial x}$ in one dimension

The equations are partial differential equations (PDEs). To obtain a solution of the PDEs of 2.8, the aforementioned six parameters are not enough, so at least one of the three boundary conditions for heat transfer (Table 2.1), one of the two boundary conditions for moisture transfer (Table 2.2) and one initial condition need to be specified (Eq 2.9).

The initial condition represents the temperature and RH distribution in the object at the initial time ($t=0$). The three dimension expression of the initial condition is:

$$T(x, y, z, 0) = T_0(x, y, z)$$

$$RH(x, y, z, 0) = RH_0(x, y, z) \quad (2.9)$$

Table 2.1 Boundary conditions for heat transfer (Luikov 1966, Incropera 1981)

	The 1st condition Dirichlet condition	The 2nd condition Neumann condition		The 3rd condition Robin condition
Description	Constant surface temperature	Constant heat flux		Convection surface
		a) Finite heat flux	b) Adiabatic surface	
Numerical expression	$T(0, t) = T_s$	$-k \frac{\partial T}{\partial n} \Big _{n=0} = q_s$	$\frac{\partial T}{\partial x} \Big _{x=0} = 0$	$-k \frac{\partial T}{\partial x} \Big _{x=0} = h[T_\infty - T(0, t)]$
Annotation	T_s : Constant temperature ($^{\circ}\text{C}$)	q_s : Surface heat flux (W/m^2) k : Thermal conductivity (W/m K)	The direction of ∂x is orthogonal to the heat flux section.	T_∞ : ambient temperature ($^{\circ}\text{C}$) h : heat transfer coefficient ($\text{W/m}^2\text{K}$)

Table 2.2 Boundary conditions for moisture transfer (Luikov 1966, Incropera 1981)

	The 1st condition	The 2nd condition
Description	Constant surface concentration	Constant species flux
Numerical expression	$x_A(0, t) = x_{A,s}$	$-CD_{AB} \frac{\partial x_A}{\partial X} \Big _{x=0} = J_{A,s}^*$
Annotation	x_A : Concentration (mol/m^3)	C : total molar concentration (kmol/m^3)

	$x_{A,s}$: Constant species concentration (mol/m ³)	D_{AB} : mass diffusivity (m ² /s) $J_{A,s}^*$: constant species flux (mol/m ³ s)
--	--	---

The molar concentration can be converted to moisture content. In the transient state, the derivative of moisture with respect to time can be described by equation 2.10 (Portal 2011).

$$\frac{\partial w}{\partial t} = \frac{\partial w}{\partial p} \cdot \frac{\partial p}{\partial t} = \frac{\partial w}{\partial \varphi} \cdot \frac{\partial \varphi}{\partial p} \cdot \frac{\partial p}{\partial t} = \frac{\partial w}{\partial \varphi} \cdot \frac{\partial \varphi}{\partial t} \quad (2.10)$$

w : Moisture content (kg/m³)

p : Pressure (Pa)

φ : Relative humidity

t : Time (s)

Where the $\frac{\partial w}{\partial \varphi}$ is the moisture capacity which often is expressed by ξ .

To solve the PDEs, at least six input parameters, initial conditions, and boundary conditions need to be known. In addition, even when these conditions are met, the solving of the PDEs still needs an effective tool to manage conferrable calculations and complex data processing.

The following sections reviews the research status of the six essential input parameters of Moso bamboo which are density, specific heat capacity, thermal conductivity (or thermal diffusivity), water vapour permeability (or water vapour resistance factor), liquid diffusion coefficient and sorption isotherm. Moreover the initial conditions, and boundary conditions, the simulation tools and experimental works on heat and moisture transfer are also reviewed.

2.2 Density research

Density is not only a physical property of an object but also a basic input datum in the quantitative research of thermal and mechanical properties and their analyses (Steppe *et al.* 2004). Bulk density of an object is relatively easy to measure. The average density of Moso bamboo varies from 600 to 800 kg/m³ (Forest Products Service 2010 and CES EduPack, 2013).

Traditional method for bulk density calculation utilised volume and weight to calculate bulk density of the material (BS EN ISO 17828:2015). For homogenous materials, the measured density is acceptable by this method. However, simply using bulk density to conduct thermal and mechanical analysis is not appropriate for natural materials as their density often varies as

a function of position and orientation. A previous study found that the density of bamboo is highly variable in the radial direction (Huang *et al.* 2014). See figure 2.1.

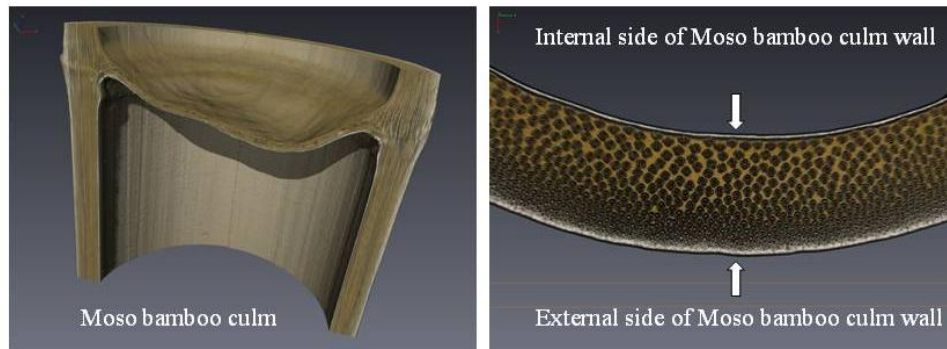


Figure 2.1 The non-homogenous section view of Moso bamboo

Limited research on density measurement of bamboo has been performed compared to timber. To accomplish the through-thickness and multi-dimensional density measurement of wood, several non-destructive technologies have been developed. A pulsed air-coupled ultrasound (ACU) method has been utilised to measure the density of particleboard (Sanabria *et al.* 2013). Microwave techniques have been found to provide an appropriate prediction of moisture content and density in Scots pine (Johansson *et al.*, 2003). The dielectric properties of wood have been utilised to conduct high frequency densitometry (Boden *et al.*, 2012). Density measurements by X-Ray techniques rely on the principle of light absorption (Benson-Cooper 1982, Mull 1984, Davis and Wells 1992, Reeves *et al.* 2012). All these methods are claimed to be sufficiently accurate to meet the requirements of density quantification research.

2.3 Specific heat capacity research

Specific heat capacity is a physical property which is defined as the amount of heat required to change a unit mass of a substance by one degree in temperature (Fourier 1878). This property is regarded as an essential input parameter in the mathematical simulation of heat transfer (Maxwell 1872). In the heat conduction equation (equation 2.2), the density and specific heat capacity are the two important properties of the energy storage term.

Specific heat capacity values of Moso bamboo varied from 1.08 to 2.29 kJ/kg·K in an early research work (Wu *et al.* 2004). Previous research by the specific heat capacity of Moso bamboo using differential scanning calorimetry (DSC) which are from 1.7 to 2.3 kJ/kg·K at 40 °C (Huang *et al.* 2014). The specific heat capacity values of bamboo fibre reinforced polyester composite ranged from 1.2 to 1.4 kJ/kg·K (Mounika *et al.* 2014).

However, research on the specific heat capacity of bamboo is still at an early stage compared to related research on wood. The average specific heat capacity values of dry wood have been investigated by many researchers. These values ranged from 0.962 to 2.114 kJ/kg·K (Beall 1968, Koch 1968, Fasina and Sokhansanj 1996 and Kristijan *et al.* 2014). The estimated specific heat capacity of pellets ranged from 1.074 to 1.253 kJ/kg·K (Guo *et al.* 2013). The specific heat capacity of softwood, softwood bark, and softwood char derived from bark were investigated by DSC. The measured values at 313 K were 1.172 kJ/kg·K, 1.364 kJ/kg·K and 0.768 kJ/kg·K respectively (Gupta *et al.* 2003).

The difficulty of measuring the specific heat capacity of biological building materials, e.g. wood and bamboo, is mainly attributed to their anatomical complexity. Biological building materials are not homogeneous compared to many metals and macromolecular compounds. Previous studies have shown the considerable variation of the density and porosity distribution of Moso bamboo in three different directions (Huang *et al.* 2014). In addition, bamboo is a hygroscopic and porous material with more than one phase. Therefore, the measured specific heat capacity value is considered as the equivalent value.



Figure 2.2 Differential scanning calorimeter (DSC)

Specific heat capacity can be measured by indirect methods and direct methods. Indirect methods require other physical properties to calculate the specific heat capacity. The flash method is an effective method to obtain the thermal diffusivity and specific heat capacity if the density of both the specimen and reference material and the specific heat capacity of the reference material are already known (Parker *et al.* 1961 and Shinzato and Baba 2001). The direct methods for specific heat capacity measurement are conducted by calorimeters, e.g. adiabatic calorimeters, reaction calorimeters, bomb calorimeters and differential scanning calorimeters (Parker *et al.* 1961, Spink and Wadsö 1976, Cao 1997). Differential scanning calorimeter and modulated differential scanning calorimeter have been utilised in wood research (Furuta *et al.* 2012, Miki *et al.* 2012). Specific heat capacity measurement by DSC is

a quick method with a relatively simple working process. See figure 2.2. The specific heat capacity results can be obtained over a wide temperature range rather than a single temperature condition. In addition, the DSC can measure the oven-dry specimen with relatively small size.

2.4 Thermal diffusivity and thermal conductivity research

Thermal diffusivity is a physical property that is defined as the ratio of the thermal conductivity to the heat capacity of a material. This property is an essential item in the transient heat conduction equation. Larger thermal diffusivity value means that a material will be quicker to reach a new equilibrium condition (Incropera 1981). See Equation 2.11 and Equation 2.12.

$$\alpha \nabla^2 T = \frac{\partial T}{\partial t} \quad (2.11)$$

$$\alpha = \frac{K}{c_p \rho} \quad (2.12)$$

α : thermal diffusivity (m²/s)

T : temperature (K)

t : time (s)

K : thermal conductivity (W/m K)

ρ : density (kg/m³)

c_p : specific heat capacity (J/kg K)

∇ : Gradient operator $\nabla T = \frac{\partial T}{\partial x}$ in one dimension

The thermal diffusivity of Moso bamboo in the longitudinal direction has previously been measured by a laser flash method (Wu *et al.* 2004). A similar method has been implemented for wood research (Harada *et al.* 1998). The thermal conductivity of Moso bamboo veneer board and laminated board has been measured (Shah *et al.* 2016). However, the thermal diffusivity data in the radial and tangential directions of the Moso bamboo culm still need to be studied. Previous studies found that Moso bamboo is non-homogenous in terms of both morphological structure and thermal properties in the radial, longitudinal and tangential directions (Huang *et al.* 2014).

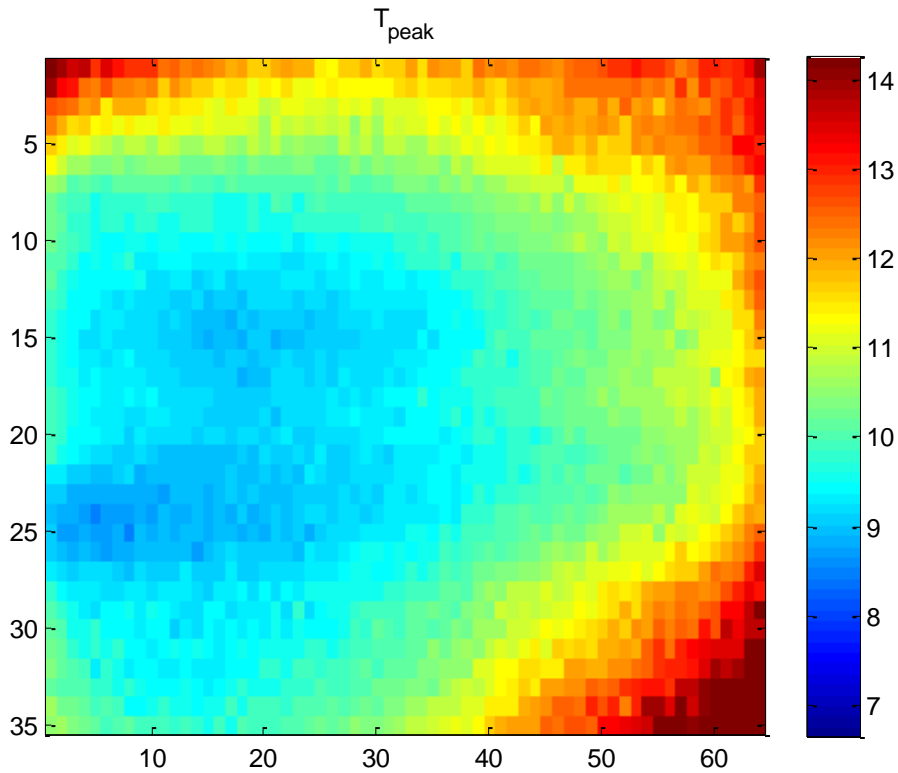


Figure 2.3 Peak temperature test image of the specimen in flash tube experiment

A number of transient methods, including Transient Plate Source (TPS), heat pulse and laser flash, have been reported as being used to measure the thermal diffusivity of biological materials (Harada *et al.* 1998, Burgess *et al.* 2001 and Duplex *et al.* 2013). These methods have been proven to be effective. However, the flash method is most suitable for Moso bamboo specimens in terms of testing time requirements and flexibility of specimen dimensions. See figure 2.3. The heat pulse method requires multiple cycles of temperature fluctuation that will require more time than the flash method. The minimum specimen size of the TPS method is restricted by the size of the transient plate sensor. However, the size of the bamboo specimens needs to be relatively small to examine the effect of microstructure variation on the thermal diffusivity. The thickness and the radius are two factors which restrict the size of specimens in the radial and tangential directions.

2.5 Water vapour diffusion resistance factor research

The water vapour diffusion resistance factor is the ratio of the water vapour permeability of the air to the water vapour permeability of the specimen. The water vapour permeability of the air can be regarded as a constant if the temperature is known. Therefore, to calculate the water vapour permeability, the value of water vapour diffusion resistance of the specimen is

required. The water vapour permeability of the specimen is the water vapour diffusion coefficient with vapour pressure as the driving potential in Fick's laws of diffusion (Time 1998). The physical definition of the water vapour permeability is the quantity of water vapour transmitted per unit time through a unit area of the material per unit of vapour pressure (BS EN 12086:2013).

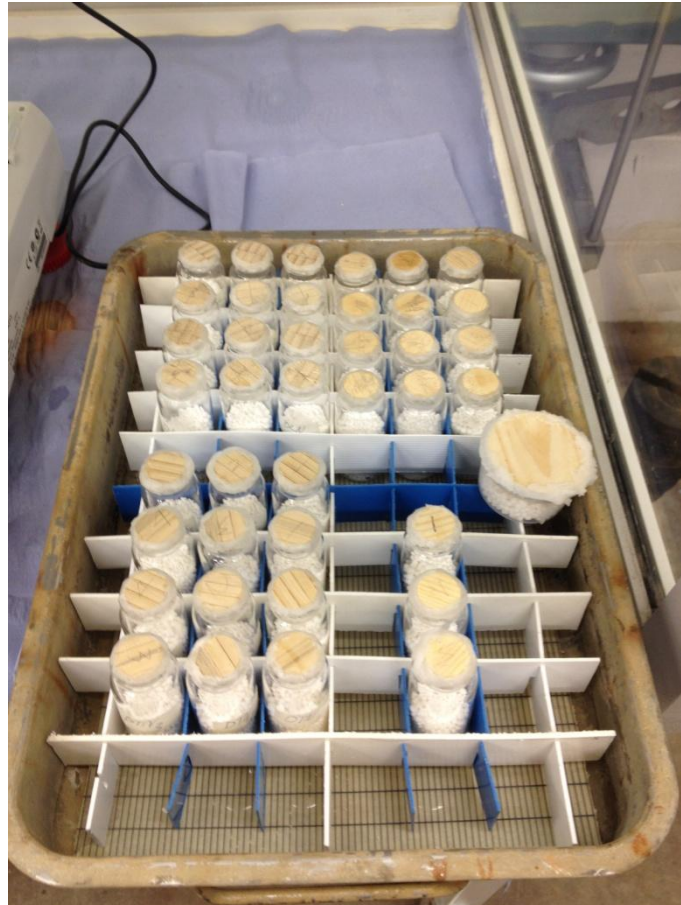


Figure 2.4 Water vapour diffusion resistance factor measurements by dry cup method

The water vapour permeability data of bamboo is insufficient in the literature compared with related research on wood. Most of the water vapour permeability research on bamboo currently focuses on knitted fabrics rather than bamboo for construction (Majumdar *et al.* 2010, Prakash *et al.* 2011). The water vapour permeability of heat treated bamboo fibre and high density polyethylene composites has been reported by Du *et al.* (2014). The water vapour permeability of Swedish pine and spruce was investigated in the radial, tangential and longitudinal directions of the log (Wadsö 1993). The density variation was considered in a research on the water vapour permeability of wood in the radial and tangential directions (Carmeliet and Derome 2008). The water vapour permeability values of wood fibre, wide-ring wood, narrow-ring wood and oriented strand board were measured by both dry cup (see

figure 2.4) and wet cup method (Vololonirina *et al.* 2014). The design values of water vapour permeability for general building materials can be found in a standard (BS EN 12524:2000).

2.6 Sorption isotherm research

Sorption isotherm curves are the fundamental data for deriving the moisture storage capacity. The moisture storage capacity is the basic input of the numerical simulation of moisture transfer for bamboo. The sorption isotherm curves are regarded as essential data for understanding the moisture transfer mechanism of bamboo. See figure 2.5.

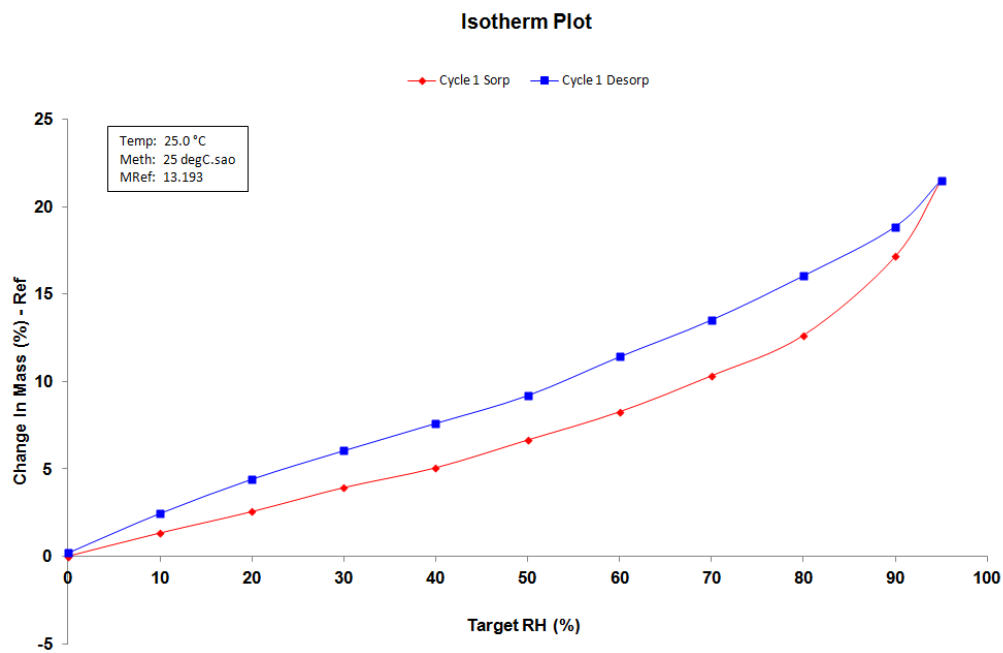


Figure 2.5 Sorption isotherm curves of Moso bamboo specimen

The sorption property of bamboo powder, bamboo blocks, parenchyma cells, and chemically macerated fibres of Moso bamboo was measured. The major conclusion was that the parenchyma cells demonstrated the highest hygroscopic capability followed by bamboo fibres, bamboo powder and bamboo blocks (Jiang *et al.* 2000 and Jiang *et al.* 2006a). Ohmae and Nakato (2009) investigated the moisture sorption properties of Moso bamboo in the longitudinal direction by a saturated solution method. Wang (2010) compared the difference of moisture sorption among bamboo blocks, bamboo fibre, lignin and hemicelluloses. The major finding was that the hygroscopic capability of the hemicelluloses was much higher than the lignin at same relative humidity. The hygroscopic capability of bamboo fibre was higher than the bamboo block.

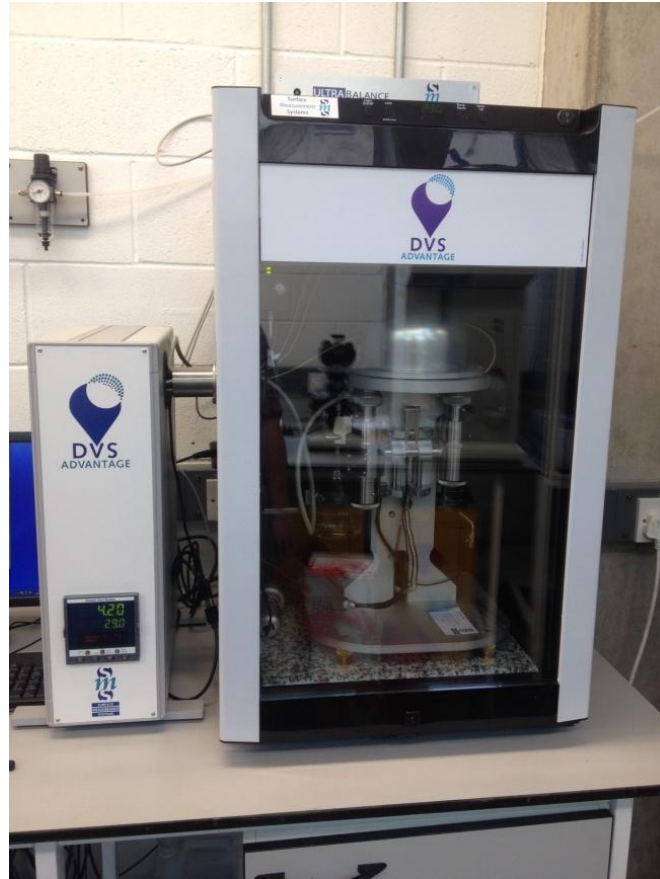


Figure 2.6 Dynamic vapour sorption (DVS) equipment

Dynamic vapour sorption (DVS) is another novel technique to investigate the hygroscopic properties of different cellulosic materials. See figure 2.6. Hygroscopic research by DVS on bamboo has not been found in the literature. However, in wood research, a number of studies have been undertaken using DVS. The dynamic water vapour sorption properties of Scots pine (*Pinus sylvestris* L.) wood samples with glutaraldehyde treatment were investigated. The glutaraldehyde treatment can lead a remarkable reduction in equilibrium moisture content of wood and the corresponding time to approach equilibrium state at each target relative humidity (RH) (Xie *et al.* 2011). The water vapour sorption properties of apple wood biochar (*Malus* sp.) have been investigated by DVS. The parallel exponential kinetics (PEK) model fitted well in this study (Popescu *et al.* 2015). The sorption isotherms, hysteresis, accessibility, and surface area of Finnish birch and spruce wood were investigated by DVS. The research concluded that the increased porosity and reduced particle size can cause negative impact on the storage properties of torrefied and charred material (Kymäläinen 2015).

The review indicated that both saturated salt solution method and DVS can be utilised to conduct the sorption isotherm research on Moso bamboo. The hygroscopic performance of

bamboo has not been discussed in the radial and tangential directions. Moreover, there is little published information on the moisture desorption of bamboo.

2.7 Liquid water diffusivity research

Liquid water movement can be described by Darcy's law if the effects of gravity are not considered. See equation 2.7.1.

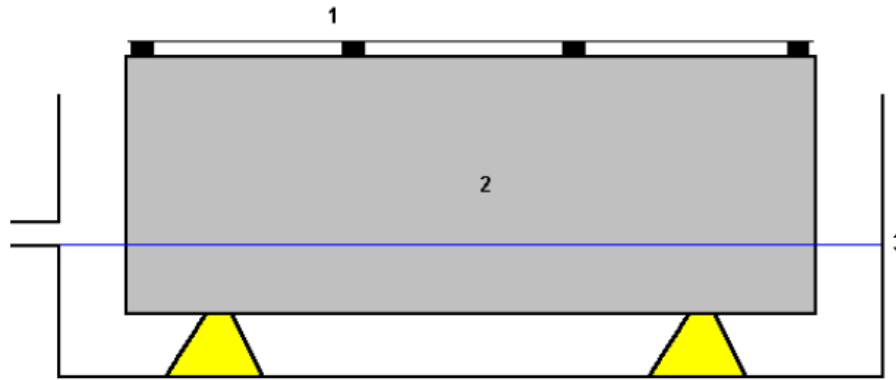
$$K = D_l \frac{\partial w}{\partial P_{suc}} \quad (2.7.1)$$

K : Coefficient of liquid water permeability (kg/m s pa)

D_l : Liquid water diffusivity (m²/s)

P_{suc} : Capillary suction stress (Pa)

The measurement of liquid water diffusivity of Moso bamboo is presently under development. Time (1998) explained the conversion method between the diffusion coefficient with moisture concentration as driving potential and the diffusion coefficient with vapour pressure as driving potential. The research also compared the experiment results of these diffusion coefficients by different authors. The liquid water diffusivity in wood was investigated by Kang and Chung (2009). The results indicated that the ratio of liquid water diffusivity divided by the intrinsic permeability of wood can be estimated by a function of saturation or moisture content. Moisture transport in wood was expressed by a mesoscopic model. The liquid water diffusivity was estimated by considering the porosity of the late wood and early wood (Zillig *et al.* 2006). Another method from WUFI software was also reported for calculation of the water diffusivity of building material (Delgado *et al.* 2012).



Key

- 1 Grid to weigh down buoyant specimens (if required)
- 2 Specimen
- 3 Water level

Figure 2.7 Water absorption coefficient measurement (BS EN ISO 15148: 2002)

The water absorption coefficient can be utilised to calculate the liquid water diffusivity (BS 15148 EN ISO 2002 and Zillig *et al.* 2006). However, this British standard (BS 15148 2002) suggests that ‘The findings for hygroscopic building materials under practical non-isothermal conditions show that it is not possible to describe moisture transport in terms of moisture dependent diffusion only. For that reason, neglecting liquid transport completely in simple prediction methods which only model diffusion will lead to a smaller error than an incorrect consideration of using moisture dependent vapour permeabilities. This means that permeability measured under dry-cup conditions should be used for such models only.’

2.8 Thermal and hygroscopic expansion

Thermal expansion, shrinking and swelling data of bamboo are still scarce in the literature compared with the related researches on wood. Thermal and moisture strain data of bamboo plywood wall were measured under periodic temperature and relative humidity conditions by Li *et al.* (2012). The effect of utilising bamboo and hybrid bamboo-precipitated calcium carbonate filler to improve the thermal expansion performance of filled plastic composites was assessed by Huang *et al.* (2012). The linear thermal expansion thermal coefficients of nine wood species and resin-bonded birch laminates were investigated in the three directions of the cylindrical coordinate system. A dilatometer was utilised in the thermal expansion measurement (Weatherwax and Stamm 1956). See figure 2.8. The hygroexpansion of three wood species under sinusoidally varying relative humidity conditions was studied by Chomcharn and Skaar. (1983). The hygroscopic swelling and shrinkage of latewood cell wall

was investigated by image processing using a stereological technology (Rafsanjani *et al.* 2014). The hygroexpansion of *Cunninghamia lanceolata* (Chinese fir) during moisture adsorption and desorption processes was reported by Ma *et al.* (2005).

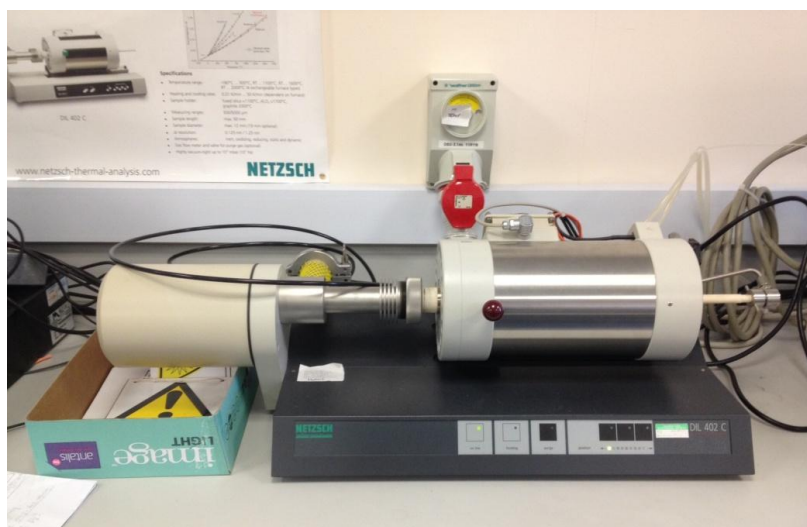


Figure 2.8 Dilatometer for thermal expansion measurement

2.9 Simulation and experiment research

Heat and moisture transfer on wood were investigated earlier than the researches on bamboo. Li *et al.* (2012) presented work on the a heat and moisture transfer work in bamboo with both experimental and simulation methods. A heat and moisture transfer model has been utilised to simulate the wood drying process (Plumb *et al.* 1985). Younsi *et al.* (2006) presented a three-dimensional simulation of heat and moisture transfer in wood which is based on the theory of coupled heat and mass transfer in capillary porous media from Luikov (1966). Wang (2010) investigated the heat and moisture transfer process in the bamboo composite wall.

The aforementioned reviews indicated that partial differential equations (PDEs) have been broadly utilised in the building physics field to describe the transient heat and moisture transfer mechanism of building materials. Due to the complexity of the PDEs, large numbers of mathematical tools were developed to provide the numerical solutions for the PDEs. Delgado *et al.* (2012) reviewed 14 hygrothermal modelling tools and suggested that versatility, visibility, renewability and user-friendliness are the features of successful hygrothermal modelling tools. To assess the accuracy of the current model for hygrothermal modelling, a British Standard provided a benchmark example (BS EN 15026 2007) for calibration. Studies from Portal (2011) and Nusser and Teibinger (2012) proved that the simulation tool from the theory of Sasic Kalagasidis (2010) and the PDEs of WUFI software can meet the requirements of the benchmark.

2.10 Summary of literature review

This chapter reviewed the basic theory of heat and moisture transfer. The PDEs to describe the heat and moisture transfer require the measurement of density, specific heat capacity, thermal conductivity (or thermal diffusivity), water vapour permeability (or water vapour resistance factor), liquid diffusion coefficient and sorption isotherm for Moso bamboo. The data for these six parameters of Moso bamboo are still under development. Especially, the data from different positions and directions need to be specified because Moso bamboo shows obvious non-homogenous characteristics in these directions and positions. The evidence was illustrated in details in Chapter 3. The temperature and RH need to be known as the initial condition. The constant surface temperature and RH, heat or moisture flux, and convection conditions are the boundary conditions for solving the heat and moisture transfer PDEs. The simulation tool from the theory of Sasic Kalagasidis (2010) and the PDEs of WUFI software can meet the requirements of the benchmark calibration.

Therefore, the following chapters will focus on the data collection of density, specific heat capacity, thermal conductivity (or thermal diffusivity), water vapour permeability (or water vapour resistance factor), liquid diffusion coefficient, and isotherm of Moso bamboo. Furthermore, the simulation and experiment studies will be presented for understanding the temperature and RH response of Moso bamboo in different climate conditions.

Chapter 3 Anatomical features, density and porosity of Moso bamboo

The research of the density of Moso bamboo was published in a peer reviewed journal: *Construction and building materials*. The research of porosity of Moso bamboo was published by another peer reviewed journal: *Wood science and technology*. (In self bibliography and published work: Huang *et al.* 2015 and Huang *et al.* 2017a).

3.1 Anatomical features of Moso bamboo

Phyllostachys edulis is the Latin name of Moso bamboo. Generally, the stem of bamboo is a hollow cylinder constituting node parts and internode parts. The vertical growing direction of the Moso bamboo is defined as the longitudinal direction. The radial direction is from the internal surface to the external surface of the bamboo culm wall. The tangential direction follows the perimeter of the bamboo culm (Figure 3.1.1) and be located in radial increments from the inside to the outside.

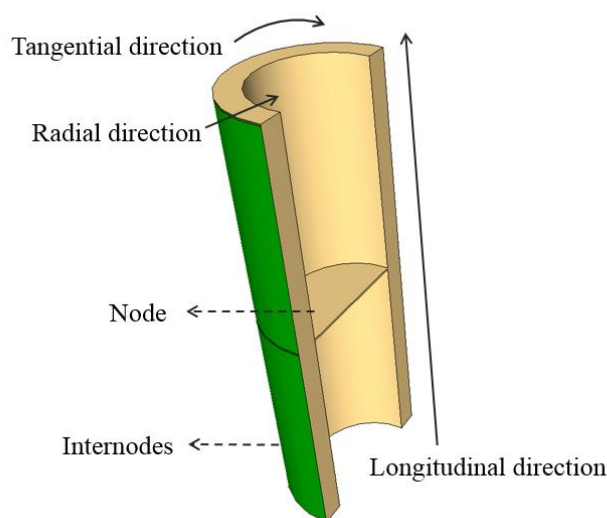


Figure 3.1.1 Terminology for a bamboo culm

In the transverse section, the main morphological feature of Moso bamboo is that the vascular bundle tissue is surrounded by the parenchymatous ground tissue. Every vascular bundle unit has two large vessels which are the main channels of water transportation (Grosser and Liese

1971). The edge of the vascular bundle vessel is surrounded by fibre strand. Figure 3.1.2 shows that the parenchymatous ground tissue is relatively uniform in size.

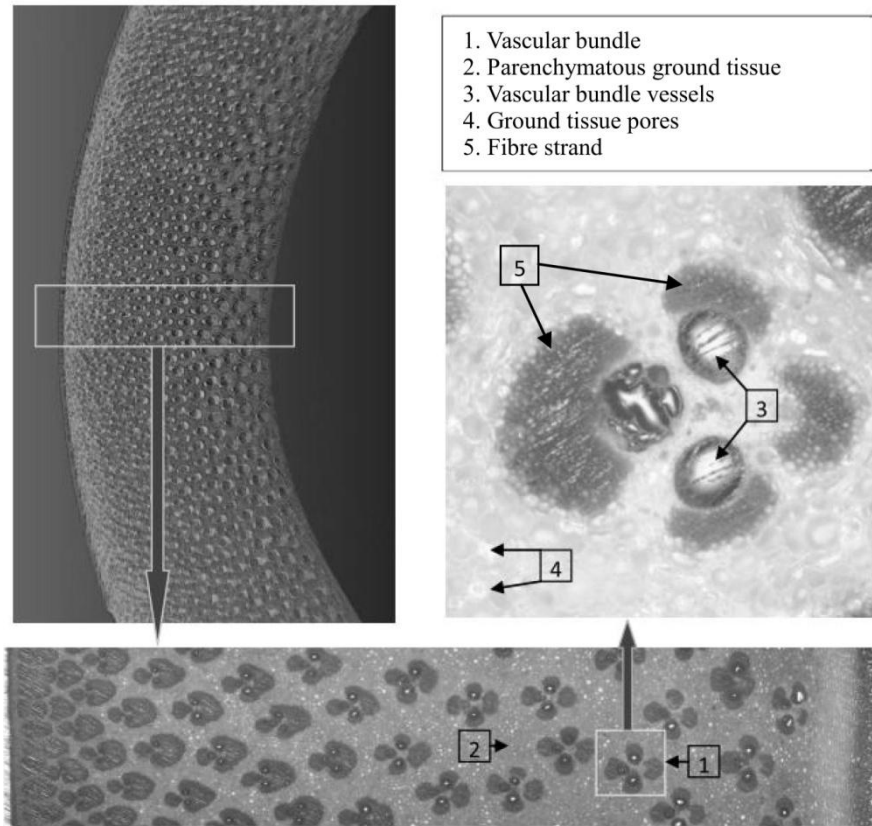


Figure 3.1.2 Anatomical features of Moso bamboo in the radial direction (Huang *et al.* 2014)

In the radial direction, for internode parts, the total size and the area of vascular bundles' vessels become larger from the external surface to the internal surface of the culm wall of the Moso bamboo. The quantity of the vascular bundle and the proportion of the lignified parenchyma cells decrease. For node parts, besides the aforementioned features, many horizontal tubular vascular bundles form a spoke-shape transverse section (Figure 3.1.3).

Longitudinally, for internode parts, parenchyma cells and lignified parenchyma cells maintain a remarkably straight alignment with the longitudinal axis of the culm (Liese 1985, Lo *et al.* 2004). The vascular bundle vessels are present as continuous vertical cavities in the longitudinal direction. The constitution of every longitudinal line is relatively homogenous. For node parts, vertical vascular bundles gradually bend towards the horizontal direction (Figure 3.1.3). These interwoven bundles are irregularly distributed in the zone between the diaphragm and the peripheral cortex of nodes (Grosser and Liese 1971).

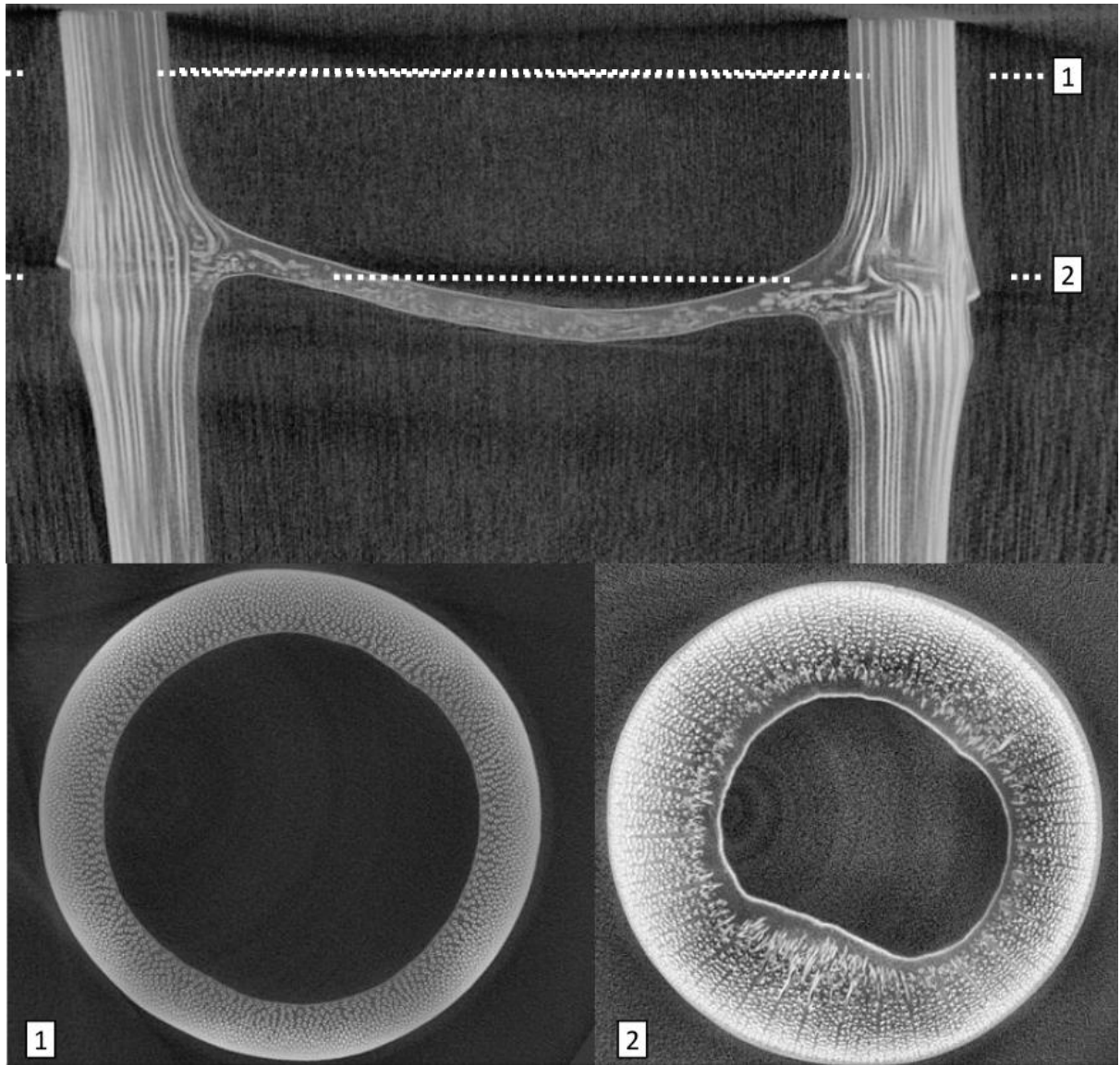


Figure 3.1.3 CT-scanned images of the morphological features of the Moso bamboo

The morphological characteristics of the Moso bamboo along the tangential direction are determined by the morphological characteristics of the radial and longitudinal direction. The orientation of vascular bundles dominates the morphological difference between the nodes and internode parts of Moso bamboo. For internode parts, the direction of the vascular bundles is perpendicular to the tangential line. For node parts, the distribution of the vascular bundles is not uniform.

3.2 Density profile of Moso bamboo

3.2.1 Research objectives

This section aims to quantify density distribution and specify the density distribution difference between internodes and node parts of *Phyllostachys edulis* (Moso Bamboo) in radial, tangential and longitudinal directions. The results of this study are prepared as the density database for the further work on Computational fluid dynamics (CFD) simulations for thermal performance of bamboo. In transient heat transfer studies, the density, thermal conductivity and specific heat capacity of the target material are three basic input parameters (Fourier 1878). Currently, there is insufficient density data for bamboo so researchers are forced to use the averaged density as the material parameter. However, the Moso bamboo is regarded as a non-homogenous natural material so density may vary as a function of position in the culm. The density variation may lead to relevant changes in other physical properties such as thermal diffusivity and specific strength. Better understanding of density distribution could provide more accuracy and clear guidance for optimum selection of certain specific parts of Moso bamboo for construction applications.

3.2.2 Methodology

Computed tomography (CT) scanning technology is a method for quantifying the inner density variation of a Moso bamboo specimen as a function of orientation. This technique provides accurate visual information, an easy operational process and a simple method for calculating density (Mull 1984, Davis and Wells 1992). There are limitations in the CT scanning technique. To obtain an acceptable resolution for density quantification, the volume of specimen needs to be restricted to a relatively small size while the scanning time needs to be as long as possible (Grundberg *et al.* 1995). The CT scanning environment needs to be fairly clean. Minimising the number of reference materials and avoiding the involvement of metals are two requirements for improving the accuracy of CT scanning (Bucur 2003). The scanning parameters will influence the results. Therefore, calibration needs to be conducted after adjusting the scanning setting (Freyburger, *et al.* 2009).

In this study, a Nikon XT H 225 CT scanner is utilised to quantify the density of the Moso Bamboo specimen. This equipment outputs greyscale images. The scanning parameters were fixed at a voltage of 106kV and current of 91 μ A. The resolution of the captured grayscale image is 1000 dots per inch (DPI). Under this condition, the linear relationship between the greyscale value and the density value of the specimen can be described by equation 1. The greyscale value is calibrated by scanning distilled water and Polypropylene (PP Homopolymer). The bulk densities of these materials are known. However, this linear relationship is only applicable to this scanning. Calibration needs to be conducted in every

time by scanning reference materials with known bulk density. The Avizo image processing software is utilised to measure the greyscale of CT scanning image. The coefficient of multiple determination (R^2) of this equation is 99.992%.

$$\rho = 39935.791Gs - 1.193 \quad (3.2.1)$$

ρ : density (kg/m^3)

Gs: greyscale

Therefore, the density of the Moso bamboo can be calculated by the greyscale measurement of the greyscale images of specimens.

Moso bamboo culm was ordered from UK Bamboo Supplies Limited in the United Kingdom. The average moisture content of the specimen was 9% determined by oven drying. The bulk density range of bamboo culms was from 601kg/m^3 to 640 kg/m^3 and the diameter of the bamboo culm varied from 52 mm to 55 mm. The thickness of the specimen varied between 7 mm and 8 mm. Specimens were prepared with a height varying from 10mm to 12mm. These dimensions result in the maximum volume of the bamboo culm (Figure 3.2.1) to achieve an acceptable resolution in the CT scanner. Parts were cut from the culm section as shown in Figure 3.2.1a. The tangential length of the specimen was one eighth of the perimeter of the culm. The longitudinal length was set to be higher than the thickness of the bamboo culm wall to optimise the CT measurement Scans were made at a node and an internode zone. The density measurement of the specimens was conducted in a radial direction, tangential direction and longitudinal direction. Scans were made according to the notation in Figure 3.2.1 and identified by the ten layer numbers and the radial angle in degrees.

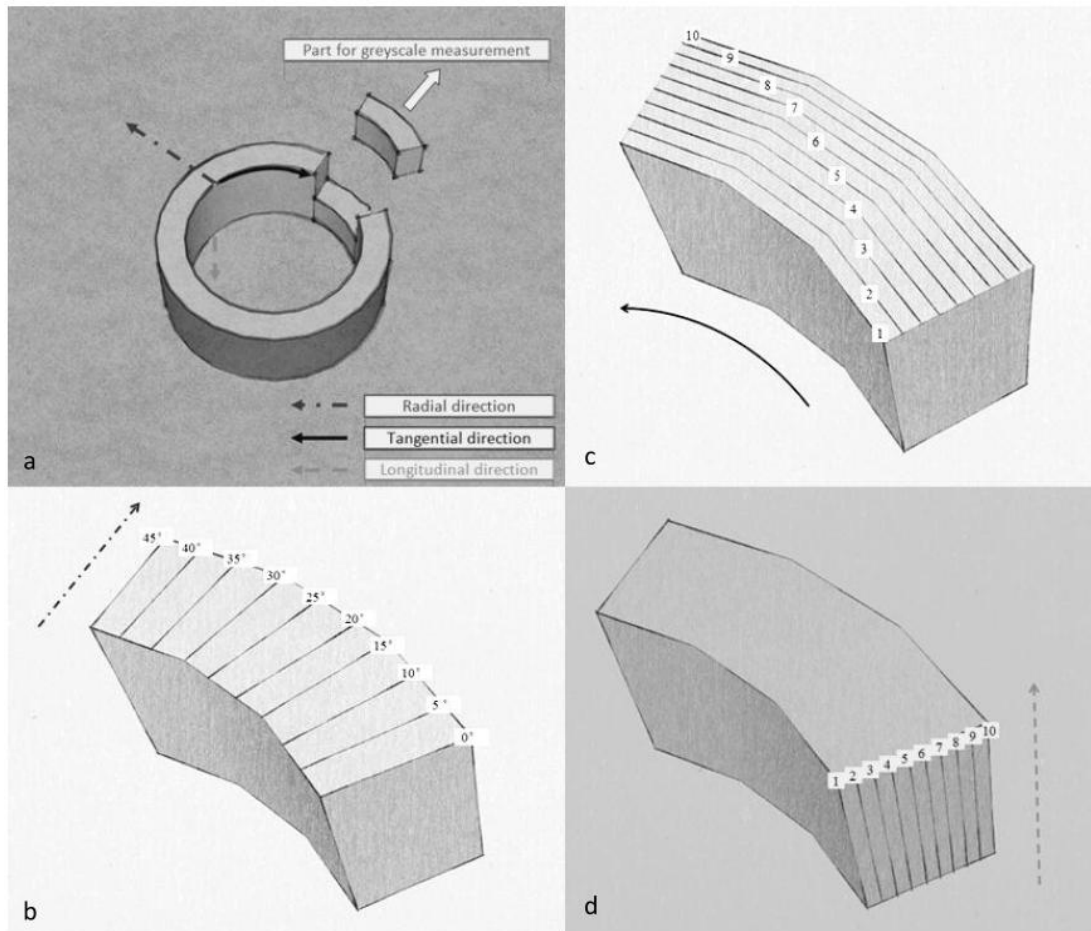


Figure 3.2.1 (a) Orientation of culm section showing a part cut for CT scanning. (b) Definition of radial elements in culm section. (c) Tangential elements in culm section. (d). Longitudinal elements in culm section.

In the radial direction measurement, ten measurement lines were equally distributed in a sector area with the central angle of 45° . The first measurement line was set to be the 0° line. The central angle of two adjacent lines is 5° . The length of each measurement line was equal to the thickness of the bamboo culm wall. (see Figure 3.2.1(b).) In the tangential direction measurement, measurement lines were arcs. From the internal surface to the external surface of the bamboo culm wall, the length of these arcs progressively increased. (see Figure 3.2.1(c).) In the longitudinal direction measurement, all measurement lines with the same length were perpendicular to the cross section of the bamboo culm. (see Figure 3.2.1(d).) Every measurements line had 10 sample points which were also equally distributed along the measurement line.

3.2.3 Results and discussion

The density variation of both internode and node parts were measured in this study by CT scanning. The results are illustrated by the waterfall charts. The left horizontal axis represents the sample points with measurement direction. The number is from 1 to 10. The right horizontal axis represents the serial number of different measurement lines. The vertical axis represents the density value. The unit of the density value is kilograms per cubic metre.

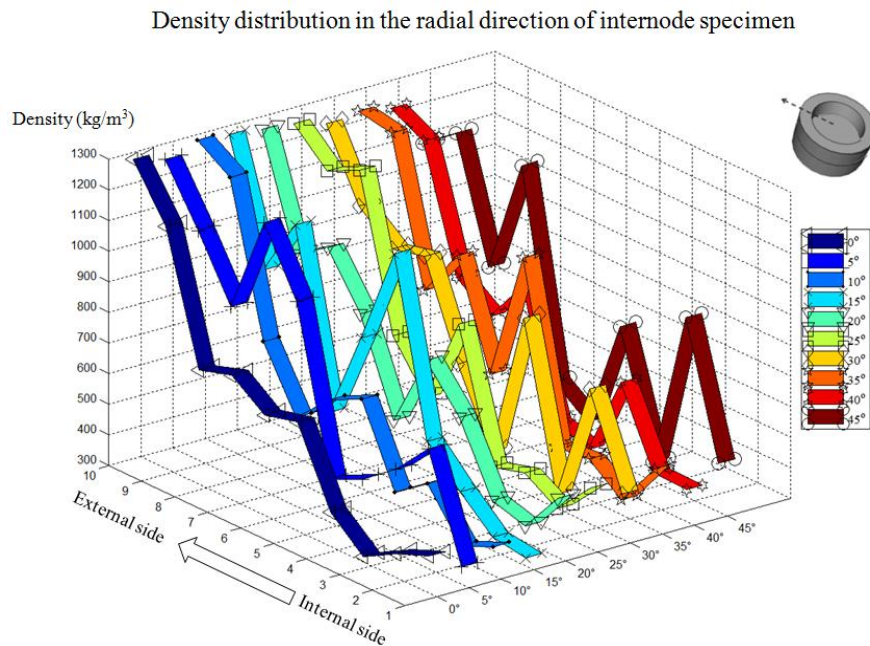


Figure 3.2.2 Density distribution in the radial direction of internode specimen

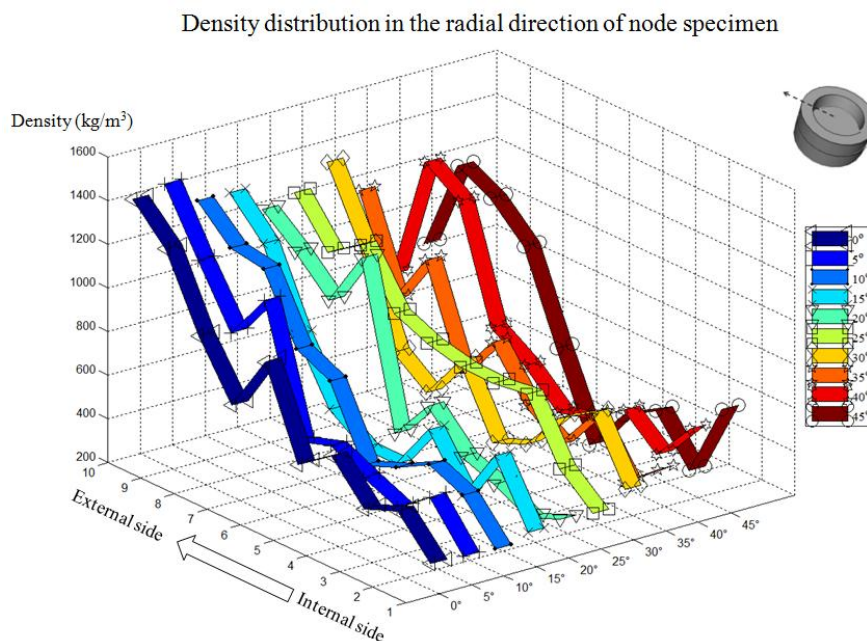


Figure 3.2.3 Density distribution in the radial direction of node specimen

In the radial direction (Figure 3.2.1c), the fluctuation in density of internode parts ranges from 336kg/m³ to 1283kg/m³ (Figure 3.2.2). For node parts, the trend in density variation is similar to that of internode parts and the density fluctuation range of node parts is from 331kg/m³ to 1407kg/m³ (Figure 3.2.3). Node parts have higher density on the external side. The average density value of measurement lines ranges from 674 kg/m³ to 759kg/m³ at internode parts and 634kg/m³ to 751kg/m³ at node parts.

The standard deviation of internode density ranges from 282kg/m³ to 336kg/m³. The standard deviation of node parts is from 240kg/m³ to 362kg/m³. The Coefficient of Variation (COV) ranges are 37.39% to 47.15% for internode parts and 33.51% to 49.46% for node parts, respectively.

In the radial direction, all density versus distance curves undulate and increase from the internal side to the external side of the bamboo culm wall (see Figures 3.2.2 and 3.2.3). These undulations are caused by the anatomical characteristics of the Moso bamboo. Figure 3.1.2 indicates that a high density of vascular bundles and fibre strand can be found at the periphery of the bamboo culm wall. From the external side to the internal side of the bamboo culm wall, the proportion of vascular bundles decreases, while more space is occupied by parenchyma ground tissue. The vascular bundle vessel is surrounded by fibre strand. The fibre strand is denser than the ground tissue cells. Therefore, the density of vascular bundle tissue is higher than the density of the ground tissue. A large proportion of vascular bundles signifies higher density. Most measurement lines show obvious fluctuation. However, the 25° measurement line at the node part should be noted. The density of this line tends to be steady in the middle zone because the line passes through a spoke-shaped radial, horizontal vascular bundle vessel. The hollow structure of the vessel is the main reason for the series of relatively uniform density values. At node parts, a remarkable feature is that vascular bundles deviate in different directions.

In the longitudinal direction, the density range is from 323kg/m³ to 1334kg/m³ at internode parts and from 402kg/m³ to 1244kg/m³ at node parts. The average density value of different measurement lines ranges from 377kg/m³ to 1304kg/m³ at internode parts and from 520kg/m³ to 1125kg/m³ at node parts. For internode parts, the standard deviation and COV of each measurement line ranges from 16kg/m³ to 46kg/m³ and 1.2% to 6.78%, respectively. At the node parts, the standard deviation ranges from 107kg/m³ to 277kg/m³. The COV is from 9.52% to 32.29%.

Density distribution in the longitudinal direction of internode specimen

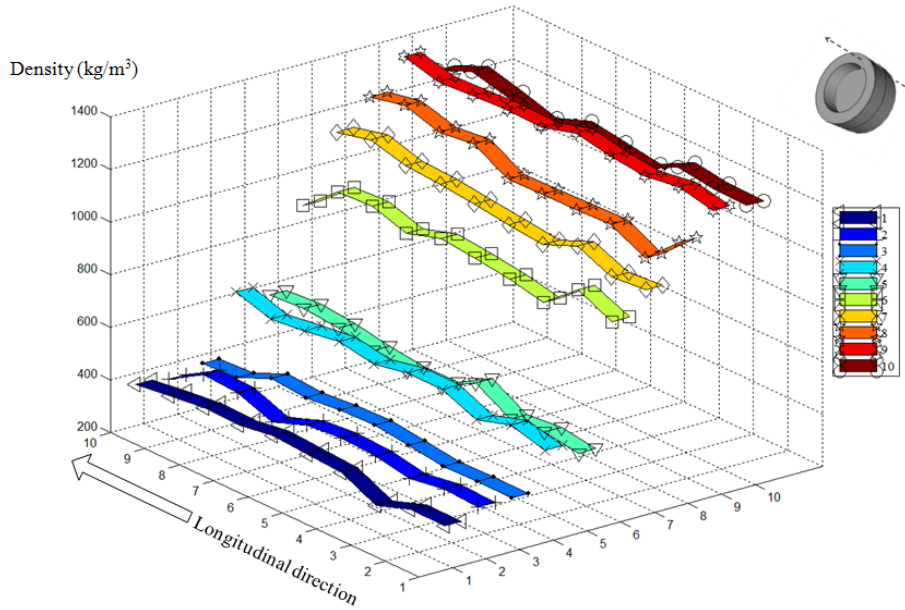


Figure 3.2.4 Density distribution in the longitudinal direction of internode specimen

Density distribution in the longitudinal direction of node specimen

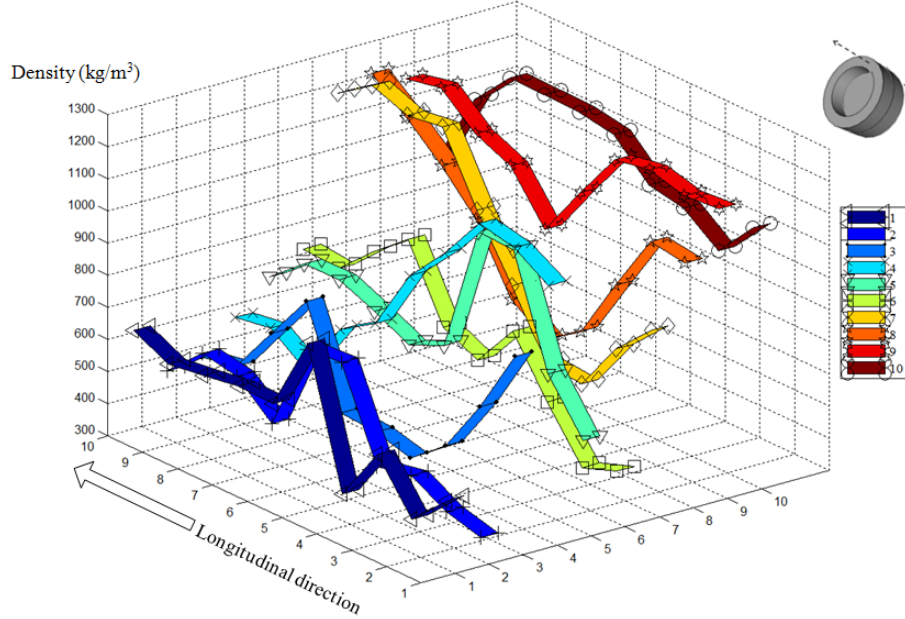


Figure 3.2.5 Density distribution in the longitudinal direction of node specimen

The standard deviation and COV data indicate that density remains almost unchanged through every single measurement line at the internode parts (Figure 3.2.4). The linearly grown vascular bundles at the internode parts in the longitudinal direction are uniform in density. The density fluctuation of every measurement line at the node parts is much more significant compared with the internode parts (Figure 3.2.5). The longitudinal axis in Figure 3.2.5

includes a central portion of node material and internode material on either side. The density fluctuates highly in the central portion because of the complex distribution of fibre bundles but is more stable on either side. There is also an underlying trend of increase in density passing from specimen 1 to specimen 10 in the radial direction.

In the tangential direction, the density ranges of internode parts are from 286kg/m^3 to 1303kg/m^3 . The density of node parts ranges from 237kg/m^3 to 1412kg/m^3 . The average density value of different measurement lines is from 442kg/m^3 to 1192.1kg/m^3 at internode parts and from 479kg/m^3 to 1055kg/m^3 at node parts. The standard deviation of each measurement line is from 89kg/m^3 to 217kg/m^3 at internode parts. The COV range is from 10.40% to 33.23%. At node parts, standard deviation is from 98kg/m^3 to 290kg/m^3 . The COV is from 19.55% to 33.80%.

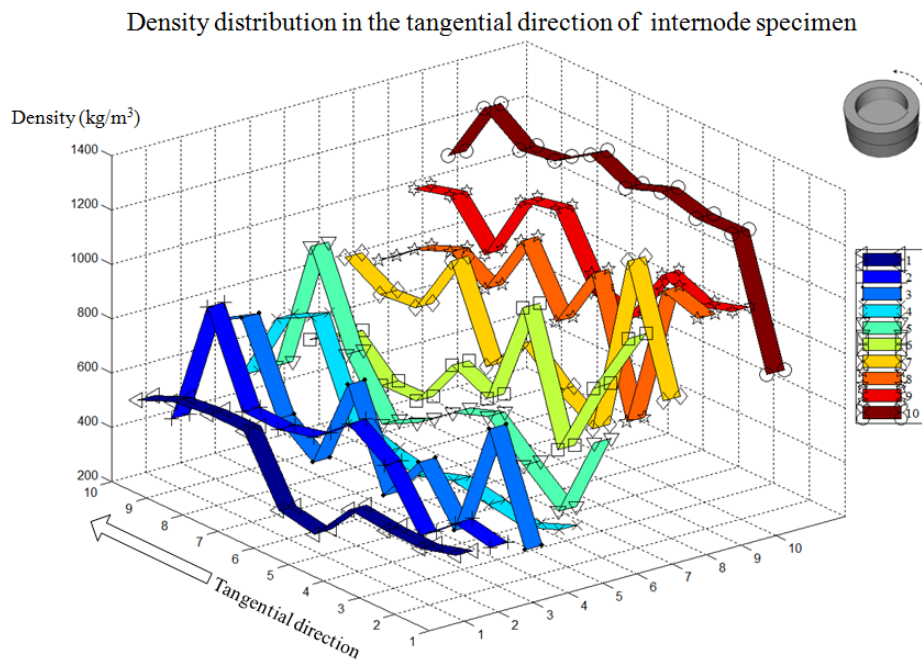


Figure 3.2.6 Density distribution in the tangential direction of internode specimen

Density distribution in the tangential direction of node specimen

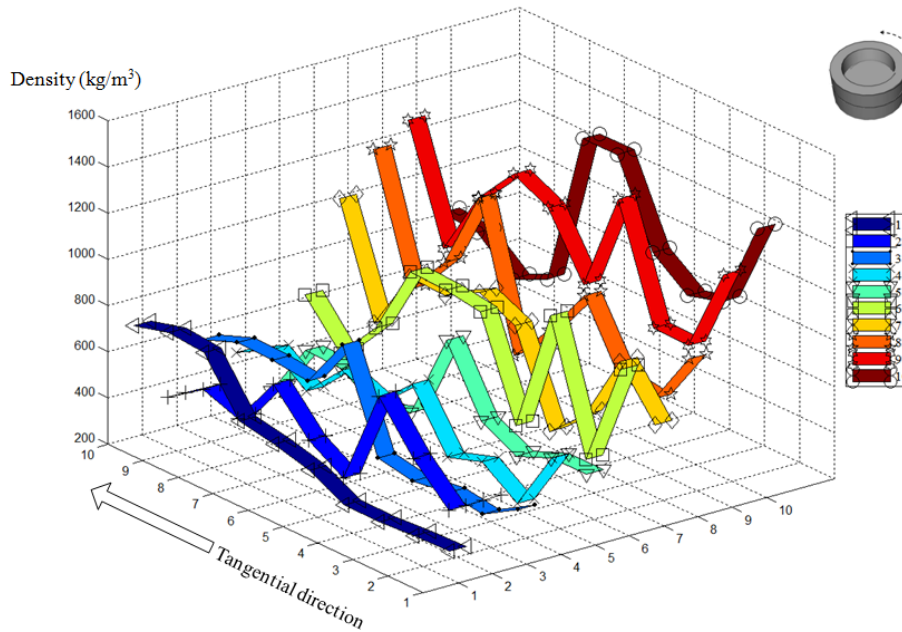


Figure 3.2.7 Density distribution in the tangential direction of node specimen

For internode parts, the standard deviation and COV data indicate that the density fluctuation range in a tangential direction (Figure 3.2.6) is more extreme than in the longitudinal direction (Figure 3.2.4), but steadier than the range of radial direction (Figure 3.2.5). The node parts' standard deviation and COV changed very little compared with the longitudinal direction. The density variation of the tangential measurement lines of internode parts and node parts has a similar trend to the longitudinal direction. (see Figures 3.2.6 and 3.2.7). The fluctuation of density could be attributed to the distribution of the vascular bundles. The irregular interwoven vascular bundles are the cause of the unsteady density data.

3.2.4 Summary

Both anatomical observation and CT density quantification have indicated that:

The density of both the internode parts and node parts of the Moso bamboo decrease from the external surface to the internal surface of the culm wall in the radial direction. The different proportions of the vascular bundle tissues and the parenchyma ground tissues dominate the density variation of the Moso bamboo in the radial direction. A high proportion of the vascular bundles' tissues are of higher density than the surrounding material, while a high proportion of parenchyma ground tissues is of low density.

In the longitudinal direction, internode parts of Moso bamboo retain relatively uniform density due to the straight vascular bundles. The density distribution for node parts is irregular.

In the tangential direction, the density fluctuation of internode parts is more significant than in the longitudinal direction. This fluctuation is caused by the distribution of vascular bundles tissue and ground tissue in the transverse section. For node parts, the density of the Moso bamboo fluctuates irregularly because the vascular bundles are organised in different directions at the node parts.

Although the bulk density of the bamboo ranges from 601kg/m^3 to 640kg/m^3 , Moso Bamboo has a relatively wide density distribution at different measurement points. The maximum and minimum densities are 237kg/m^3 and 1412kg/m^3 respectively. High density parts of Moso bamboo are concentrated on the external side of the bamboo culm wall for both internode and node parts. Low density parts of Moso bamboo appear on the internal side of the bamboo culm wall of internode parts.

The results of this section indicate that obvious variations exist in different orientations of the Moso bamboo culm. To enhance the reliability of the simulation models in thermal and mechanical fields, variation of the density must be considered.

The results of this section also contributes to supplement the insufficient density data of Moso bamboo, albeit the data could be more universal and refined by considering the samples in different locations within the bamboo culm and higher resolution for CT Scanning*.

(*The content of this section is from a published work of author. See self bibliography (Huang *et al.* 2015))

3.3 Porosity of Moso bamboo

3.3.1 Research objectives

This section aims to quantify the porosity in the cross section of *Phyllostachys edulis* (Moso bamboo) culm wall. The results of this study will form the porosity database for conducting a heat and moisture transfer simulation. The porosity data could also be transferred to a fraction model to derive the basic equivalent thermal properties of Moso bamboo (e.g. equivalent thermal conductivity, heat capacitance).

To evaluate the thermal and moisture performance of bamboo at the material level, the knowledge of hygrothermal behaviour of the material is indispensable. The porosity, density, thermal conductivity, specific heat capacity, vapour permeability, and moisture capacity are the essential hygrothermal properties required to conduct heat and moisture transfer simulations in the thermal performance of porous materials. Among these properties, the porosity could be regarded as the foundation parameter. Another name for porosity is void

fraction which refers to the ratio of the void volume to the total volume. The phase of the void part of bamboo could be gas and liquid while the phase of the skeletal part is solid. (e.g. hemicellulose, cellulose and lignin). Remarkable differences in the physical properties exist in the different phases of bamboo. For example, the density of the air and water are 1.184kg/m^3 and 997kg/m^3 respectively at $25\text{ }^\circ\text{C}$. Density study in this chapter found that the bulk density of Moso bamboo could reach to 1412 kg/m^3 . Therefore, the skeletal density of the Moso bamboo is higher than this value. The fraction variation of the phases leads to the variations in other hygrothermal properties (Wu *et al.* 2013).

The porosity research on bamboo species is still under development compared with the similar research on wood. Mercury intrusion porosimetry (MIP), Gas pycnometry (GP), microscopy image processing and computed tomography are some well established technologies for porosity measurement in the wood research field. The application, strengths and limitations of these technologies are investigated as follows.

The porosity of five hard wood species and one soft wood species has been investigated by MIP (Ding *et al.* 2008). The authors consider MIP as an effective method to measure the porosity of wood. Meanwhile, the limitation of MIP has also been stated as follows: High pressure may cause deformation of pores (Stone, 1964 cited in Ding *et al.*, 2008; Hill and Papadopoulos, 2001). The theory of the MIP assumes that all pores are circular (Cook and Hover, 1993). MIP may measure the pore entrance size rather than the actual pore size distribution (Roels *et al.*, 2001, Giesche 2006). The anisotropic characteristics, e.g. density and porosity variation of the specimens in different locations, need to be carefully discussed (Almeida and Hernandez, 2006).

Gas pycnometry (GP) has been utilised in many papers on porosity research on wood. In Zauer's research (2013, 2014), the porosity and cell-wall density of Norway spruce (*Picea abies*), sycamore maple (*Acer pseudoplatanus*), and European ash (*Fraxinus excelsior*) were analysed by the GP method. This method can achieve relatively high accuracy in the measurement of skeletal density and porosity. However, differences in preparation methods, measurement conditions and the displacement media can result in apparently different results (Stamm and Hansen 1937). The number of mesopores and macropores can be underestimated by some common absorption methods. Also, the result of pore size distribution in GP corresponds to the pore size rather than the morphological porosity distribution.

Other porosity measurement methods are based on the stereological technologies which include three dimensional reconstruction and image processing. The working principles, effective resolution and advantages of X-ray microtomography(X- μ CT), light microscopy (LM), scanning electron microscopy (SEM) and field-emission SEM (FE-SEM) have been

illustrated in Chinga-Carrasco's study (2002). The development of SEM and FE-SEM technologies allows the researchers to capture the image of their specimens at the nanometre level. With the help of image recognition and processing software, the cell wall and lumen can be extracted for the purpose of calculating the porosity. Pan and Kudo (2011) have contributed a number of substantial insights to the segmentation of pores from the microscopic images of wood. A systematic algorithm has been utilised to recognize three different kinds of pore distributions in wood microscopic images (Pan and Kudo 2011). The two dimensional cell porosity and thickness of the cell wall of Norway spruce has been investigated in a recent research (Derome et al. 2012). Although SEM images are often utilised for morphology studies of many wood species, the quantification of solid porosity from SEM images is rarely undertaken by researchers. Computed tomography (CT) scanning technology is a non-destructive method for obtaining the morphological information inside specimens (Iassonov et al. 2009). The X-ray computed tomography imaging has been utilised for the porosity measurement of rocks (Taud et al. 2005). The application of CT scanning in the wood industry could be traced back to 1980s (Benson-Cooper 1982). The pore size and porosity of beech vessels has been investigated by X-ray tomographic microscopy (Hass et al. 2010). Although, a relatively high resolution has been achieved by the CT scanning method, the image recognition of porosity still remains at the level of vascular bundle vessels rather than the level of ground tissue pores. The main strength of using stereological technologies is that the actual morphological pore distribution of the specimen can be displayed directly. That means the porosity can be obtained as a certain orientation. The destruction of the specimen during the process of porosity measurement is less than other aforementioned methods. A limitation of this technology is that the porosity measurement from SEM of the cross section is the two dimensional porosity. In the image processing stage, it is difficult to provide a uniform standard for threshold transformation. The porosity measurement depends on the image quality. A large amount of time is needed for transforming the visual information into numerical results.

The aforementioned techniques are summarised in the table 3.3.1.

Table 3.3.1 Summary of current techniques on the porosity measurement

Techniques	Strengths	Limitations	References
MIP	<ul style="list-style-type: none"> • Effective for woods 	<ul style="list-style-type: none"> • Sample Deformation • Assume all pores are circular • Porosity result is corresponded to the pore size of the sample 	(Ding <i>et al.</i> 2008), (Stone 1964), (Hill and Papadopoulos 2001), (Cook and Hover, 1993), (Roels <i>et al.</i> 2001),(Giesche 2006) (Almeida and Hernandez, 2006)
GP	<ul style="list-style-type: none"> • High accuracy 	<ul style="list-style-type: none"> • Sample preparation and displacement media need to be treated carefully. • Porosity result is corresponded to the pore size of the sample 	(Zauer <i>et al.</i> 2013), (Zauer <i>et al.</i> 2014), (Stamm and Hansen 1937)
LM \SEM	<ul style="list-style-type: none"> • High resolution • Non-destructive • Porosity result is corresponded to the real position of the sample 	<ul style="list-style-type: none"> • 2D measurement • Highly rely on the image quality • No specific image processing standard 	(Chinga-Carrasco 2002), (Pan and Kudo 2011), (Derome <i>et al.</i> 2012),
CT\X-ray	<ul style="list-style-type: none"> • 3D measurement • Non-destructive • Porosity result is corresponded to the real position of the sample 	<ul style="list-style-type: none"> • Low resolution • Slow in digitizing 	(Iassonov <i>et al.</i> 2009), (Taud <i>et al.</i> 2005), (Benson-Cooper 1982), (Hass <i>et al.</i> 2010)

Due to the importance and the influence of the porosity on the hydro-thermal properties of the Moso bamboo, this study aims to investigate and quantify the porosity in the cross section of the *Phyllostachys edulis* (Moso bamboo) culm wall. By considering the strengths and limitation of the existing porosity measurement technologies, both SEM and CT scanning method are utilised in this study. The main reason is that these two methods can determine the porosity distribution as the function of the orientation within Moso bamboo. The density study has proved that the density and the fraction of vascular bundle tissue to ground tissue decrease from the external surface to the internal surface of the bamboo culm wall. It is expected that the porosity has a similar trend with density.

3.3.2 Specimen preparation and methods

Eight Moso bamboo culms, which were cut from different heights, were ordered from a bamboo supplier in the United Kingdom. The external diameter of these culms and recognition numbers are listed in the Table 3.3.2. The specimens from each culm are divided into two major groups. The specimens of one group are cut from internode part of the bamboo culm. The specimens of the other group are from nodes part. See Figure 3.3.1.

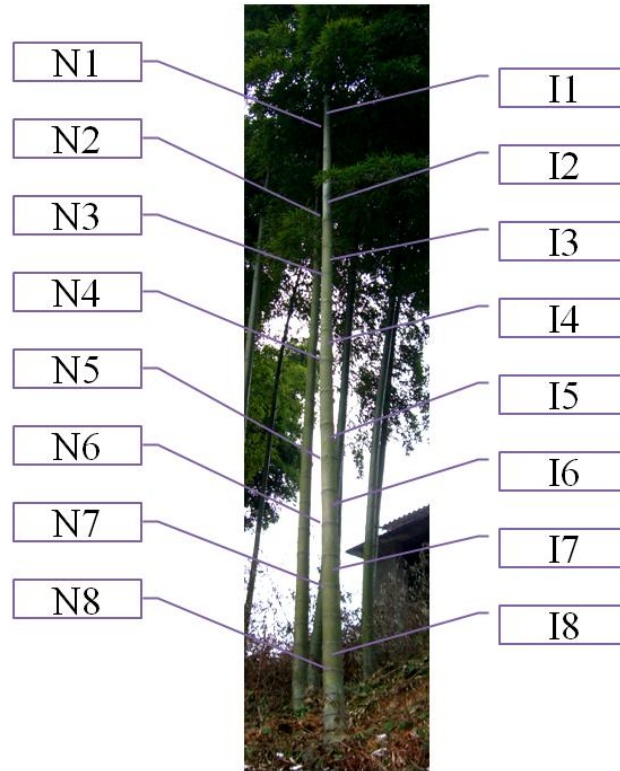


Figure 3.3.1 Group number and cutting position of Moso bamboo

Table 3.3.2 Nomenclature of each specimen by external diameter sequence

External diameter (mm)	20-25	30-35	40-45	50-55	60-70	70-80	100-120	120-150
The height of the cutting position (m)	>7	6.5-7	5.5-6.5	4.5-5.5	3.5-4.5	2.5-3.5	1.5-2.5	0-1.5
Internode	I1	I2	I3	I4	I5	I6	I7	I8
Node	N1	N2	N3	N4	N5	N6	N7	N8

Bamboo specimens were oven dried to eliminate the moisture at $103\text{ }^{\circ}\text{C}\pm 2\text{ }^{\circ}\text{C}$ for 24 hours. Then the specimens were stored in the desiccators with Calcium Chloride (CaCl_2) to avoid the moisture absorption. The specimens were cut into small pieces. The specimens were firstly utilised for CT scanning measurement. The same specimens were softened by water soaking at $70\text{ }^{\circ}\text{C}$. The softened specimens needed to be further cut by blades to form a flat surface for the SEM measurement. After the cutting stage, the specimens were oven dried again. Vacuum storing and gold sputter coating were conducted before the SEM measurement. The coating time was three minutes.

The CT scanning aims to obtain the bulk density of the specimens. The Nikon XT H 225 CT scanner are utilised to capture the greyscale image of Moso bamboo specimens. The scanning parameters were fixed at a voltage of 90 kV and current of 108 μ A. Polypropylene (PP Homopolymer) and Acrylic were scanned simultaneously with the bamboo specimens to obtain the linear relationship between the greyscale value and their actual bulk density. The bulk densities of these materials are known. The linear relationship could be expressed by the 3.3.1.

$$\rho_{bulk} = 40.6Gs - 70.4 \quad 3.3.1$$

ρ_{bulk} : Density (kg/m³)

Gs : Greyscale

Density study in this chapter found that the linear relationship is only applicable for one single scanning. Any change on the settings will lead to a different linear relationship. Calibration needs to be conducted in every time by scanning reference materials with known bulk density. The Avizo software is utilised to conduct the measurement of the greyscale of CT scanning image.

Five scan lines were placed in the cross section of each Moso bamboo specimen. The line thickness is 0.1mm. The distance between two adjacent lines is approximately 0.5mm. The CT scanning area with 5 lines, which is a representative area, is also as same as the area from backscattered electron (BSE) image. See Figure 3.3.2. Every measurement line could obtain 500 greyscale values.

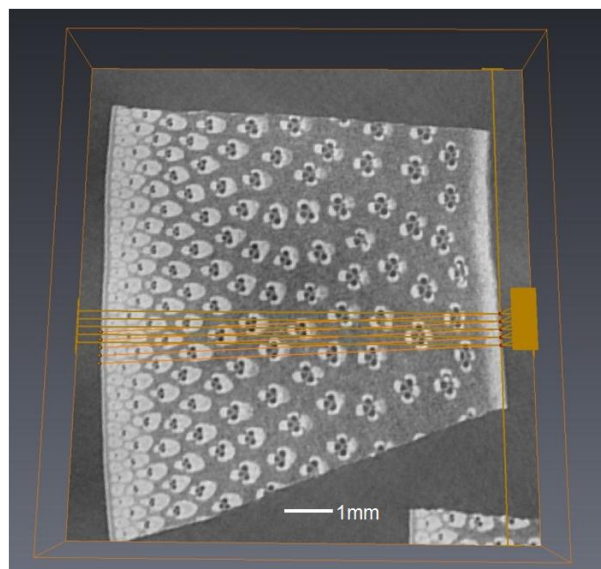


Figure 3.3.2 CT scanning measurement area of a Moso bamboo specimen

The average values of the five measurement lines are utilised as the bulk density to calculate the porosity by equation 3.3.2.

$$\rho_{bulk} = \rho_s * (1 - \phi) + \rho_{air}\phi \quad 3.3.2$$

ρ_{bulk} : Bulk density (kg/m³)

ρ_s : Skeletal density (kg/m³)

ϕ : Porosity

ρ_{air} : Air density (1.184 kg/m³ at 1atm, 25 °C)

If the bulk density and skeletal density are known, the porosity value can be obtained. The bulk density is obtained by CT scanning measurement. The cell wall density range of Moso bamboo is assumed in the range between 1425 to 1524kg/m³. This range is obtained by the peak density value of the bamboo specimens in the CT scanning. The peak values generally appear at the epidermis side of the bamboo culm. The epidermis side are regarded as the side where the porosity tends to zero. The later observation by SEM found that more pores, which the diameter is less than 1µm, appeared in the cell wall of internal side of the bamboo culm. Wood researchers often use 1500 kg/m³ as the approximate cell wall density (Siau 1984). Three types of displacement media were utilised to measure the cell wall density of ten wood species. The measured density is from 1466 to 1548 kg/m³ (Stamm 1928). In Kellogg and Wangaard's research (1969), the cell wall density for wood species ranges from 1497 to 1529 kg/m³. It could be noticed that the cell wall density range of Moso bamboo is similar to the literature values of wood species.

Backscattered electron (BSE) image of the Moso bamboo specimens were captured by JEOL JSM-6480 scanning electron microscope (SEM) in the high vacuum mode. The beam accelerating voltage of the BSE is 15kV in this study. The magnification of the BSE is X60. The working distance and probe diameter are approximately 22mm and 60nm respectively. The BSE signal is from the elastically scattered electron which is deflected back from the specimen. The higher atomic mass elements have higher capability to backscatter the incident beam of electrons than the lower atomic mass elements. The result of this fact is that heavier elements contribute brighter pixels than lighter elements to the images (Solomonov *et al.* 2014). The high contract BSE image are more helpful for distinguishing the air phase and bamboo cell wall phase. Figure 3.3.3 clearly showed the difference between the secondary electron (SE) image and BSE image.

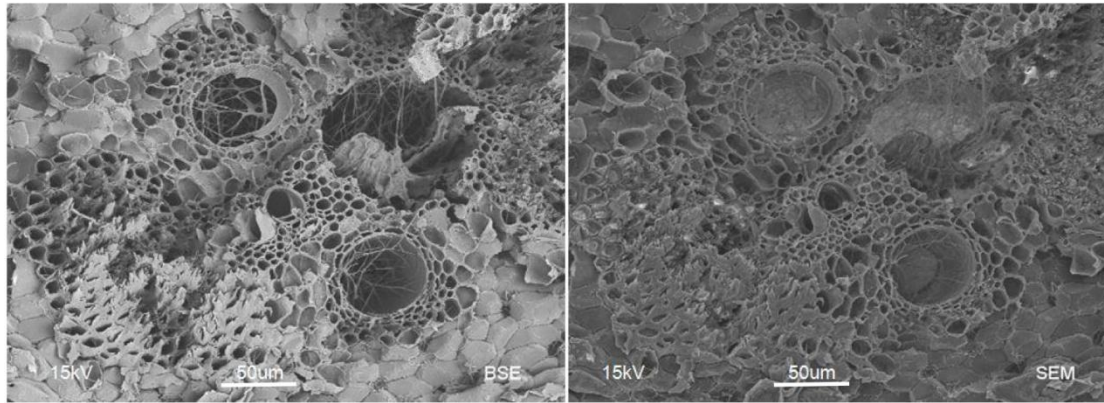
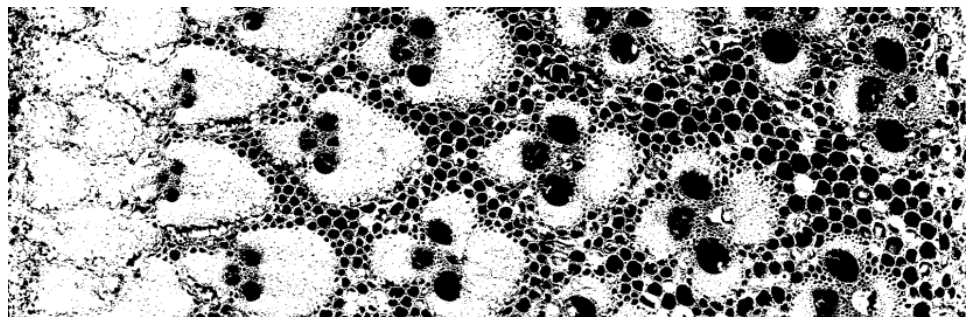
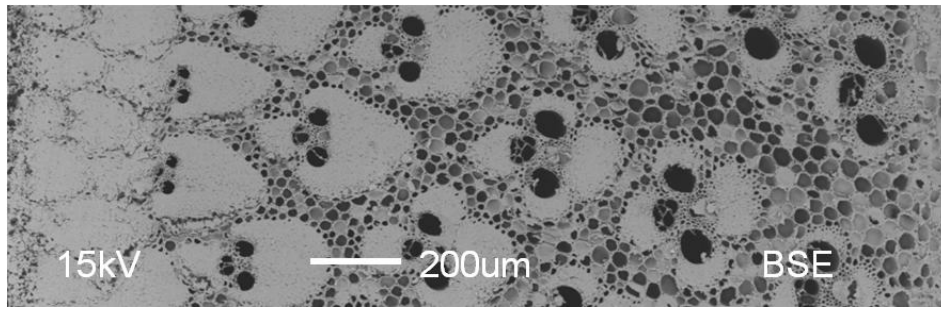


Figure 3.3.3 Comparison between the BSE image and secondary electron (SEM) image

The area of each pixel is $1\mu\text{m}^2$. The captured BSE images were merged by Adobe Photoshop software. Then merged images were processed by image J software (National Institutes of Health). By adjusting the threshold, the BSE images were transferred into binary images. Binary image can be saved as a result file in matrix form. The greyscale value of white pixels is 0 which represented the bamboo cell wall phase while the greyscale value of black pixels is 255 which represented the pore (air) phase. By calculating the average fraction between the 0 and 255 of every column of the matrix, the average porosity of bamboo specimens could be acquired. Figure 3.3.4 illustrated the procedure of BSE image processing.



...
...	255	255	255	255	255	...
...	255	0	255	255	255	...
...	0	0	0	255	255	...
...	255	255	255	255	255	...
...	255	255	255	255	255	...
...	255	0	0	0	0	...
...	255	0	0	0	255	...
...	255	255	255	255	255	...
...

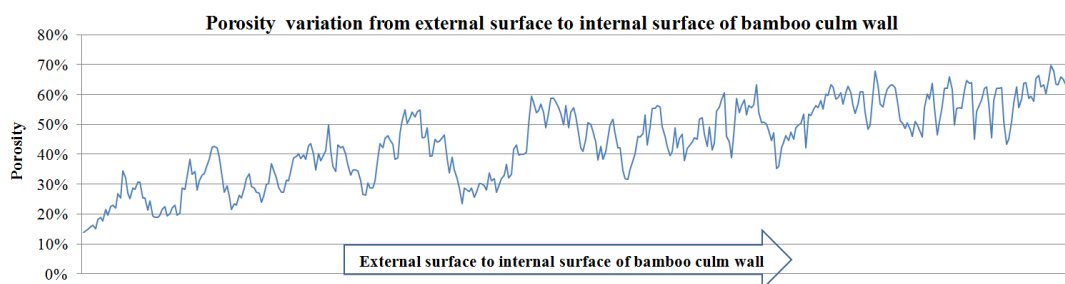


Figure 3.3.4 The transfer procedure from BSE image to porosity values

3.3.3 Results and discussions

Macro data statistics of BSE and CT scanning aims to provide the average porosity, standard deviation (SD) and coefficient of variation (COV) of each group. Pearson product-moment correlation coefficient (PPMCC) was calculated to measure the linear correlation between the BSE results and CT scanning results (See table 3). Both BSE and CT scanning methods could generate at least 400 sampling points. The number of sampling points depends on the thickness of the bamboo culm wall. The PPMCC values were calculated by the equation 3.3.3:

$$r_{xy} = \frac{n \sum xy - \sum x \sum y}{\sqrt{n \sum x^2 - (\sum x)^2} \sqrt{n \sum y^2 - (\sum y)^2}} \quad (3.3.3)$$

r_{xy} : Pearson product-moment correlation coefficient (PPMCC)

x,y: The two groups of data

The maximum and minimum CT scanning results are shown in table 3.3.3, their variation trend is exactly same. Therefore, the PPMCC values between BSE results and maximum CT scanning results are equal to the PPMCC values between BSE results and minimum CT scanning results.

Table 3.3.3 Macro data statistics of BSE and CT scanning

	No.	Average Porosity (%)			SD (%)			COV (%)			PPMCC ¹ (%)
		BSE	CT _{Min}	CT _{Max}	BSE	CT _{Min}	CT _{Max}	BSE	CT _{Min}	CT _{Max}	BSE/CT ²
I N T E R N O D E	I 1	43.9	44.9	48.5	13.1	15.3	14.4	29.8	34.2	29.6	78.8
	I 2	58.8	60.9	63.4	21.6	23.6	21.5	49.3	52.5	34.0	70.3
	I 3	52.4	54.4	57.4	18.2	18.6	17.0	41.5	41.5	29.7	80.8
	I 4	47.6	49.9	53.2	17.5	16.0	14.7	39.9	35.6	27.7	68.0
	I 5	51.9	53.6	56.6	18.5	19.7	18.1	42.3	43.8	31.9	71.1
	I 6	57.5	56.6	59.4	21.4	20.7	18.9	48.8	46.1	31.8	76.8
	I 7	53.6	53.0	56.1	16.5	15.7	14.3	37.7	35.0	25.5	72.2
	I 8	49.8	50.9	54.1	14.7	16.1	14.9	33.4	35.9	27.5	75.9
N O D E	N 1	37.4	32.1	36.5	13.8	18.4	17.7	31.5	40.9	48.5	57.7
	N 2	41.0	42.8	46.5	14.2	19.5	18.4	32.3	43.5	39.5	65.5
	N 3	56.6	59.6	62.2	23.3	23.7	21.7	53.1	52.8	34.8	70.7
	N 4	46.7	51.9	55.1	20.0	20.0	18.4	45.6	44.5	33.5	75.1
	N 5	43.0	46.4	49.9	21.5	18.1	16.9	48.9	40.3	33.8	68.1
	N 6	45.5	47.5	50.9	16.2	17.2	15.9	37.0	38.2	31.3	54.3
	N 7	48.0	49.1	52.4	8.6	14.1	12.9	19.5	31.3	24.6	47.2
	N 8	47.1	49.7	53.0	16.3	15.8	14.5	37.3	35.1	27.4	67.3

1. The PPMCC values were calculated to measure the linear correlation between BSE results and CT scanning results.

2. PPMCC value between BSE/CTmin and BSE/CTmax is the same because they use the same bulk density value in equation 3.3.2.

In internode specimens, the average porosity is from 43.9% to 58.8% by BSE measurement. The average porosity from CT scanning measurement is 44.9% to 60.9% and 48.5% to 63.4% by minimum skeletal density calculation and maximum skeletal density calculation respectively. The SD value is from 13.1% to 21.6% by using BSE measurement. The SD from CT scanning measurement is 15.3% to 23.6% and 14.3% to 21.5% by minimum skeletal density calculation and maximum skeletal density calculation respectively. The COV value is from 29.8% to 49.3% by using the BSE measurement. The COV from the CT scanning measurement is 34.2% to 52.5% and 25.5% to 34.0% by minimum skeletal density calculation and maximum skeletal density calculation respectively. The PPMCC between the BSE results and CT scanning results ranges from 68.0% to 80.8%.

In node specimens, the average porosity is from 37.4% to 56.6% by BSE measurement. The average porosity from CT scanning measurement is 32.1% to 59.6% and 36.5% to 62.2% by minimum skeletal density calculation and maximum skeletal density calculation respectively. The SD value is from 8.6% to 23.3% by BSE measurement. The SD from CT scanning measurement is 14.1% to 23.7% and 12.9% to 21.7% by minimum skeletal density calculation and maximum skeletal density calculation respectively. The COV value is from 19.5% to 53.1% by BSE measurement. The COV from CT scanning measurement is 31.3% to 52.8% and 24.6% to 48.5% by minimum skeletal density calculation and maximum skeletal density calculation respectively. The PPMCC between the BSE results and CT scanning results ranges from 47.2% to 75.1%.

The PPMCC results indicated that the correlation coefficient is at the moderate correlation level to the strong correlation level (Dancey and Reidy 2004). The PPMCC of internode specimens is higher than the node specimens. The strength of the CT scanning is that porosity in the cell wall phase of the bamboo specimens can be obtained in three dimensions while BSE results are two dimensional.

The typical porosity results aims to present the non-homogeneity on the pore distribution of the Moso bamboo. Both BSE and CT scanning methods could generate at least 400 sample points. Figure 3.3.5 illustrates a typical porosity result of the Moso bamboo specimens. Results of I1 are from both CT scanning method and BSE image processing method.

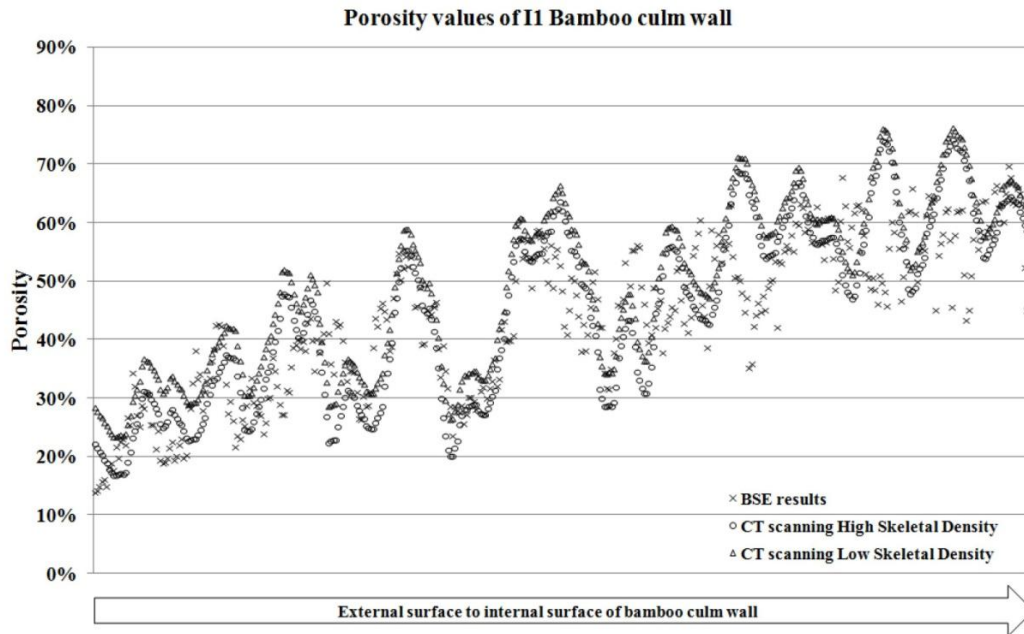


Figure 3.3.5 Typical porosity results of a specimen from CT scanning and BSE

The porosity was measured from the external surface to the internal surface of the cross section of the bamboo culm wall. Figure 3.3.5 indicates the porosity values increased with remarkable fluctuations in this direction. The result indicated that the results from the BSE image demonstrated similar trend with the results from CT scanning images. However, a number of different values appeared between the two methods. The reason may include two aspects. One is that BSE method cannot detect the porosity of the cell wall phase but CT scanning measurement can be conducted in the three dimensional space. The other is that threshold image processing may cause some errors from the light and dark points of the BSE images.

Both macro data statistics and the typical results in Figure 3.3.4 indicated that the porosity data showed remarkable fluctuation and high variation from the external side to the internal side of bamboo culm wall. If all 400 data points and all groups were included in one diagram, the trend would be relatively difficult to describe. Furthermore, the huge data in the numerical simulation of the heat and moisture transfer will lead to longer computing time. In addition, the length of several small specimens is less than 4mm. It is not worth to divide 4mm into 400 times by the manufacturing machines in the wood industry.

Therefore, a further statistics were made with the consideration of the ease of data comparison, the efficiency of numerical simulation and the manufacturing cost efficiency of the wood work machines. In detail, 400 data points of each specimen were divided into 10 equal portions from the external side to the internal side of the bamboo culm wall. For every

portion, namely 40 data points, an average value was generated. For example, the first value is the average of the first 40 samples points from external side of the bamboo culm. The number 10 is the average of the last 40 sample points from external side of the bamboo culm.

Figure 3.3.6 and Figure 3.3.7 illustrate the porosity results of internode and node specimens respectively from the BSE and CT results. BSE results are displayed in the left side of the figure. The CT results are displayed in the right side of the figure. The horizontal axis represents the sequence number of the average values. The vertical axis represents the porosity values. Every figure has 8 data series. In BSE side, each series includes a single data line. In CT side, each series includes a maximum porosity line and a minimum porosity line.

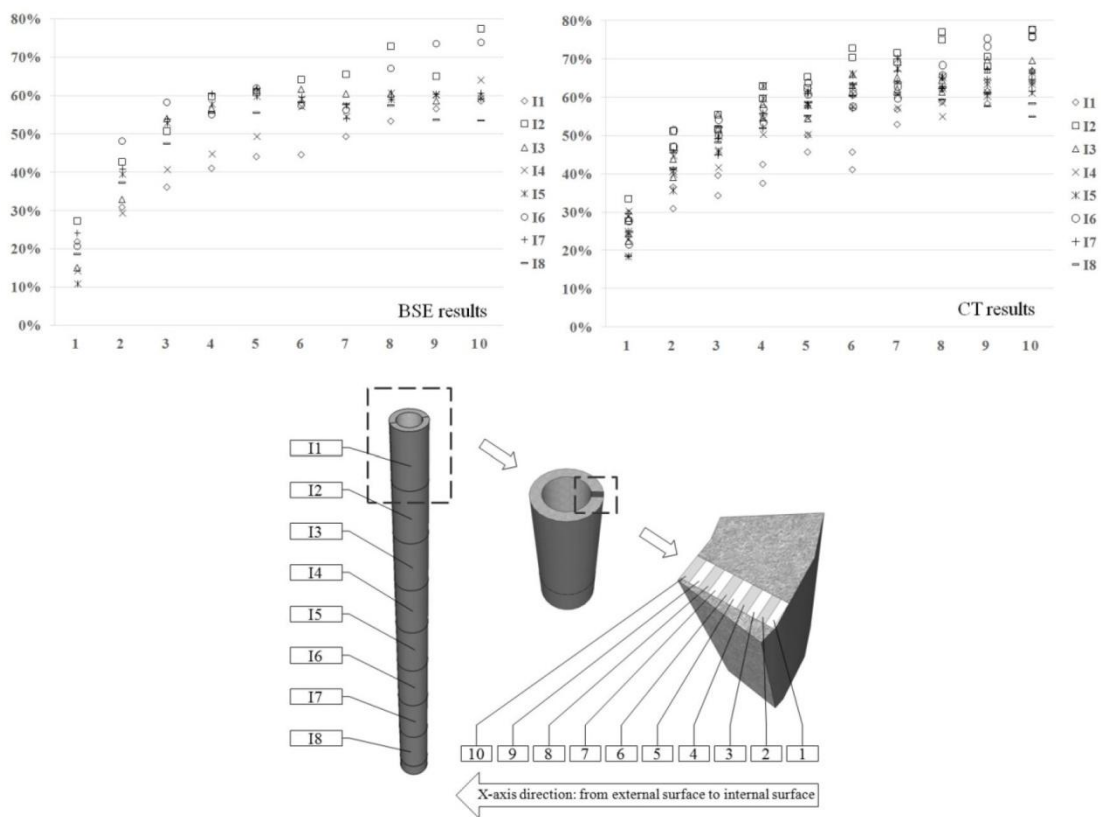


Figure 3.3.6 Porosity results of internode specimens from BSE and CT results by group comparison

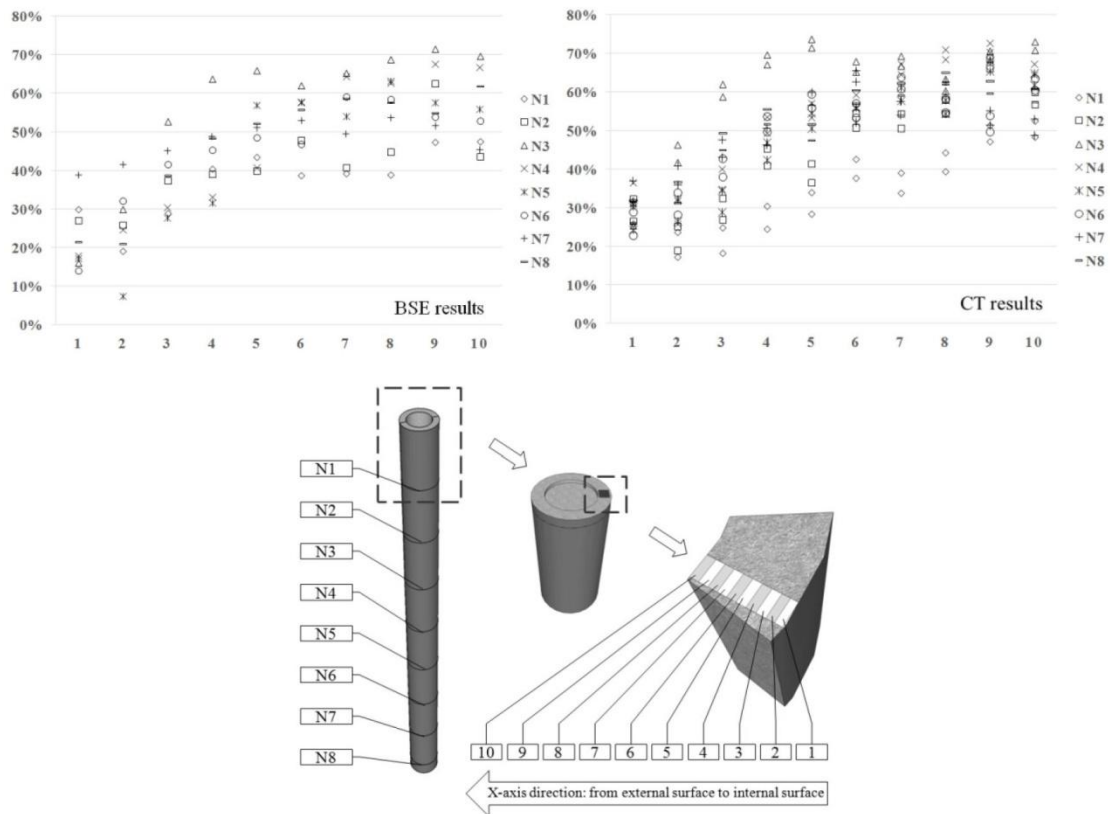


Figure 3.3.7 Porosity results of node specimens from BSE and CT results by group comparison

The porosity of both internode and node specimens increases from the external side to the internal side of bamboo culm. The CT scanning results showed similar trend with the BSE results. The lowest porosity values of both internode and node specimens are mainly from the smallest external diameter of the bamboo culms. The N5 specimen needs to be noticed. In the BSE result, the N5 specimen shows the lowest porosity at portion 2 but it did not show similar trend in CT results. The reason is that the growing direction of vascular bundle tissue became irregular in the node specimen. The BSE results are based on the cross section image. If porous vascular bundle tissue grows in the cross section, the pore will not be included in the cross section image. But this tissue could be detected in the three dimension CT measurement line. For internode specimens, the difference among I4, I5, I7 and I8 is not considerable. Both I2 and I6 showed high porosity. For node parts, N3 had the highest porosity. The fluctuation of nodes specimens was stronger than the internodes specimens.

As shown in table 3.3.2, the external diameter of the bamboo culm decreases with the height in the stem. From I1 or N1 to I8 or N8, the height of cutting position is decreasing. Figure 3.3.6 and Figure 3.3.7 present the relationship between the porosity and the height of cutting position. The porosity of the specimen from the highest cutting position is lowest for both

internode and node samples. The highest porosity is not found at the lowest cutting position. The porosity from I2 and N3 showed the highest porosity at internode part and node part respectively.

Figure 3.3.6 and Figure 3.3.7 compared the difference among the specimens with different external diameter of bamboo culms. Each series represents a specimen. Figure 3.3.8 and Figure 3.3.9 are utilised to compare the difference among ten portions. Each series represents a portion number. The porosity is increasing from portion 1 to portion 10.

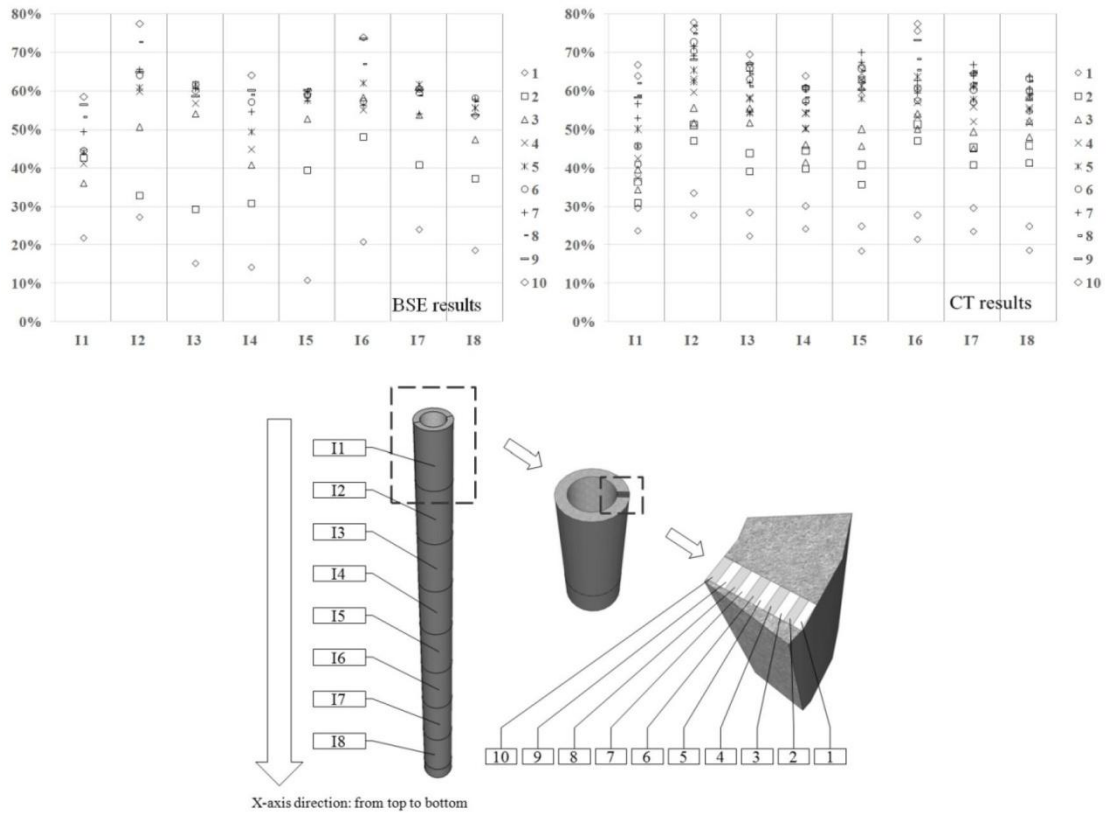


Figure 3.3.8 Porosity results of internode portions from BSE and CT results by portion comparison

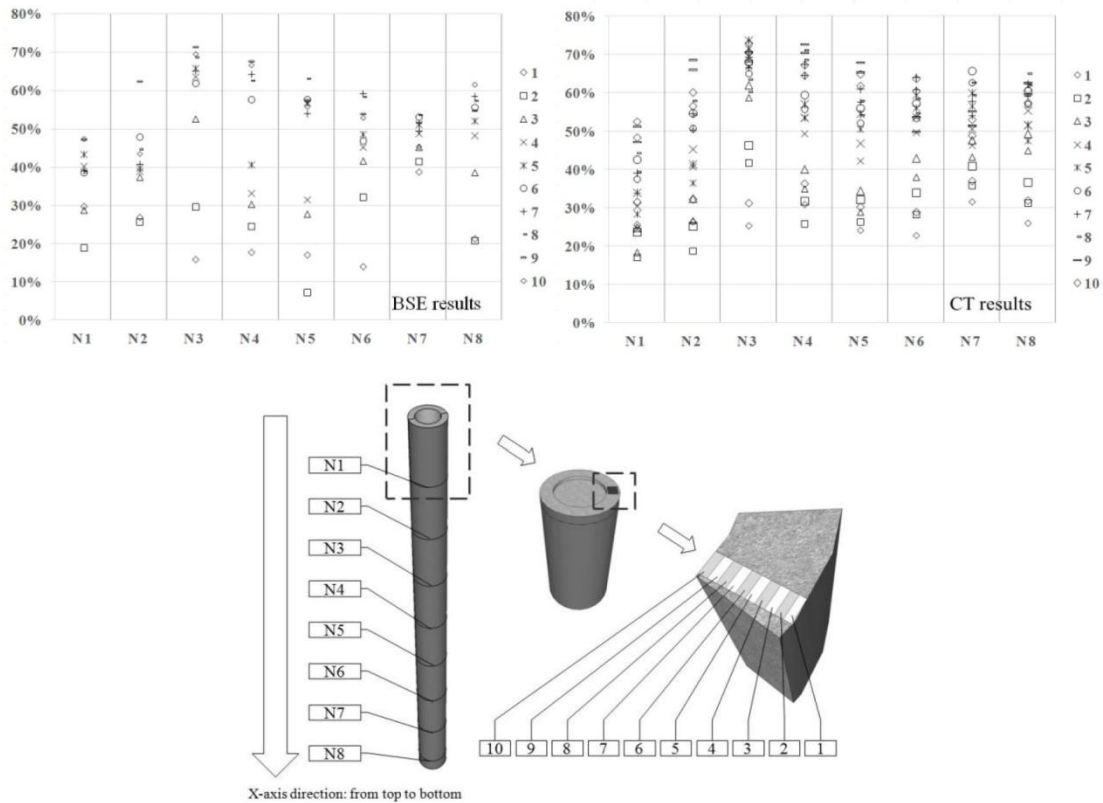


Figure 3.3.9 Porosity results of nodes portions from BSE and CT results comparison by portions

In portions comparison, the porosity fluctuation of internode specimens is similar to the Sine or Cosine curve. The porosity fluctuation of node specimens demonstrated larger fluctuation in each single line than the internode specimens. The similarity between the BSE and CT results is lower in the nodes specimens than the internode specimens. The aforementioned PPMCC comparison has already shown this fact.

The porosity increases with the portion number, namely the distance to the external side of the bamboo culm wall. This trend is more significant than trend of the height and the porosity. The porosity of BSE results is lower than the CT results at portion 1 and portion 2 from both internode and node specimens, especially for I3 and I5 specimens.

3.3.4 Summary

Computed Tomography (CT) and Back-Scattered Electron (BSE) imaging are the two effective technologies to measure the actual morphological porosity distribution from the external side to the internal side of the bamboo culm wall. The CT scanning results showed similar trends with BSE results. The correlation relationship between BSE and CT results approached moderate correlation to strong correlation level. The average porosity of internode specimens was from 43.9% to 58.8% by BSE measurement and from 44.9% to 63.4% by CT measurement. The average porosity of node specimens was from 37.4% to 56.6% by using BSE measurement and from 32.1% to 62.2% by CT measurement. Macro statistics, typical porosity results from 400 sampling points and 10 portions average porosity results indicated that the BSE porosity results were lower than the CT results. The reason is that the BSE results are based only on the cross section image. If the pores are in the cross section, it will not be included in the cross section image but these pores can be calculated in the three dimensional CT measurement line. The porosity fluctuation of node specimens demonstrated larger fluctuations in each single line than internode specimens. The PPMCC determined that the similarity between the BSE and CT results is lower in the nodes specimens than the internode specimens. The porosity increases with the portion number, namely the distance from the external side of the bamboo culm wall.

The limitation of this section includes four aspects. First, the BSE porosity measurement based on the image processing method, the accuracy is influenced by the image quality. Second, the BSE porosity measurement is two dimensional. Third, the CT measurement depends on the accuracy of the skeletal cell wall density. This density has relatively wide range which leads to relatively wide porosity ranges. Finally, compromises need to be made between the time taken and the number of the measurement specimens, as well as the area of the measurement.

Nevertheless, this section has provided a large number of porosity data from 8 bamboo culms with different external diameters and culm wall thickness. Both internodes and node position were included in this study. The porosity variation in the radial direction of Moso bamboo culm wall has been illustrated. The porosity results are expected to be utilised in the heat and moisture transfer simulation studies in the future*.

(*The content of this section is from the accepted manuscript of author. See self bibliography (Huang *et al.* 2017a))

Chapter 4 Specific heat capacity of Moso bamboo

The content of this chapter was published in a peer reviewed journal: *Construction and building materials*. (In self bibliography and published work: Huang *et al.* 2016a).

4.1 Research objectives

This study measured the specific heat capacity of the Moso Bamboo in three directions of the cylindrical coordinate system. Due to the lack of knowledge on the specific heat capacity, the strengths of the differential scanning calorimetry (DSC), and requirements of the heat and moisture simulation on Moso bamboo, this study measured the specific heat capacity of Moso bamboo by DSC. To investigate the variation of the specific heat capacity in different directions of bamboo culms, the measurements were conducted in the radial, longitudinal and tangential directions. The results of this study will be utilised as a physical property database for the future work on the heat and moisture transfer simulation of Moso bamboo.

4.2. Methodology

4.2.1 Specimen preparation

The Moso bamboo culms were ordered from the UK Bamboo Supplies Limited. The external diameters of the bamboo culms ranged from 70 mm to 100 mm. The specimens were cut from these culms. The specimens were cut into thin discs to fit the sample chamber of the DSC. The diameter of the discs was 6 ± 0.2 mm. The thickness of the discs was 1 ± 0.2 mm (Figure. 4.2.1).

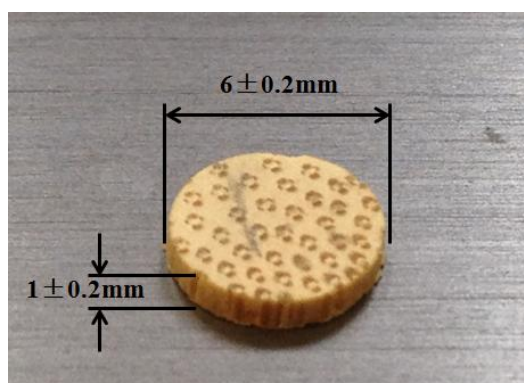


Figure 4.2.1 The dimension of the bamboo specimen

The specimens were cut from radial, tangential and longitudinal directions within both the internode part and the node part of Moso bamboo culms. A bamboo culm can be regarded as a hollow cylinder. So a coordinate system is utilised to illustrate three sampling directions. In this study, three directions of the specific heat capacity, namely radial, tangential, and longitudinal directions, refer to the heat flow directions which are perpendicular to the circular flat surface of the bamboo specimens (Figure. 4.2.2).

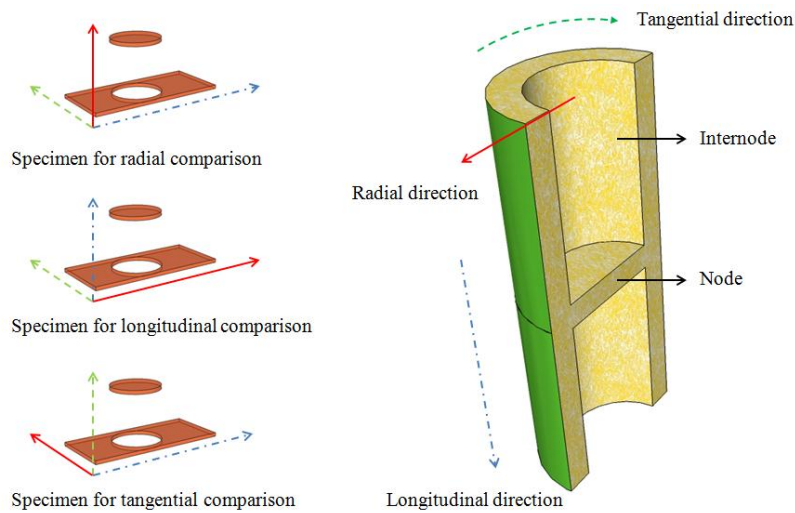


Figure 4.2.2 Nomenclature of the directions of specific heat capacity measurements

In the radial direction, specimens were cut from three positions which refer to the external surface, the middle position and the internal surface of the culm wall. In the tangential direction, specimens were cut from four positions. An interval of 90° was set between adjacent positions. In the longitudinal direction, specimens were cut from three positions. The distance between two adjacent positions is 10 ± 1 mm in the internode part and 3 ± 1 mm in the node part respectively. This distance is determined by the length of the internode and node parts of bamboo culms. Three specimens were prepared at each position for specific heat capacity measurement (Figure. 4.2.3).

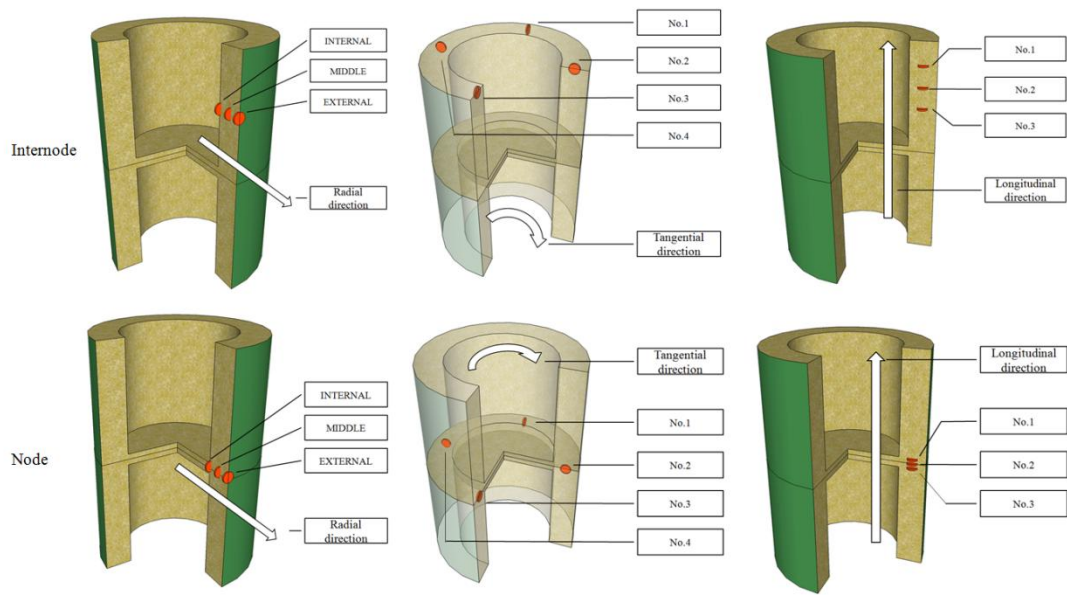


Figure 4.2.3 The cutting positions and numbers of bamboo specimens.

4.2.2 Specific heat capacity measurement by DSC

The specimens were oven dried to eliminate water at 103 °C. Calcium Chloride (CaCl₂) was used as desiccant to store the specimens to avoid moisture absorption. The specific heat capacity was measured using a TA instruments Q200 modulated differential scanning calorimeter with a scan rate of 3 °C/min, a modulation of ± 1 °C per 100 s, and an oxygen-free nitrogen gas flow rate of 25 ml/min. Scans were made with the temperature increasing from 5 °C to 40 °C. Specific heat capacity values were extracted from the total heat flow signal.

4.3 Results and discussions

4.3.1 Results from three directions

The results are illustrated by bar charts with standard deviations in Figure 4.3.1 to 4.3.7. Both internode and node parts of Moso bamboo specimens are reported. The vertical axis represents the specific heat capacity. The unit of the specific heat capacity is kJ/kg·K. The horizontal axis represents the temperature. The temperature ranges from 5 °C to 40 °C. This temperature range covers the majority of the service range of building materials. The temperature range from 5 °C to below 0 °C is not discussed in this study.

In the radial direction, Moso bamboo specimens were cut from three positions. Three positions refer to the external surface, the midpoint and the internal surface of a bamboo culm wall. Three specimens were measured at each position. The results of both internode and node parts indicate that the specific heat capacity decreases from the external surface to the internal surface. Specific heat capacity values increase with temperature. The difference among three positions is higher at node parts. See Figure. 4.3.1 and Figure. 4.3.2.

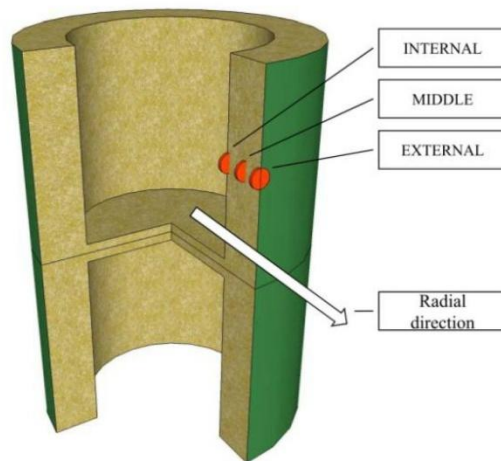
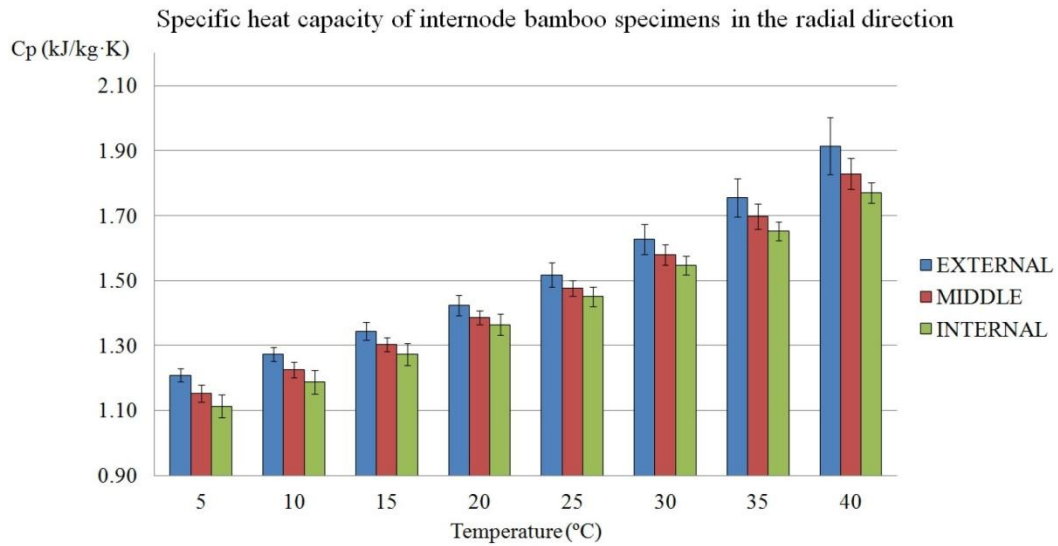


Figure 4.3.1 Specific heat capacity of internode bamboo specimens in the radial direction.

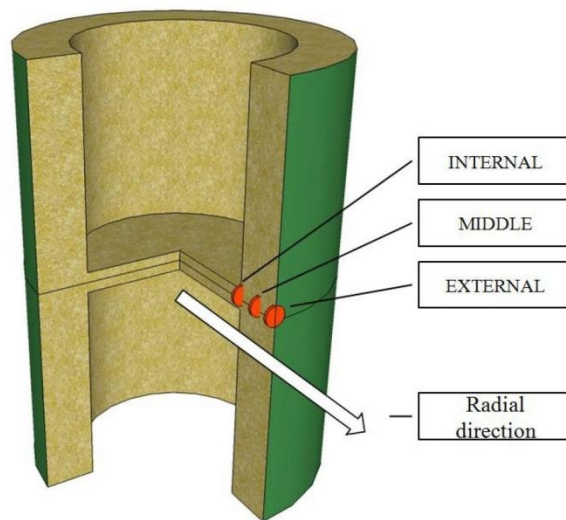
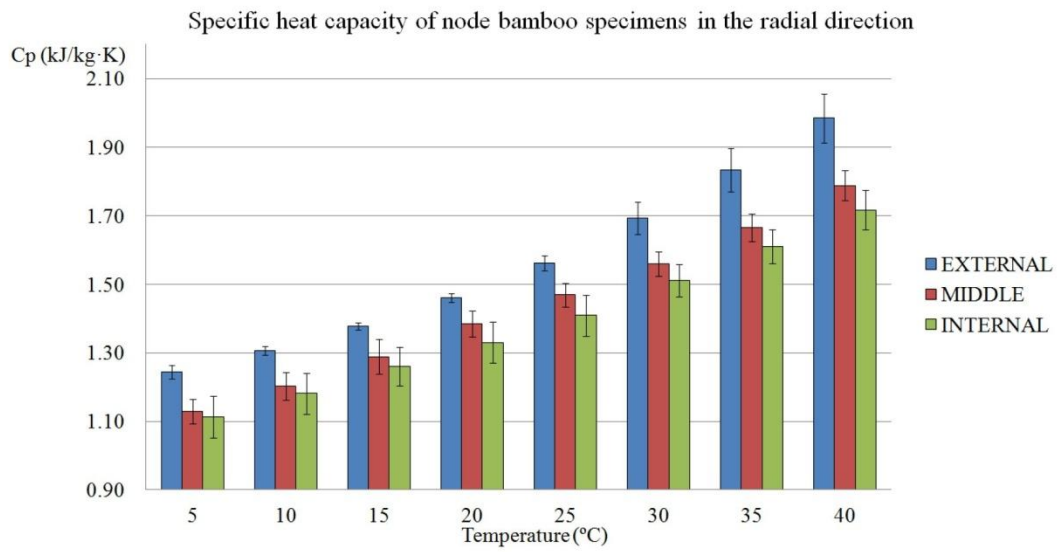


Figure 4.3.2 Specific heat capacity of node bamboo specimens in the radial direction.

In the tangential direction, Moso bamboo specimens were cut from four representative positions. The azimuth between two adjacent positions is 90°. Three specimens were measured at each position. The average specific heat capacity values of four positions present an irregular trend. No specific gradient is found in tangential direction. See Figure 4.3.3 and Figure 4.3.4.

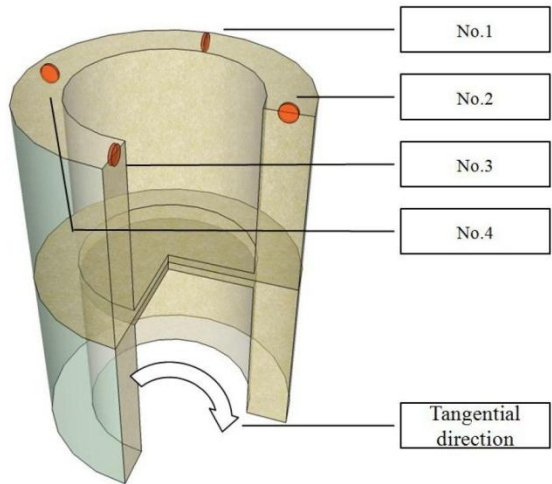
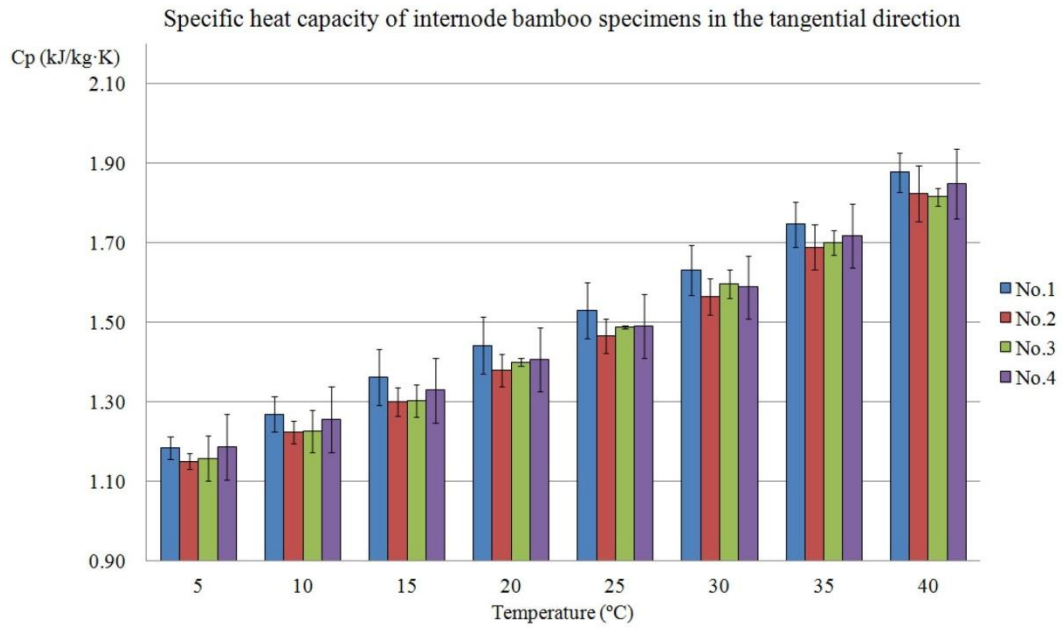


Figure 4.3.3 Specific heat capacity of internode bamboo specimens in the tangential direction.

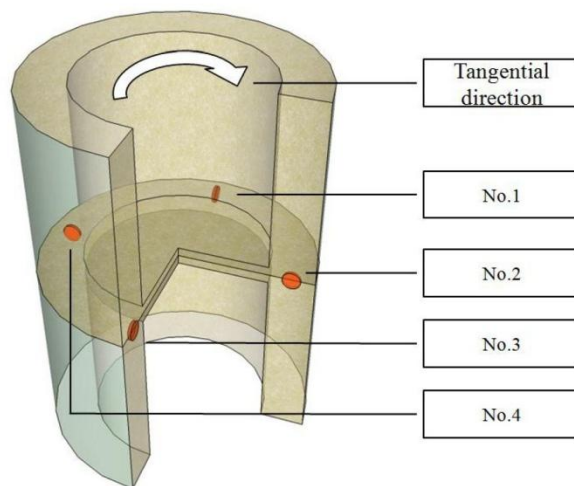
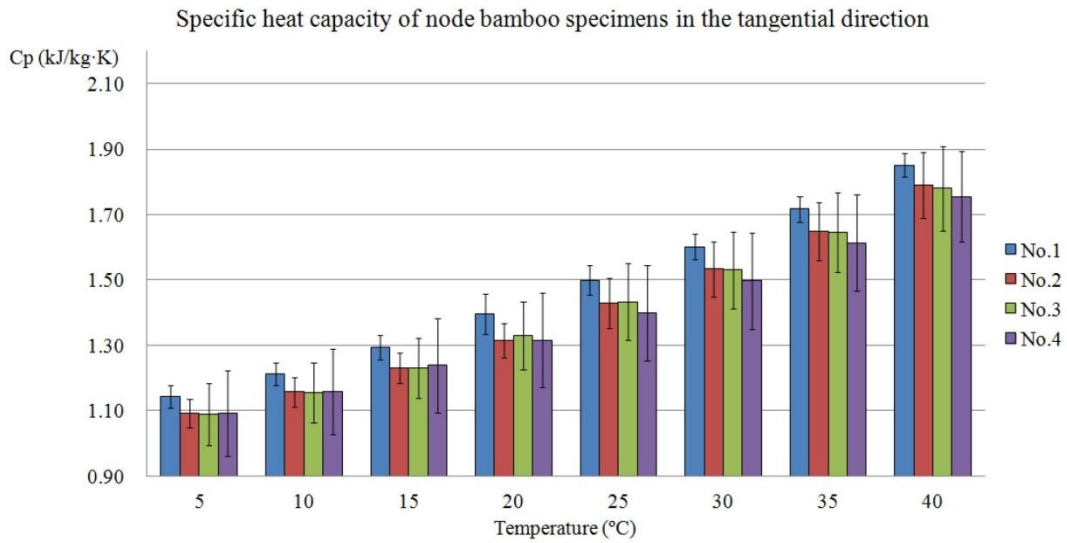


Figure 4.3.4 Specific heat capacity of node bamboo specimens in the tangential direction.

In the longitudinal direction, specimens were cut from three positions. The distance between two adjacent positions is 3 ± 1 mm at node part and 10 ± 1 mm at internode part respectively. This distance is determined by the length of node part and internode part of bamboo culms. Three specimens were prepared at each position for specific heat capacity measurement. See Figure 4.3.5 and Figure 4.3.6.

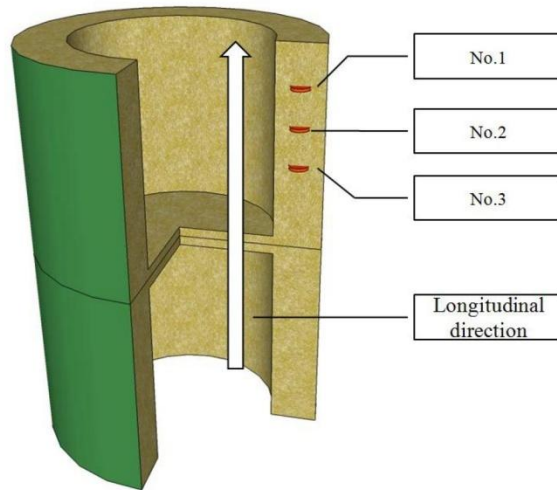
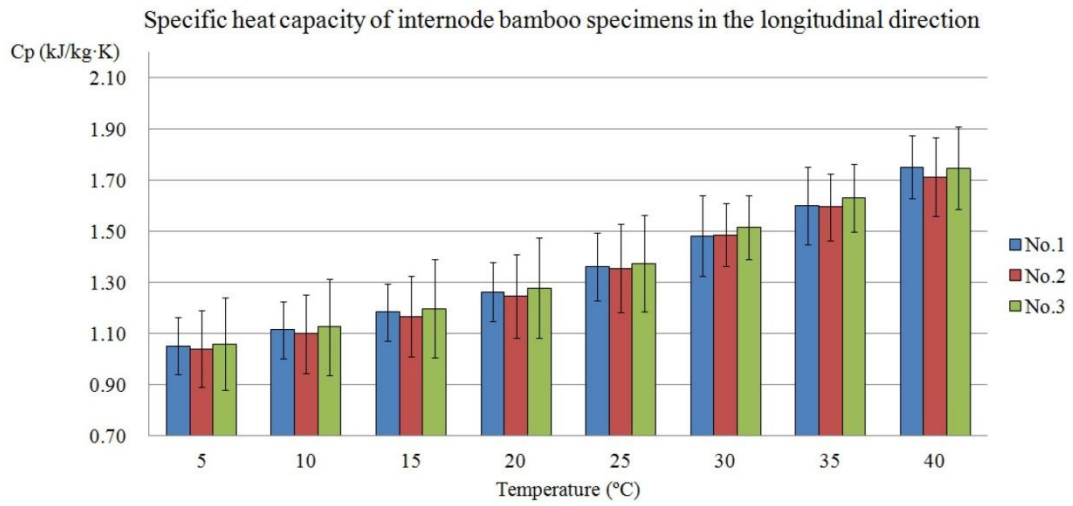


Figure 4.3.5 Specific heat capacity of internode bamboo specimens in the longitudinal direction

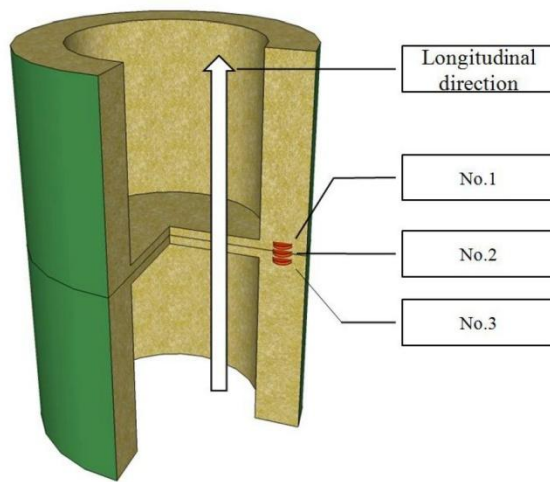
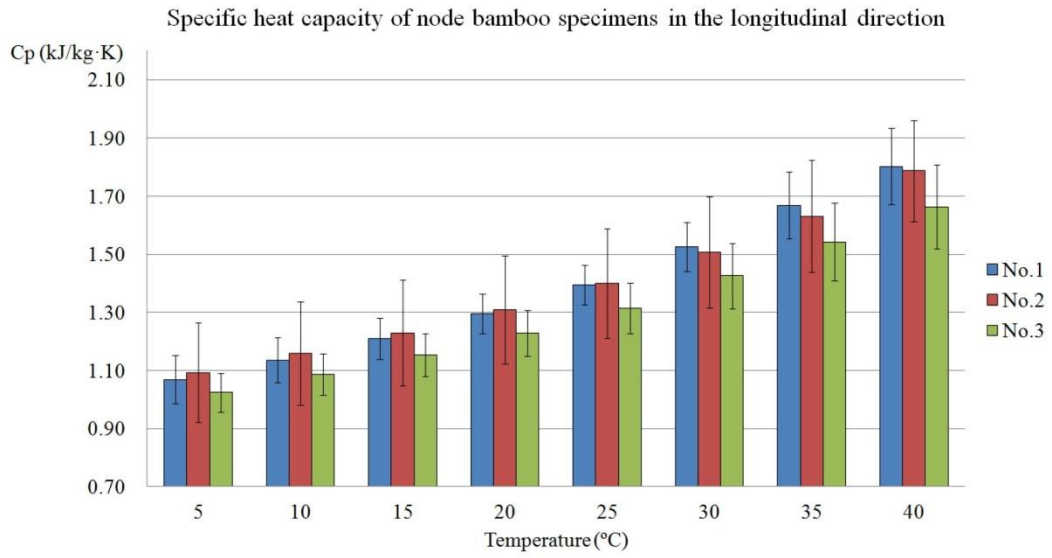


Figure 4.3.6 Specific heat capacity of node bamboo specimens in the longitudinal direction

4.3.2 Typical results summery

The average specific heat capacity results at 25 °C are compared in Figure 4.3.7.

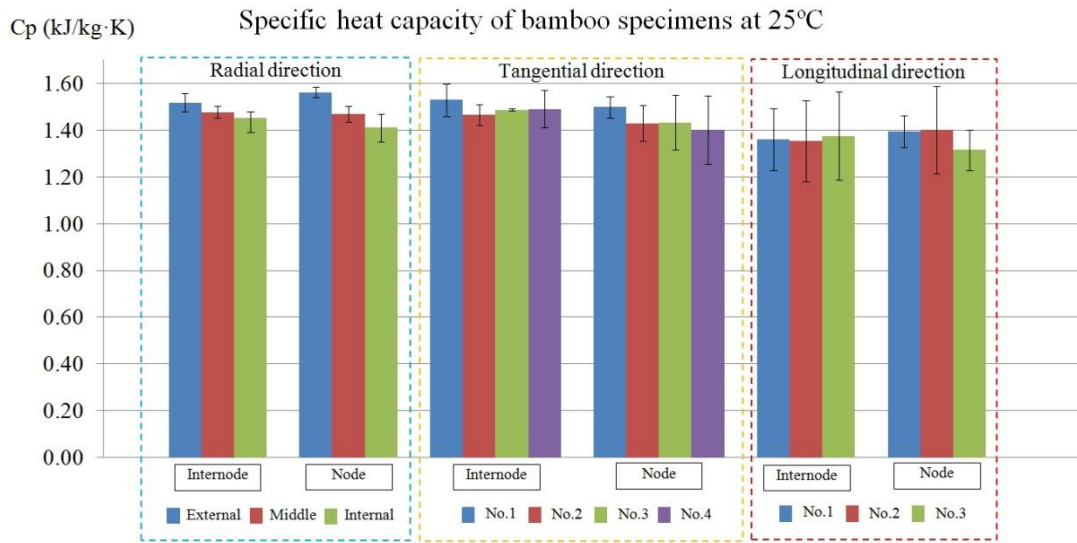


Figure 4.3.7 Average specific heat capacity comparison at 25 °C.

In the radial direction, the average specific heat capacity values of both internode and node parts feature a gradient decreasing trend from the external surface to the internal surface of the bamboo culm wall. This trend is not discovered in the tangential and longitudinal direction. In the radial and tangential direction, the majority of specimens from node parts show higher standard deviations than the internode parts. In the longitudinal direction, only the No.2 specimen from the node part presents a higher standard deviation range than the internode part of bamboo specimens. The average specific heat capacity values in the longitudinal direction are lower than the values in the radial direction and tangential direction. The results in table 4.3.1 indicate that the average specific heat capacity values are lower than 1.40 kJ/kg·K in the longitudinal direction. The values in the radial direction and tangential direction are higher than 1.40 kJ/kg·K.

Table 4.3.1 Specific heat capacity results at 25 °C.

Specific heat capacity at 25 °C (kJ/kg K)		Radial direction			Tangential direction				Longitudinal direction		
		External	Middle	Internal	No.1	No.2	No.3	No.4	No.1	No.2	No.3
Internode	Average	1.52	1.48	1.45	1.53	1.47	1.49	1.49	1.36	1.35	1.37
	Maximum	1.55	1.50	1.48	1.61	1.51	1.49	1.58	1.48	1.47	1.51
	Minimum	1.48	1.45	1.42	1.48	1.42	1.48	1.44	1.22	1.16	1.16
	SD	0.04	0.02	0.03	0.07	0.04	0.004	0.08	0.13	0.17	0.19
Node	Average	1.56	1.47	1.41	1.50	1.43	1.43	1.40	1.40	1.40	1.32
	Maximum	1.58	1.51	1.48	1.55	1.49	1.56	1.53	1.46	1.56	1.38
	Minimum	1.54	1.44	1.36	1.47	1.34	1.33	1.24	1.32	1.20	1.22
	SD	0.02	0.03	0.06	0.05	0.08	0.12	0.15	0.07	0.19	0.09

4.3.3 Discussion

All results demonstrate that the specific heat capacity of the bamboo specimens increases with temperature. This phenomenon has been mentioned in many papers on wood (Volbehr 1896, Beall 1968, Koch 1968, and Simpson and Tenwolde 1999). As aforementioned, the measured specific heat capacity is an equivalent value of many different phases due to the morphological complexity of biological materials. For example, the equivalent specific heat capacity of the bamboo can be described by Equation 4.3.1.

$$C_p = C_{pB} + C_{pL} + C_{pG} \quad (4.3.1)$$

C_p : Total specific heat capacity (kJ/kg·K)

C_{pB} : Specific heat capacity of the bamboo solid phase (kJ/kg·K)

C_{pL} : Specific heat capacity of the liquid phase, e.g. water. (kJ/kg·K)

C_{pG} : Specific heat capacity of the gas phase, e.g. water vapour and air. (kJ/kg·K)

In this study, the specimens were treated to eliminate the water. The absorbed water during the loading process of specimens was assumed to be negligible. The total specific heat capacity mainly includes two phases, one is the bamboo solid phase, and the other is the dry air phase. Although the specific heat capacity of the air increases with the temperature, from 5 °C to 40 °C the values are confined to the narrow range of 1.007 to 1.008 kJ/kg·K. Therefore, the air phase can be regarded as a constant component of the total specific heat capacity value. The bamboo solid phase can be regarded as the component in which the specific heat capacity increases with temperature.

Table 4.3.2 T-test of the specific heat capacity of bamboo specimens

Independent Samples Test										
		Levene's Test for Equality of Variances		T-test for Equality of Means						
		F	Sig.	t	df	Sig. 2-tailed	Mean Difference	Std. Error Difference	95% Confidence Interval of the Difference	
									Lower	Upper
External Radial	Equal variances assumed	0.953	0.384	-1.724	4	0.160	-0.04400	0.02553	-0.11487	0.02687
	Equal variances not assumed			-1.724	3.220	0.177	-0.04400	0.02553	-0.12218	0.03418
Middle Radial	Equal variances assumed	0.681	0.456	0.302	4	0.778	0.00733	0.02431	-0.06016	0.07482
	Equal variances not assumed			0.302	3.628	0.779	0.00733	0.02431	-0.06298	0.07765
Internal Radial	Equal variances assumed	2.057	0.225	1.053	4	0.352	0.04067	0.03863	-0.06659	0.14793
	Equal variances not assumed			1.053	2.947	0.371	0.04067	0.03863	-0.08354	0.16488
No.1 Tangential	Equal variances assumed	1.125	0.349	0.647	4	0.553	0.03100	0.04789	-0.10198	0.16398
	Equal variances not assumed			0.647	3.432	0.558	0.03100	0.04789	-0.11113	0.17313
No.2 Tangential	Equal variances assumed	1.783	0.253	0.716	4	0.513	0.03633	0.05072	-0.10448	0.17714
	Equal variances not assumed			0.716	3.152	0.523	0.03633	0.05072	-0.12075	0.19341
No.3 Tangential	Equal variances assumed	6.074	0.069	0.806	4	0.465	0.05433	0.06739	-0.13278	0.24145
	Equal variances not assumed			0.806	2.004	0.505	0.05433	0.06739	-0.23505	0.34372
No.4 Tangential	Equal variances assumed	0.937	0.388	0.945	4	0.398	0.09067	0.09589	-0.17558	0.35691
	Equal variances not assumed			0.945	3.095	0.412	0.09067	0.09589	-0.20930	0.39063
No.1 Longitudinal	Equal variances assumed	1.497	0.288	-0.401	4	0.709	-0.03433	0.08560	-0.27200	0.20333
	Equal variances not assumed			-0.401	2.998	0.715	-0.03433	0.08560	-0.30687	0.23820
No.2 Longitudinal	Equal variances assumed	0.007	0.939	-0.314	4	0.769	-0.04633	0.14768	-0.45636	0.36369
	Equal variances not assumed			-0.314	3.973	0.770	-0.04633	0.14768	-0.45747	0.36481
No.3 Longitudinal	Equal variances assumed	3.199	0.148	0.492	4	0.648	0.05900	0.11981	-0.27365	0.39165
	Equal variances not assumed			0.492	2.815	0.658	0.05900	0.11981	-0.33690	0.45490

T-tests were conducted to evaluate the significance of the specific heat capacity difference between the internode specimens and node specimens. The significance probability (Sig.) results indicated that the specific heat capacity difference between the internode specimens and node specimens is not significant (See Table 4.3.2). Analysis of variance (ANOVA) was made to identify the significance of the specific heat capacity among the cutting positions. The results indicated that significant differences only exist in the radial direction. It is apparent that the specific heat capacity difference between the external position and internal position is significant. For internode specimens, the specific heat capacity in the middle position showed no significant difference when they compared with specimens in the external position and internal position respectively. For node specimens, the specific heat capacity in the middle position shows no significant difference when they compare with specimens in the internal position. This fact implies that non-linear specific heat capacity values distribute from the external side to the internal side of the bamboo culm wall at both internode and node parts (See Table 4.3.3).

Table 4.3.3 ANOVA of the specific heat capacity of bamboo specimens

	Compare groups		Mean Difference (I-J)	Std. Error	Sig.	95% Confidence Interval	
						Lower Bound	Upper Bound
Radial direction at internode part	external	middle	0.04100	0.02565	0.161	-0.0218	0.1038
		internal	0.06700	0.02565	<u>0.040</u>	0.0042	0.1298
	middle	external	-0.04100	0.02565	0.161	-0.1038	0.0218
		internal	0.02600	0.02565	0.350	-0.0368	0.0888
	internal	external	-0.06700	0.02565	<u>0.040</u>	-0.1298	-0.0042
		middle	-0.02600	0.02565	0.350	-0.0888	0.0368
Radial direction at node part	external	middle	0.09233	0.03414	<u>0.035</u>	0.0088	0.1759
		internal	0.15167	0.03414	<u>0.004</u>	0.0681	0.2352
	middle	external	-0.09233	0.03414	<u>0.035</u>	-0.1759	-0.0088
		internal	0.05933	0.03414	0.133	-0.0242	0.1429
	internal	external	-0.15167	0.03414	<u>0.004</u>	-0.2352	-0.0681
		middle	-0.05933	0.03414	0.133	-0.1429	0.0242
Tangential direction at internode part	No. 1	No. 2	0.06433	0.04663	0.205	-0.0432	0.1719
		No. 3	0.04233	0.04663	0.390	-0.0652	0.1499
		No. 4	0.03933	0.04663	0.423	-0.0682	0.1469
	No. 2	No. 1	-0.06433	0.04663	0.205	-0.1719	0.0432
		No. 3	-0.02200	0.04663	0.650	-0.1295	0.0855
		No. 4	-0.02500	0.04663	0.606	-0.1325	0.0825
	No. 3	No. 1	-0.04233	0.04663	0.390	-0.1499	0.0652
		No. 2	0.02200	0.04663	0.650	-0.0855	0.1295
		No. 4	-0.00300	0.04663	0.950	-0.1105	0.1045
	No. 4	No. 1	-0.03933	0.04663	0.423	-0.1469	0.0682
		No. 2	0.02500	0.04663	0.606	-0.0825	0.1325
		No. 3	0.00300	0.04663	0.950	-0.1045	0.1105
Tangential direction at node part	No. 1	No. 2	0.06967	0.08442	0.433	-0.1250	0.2643
		No. 3	0.06567	0.08442	0.459	-0.1290	0.2603
		No. 4	0.09900	0.08442	0.275	-0.0957	0.2937
	No. 2	No. 1	-0.06967	0.08442	0.433	-0.2643	0.1250
		No. 3	-0.00400	0.08442	0.963	-0.1987	0.1907
		No. 4	0.02933	0.08442	0.737	-0.1653	0.2240
	No. 3	No. 1	-0.06567	0.08442	0.459	-0.2603	0.1290
		No. 2	0.00400	0.08442	0.963	-0.1907	0.1987
		No. 4	0.03333	0.08442	0.703	-0.1613	0.2280
	No. 4	No. 1	-0.09900	0.08442	0.275	-0.2937	0.0957
		No. 2	-0.02933	0.08442	0.737	-0.2240	0.1653
		No. 3	-0.03333	0.08442	0.703	-0.2280	0.1613
Longitudinal direction at internode part	No. 1	No. 2	0.00667	0.13569	0.962	-0.3254	0.3387
		No. 3	-0.01300	0.13569	0.927	-0.3450	0.3190
	No. 2	No. 1	-0.00667	0.13569	0.962	-0.3387	0.3254
		No. 3	-0.01967	0.13569	0.890	-0.3517	0.3124
	No. 3	No. 1	0.01300	0.13569	0.927	-0.3190	0.3450
		No. 2	0.01967	0.13569	0.890	-0.3124	0.3517
Longitudinal direction at node part	No. 1	No. 2	-0.00533	0.10287	0.960	-0.2571	0.2464
		No. 3	0.08033	0.10287	0.465	-0.1714	0.3321
	No. 2	No. 1	0.00533	0.10287	0.960	-0.2464	0.2571
		No. 3	0.08567	0.10287	0.437	-0.1661	0.3374
	No. 3	No. 1	-0.08033	0.10287	0.465	-0.3321	0.1714
		No. 2	-0.08567	0.10287	0.437	-0.3374	0.1661

In addition, the specific heat capacity results in the longitudinal direction are lower than the other two directions. The morphological structure in backscattered electron (BSE) images of Moso bamboo may explain this variation (See Figure 4.3.8). Fig. 4.3.8a is the section view of the longitudinal specimens. Figure 4.3.8b is the section view of the radial specimens. Figure 4.3.8c is the section view of the tangential specimens. Figure 4.3.8d is a high magnification backscattered electron image of the ground tissue cell.

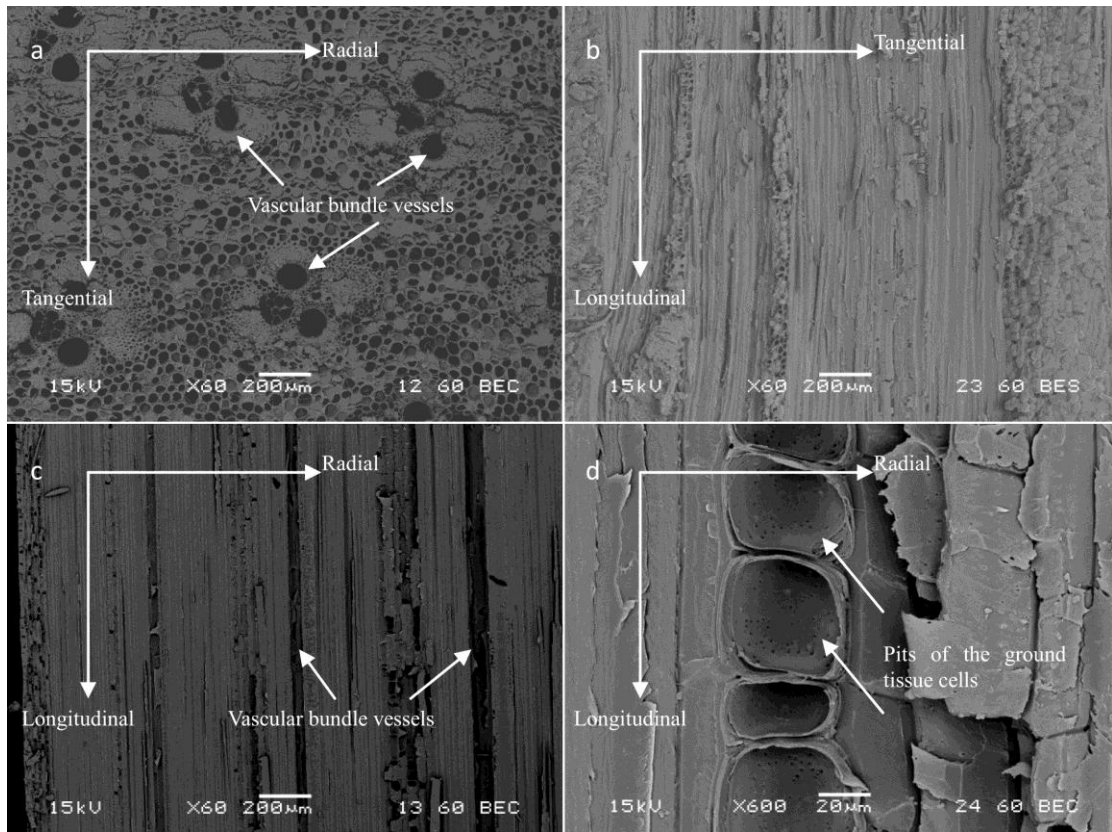


Figure 4.3.8 (a) The radial-tangential section view of the Moso bamboo BSE image. (b) The tangential-longitudinal section view of the Moso bamboo BSE image. (c) The radial - longitudinal section view of the Moso bamboo BSE image. (d) The radial -longitudinal section view of the Moso bamboo BSE image at a high magnification.

In the DSC measurement process, when the heat flow is along the longitudinal direction, the convective heat lost may be higher than the other two directions. The vascular bundles provide many straight tunnels for the air ventilation. The specific heat capacity can also be considered as the parameter to describe the heat sink ability when the energy is input. Relatively small pits, holes and tightly arranged cells could be assumed as the features of higher specific heat capacity because these features provide considerable barriers to convective heat loss. This assumption can explain why the results of the external specimens in

the radial direction possess the highest specific values while specimens in the longitudinal direction possess lower specific heat capacity.

4.4. Summary

The specific heat capacity of the Moso bamboo specimens were measured by DSC. The measurements were conducted in all directions of the cylindrical coordinates system at both internode parts and node parts. All results demonstrate that the specific heat capacity of the bamboo specimens increases with the temperature. Relatively small pits, holes and tightly arranged cells result in higher specific heat capacity. In the radial direction, the results for both internode and node parts indicate that the specific heat capacity decreases from the external surface to the internal surface. In tangential and longitudinal direction, average specific heat capacity values present an irregular trend. No specific gradient are found in these two directions*.

(*The content of this chapter is from a published work of author. See self bibliography (Huang *et al.* 2016a))

Chapter 5 Thermal diffusivity of Moso bamboo

The content of this chapter was published in a peer reviewed journal: *Holzforschung*. (See self bibliography Huang *et al.* 2017b)

5.1 Research objectives

Thermal diffusivity is a physical property that is defined as the ratio of the thermal conductivity to the heat capacity of a material. This property is an essential item in the transient heat conduction equation. Larger thermal diffusivity value means that a material will be quicker to reach a new equilibrium condition (Incropera 1981). See Equation 5.1.1 and Equation 5.1.2.

$$\alpha \nabla^2 T = \frac{\partial T}{\partial t} \quad (5.1.1)$$

$$\alpha = \frac{\lambda}{c_p \rho} \quad (5.1.2)$$

α : Thermal diffusivity (m²/s)

∇^2 : Laplace operator

T : Temperature (K)

t : Time (s)

λ : Thermal conductivity (W/m K)

ρ : Density (kg/m³)

C_p : Specific heat capacity (J/kg K)

This study measured the thermal diffusivity of Moso bamboo using the flash method. The measurement was conducted in the radial, longitudinal and tangential directions for the purpose of understanding the effect of anisotropy on thermal diffusivity.

5.2 Methodology

5.2.1 Specimen preparation

The Moso bamboo culms were purchased from UK Bamboo Supplies Limited. The external diameter of the bamboo culms ranged from 70mm to 100mm. The specimens were cut into thin square pieces from these culms. The side length of the square pieces was 10 ± 0.5 mm. The thickness of the specimen was 1 ± 0.2 mm. The specimens were oven dried to eliminate the water at $103 \text{ }^\circ\text{C}$. Then specimens were stored in a container with calcium chloride (CaCl_2) to prevent moisture absorption. Before measurement, all specimens were embedded into acrylic boards to fit the frame of the flash tube heat source (Figure 5.2.1).

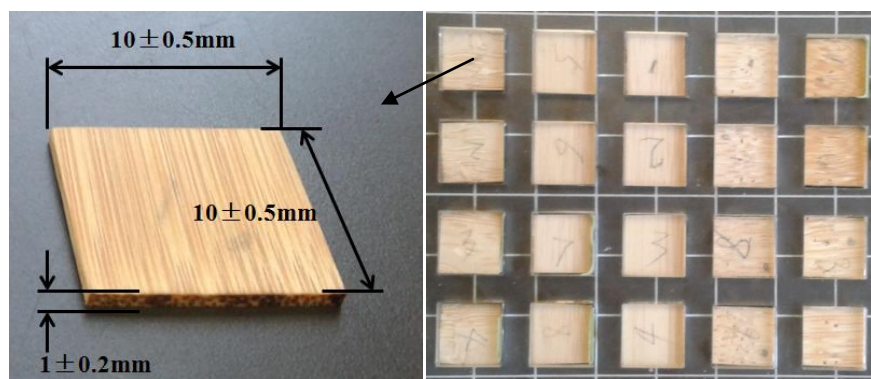


Figure 5.2.1 The dimension and fixation of Moso specimens

The specimens were cut in radial, tangential and longitudinal directions from both internode part and node part of Moso bamboo culms. In the radial direction, specimens were cut from three positions which are the external surface, middle position and internal surface of the bamboo culm wall. In the tangential direction, specimens were cut from four positions. An interval of 90° was set between adjacent positions. In the longitudinal direction, specimens were cut from three positions. The distance between two adjacent positions is $3\text{mm} \pm 1\text{mm}$ for the node parts and $10\text{mm} \pm 1\text{mm}$ for internode parts respectively. This distance was determined by the length of the node part and internode part of bamboo culms. Three specimens were prepared at each position for thermal diffusivity measurement (see Figure 5.2.2).

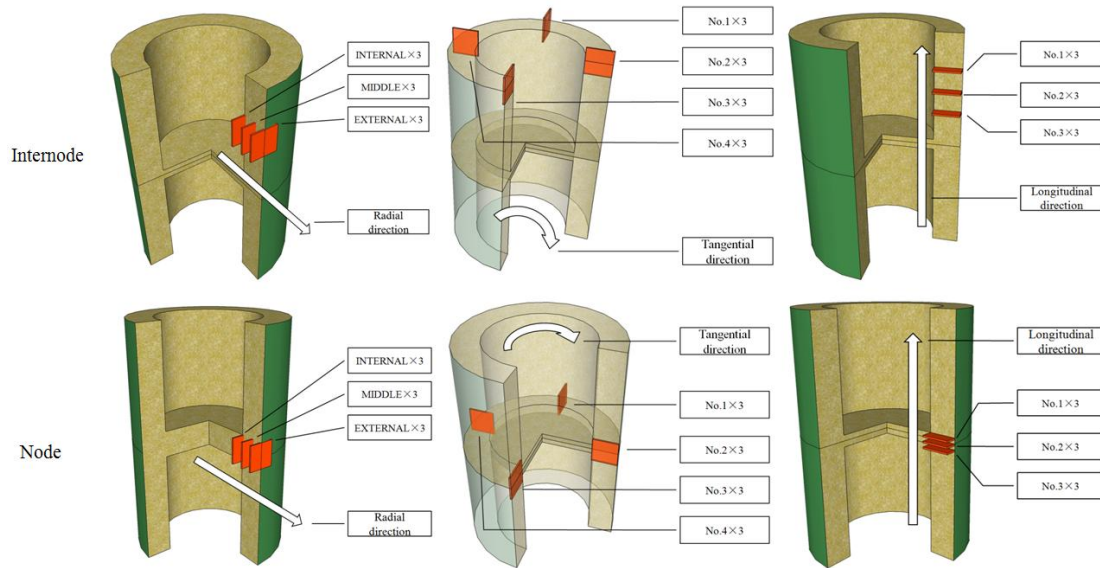


Figure 5.2.2 The cutting position of Moso bamboo specimens

5.2.2 Thermal diffusivity measurement by flash tube method

The thermal diffusivity was calculated using equation 3. The detailed theory was described in a previous research paper (Parker *et al.* 1961).

$$\alpha = 1.38 \cdot \frac{L^2}{\pi^2 \cdot t_{\frac{1}{2}}} \quad (5.2.1)$$

α : Thermal diffusivity (m²/s)

L : The thickness of the specimen (m)

$t_{\frac{1}{2}}$: The half time for the rear surface reaching peak temperature (s)

The thermal diffusivity measurement was conducted using a Thermal Waving Imaging (TWI) Ecotherm flash tube system. The flash tube system included a pulse generator, a flash tube heat source, a Mid-Wave Infrared (MWIR) camera, a controller and data recording PC system (See Fig 5.2.3). The acrylic board with embedded Moso bamboo specimens was fixed in front of the flash tube heat source. The temperature of the rear surface of the specimens was monitored by the MWIR camera and saved as by data recording PC.

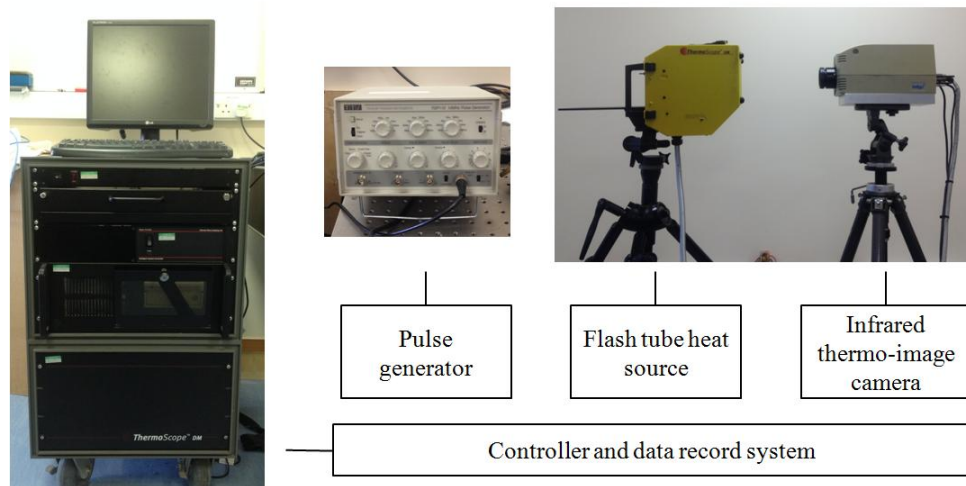


Figure 5.2.3 Flash tube system for thermal diffusivity measurement

The database files were processed using a MATLAB programme to identify the flash time and the time at which the rear surface achieves its peak temperature. After inputting the thickness of the bamboo specimens, the thermal diffusivity results can be calculated directly by this programme using equation 5.2.1.

5.3 Results and discussions

5.3.1 Thermal diffusivity results

The thermal diffusivity results including average and standard deviation (SD) in three directions are summarised in table 5.3.1.

Table 5.3.1 Thermal diffusivity results

Thermal diffusivity ($10^{-7} \text{ m}^2/\text{s}$)		Radial direction			Tangential direction				Longitudinal direction		
		External	Middle	Internal	No.1	No.2	No.3	No.4	No.1	No.2	No.3
Internode	Average	6.36	1.74	1.28	1.47	1.48	1.64	1.60	2.09	2.12	2.09
	SD	0.72	0.09	0.004	0.02	0.16	0.04	0.05	0.02	0.17	0.08
Node	Average	7.81	1.61	1.27	1.43	1.47	1.58	1.48	2.22	2.14	2.39
	SD	0.56	0.01	0.02	0.04	0.04	0.09	0.06	0.01	0.12	0.02

In the radial direction, specimens were cut from the external surface, midpoint and internal surface of bamboo culm wall at the internode (Figure 5.3.1) and node (Figure 5.3.2). Three specimens were prepared in each position. The vertical axis represents the thermal diffusivity value of the Moso bamboo specimens. The unit of the vertical axis is m^2/s .

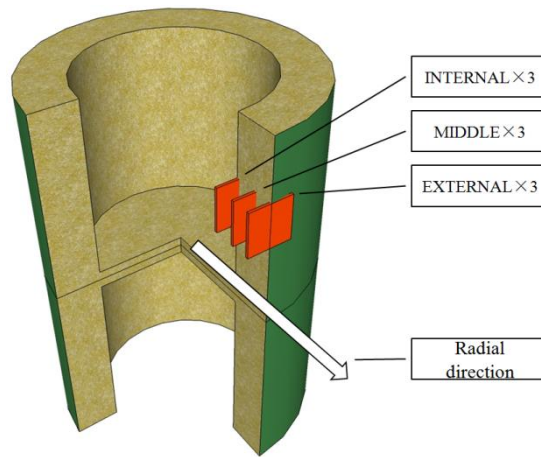
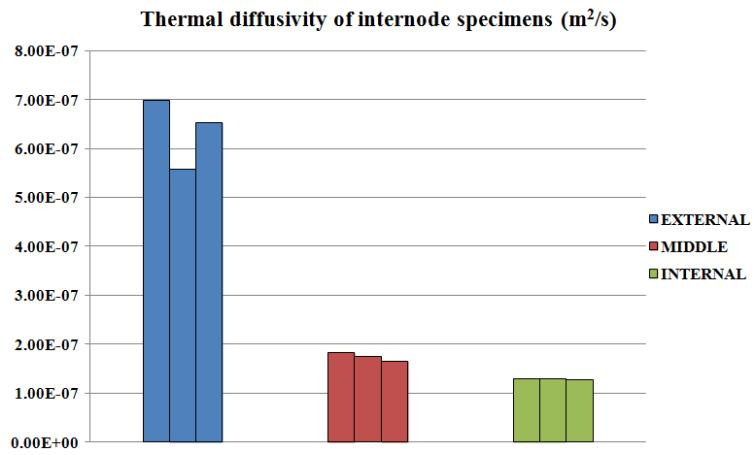


Figure 5.3.1 Thermal diffusivity of internode bamboo specimens in the radial direction

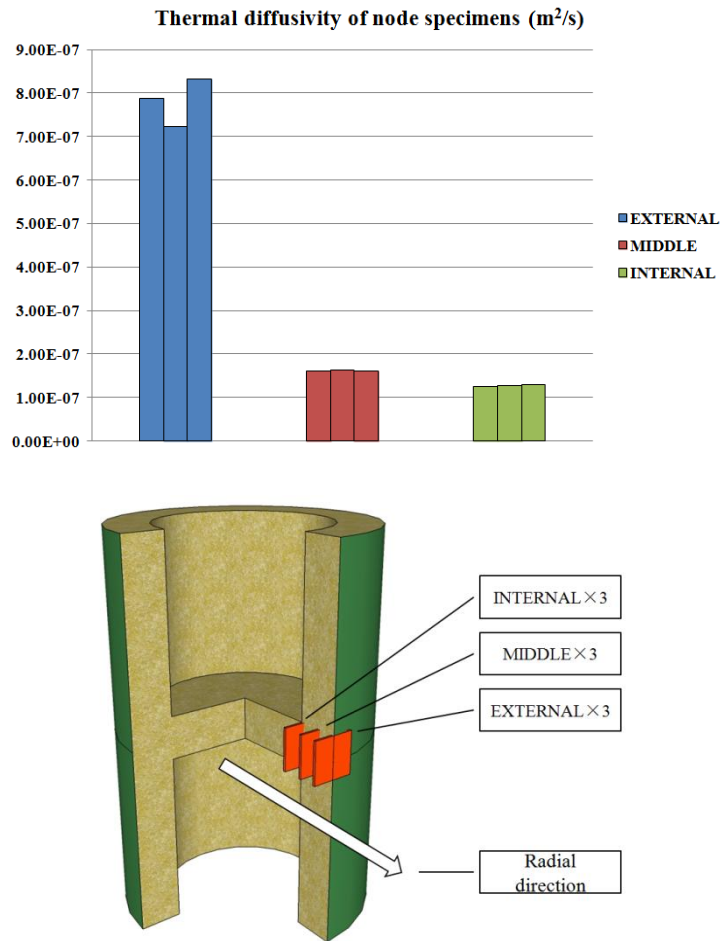


Figure 5.3.2 Thermal diffusivity of node bamboo specimens in the radial direction

The results indicated that the thermal diffusivity of the bamboo specimen from the external surface is significantly higher than the middle specimens and internal specimens with the thermal diffusivity decreasing from the external surface to the internal surface.

In the tangential directions, a specimen was cut every 90 degree at a same vertical height in the bamboo culm wall. Four representative cutting positions were evenly distributed around a circular area. Three specimens were measured at each position (See Figure 5.3.3 and Figure 5.3.4).

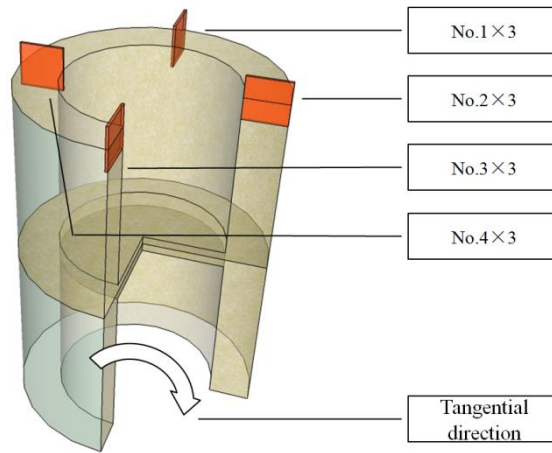
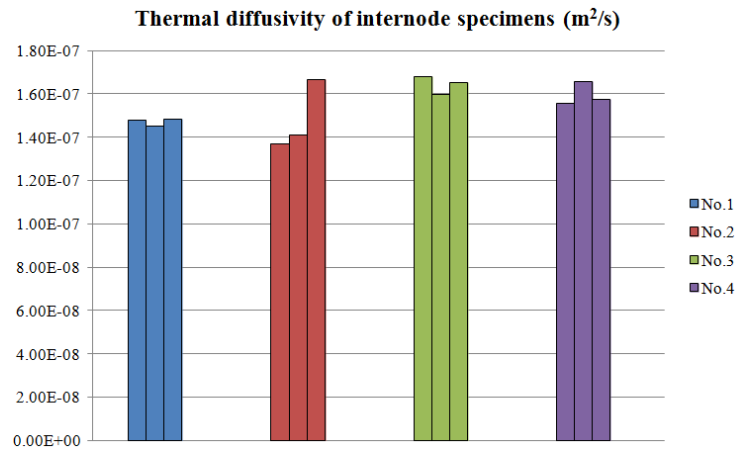


Figure 5.3.3 Thermal diffusivity of node bamboo specimens in the tangential direction

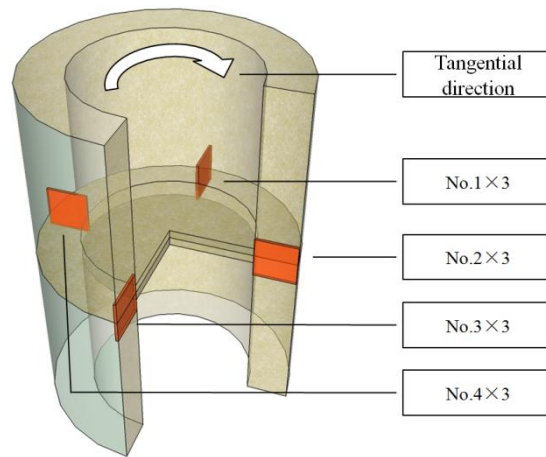
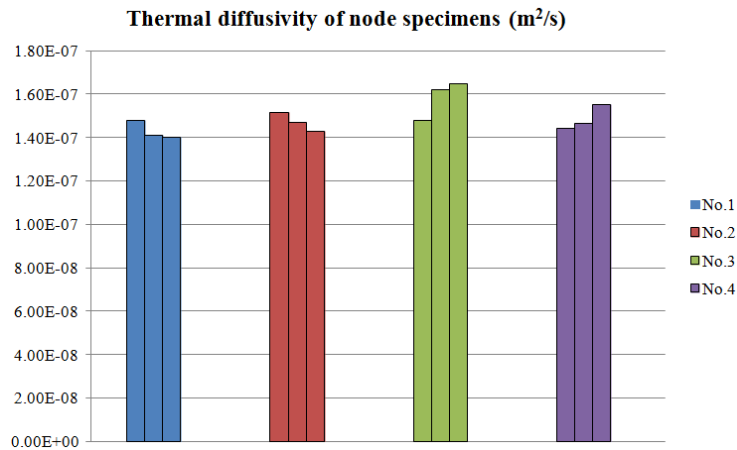


Figure 5.3.4 Thermal diffusivity of node bamboo specimens in the tangential direction

The average thermal diffusivity results demonstrated negligible differences in four representative positions for both internode part and node part.

In the longitudinal direction, specimens were taken from three positions. Due to the length difference between the internode part and the node part, the cutting interval between two adjacent positions was $10\text{mm} \pm 1\text{mm}$ for the internode parts and $3\text{mm} \pm 1\text{mm}$ for the node parts respectively. Three specimens were cut from each position for measurement (See Figure 5.3.5 and Figure 5.3.6).

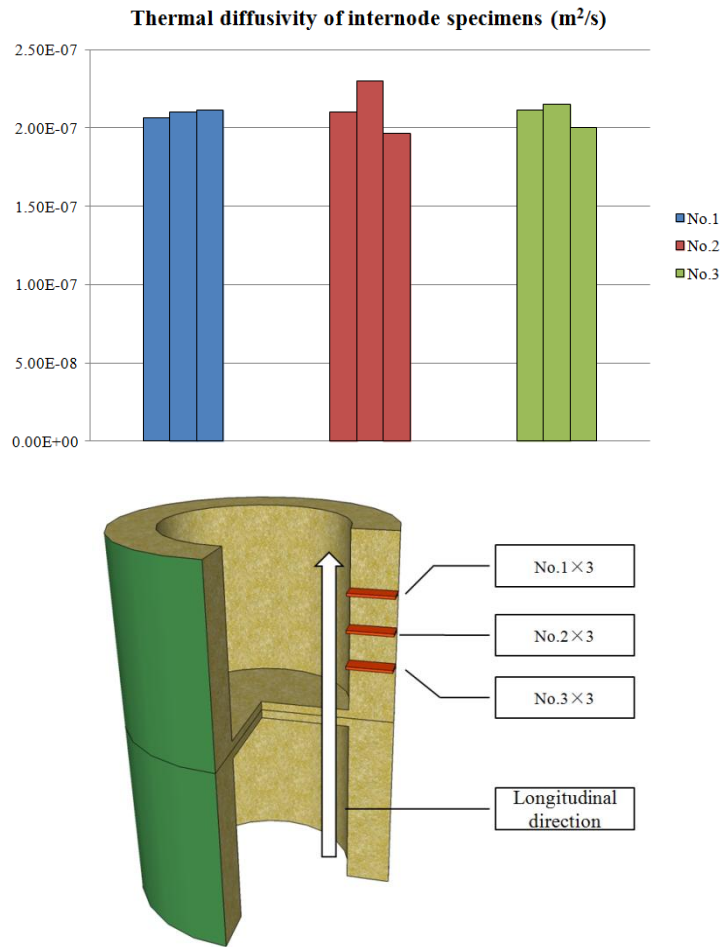


Figure 5.3.5 Thermal diffusivity of internode bamboo specimens in the longitudinal direction

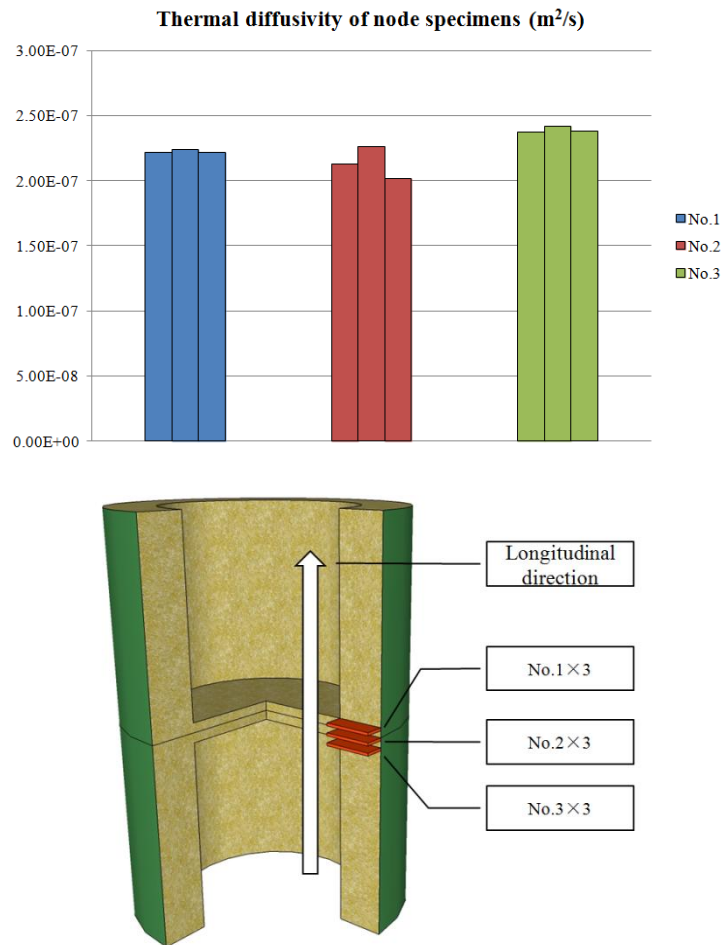


Figure 5.3.6 Thermal diffusivity of node bamboo specimens in the longitudinal direction

The average thermal diffusivity results indicated that no remarkable difference in the three cutting positions from the internode parts or node parts. The average thermal diffusivity of the node specimens is slightly higher than the value of the internode specimens.

5.3.2 Discussion

Thermal diffusivity results indicated that the obvious difference in measurement positions was only found in the radial direction rather than tangential direction or longitudinal direction. The reason can be explained by the morphological characteristics of Moso bamboo. Previous studies on the bulk density measurement provided the detailed data in three directions of the cylindrical coordinates system (Huang *et al.* 2015). The bulk density data demonstrated gradually decreasing trend from the external surface to the internal surface of the bamboo culm wall. However, the data from Figure 5.3.7 indicated that density is not the decisive factor for determining the thermal diffusivity of the material. The materials in Figure 5.3.7 shown a trend that the pure solid materials have relatively higher thermal diffusivity values followed by gases and alloys. The thermal diffusivity of polymers and porous materials is at a relatively lower level (James 1968, Blumm and Lindemann 2003, Wilson

2007, Casalegno *et al.* 2010 and Bergman *et al.* 2011.). It was postulated that the porosity is a factor which may influence the thermal diffusivity. The porosity data in the radial direction has been quantified by computed tomography scanning and backscattered electron (BSE) methods. Both methods indicated that the porosity increased from the external surface to the internal surface of the bamboo culm wall.

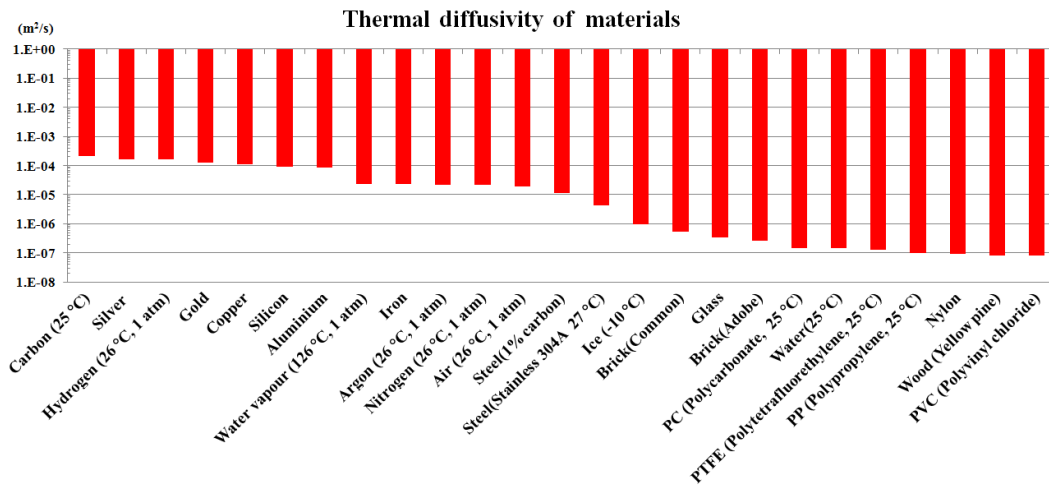


Figure 5.3.7 Thermal diffusivity of materials

Higher porosity can lead to a higher internal surface area which provides a larger area for heat propagation. Increasing porosity could be regarded as a sign of thermal diffusivity decreasing. Similar view has been voiced by some previous research on the porous materials (Zalameda and Winfree 1990 and Thomson 2010). The thermal diffusivity variation is also attributed to the tissue structure and interconnectivity of pores. Research on the thermal diffusivity of bread is a typical example of a material with high interconnectivity (Zanoni *et al.* 1995). Since the water content of the specimens is assumed as a negligible factor, only two phases existed in the bamboo specimens. The gas phase is the air, of which thermal diffusivity ranges from $1.9 \times 10^{-5} \text{m}^2/\text{s}$ to $2.28 \times 10^{-5} \text{m}^2/\text{s}$ (Wang and Mandelis 1999), and the solid phase is the bamboo cell wall. The results of this study implied that the thermal diffusivity of the bamboo cell wall is much less than the thermal diffusivity of air. If one just considers the fraction ratio, regions with high porosity and high interconnectivity will provide high thermal diffusivity values. However, the results of this study are not in a good agreement with this assumption. The interconnectivity of Moso bamboo is not large enough to counteract the influence of the high porosity. For Moso bamboo, porosity is a more decisive factor than interconnectivity in terms of the thermal diffusivity.

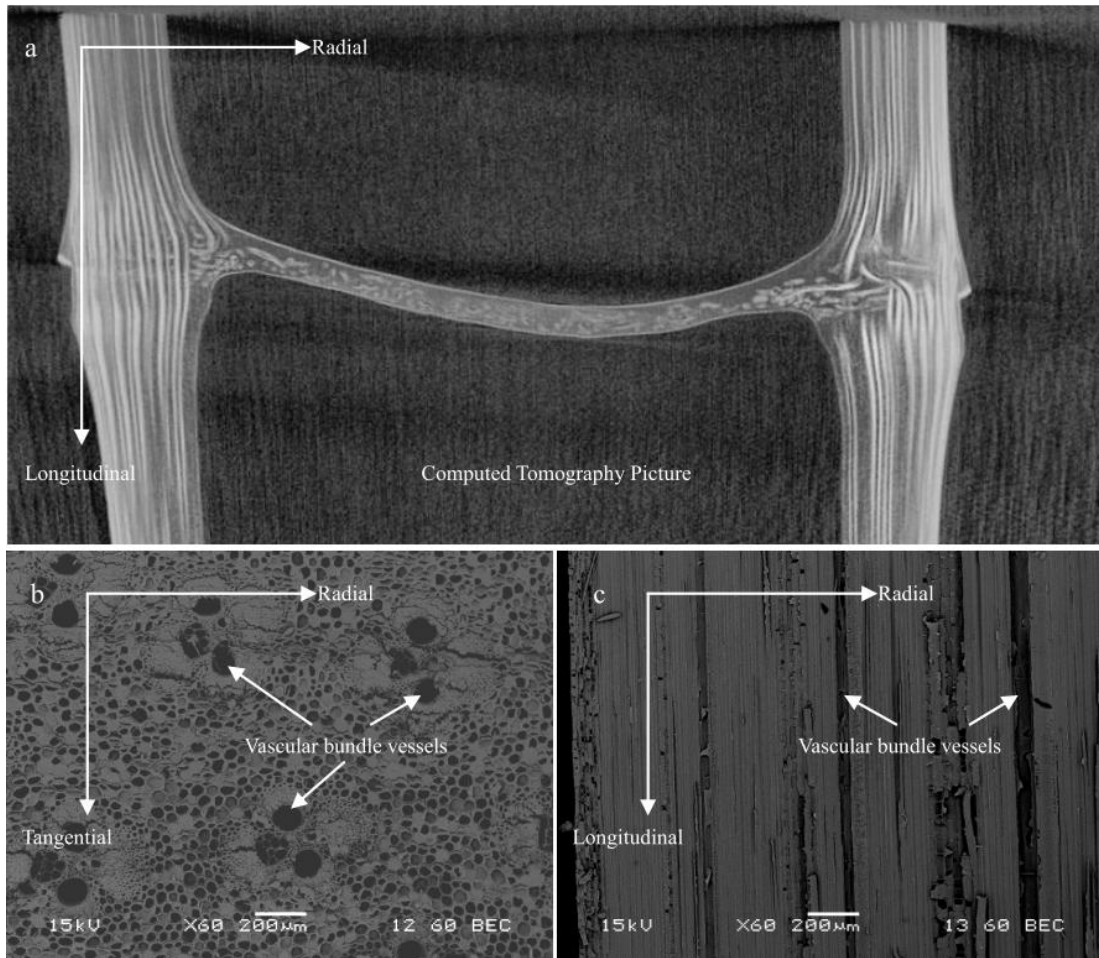


Figure 5.3.8 CT and BSE pictures of Moso bamboo specimens

Moso bamboo specimens in the longitudinal direction presented higher thermal diffusivity values than the specimens in the tangential directions and the specimens from middle and internal positions in the radial direction. The reason can be found in the Computed Tomography (CT) picture and back-scattered electron (BSE) pictures of Moso bamboo specimens. Morphologically, vertically grown fibres provided shorter routes for heat propagation while the vascular bundle vessels allowed more interconnectivity for air (See Figure 5.3.8a and 5.3.8c). The Figure 5.3.8b illustrated that the route of heat propagation was though more complex routes in radial and tangential direction than the longitudinal direction.

5.4. Summary

The thermal diffusivity of the Moso bamboo specimens was measured by a flash tube system. The specimens were measured in all directions of the cylindrical coordinates system at both internode parts and node parts. An obvious difference in the thermal diffusivity results was found between the measurement positions in the radial direction. The remarkable differences of porosity and complexity of heat propagation area in the radial direction are regarded as factors to influence the thermal diffusivity. Higher thermal diffusivity values appeared for specimens in the longitudinal direction than the specimens in the tangential directions and the specimens from middle and internal positions in the radial direction. This phenomenon can be attributed to vertically grown fibres and permeable vascular bundle vessels in the longitudinal direction*.

(*The content of this chapter is from a published paper of author. See self bibliography (Huang *et al.* 2017b))

Chapter 6 Water vapour diffusion resistance factor of Moso bamboo

The content of this chapter was published in a peer reviewed journal: *Construction and building materials*. See self bibliography (Huang *et al.* 2017c).

6.1 Research objectives

The aim of this chapter is to investigate the water vapour permeability or water vapour diffusion resistance factor of Moso bamboo in both internode and node specimens. It is intended that moisture movement mechanisms within bamboo panels may be elucidated when the spatial arrangement of the raw materials is considered. Better understanding of moisture transfer mechanisms of building materials is important for several reasons, for assessing the equivalent thermal resistance, for estimating the condition under which mould will grow, and for predicting the expansion where will happen.

6.2 Methodology

6.2.1 Specimen preparation and water vapour diffusion resistance factor measurement

Figure 6.2.1 illustrates the cutting position of specimens. The radial direction refers to the direction of the bamboo culm wall thickness. The longitudinal direction is the bamboo vertical growing direction. The tangential direction is along the radial direction of the bamboo culm wall. Three types of cylindrical specimens were prepared for water vapour permeability measurement. The measurement direction is perpendicular to the circular surface. For example, the tangential-longitudinal surface is perpendicular to the radial direction. The cylindrical specimen with circular tangential-longitudinal surface is the specimen for the radial direction measurement of water vapour permeability because the water vapour is transmitted in the radial direction. The cutting position is described in detail in Figures. 6.2.2, 6.2.3 and 6.2.4.

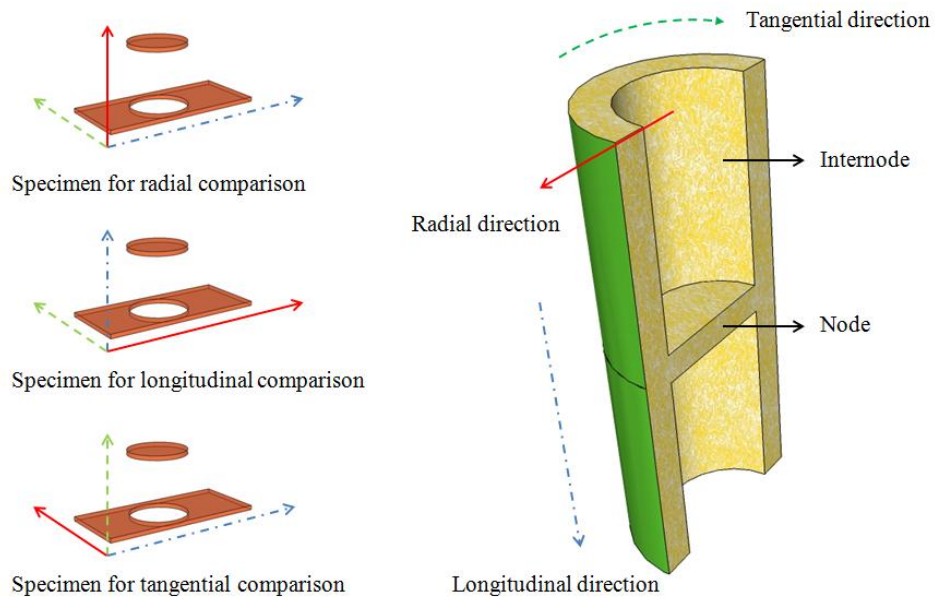


Figure 6.2.1 Nomenclature for a bamboo culm and orientation of specimens

In the radial direction (Figure. 6.2.2), specimens were cut from both the internode and the node position. Three cutting positions are defined as internal, middle and external positions from the internal surface to the external surface of the bamboo culm wall. Five specimens were prepared for each position. These specimens were prepared to demonstrate the water vapour permeable trend of the bamboo in the radial direction.

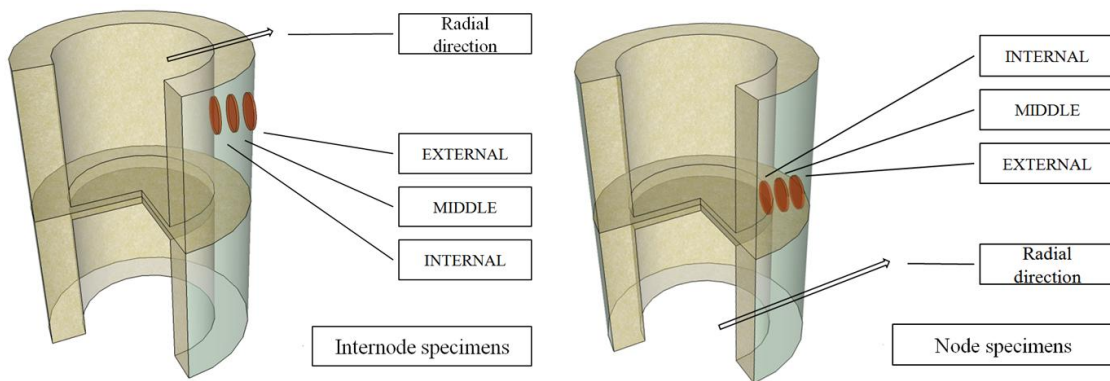


Figure 6.2.2 The cutting position of bamboo specimens in the radial direction

In the tangential direction (Figure 6.2.3), specimens were designated Nos.1 to 4. The interval of two adjacent cutting positions is 90° . Five specimens were prepared for each position. The middle point of the node specimens were aligned with the node line of the bamboo culm wall. These specimens were utilised to identify the water vapour permeable trend of the bamboo in the tangential direction.

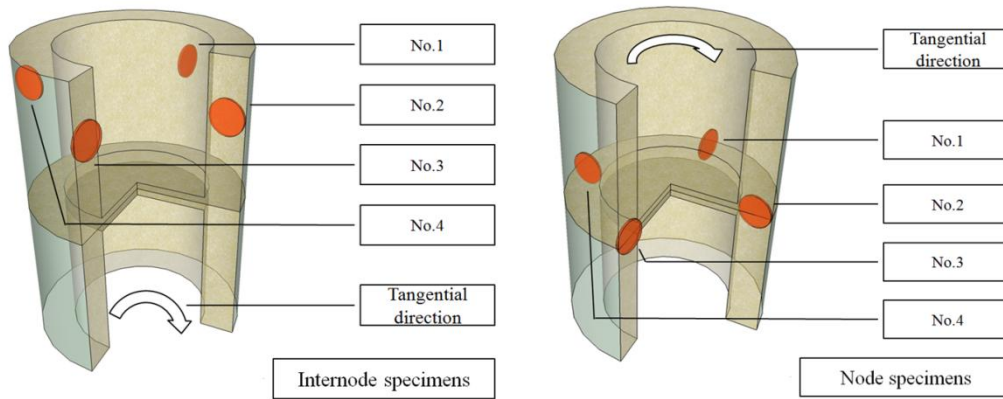


Figure 6.2.3 The cutting position of bamboo specimens in the tangential direction

In the longitudinal direction (Figure 6.2.4), specimens were designated Nos.1 to 3. The distance between two adjacent specimens was equal. Five specimens were prepared for each position. These specimens were prepared to assess the water vapour permeable trend of the bamboo in the tangential direction.

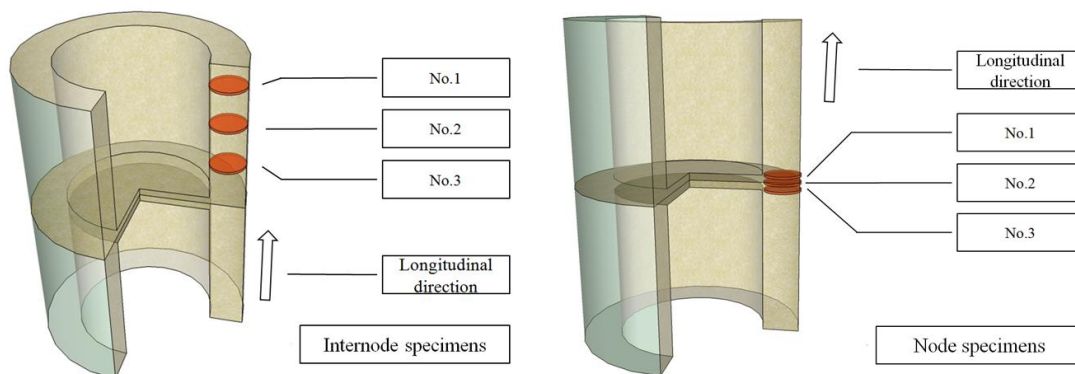


Figure 6.2.4 The cutting position of bamboo specimens in the longitudinal direction

The diameter of all specimens was 14 ± 1 mm and the thickness was 3 ± 0.5 mm. These specimens were stored in a climate chamber for 24 hours with a temperature and relative humidity of 23 ± 1 °C and 50% respectively.

The water vapour permeability measurement was conducted by a dry cup method (BS EN 12086 2013). Bamboo specimens were assembled within glass containers. Calcium chloride (CaCl_2) was prepared as the desiccant to provide 0% RH within the glass containers. The air space between the desiccant and the test specimen was 15 ± 5 mm. Crystalline wax was utilised to seal the gap between the bamboo specimen and the glass container (Figure 6.2.5). After measuring the initial mass with an electronic scale, the sealed assemblies were stored in the climate chamber. The weight of every assembly was monitored every 24 hours. The

monitoring was terminated when the mass change was less than 5%. The readability of the electronic scale is 0.001g.

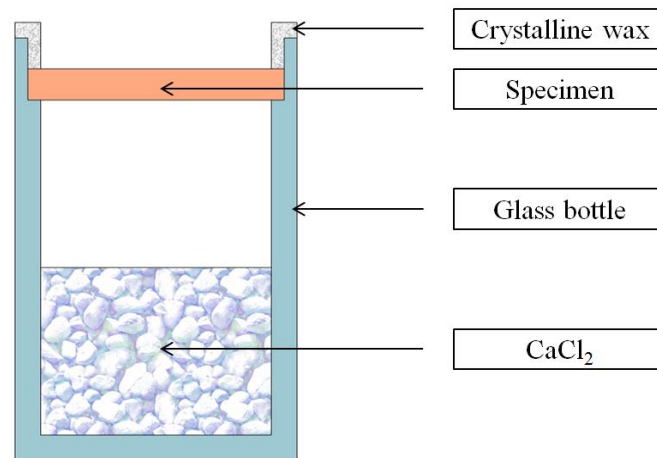


Figure 6.2.5 Assemblies for water vapour diffusion resistance factor measurement

6.2.2 Water vapour permeability calculation

The water vapour permeability was calculated by equation 6.2.1.

$$\delta_p = \frac{\Delta m \cdot d}{\Delta t \cdot A_{ex} \cdot \Delta p} \quad (6.2.1)$$

δ_p : Water vapour permeability (kg/m s Pa)

Δm : Mass change in 24 hours (kg)

d : Thickness of the specimen (m)

Δt : Time interval=24 (h)

A_{ex} : Exposed area (m²)

Δp : The water vapour pressure difference=1400 (Pa)

The water vapour permeable capability of a construction material is often expressed by the water vapour diffusion resistance factor. The water vapour diffusion resistance factor was calculated by equation 6.2.2.

$$\mu = \frac{\delta_{air}}{\delta_p} \quad (6.2.2)$$

μ : Water vapour diffusion resistance factor, dimensionless

δ_{air} : Water vapour permeability of air (kg/m s Pa)

δ_p : Water vapour permeability of the specimen (kg/m s Pa)

The water vapour permeability of air can be calculated by equation 5.2.3 (Schirmer 1938).

$$\delta_{air} = \frac{2.306 \cdot 10^{-5} \cdot P_0}{R_v \cdot T \cdot P_a} \left(\frac{T}{273.13} \right)^{1.81} \quad (6.2.3)$$

δ_{air} : Water vapour permeability of air (kg/m s Pa)

P_0 : Standard atmospheric pressure (101325 Pa)

R_v : Gas constant for water (461.5 J/K kg)

T : The temperature (K)

P_a : Ambient air pressure (Pa)

6.3 Results and discussion

The results of Moso bamboo specimens were displayed in the form of the water vapour diffusion resistance factor (μ). The horizontal axis represents the μ value. The vertical axis displays the group name of bamboo specimens from different directions in both internode and node parts. The variation ranges of each group were provided. See Figure 6.3.1.

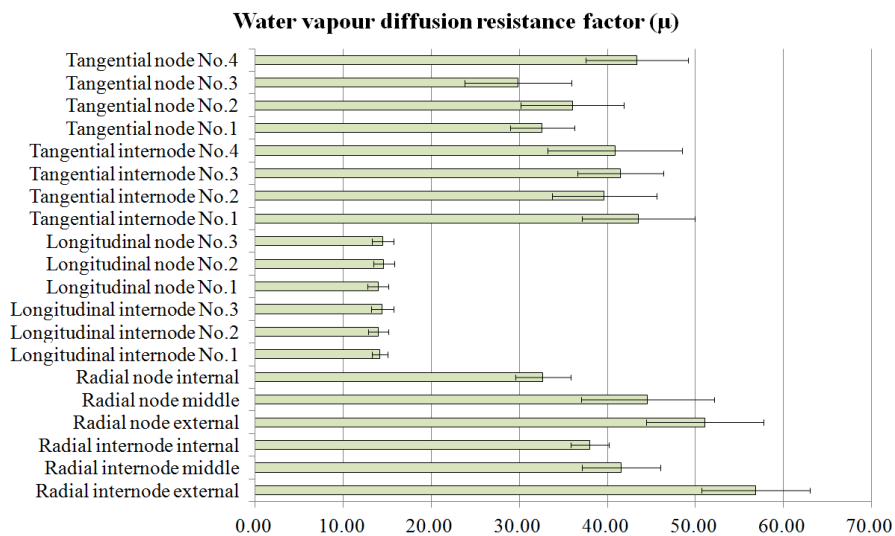


Figure 6.3.1 Water vapour diffusion resistance factor (μ)

The water vapour diffusion resistance factor results for Moso bamboo specimens in the radial direction exhibit an obvious decreasing trend from the external surface to the internal surface for both internode and node parts which is explained by the morphological features of bamboo. The main structure of the bamboo culm can be regarded as a mixture of vascular bundle tissue and the parenchyma ground tissue. From the external surface to the internal surface, the content of vascular bundle tissue decreases while the content of parenchyma ground tissues increases (Figure 6.3.2). The large numbers of fibre cells around the vascular bundle vessels are highly lignified with relatively small cavities and thick cell walls. Even the parenchyma ground cells between two vascular bundles are smaller than the parenchyma ground cells in other parts of the bamboo culm wall (Figure 6.3.3). On the external side, the vascular bundle tissues occupy a large proportion of the area. The gap between parenchyma ground cells is much larger than the tightly arranged fibre cells at 600 times magnification (Figure 6.3.5). Furthermore, many tiny pits are distributed on the cell wall of the parenchyma ground tissue cells. The diameter of these pits is around 1 μm . However, these pits are rarely found on the cell wall of the vascular bundle cells. In addition, the quantified bulk density data demonstrates a decreasing trend from the external surface to the internal surface (Huang *et al.* 2015). Therefore, the difficulty for water vapour to diffuse through the external side of bamboo culm wall is higher than that through the internal side.

Another feature of the results is that the water vapour diffusion resistance factor of bamboo specimens in the longitudinal direction is remarkably lower than the water vapour diffusion resistance factor of bamboo specimens in the radial and tangential directions. The water vapour diffusion resistance factor of bamboo specimens in the longitudinal direction is around 14. The values in the radial and tangential directions range from 30 to 57. The main reason is that vascular bundle vessels provide many straight conduits for the transportation of water vapour. The interconnectivity of the vascular bundle vessel is considerable in the tangential direction (Figure 6.3.4). The vascular bundle vessel can be regarded as a tube with many tiny pits. No obvious partition appears in the longitudinal direction of the vascular bundle vessel (Liese 1985 and Wang 2010). The diameter of the vascular bundle vessels can reach 100 μm . However, no tissue with straight conduits and high interconnectivity can be found in the radial and tangential directions (Figure 6.3.5).

In addition, the results indicate that the majority of the node specimens pose a lower water vapour diffusion resistance factor than internode specimens in the radial and tangential directions. This phenomenon may be attributed to the irregularly growing vascular bundle tissues in the node parts of the bamboo culm. Figure 6.3.6 is a computed tomography (CT) image of a bamboo specimen from the node parts. The greyscale of the image clearly showed the density difference between the vascular bundle tissues and the parenchyma ground tissues.

Figures 6.3.6 and 6.3.7 illustrate that the growth of the vascular bundle tissue in the node part is not as straight as it is in the internode part. The direction of the vascular bundle tissue also changes from the longitudinal direction to other directions. Therefore, water vapour may be transported via these irregularly growing vascular bundle vessels which can provide higher interconnectivity than other tissues.

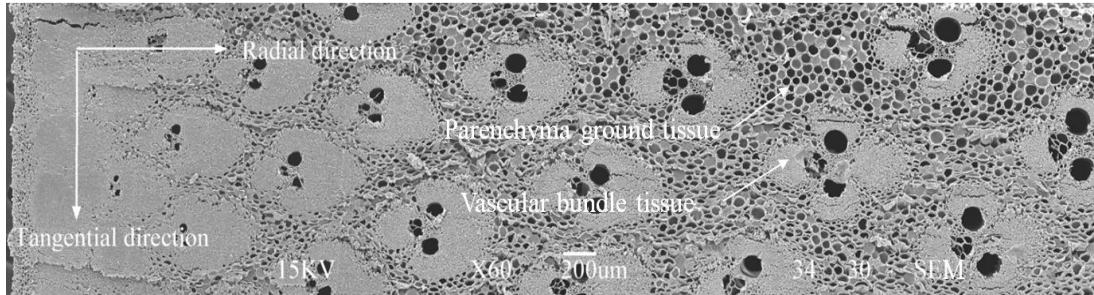


Figure 6.3.2 The SEM image of a bamboo specimen ($\times 60$)

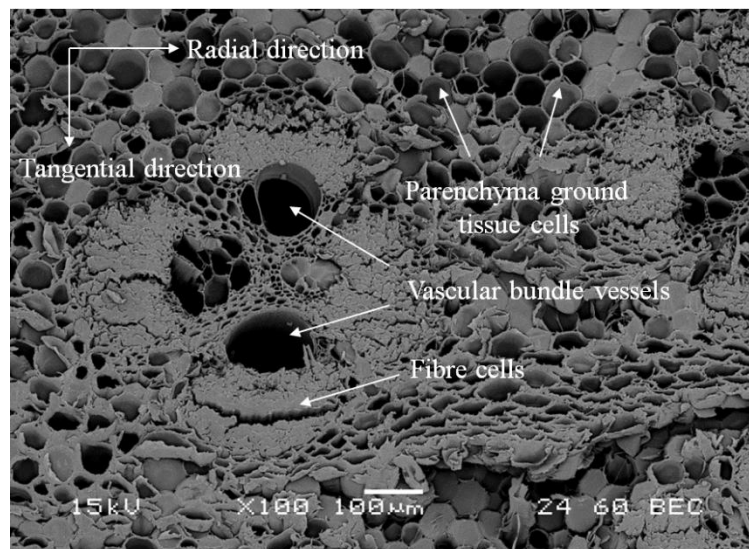
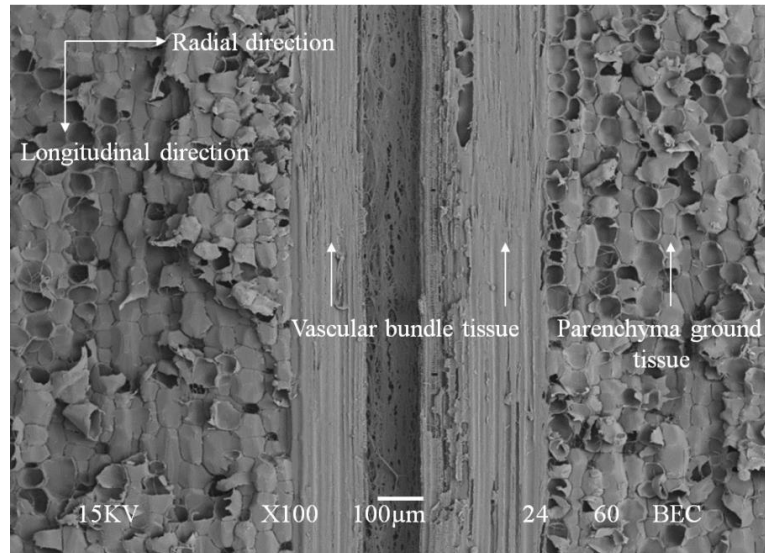


Figure 6.3.3 A BSE image of a bamboo cross-section ($\times 100$)



Figures 6.3.4 A BSE image of a bamboo radial-longitudinal section ($\times 100$)

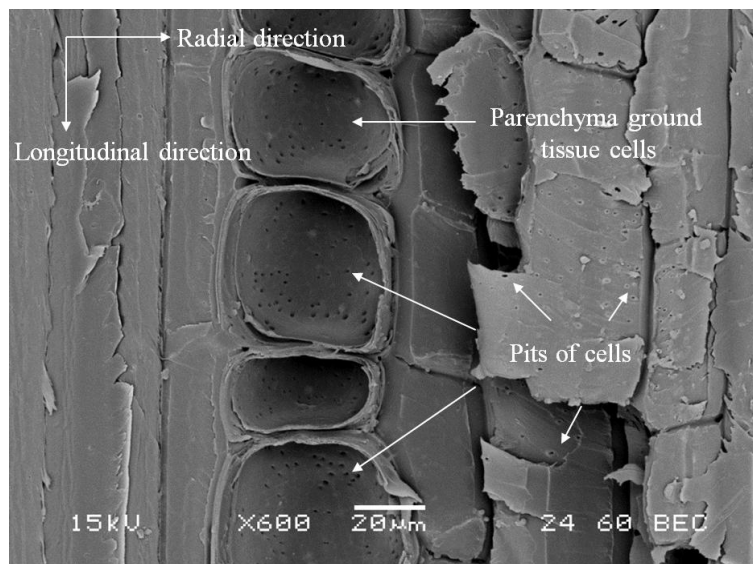


Figure 6.3.5 The BSE image of a radial-longitudinal section ($\times 600$)

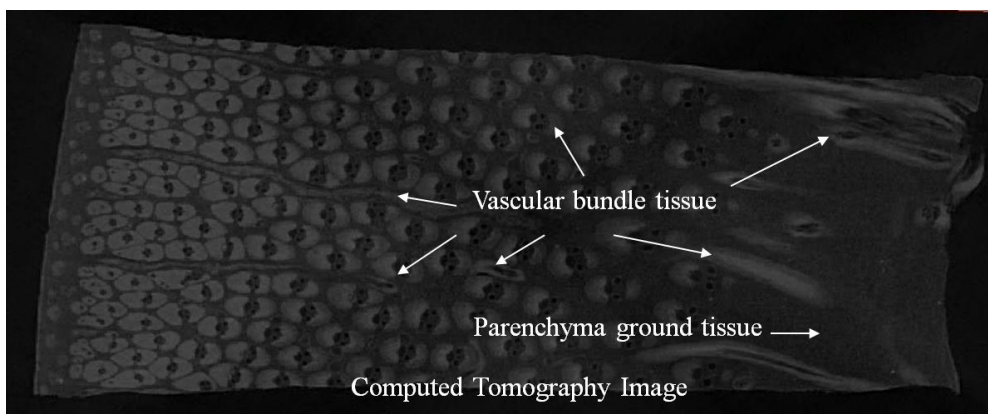


Figure 6.3.6 A computed tomography image of a bamboo cross-section

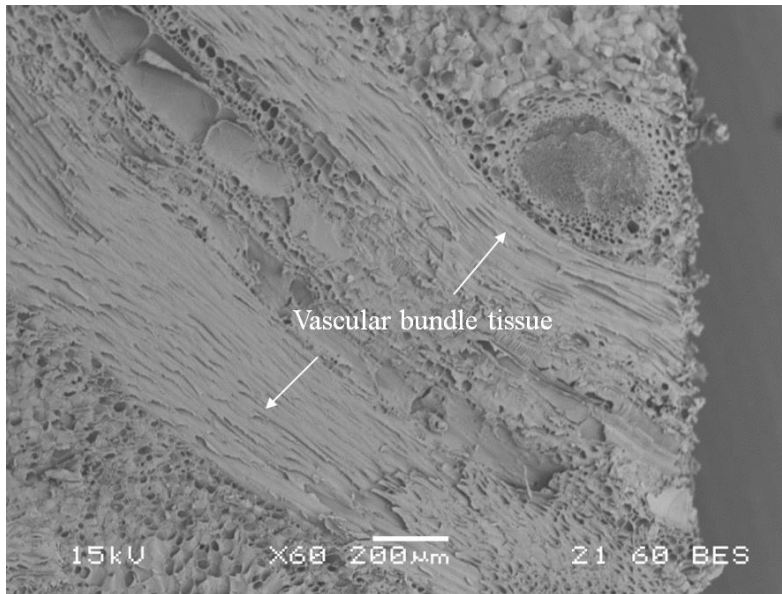


Figure 6.3.7 A BSE image of a section through a node. ($\times 60$)

The results of the water vapour diffusion resistance factor study indicate that different fibre directions can lead to significant variation of the water vapour diffusion performance. The variation needs to be considered in the manufacturing of bamboo-based building envelope components. In addition, the wide variation range of the water vapour diffusion factors implies that simply using average value is not appropriate in the heat and moisture transfer research. The selection of the water vapour diffusion factors should consider the fibre direction and cutting position of bamboo specimens.

6.4 Summary

The water vapour diffusion resistance factor of the Moso bamboo specimens was measured by a dry cup method. The specimens were measured in all directions of the cylindrical coordinates system for both internode parts and node parts. The water vapour diffusion resistance factor results for Moso bamboo specimens demonstrated a decreasing trend from the external surface to the internal surface in the radial directions. This fact may be attributed to the more densified fibre cells and low quantity of pits at the external surface. The water vapour diffusion resistance factor of bamboo specimens is remarkably lower in the longitudinal direction than in the radial and tangential directions. The large diameter, high interconnectivity and straight structure of the vascular bundle vessels are the factors which lead to this lower water vapour diffusion resistance factor in the longitudinal direction. The majority of the node specimens demonstrated lower water vapour diffusion resistance factor values than internode specimens in the radial and tangential directions due to the irregularly growing vascular bundle vessels which are oriented in different directions*.

(*The content of this chapter is from a submitted manuscript of author. See self bibliography (Huang *et al.* 2017c))

Chapter 7 Sorption isotherm and liquid transport coefficient of Moso bamboo

Part of the content of in this Chapter was sent to a peer reviewed journal: *Construction and building materials*. See self bibliography (Huang *et al.* 2016b)

7.1 Sorption isotherm of Moso bamboo

7.1.1 Research objectives

This section measured sorption isotherm curves for the moisture sorption and desorption of *Phyllostachys edulis* (Moso bamboo) specimens in three directions of the cylindrical coordinate system. These sorption isotherm curves are the fundamental data for deriving the moisture storage capacity. The moisture storage capacity is the basic input of the numerical simulation of moisture transfer for bamboo. The sorption isotherm curves are regarded as essential data for understanding the moisture transfer mechanism of bamboo.

7.1.2 Methodology

Figure 7.1.1 indicates the cutting positions of the specimens. The radial direction refers to the direction of the bamboo culm wall thickness. The longitudinal direction is the bamboo vertical growing direction. The tangential direction is along the radian of the bamboo culm wall (See Figure 7.1.1). Three types of specimens were prepared for hygroscopic measurement. The shortest side of the specimen is defined as the main direction for data comparison. The reason is that the surface with the largest hygroscopic area can be perpendicular to the main direction. The cutting position in three main directions is further explained in Figures 7.1.2 to 7.1.4.

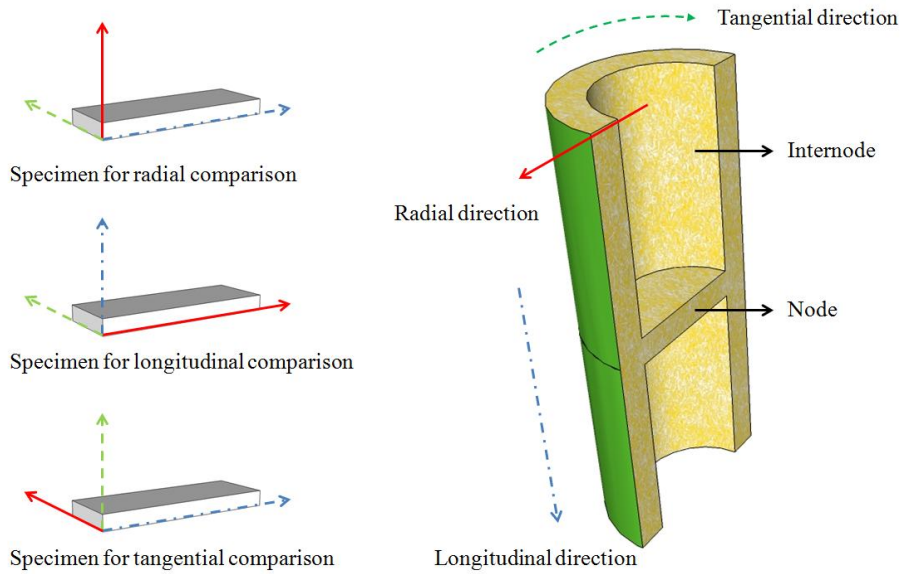


Figure 7.1.1 Nomenclature for a bamboo culm

In the radial direction, three specimens were cut from the internode and the node positions respectively. Three specimens are defined as internal, middle and external specimens passing from the internal surface to the external surface of the bamboo culm wall (Figure. 7.2.2). These specimens were prepared to demonstrate the hygroscopic trend of the bamboo in the radial direction.

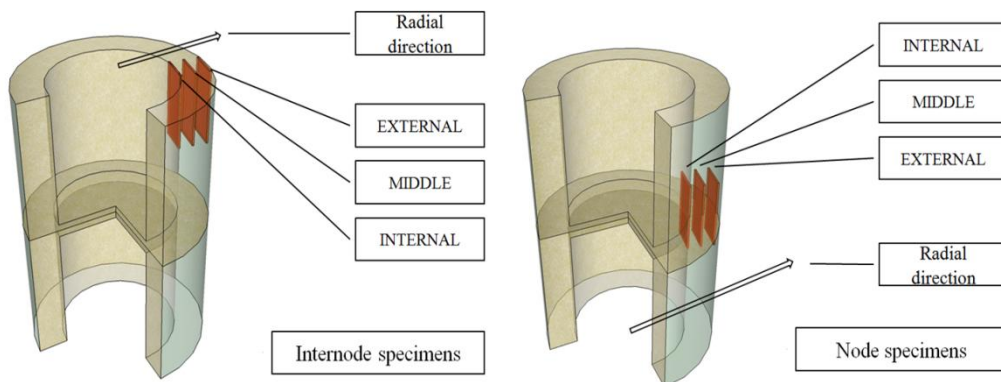


Figure 7.1.2 The cutting position of bamboo specimens in the radial direction

In the tangential direction, four specimens were cut and designated No.1 to No.4 for both internode and node position (Figure. 7.1.3). The interval of two adjacent cutting positions is 90°. The middle point of the node specimen is aligned with the node line of the bamboo culm wall. These specimens are utilised to identify the hygroscopic trend of the bamboo in the tangential direction.

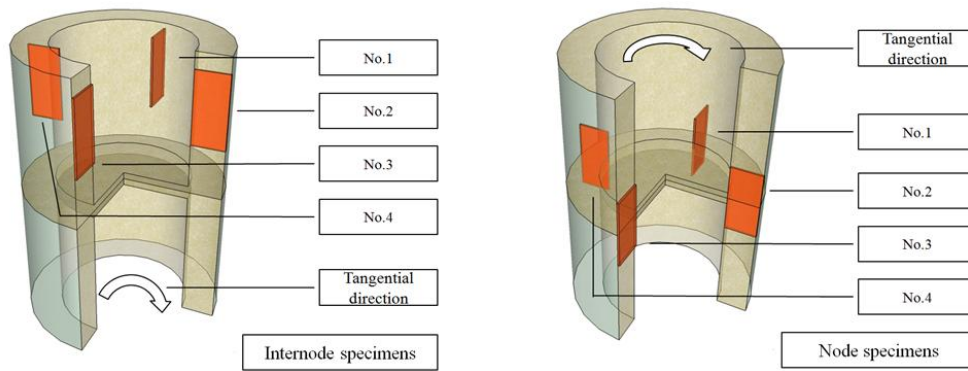


Figure 7.1.3 The cutting position of bamboo specimens in the tangential direction

In the longitudinal direction, three specimens were cut and designated No.1 to No.3 for both internode and node position (Figure. 7.1.4). Due to the restriction of the radial dimension, each specimen was glued together by Phenol-Resorcinol-Formaldehyde (PRF) from 11 small cuboids from the same vertical level. These specimens were manufactured to measure the hygroscopic response of the bamboo in the longitudinal direction.

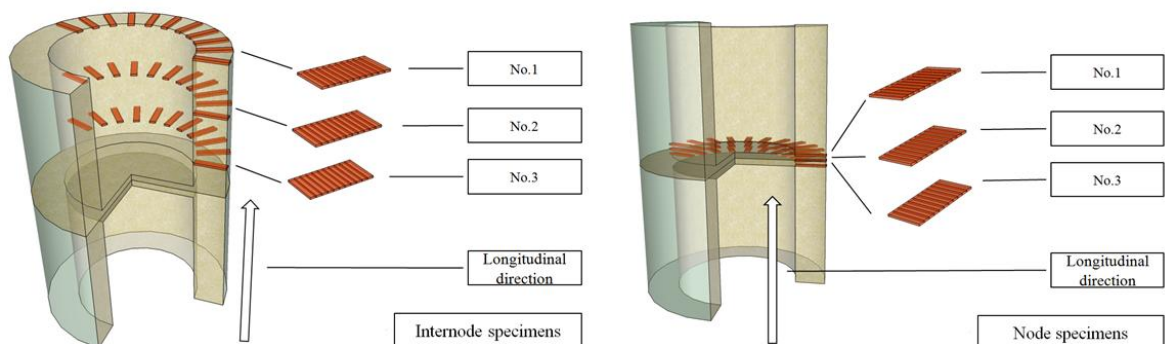


Figure 7.1.4 The cutting position of bamboo specimens in the longitudinal direction

The size of all specimens is $(45 \text{ mm} \pm 1 \text{ mm}) \times (15 \text{ mm} \pm 1 \text{ mm}) \times (5 \text{ mm} \pm 1 \text{ mm})$. All specimens were oven dried to eliminate moisture at $103 \pm 2 \text{ }^\circ\text{C}$. Then, the specimens were stored in desiccators with calcium chloride (CaCl_2). Except for the two surfaces with the largest hygroscopic area, the other four surfaces were covered by aluminium foil to minimise the hygroscopic influence of the other two directions (Figure 7.1.5).

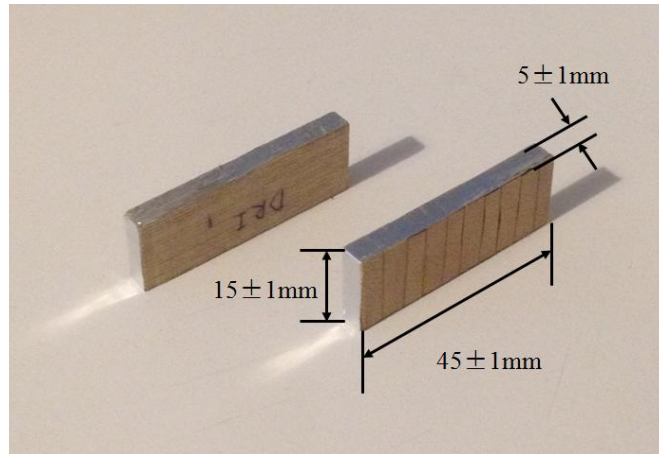


Figure 7.1.5 The size of specimens

The sorption and desorption experiments were conducted by the use of desiccators containing saturated salt solutions. The temperature of the experiment was $23 \pm 2 \text{ }^\circ\text{C}$ (Figure 7.1.6). The saturated solutions provide a steady relative humidity (RH) in each desiccator. Six saturated solutions were utilised to produce the relative humidity conditions required in each desiccator. Dettol fungicide was added to the potassium chloride (KCl) solution and potassium nitrate (KNO_3) solution to avoid undesired mould and mildew growing on the bamboo specimens. The actual relative humidity conditions were also monitored by relative humidity sensors.



Figure 7.1.6 The desiccator assembly

The theoretical and real relative humidities at 23°C are listed in Table 7.1.1.

Table 7.1.1 Relative humidities in desiccators

Substance	Theoretical RH	Real RH
KOH	9%	7%
MgCl ₂ 6H ₂ O	33%	27%
NaBr	57%	54%
NaCl	75%	76%
KCl	85%	88%
KNO ₃	93%	95%

The sorption and desorption experiments were conducted by referencing a British standard (BS EN ISO 12571:2013). After oven drying, all bamboo specimens were put into a desiccator with KOH at first. Then, these specimens were weighed every 24 hours until the change of mass between three consecutive weighings was less than 0.1%. The moisture content of each specimen was calculated at this equilibrium state by equation 7.1.1.

$$u = \frac{m - m_0}{m_0} \quad (7.1.1)$$

u : Moisture content in equilibrium state

m : mass of the specimen in equilibrium state (g)

m_0 : mass of the specimen in oven dry state (g)

After the moisture content was recorded, all specimens were moved to a new desiccator. In sorption processes, the moving sequence of desiccators was from oven dry to KOH to MgCl₂ 6H₂O to NaBr to NaCl to KCl to KNO₃. In desorption processes, the sequence of desiccators was from KNO₃ to KCl to NaCl to NaBr to MgCl₂ 6H₂O to KOH to oven dry.

7.1.3 Results and discussion

The sorption isotherm curves of Moso bamboo specimens in the radial direction are shown in Figure 7.1.7. The solid lines represent the sorption data. The dashed lines represent the desorption data. The vertical axis is the moisture content. The horizontal axis is the RH. The internal, middle and external specimens were designated as I, M and E in the legend.

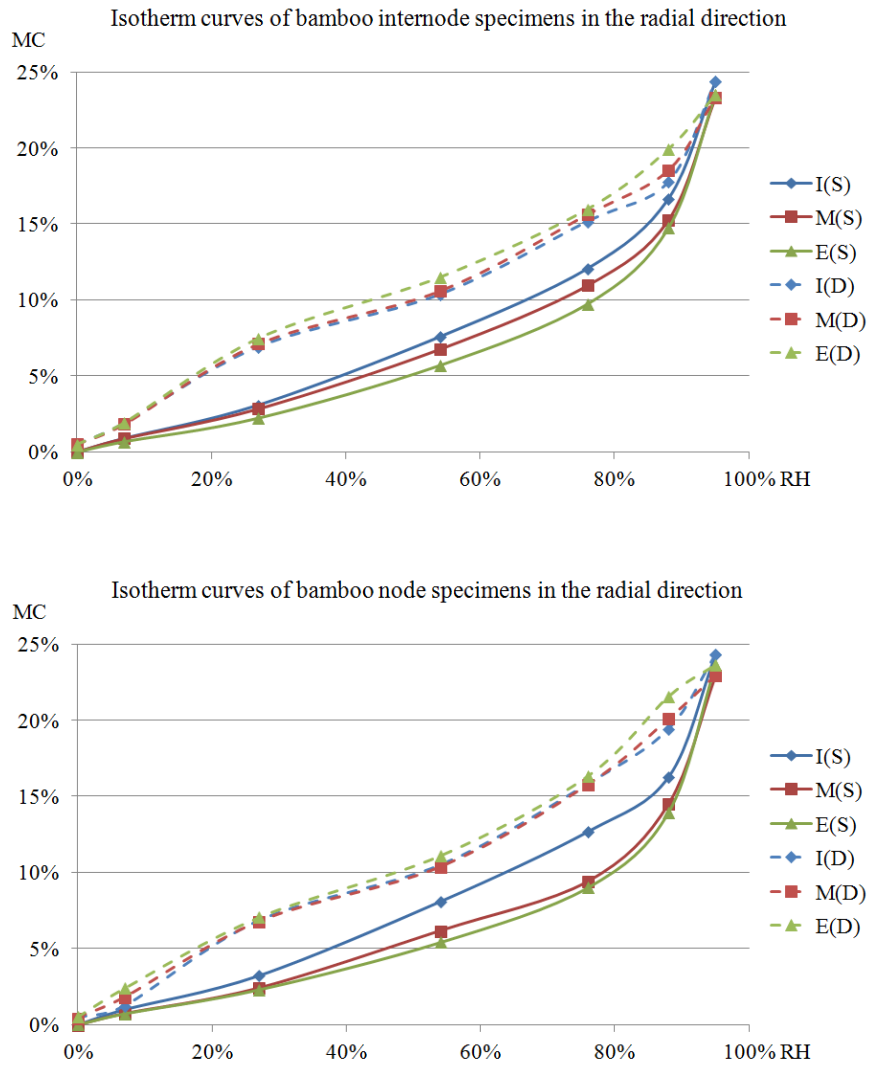


Figure 7.1.7 Sorption isotherm curves in the radial direction

The results of Figure 7.1.7 indicate that the hygroscopicity increases from the external to the internal position in the sorption process for both internode and node specimens. In the desorption process, moisture content decreases from the external to the internal position at the same RH. The term ‘hysteresis’ is defined as the difference between adsorption and desorption values (Banerjee and Tyagi 2011). The results of these two observations imply that the hysteresis between sorption curve and desorption curve also decreases from the external to the internal position. The hysteresis between the external specimen and the other two specimens is relatively higher for node position than internode position. The moisture content difference between sorption curve and desorption curve of specimens is higher at the node than the internode position at 88% RH.

The sorption isotherm curves of Moso bamboo specimens in the tangential direction are shown in Figure 7.1.8. The position of the four specimens is illustrated in Figure 7.1.3.

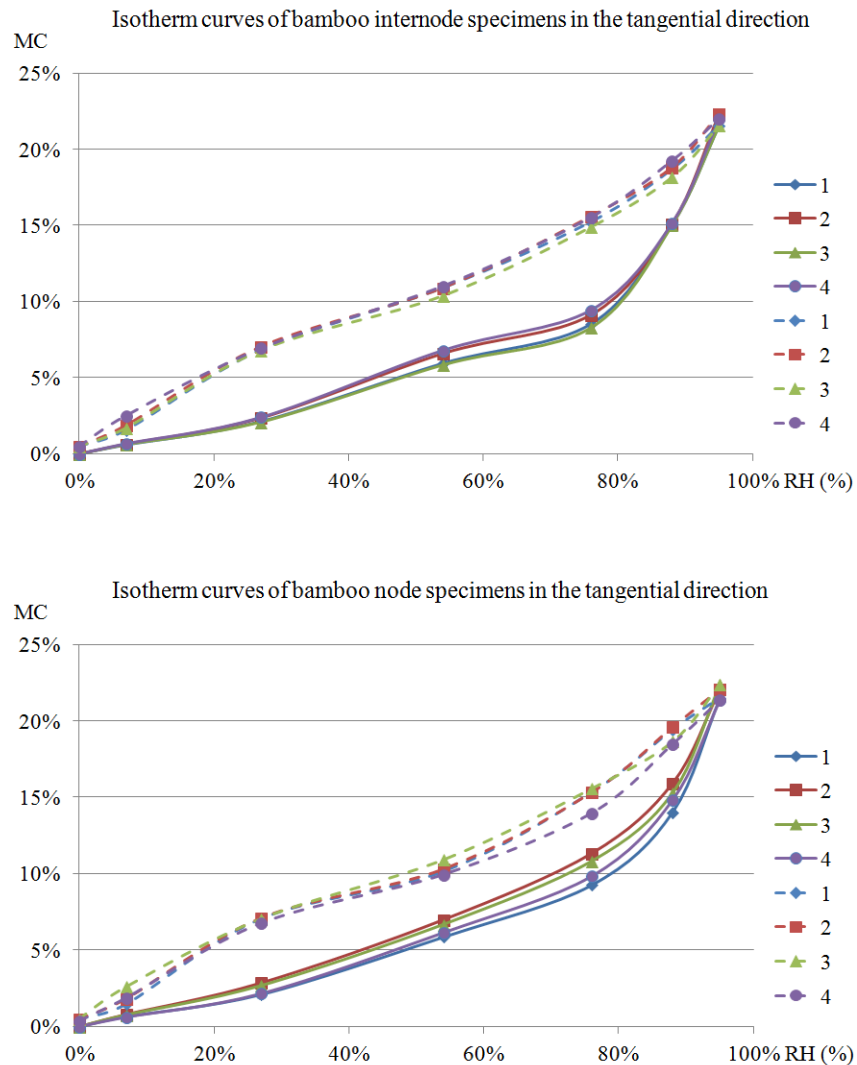


Figure 7.1.8 Sorption isotherm curves in the tangential direction

The results of Figure 7.1.8 indicate that the difference in the sorption and desorption curves for the four specimens is relatively small at internode positions compared with the node positions.

The sorption isotherm curves of Moso bamboo specimens in the longitudinal direction are shown in Figure 7.1.9. The position of the three specimens is illustrated in Figure 7.1.4.

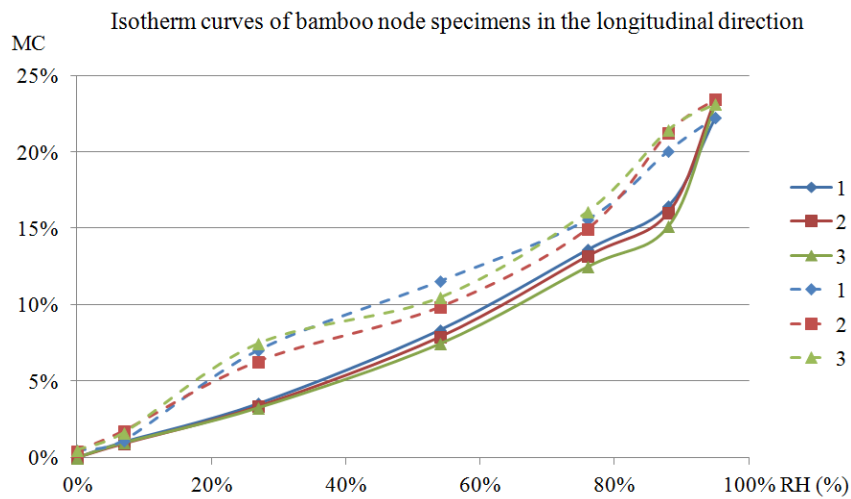
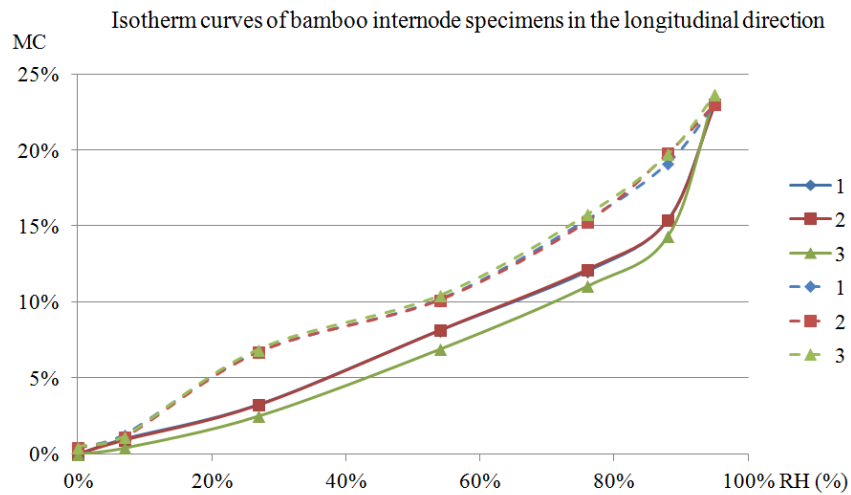


Figure 7.1.9 Sorption isotherm curves in the longitudinal direction

The results of Figure 7.1.9 indicate that the difference between the sorption and desorption curves is remarkably small between the No.1 and No.2 specimens at the internode position. The difference of sorption and desorption curves among three specimens is relatively higher at node position comparing with internode position.

Figure 7.1.10 and Figure 7.1.11 illustrate the moisture content of all specimens at different RHs in both the sorption and the desorption process. The results indicate that a trend of moisture content versus position in the culm only occurs in the radial direction.

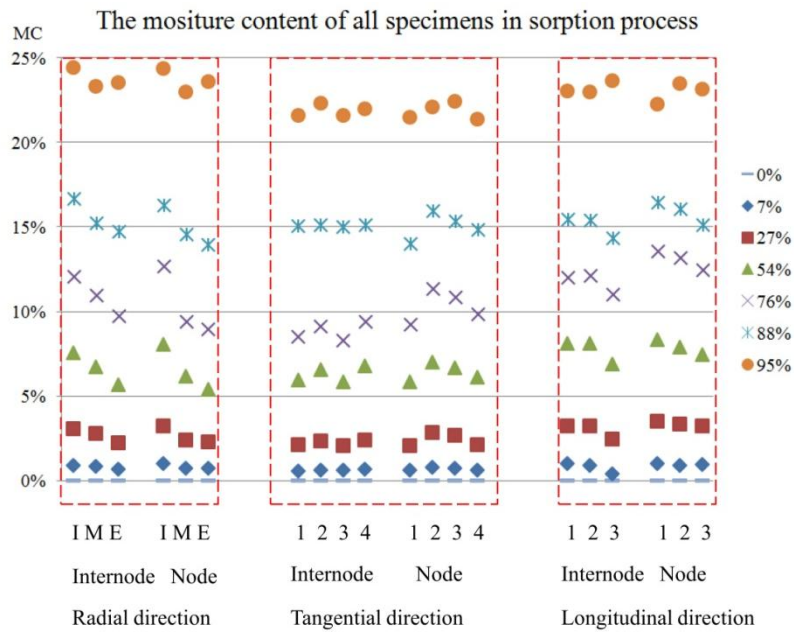


Figure 7.1.10 The moisture content of all specimens in sorption process

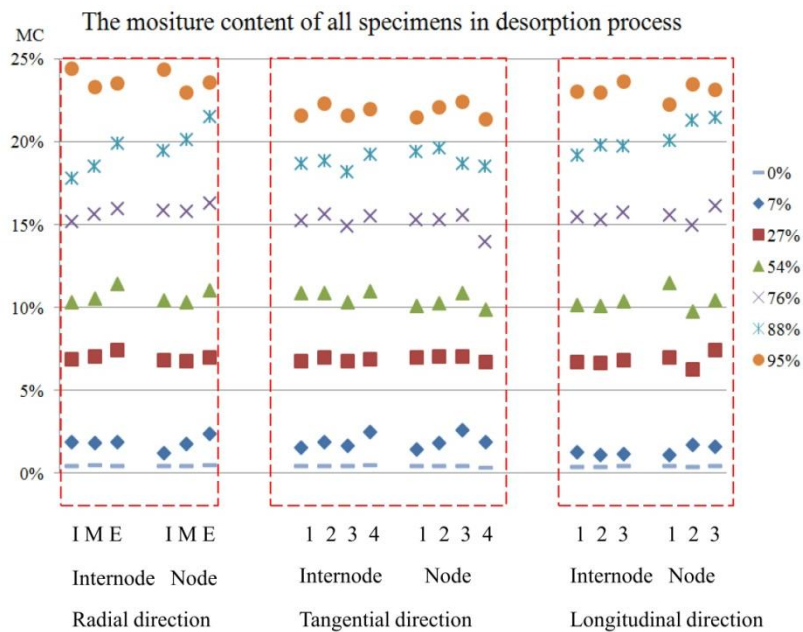


Figure 7.1.11 The moisture content of all specimens in desorption process

Figure 7.1.12 shows the hysteresis between sorption curve and desorption curve of all specimens. A gradient in moisture content difference between sorption curve and desorption curve can be found in the radial direction. The moisture content difference between sorption curve and desorption curve of specimens in longitudinal direction at the majority RH values is lower than the hysteresis of specimens in other directions.

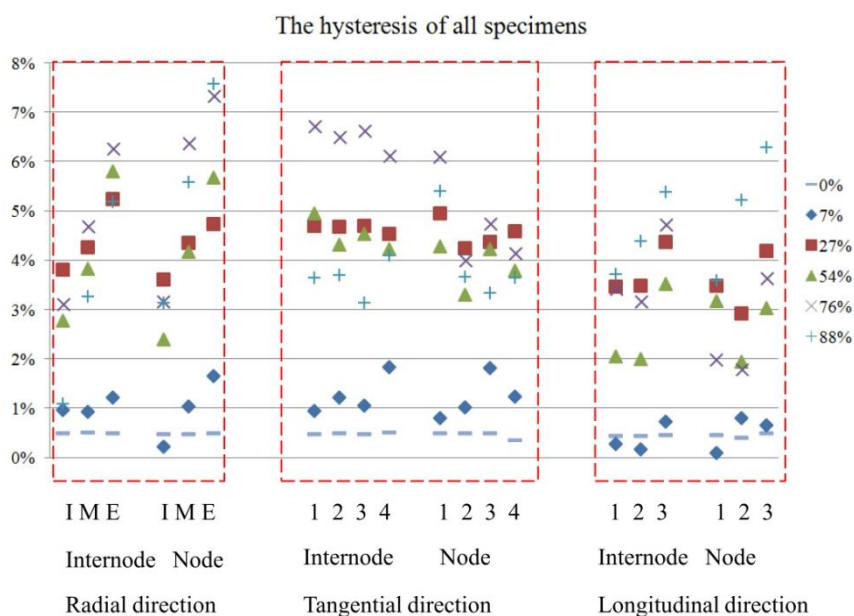


Figure 7.1.12 The hysteresis between sorption curve and desorption curve of all specimens

In the radial direction, a hygroscopic gradient appears for both sorption and desorption process. The bulk density and porosity gradient of Moso bamboo in the radial direction have been quantified in chapter 3. Low density and high porosity are the features of internal specimens while high density and low porosity are the features of external specimens. By comparing the results between the previous study and this study, a phenomenon can be discerned whereby specimens with low bulk density and high porosity can absorb more water in the sorption process and desorb more water in the desorption progress. In contrast, specimens with high density and low porosity can absorb less water in the sorption progress and desorb less water in the desorption progress. However, the hygroscopic trend is not linear with the bulk density.

The bulk density variation of bamboo in the radial direction is dominated by the distribution of the vascular bundle tissue and the parenchyma ground tissue. Specimens with a high density of vascular bundle tissue have been shown to absorb less water than specimens with a high density of parenchyma ground tissue (Ohmae and Nakato 2009). In vascular bundle tissue, a large amount of fiber cells with thick cell walls and tiny lumens provide more barriers to water absorption than the cells in parenchyma ground tissue (Liese 1985, Wang 2010). A previous study indicated that the hygroscopicity of parenchyma cells is higher than the fiber from 40% RH to higher RH levels (Jiang *et al.* 2006b).

Another feature of the hygroscopicity of bamboo specimens is that the difference between specimens from internodes is less significant than specimens from nodes. The direction and distribution of vascular bundles are possible factors which influence the hygroscopicity of bamboo specimens. Figure 7.1.13 is a Computed Tomography picture of a bamboo culm. In the internode position, the growth of vascular bundles presents a uniform vertical pattern. The direction of vascular bundles is the same. In the node position, the direction and distribution of vascular bundles present an irregular interwoven pattern.

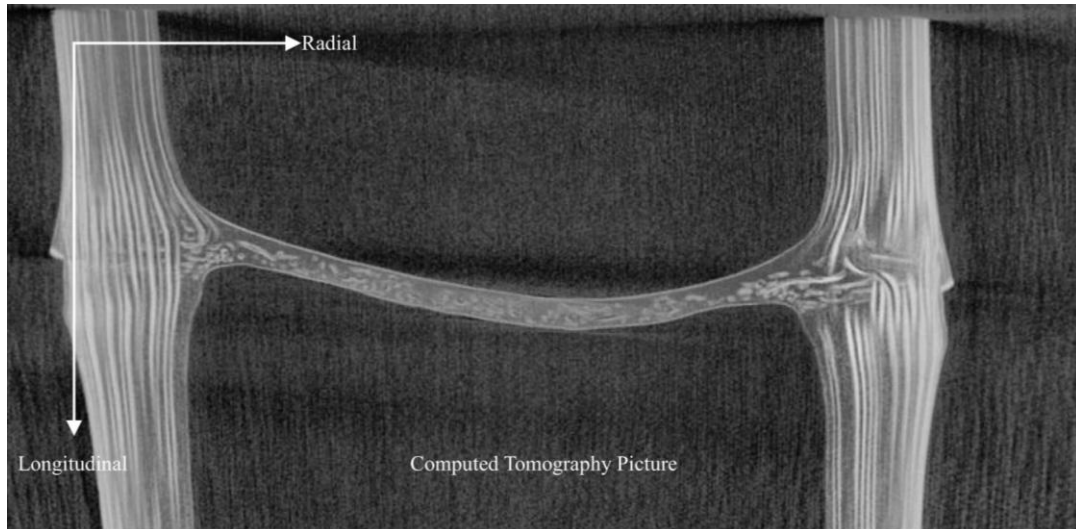


Figure 7.1.13 Computed tomography picture of a Moso bamboo culm

The hysteresis in the longitudinal direction at the majority of RH levels is less than for specimens in other directions. Figure 7.1.14 indicates that large number of vascular bundle vessels can be found in the cross-sectional (RT plane), perpendicular to the longitudinal direction. Figure 7.1.15 shows that the vascular bundle vessel has considerable interconnectivity in the longitudinal direction. Both Figure 7.1.14 and Figure 7.1.15 imply that it is relatively easy for the sorption or desorption of water through the vascular bundle vessels.

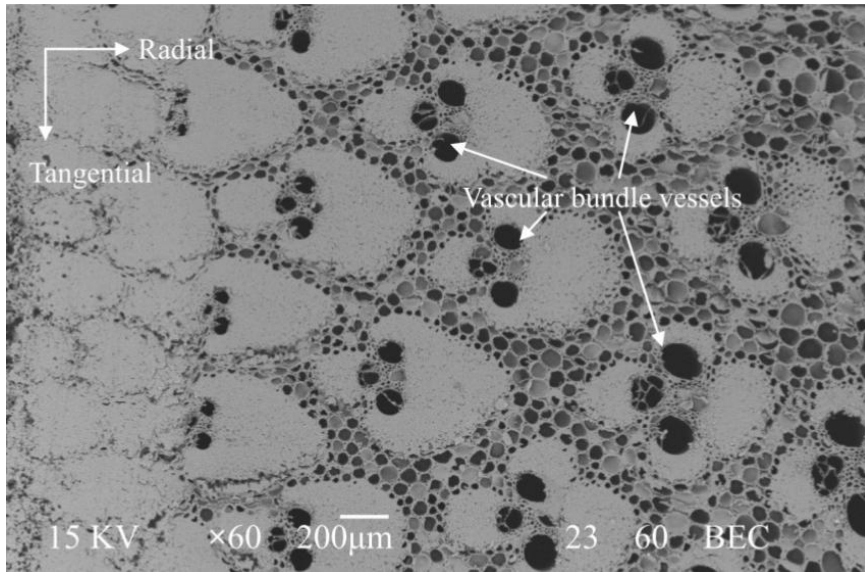


Figure 7.1.14 A backscattered electron image of the cross-section (RT plane) of Moso bamboo

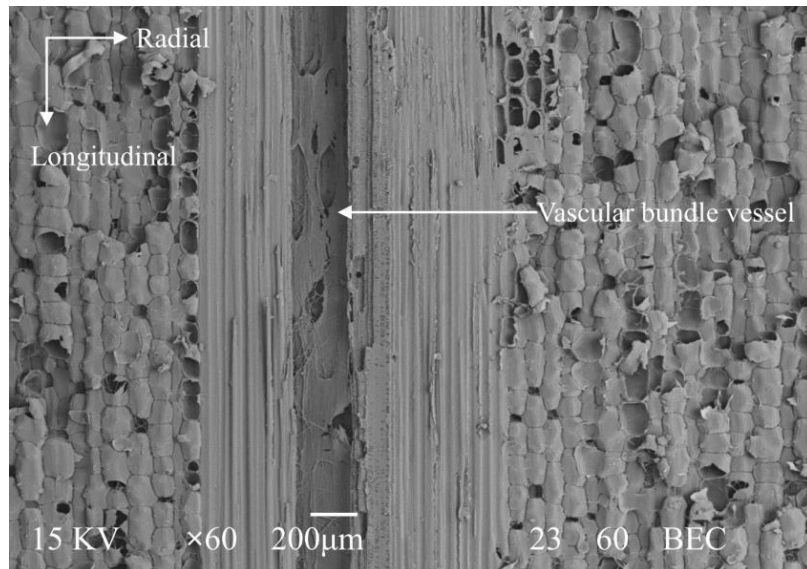


Figure 7.1.15 A backscattered electron image in the radial-longitudinal plane of Moso bamboo

7.1.4 Summary

The hygroscopic property of the Moso bamboo specimens was measured by a saturated salt solutions method. The specimens were measured in all directions of the cylindrical coordinates system at both internode parts and node parts. Both sorption and desorption processes were included in this study. The evidence from density and microstructural studies was used to indicate that a hygroscopic gradient exists in both the sorption and desorption processes in the radial direction. External specimens absorbed less water in the sorption progress and desorbed less water in the desorption progress than internal specimens. The hygroscopic difference of specimens at internodes is less significant than specimens at nodes

due to the distribution of vascular bundles. Considerable interconnectivity in the longitudinal direction can explain why the moisture content difference between sorption curve and desorption curve of specimens in the longitudinal direction at the majority of RHs is less than specimens in other directions*.

(*The content of this section is from a submitted manuscript of author. See self bibliography (Huang *et al.* 2016b))

7.2 Liquid water diffusivity assumption

7.2.1 Research objective

This section aims to quantify the liquid water diffusivity in the cross section of *Phyllostachys edulis* (Moso bamboo) culm wall. However, due to the size restriction of Moso bamboo, this section attempted to provide some assumption values of liquid water diffusivity.

7.2.2 Methods

The review of the liquid water diffusivity indicated that the related research of bamboo is still under development. A method for liquid water diffusivity estimation considered the porosity and density of the material (Zillig *et al.* 2006). The equations 7.2.1 to 7.2.3 can be utilised to calculate the liquid water diffusivity.

$$D_l = D_{wcap} \exp F \left(\frac{w - w_{cap}}{w_{cap}} \right) \quad (7.2.1)$$

$$D_{wcap} = f(F) \cdot \left(\frac{A_{cap}}{w_{cap}} \right)^2 \quad (7.2.2)$$

D_l : Liquid water diffusivity (m²/s)

D_{wcap} : Capillary saturation liquid water diffusivity (m²/s)

A_{cap} : The water adsorption coefficient (kg/m²s^{0.5})

w : Water content (kg/m³)

w_{cap} : Capillary saturation moisture content (kg/m³)

Where F and $f(F)$ describe the steepness of the moisture front:

$$f(F) = \frac{F^2}{2 \cdot F - 1 - (F - 1 + (\frac{3}{2} - \frac{4}{\pi}) \cdot F^2) \cdot e^{-F}} \quad (7.2.3)$$

F : Steepness of the moisture front is usually in the range of 5 to 10 (Carmeliet and Roels 2002 and Zillig *et al.* 2006).

This method indicated that the water adsorption coefficient, capillary saturation moisture content, and the water content need to be obtained for moisture diffusivity calculation. Water content can be obtained from sorption isotherm curves. The water adsorption coefficient and capillary saturation moisture content can be measured by (BS EN ISO 15148: 2002).

However, the water adsorption coefficient cannot be measured in radial direction by the method in BS EN ISO 15148: 2002 due to the small size of the bamboo specimen. The author of this thesis has cut some specimens at both internode and node from the external surface to the internal surface of a Moso bamboo culm. The cutting positions were shown in the Figure 7.2.1.

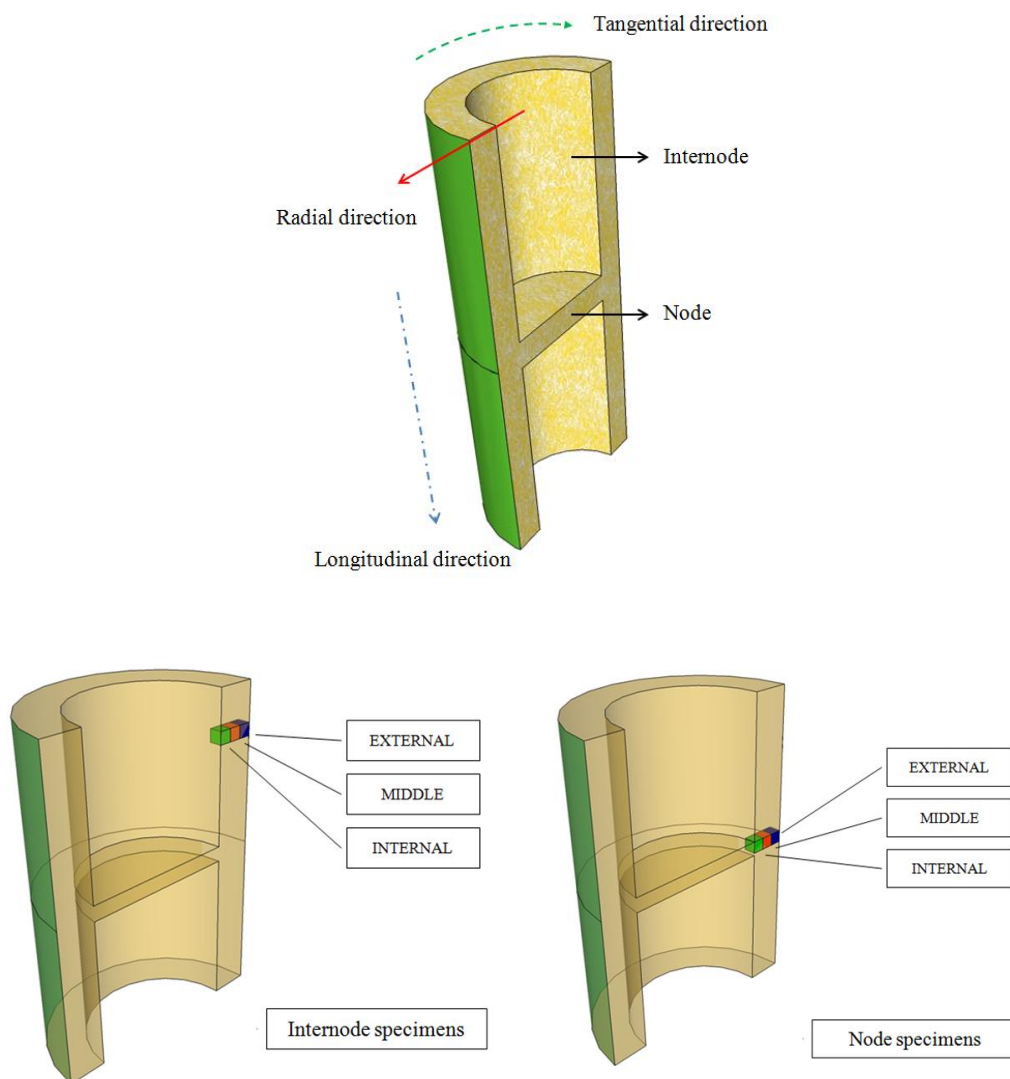


Figure 7.2.1 Cutting position of Moso bamboo specimens for water adsorption coefficient measurement

The apparatus prepared for water adsorption coefficient measurement. The maximum thickness of the bamboo specimens is 4mm in radial direction. The thickness is not enough to meet the requirement from BS EN ISO 15148: 2002. The height and length are also restricted in a relatively small size. The small volume of the bamboo specimens lead to very quick water suction and drying time. In that situation, it is impossible to obtain an accurate mass change value in a certain short time interval. Therefore, this thesis made an assumption that the liquid water diffusivity of bamboo is similar to the liquid water diffusivity of wood. Results from the chapter 3 indicated that the density and porosity of the external side of bamboo culm wall is similar to the latewood, the internal side of bamboo culm wall is similar to the earlywood.

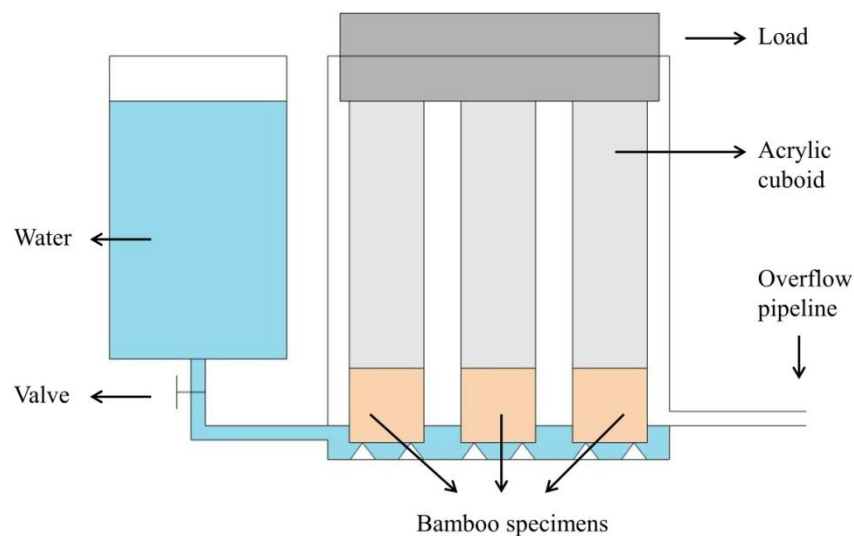


Figure 7.2.2 Testing apparatus for water adsorption coefficient measurement

7.2.3 Summary

This thesis made an assumption that the liquid water diffusivity of bamboo is similar to the liquid water diffusivity of wood. The water adsorption coefficients were set as 0.014, 0.008, and $0.0019 \text{ kg/m}^2\text{s}^{0.5}$ for external, middle, and internal parts of bamboo culm wall respectively. The capillary saturation moisture contents were set as 572, 479, and 385 kg/m^3 for external, middle, and internal parts of bamboo culm wall respectively (Zillig *et al.* 2006).

Using equation 7.2.1 to 7.2.3 on the calculation of water diffusivity of bamboo, the results are 3.7×10^{-10} to $8.6 \times 10^{-10} \text{ m/s}^2$, 2.2×10^{-12} to $3.1 \times 10^{-12} \text{ m/s}^2$, and 2×10^{-14} to $5.7 \times 10^{-13} \text{ m/s}^2$ for external, middle, and internal parts of bamboo culm wall respectively.

Chapter 8 Thermal and hygroscopic expansion characteristics of Moso bamboo

The content of this chapter has been submitted to a peer reviewed journal: *Proceedings of the Institution of Civil Engineers, Structures and Building*. See self bibliography (Huang *et al.* 2016c)

8.1 Research objectives

This study investigated the linear thermal and hygroscopic expansion characteristics of *Phyllostachys edulis* (Moso bamboo) in three directions with respect to the cylindrical coordinate system. Temperature and humidity are two common driving potentials of the expansion or contraction for bamboo. Thermal expansion is utilised to describe the deformation by temperature variation while the hygroscopic expansion, namely shrinking and swelling, are used for deformation caused by relative humidity.

8.2 Methodology

Figure 8.2.1 explains the cutting positions and directions of bamboo specimens. Three cube specimens and three cuboid specimens were respectively cut at both internode and node from the external surface to the internal surface of a Moso bamboo culm. The side length of the cube specimens was 3 ± 0.5 mm. The side length of cuboid specimens was equal to cube specimens in the radial and tangential directions. The side length of cuboid specimens in the longitudinal direction was 23 ± 0.5 mm. The cube specimens were utilised for thermal expansion measurements while the cuboid specimens were utilised for hygroexpansion measurements for the following reasons. After a number of initial measurements, the results indicated that the hygroexpansion of bamboo specimens in the longitudinal direction is in a relatively small range. The accuracy of the micrometer for hygroexpansion measurements is not enough to measure the cube specimens in the longitudinal direction. Likewise, due to the relatively higher length of the cuboid specimens in the longitudinal direction, the thermal expansion measurements in the radial and tangential directions of cuboid specimens cannot be conducted in the chamber of the dilatometer. To assess the thermal expansion in the radial and tangential directions, the size of cube specimens is more suitable for thermal expansion

measurements. The moisture content of all bamboo specimens was reduced to zero in an oven at 103 ± 2 °C. Then, the specimens were stored in a desiccator with Calcium Chloride (CaCl_2).

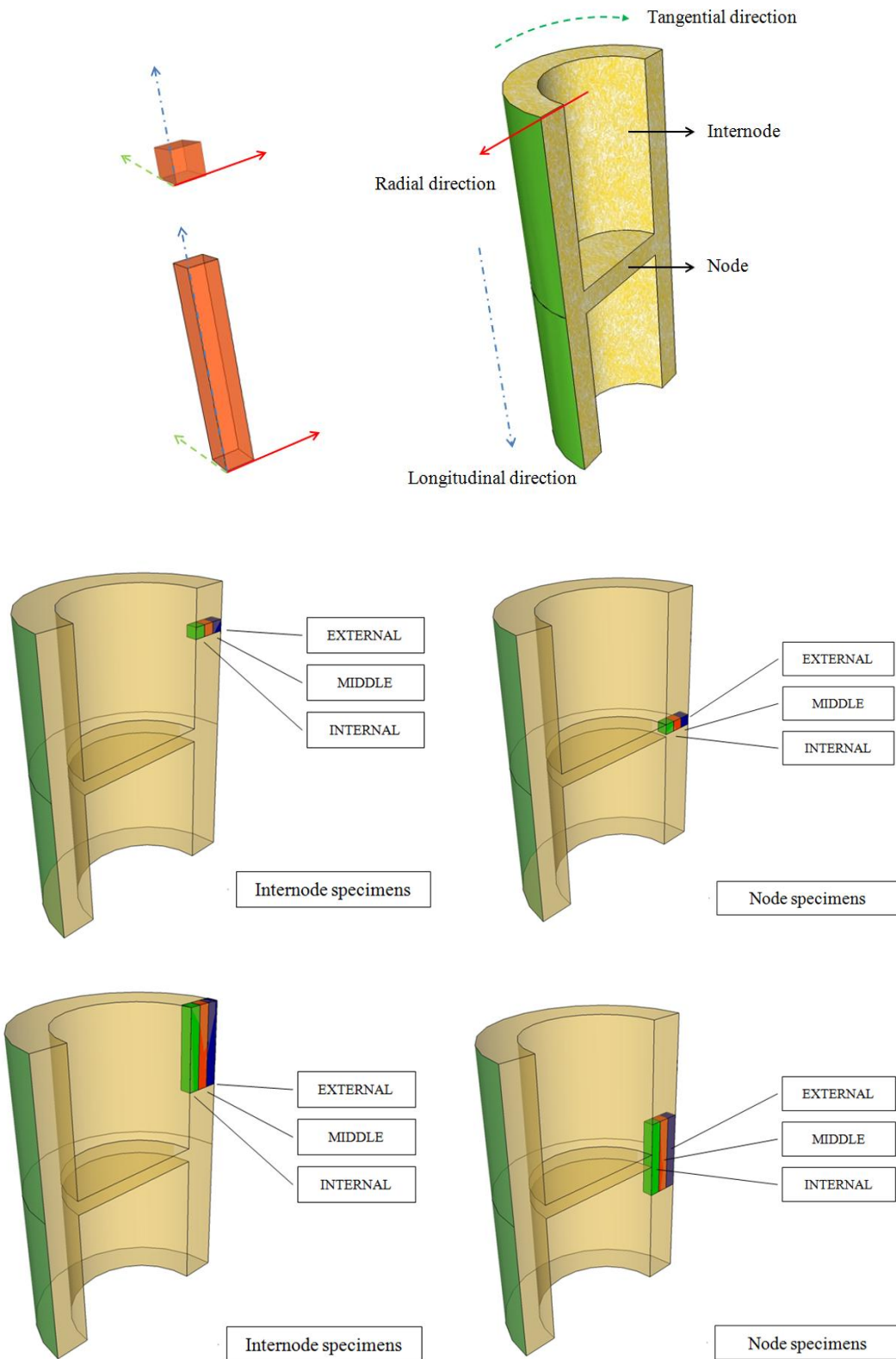


Figure 8.2.1 Cutting position and directions of bamboo specimens

The thermal expansion measurements of the bamboo specimens were conducted with a Netzsch DIL 402C dilatometer. The temperature settings of the linear thermal expansion measurement were from room temperature to 23 °C, from 23 °C to 70 °C, maintained at 70 °C for 30 minutes and from 70 °C to 23 °C. The temperature changing rate was 2 °C/min. The thermal expansion of the cube specimens was measured in the radial, tangential and longitudinal directions.

The hygroexpansion measurements were conducted in desiccators with saturated solutions. The temperature of the experiment was 23 ± 2 °C. The saturated solutions provide a steady relative humidity (RH) in a desiccator. Four saturated solutions were utilised to determine the relative humidity conditions in desiccators. Dettol fungicide was added in the Potassium nitrate (KNO_3) solution to avoid undesired mould and mildew growing of bamboo specimens. The real relative humidity conditions were also monitored by relative humidity sensors. See Figure 8.2.2.



Figure 8.2.2 The desiccator assemblies for the hygroexpansion experiment

The theoretical and actual relative humidities of the desiccators at 23 °C are listed in the Table 8.2.1.

Table 8.2.1 Relative humidities in desiccators

Substance	Theoretical RH	Real RH
MgCl ₂ 6H ₂ O	33%	27%
NaBr	57%	54%
NaCl	75%	76%
KNO ₃	93%	95%

After oven drying, all bamboo specimens were initially put into a desiccator with MgCl₂ 6H₂O saturated solution. Then, these specimens were weighed every 24 hours until the change of length among three consecutive measurements was less than 0.1%. The hygroexpansion of each specimen was calculated at this equilibrium state by equation 8.2.1.

$$S = \frac{l - l_0}{l_0} \quad (8.2.1)$$

After recording the hygroexpansion, all specimens were moved to a new desiccator. In the sorption procedure, the moving sequence of desiccators is from oven dry to MgCl₂ 6H₂O to NaBr to NaCl to KNO₃. In the desorption procedure, the moving sequence of desiccators is from KNO₃ to NaCl to NaBr to MgCl₂ 6H₂O to oven dry.

8.3 Results and discussion

8.3.1 Thermal expansion results and discussion

The thermal expansion results for the Moso bamboo specimens are illustrated in Figures 8.3.1 to 8.3.6. The left vertical axis is the linear thermal expansion. The right vertical axis represents the temperature of the dilatometer chamber. The horizontal axis shows the experiment time. The set temperature of the dilatometer is marked by a red solid line. For the radial experiment, the thermal expansion of the external specimen, middle specimen and internal specimen were designated as No.1, No.2 and No.3. The data marker of the No.1, No.2 and No.3 are solid squares with solid line, crosses with solid line and triangles with solid line. The actual temperatures of the three radial specimens in the dilatometer are marked by squares, crosses and triangles respectively.

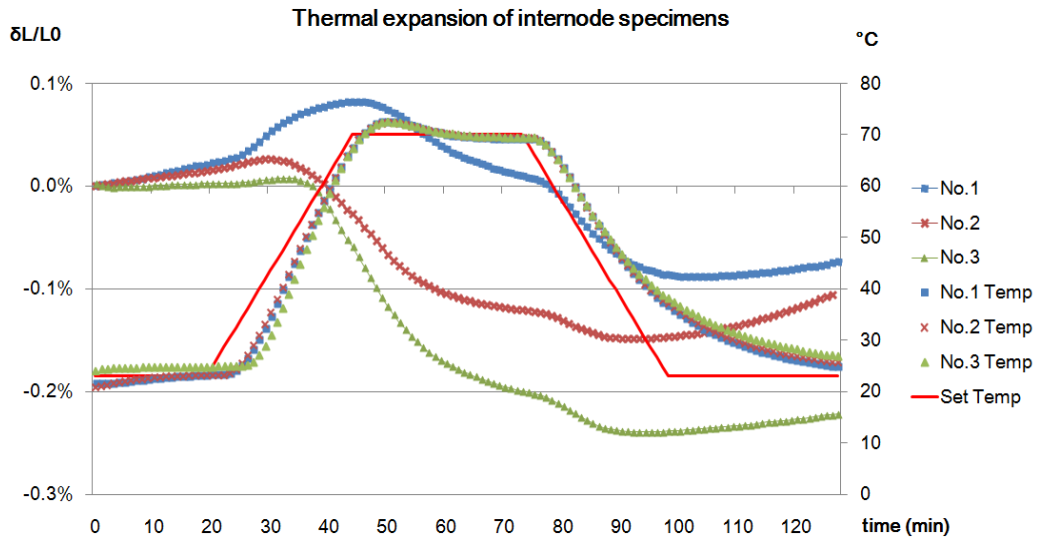


Figure 8.3.1 The thermal expansion of internode specimens in the radial direction

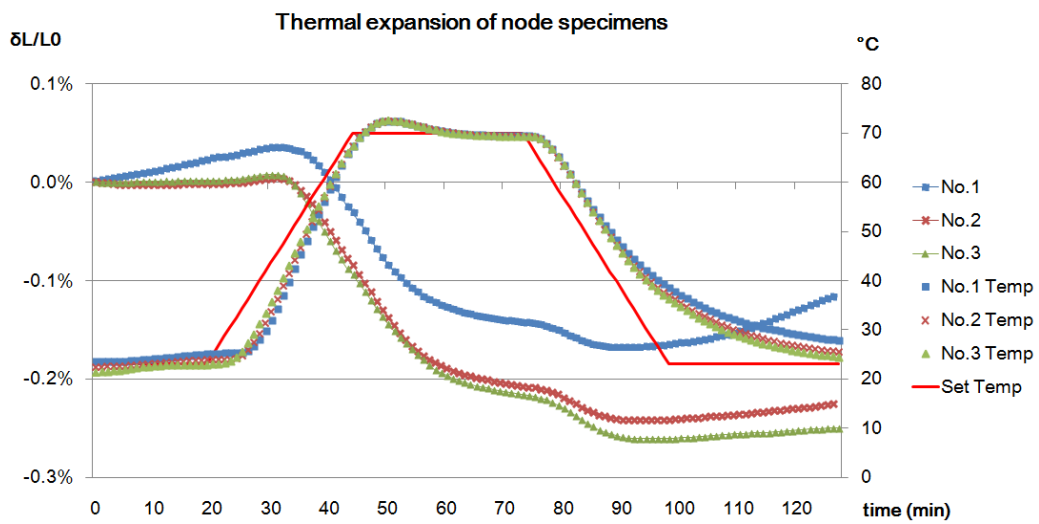


Figure 8.3.2 The thermal expansion of node specimens in the radial direction

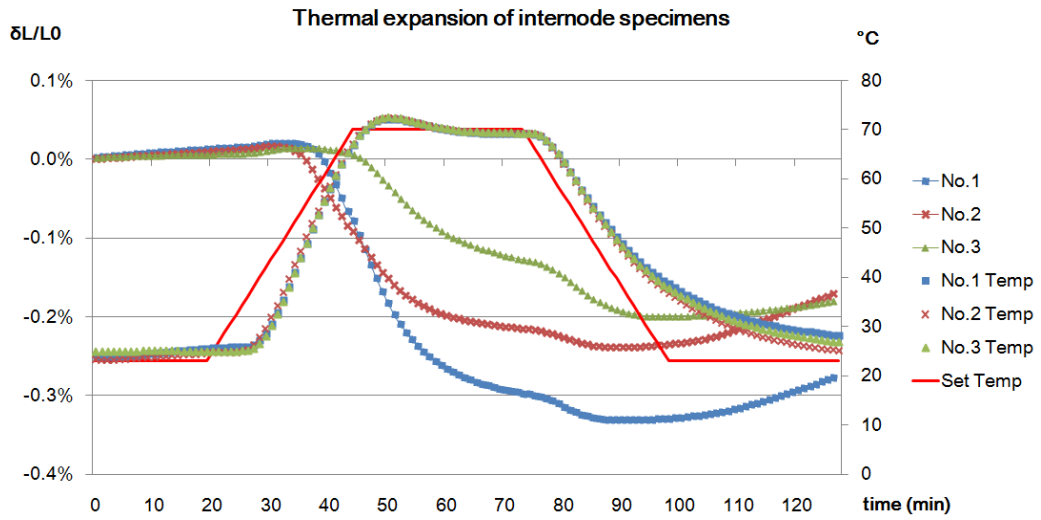


Figure 8.3.3 The thermal expansion of internode specimens in the tangential direction

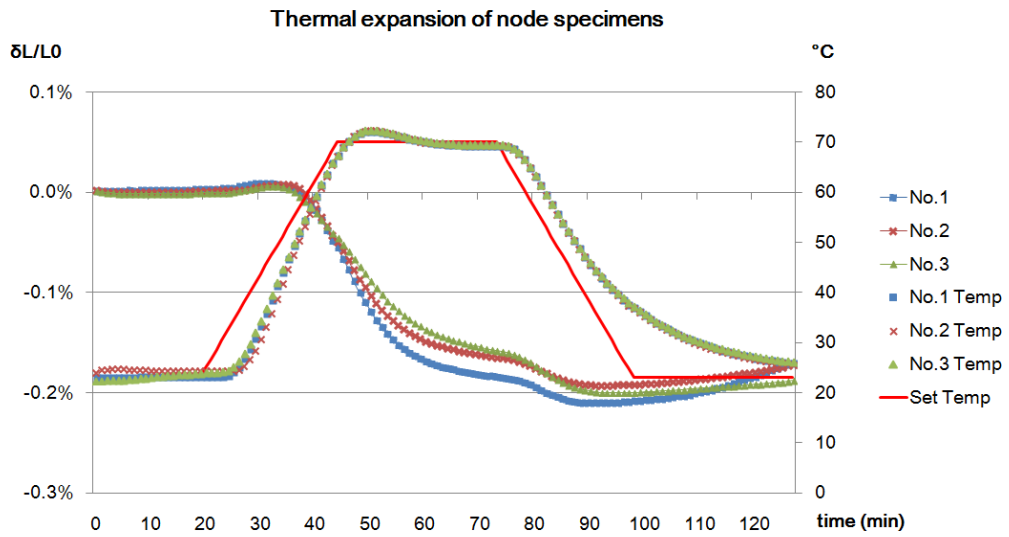


Figure 8.3.4 The thermal expansion of node specimens in the tangential direction

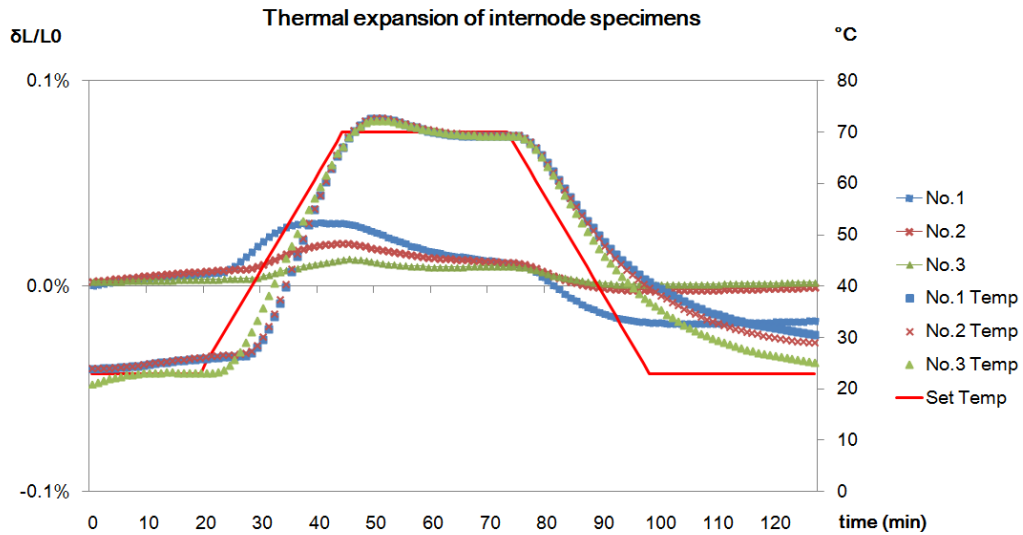


Figure 8.3.5 The thermal expansion of internode specimens in the longitudinal direction

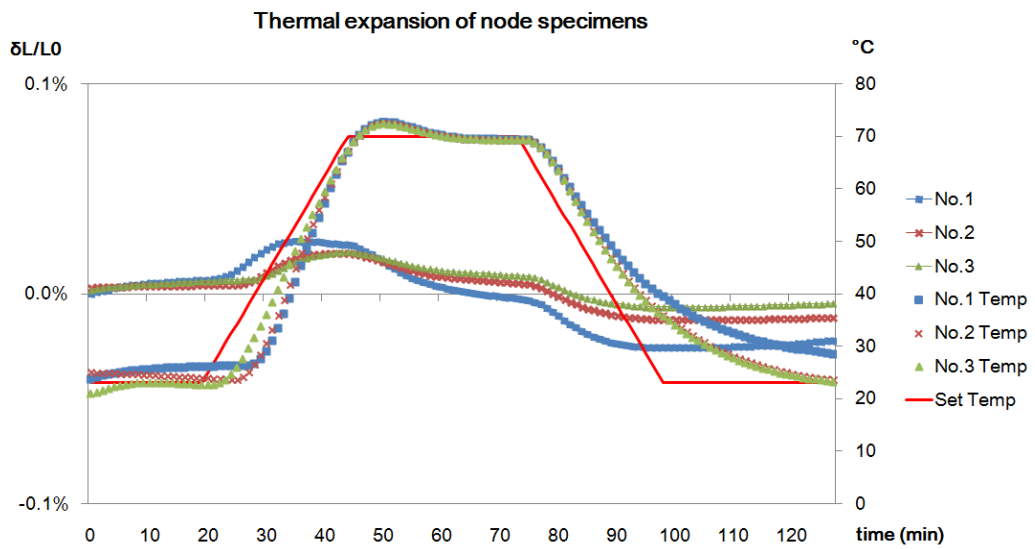


Figure 8.3.6 The thermal expansion of node specimens in the longitudinal direction

The thermal expansion results indicated that all specimens demonstrated ascent trend in the temperature ascent process. When temperature was held at 70 $^{\circ}\text{C}$, contraction occurred in all specimens. During the temperature descent process, a further contraction could be observed in the results. The contraction was mitigated once the temperature was back to room temperature. Previous studies in thermogravimetric and differential scanning calorimetry analysis reported that a noticeable weight loss, peak value of specific heat capacity and thermal conductivity can be found around 70 $^{\circ}\text{C}$ (Wu et al. 2004, Sun et al. 2006 and Li et al. 2011). This contraction was attributed to the dehydration of specimens by many researchers (e.g. Sun et al. 2006, Li et al. 2011 and Dong and Xiong 2014). In the temperature ascent process, the

thermal expansion values from high to low are external specimens, middle specimens and internal specimens. The density of these specimens increased from the internal side to the external side of the bamboo culm wall, previous thermal expansion research on nine wood species indicated that the density can be considered as a factor which influences the thermal expansion (Weatherwax and Stamm 1956). The thermal expansion of the bamboo specimen in the radial and the tangential direction is one order of magnitude higher than the thermal expansion in the longitudinal direction. This phenomenon has been reported in many previous papers on wood (Hendershot 1924, Stevens 1960 and Pizzo et al. 2002). A reason is that the bond energy of fibre tissue is higher along the longitudinal direction than the radial and the tangential directions (Pizzo et al. 2002 and Tu and Xu 2008). Hori and Wada (2005) concluded that the crystal structure of the wood cellulose dominated the anisotropic thermal expansion in the three coordinate directions and the macroscopic thermal behaviour of solid wood.

8.3.2 Hygroexpansion results and discussion

The hygroexpansion results of Moso bamboo specimens are illustrated by Figures 8.3.7 to 8.3.12. The vertical axis represents the hygroexpansion value. The horizontal axis shows the humidity condition of the desiccators. The squares, crosses and triangles represent the external, middle and internal specimens respectively. The data marked with solid lines are the data from the sorption process. The data marked with dashed lines are the data from the desorption process.

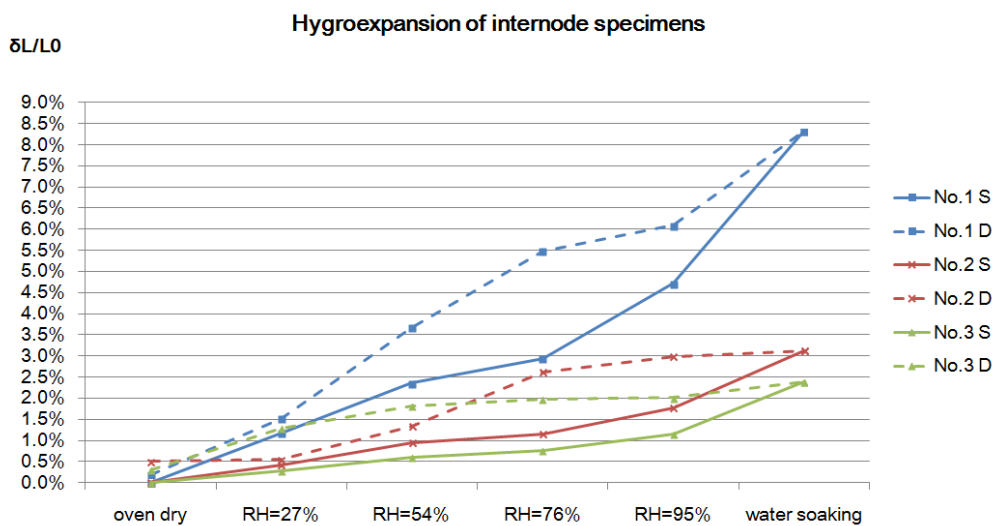


Figure 8.3.7 The hygroexpansion of internode specimens in the radial direction

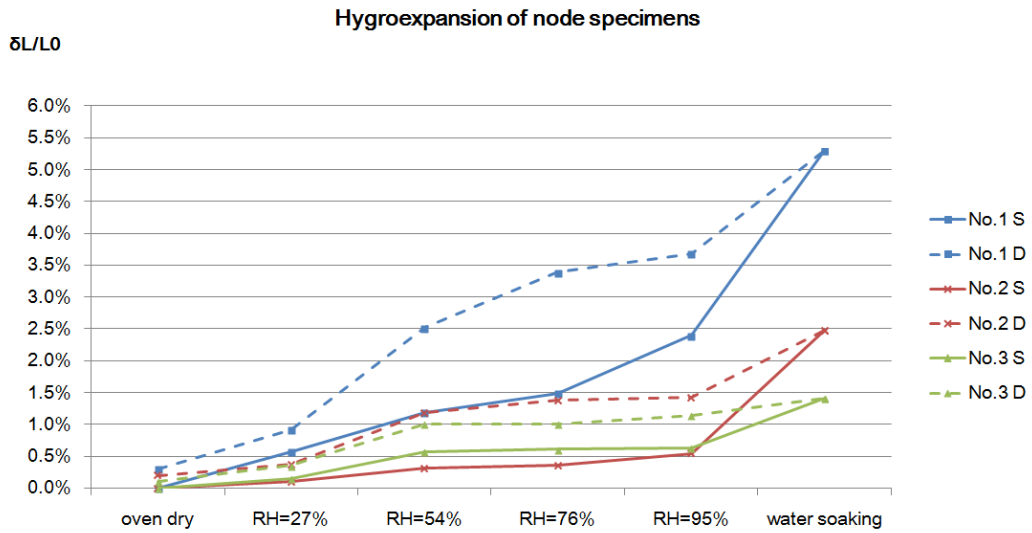


Figure 8.3.8 The hygroexpansion of node specimens in the radial direction

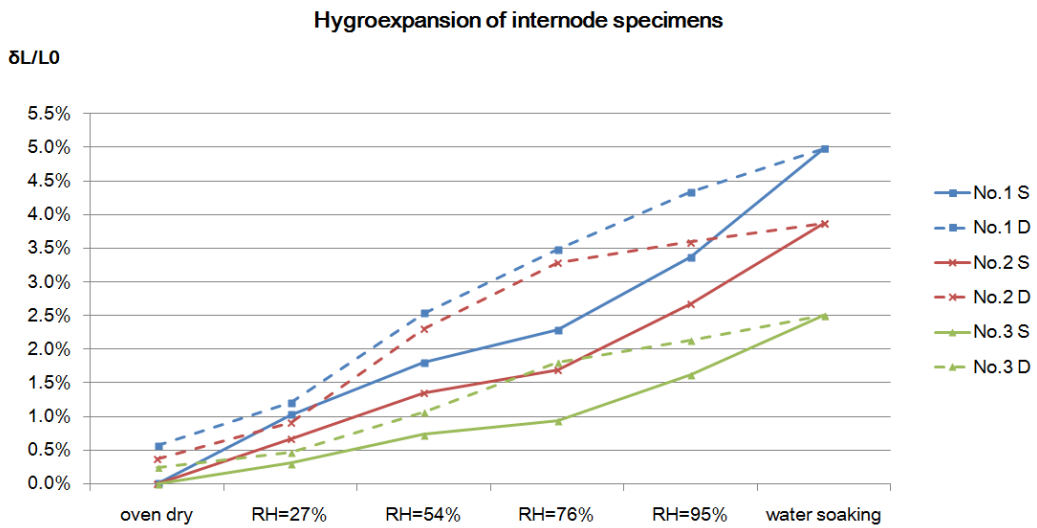


Figure 8.3.9 The hygroexpansion of internode specimens in the tangential direction

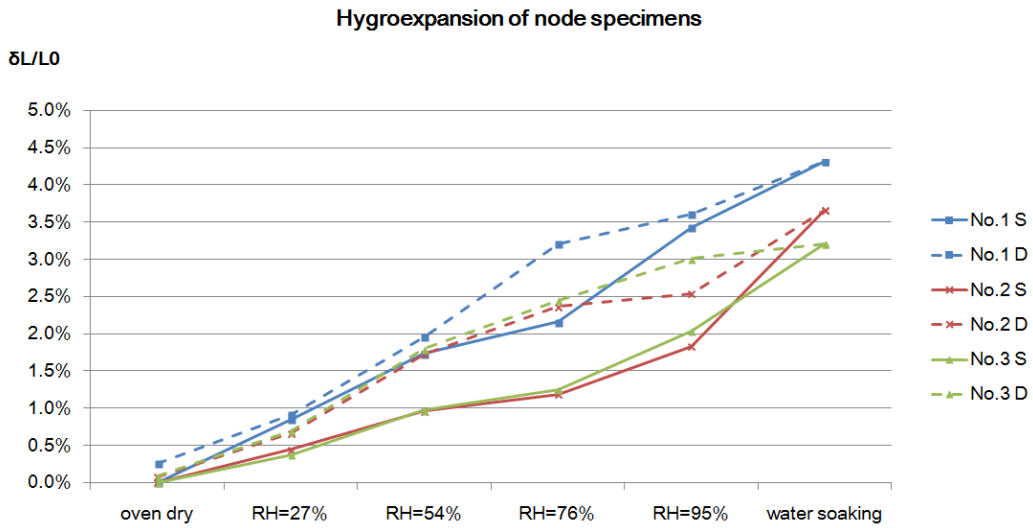


Figure 8.3.10 The hygroexpansion of node specimens in the tangential direction

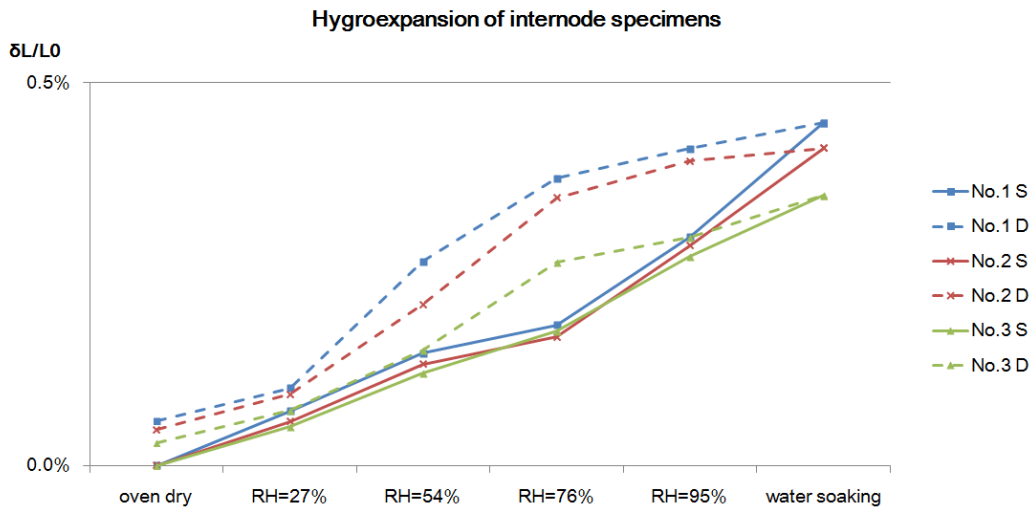


Figure 8.3.11 The hygroexpansion of internode specimens in the longitudinal direction

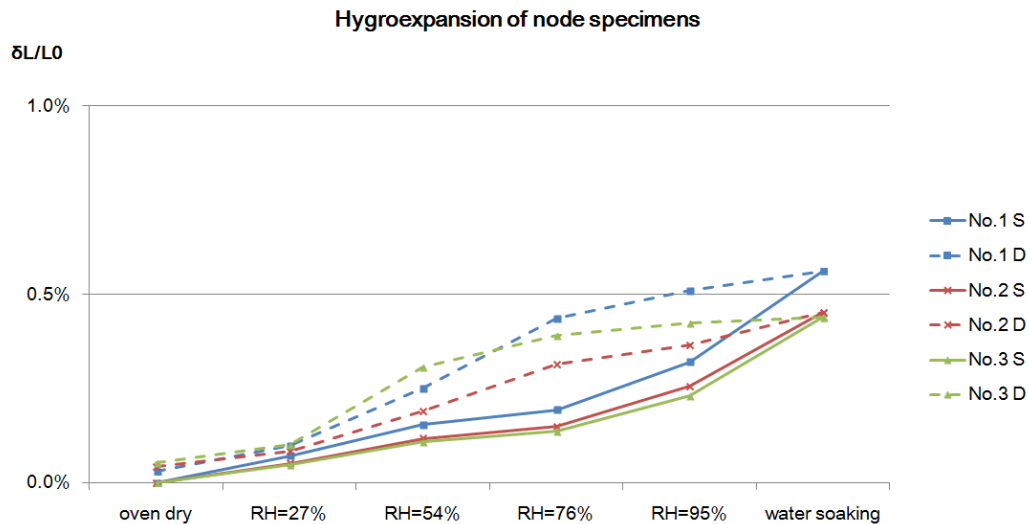


Figure 8.3.12 The hygroexpansion of node specimens in the longitudinal direction

The hygroexpansion results illustrated that the swelling of bamboo specimens increases with the relative humidity, while the expansion of bamboo specimens decreased with the relative humidity. In the radial direction, the data indicated that the hygroexpansion values from high to low were the external specimen, the middle specimen and the internal specimen. The hygroexpansion in the longitudinal direction is one order of magnitude lower than hygroexpansion in the radial and tangential directions. Tu and Xu (2008) concluded that the high proportion of vascular bundle tissue and vessels were regarded as the feature of the high hygroexpansion.

The gross wood structure, the fibre alignment and the cell-wall laying has been considered as the factors to influence the hygroexpansion in the radial and tangential directions (Pentoney 1953). The microfibril angle (MFA) theory was utilised to explain the anisotropic hygroexpansion of wood specimens (Barber and Meylan 1964). However, previous studies on the MFA of the Moso bamboo indicated that the MFA variation of Moso bamboo specimens in the radial and tangential directions was much smaller than the MFA variation of wood (Tu and Xu 2008). The MFA cannot be regarded as a decisive factor which influences hygroexpansion of bamboo (Jiang et al. 2000 and Yu et al. 2007) in these directions. However, the MFA determined that water can enlarge the distance between microfibrils but cannot enlarge the length of microfibrils (Tu and Xu 2008).

Researches on the late wood and early wood indicated that the hygroexpansion of the early wood is highly dominated by the late wood (Pentoney 1953 and Skaar 1988). Although no growth rings can be found in the anatomic structure of bamboo, remarkable density difference between the vascular bundle tissue and parenchyma ground tissue is similar to the density difference between the early wood and late wood. High density may lead to large thermal expansion for bamboo.

The thermal expansion and hygroexpansion results showed that the swelling or shrinkage which is caused by moisture variation is much higher than that caused by temperature variation. The driving potential of the thermal expansion can be attributed to that the amplitude of the lattice vibration increasing when the temperature is increased. For hygroexpansion, the water replaces the space to fill the holes between the solid subjects of bamboo when the moisture content is increasing. The difference of driving potentials of the mass transfer and energy transfer leads to the different levels of deformation. Therefore, the effect of moisture variation on the expansion of Moso bamboo based building materials is much greater than temperature variation.

8.4 Summary

The thermal expansion and hygroexpansion of Moso bamboo specimens have been measured whilst increasing and then decreasing the temperature and moisture content respectively. The thermal expansion measurements were conducted with a dilatometer. The hygroexpansion of bamboo specimens was measured with a micrometer and desiccators using different saturated salt solutions.

The thermal expansion of the bamboo specimen in the radial and the tangential direction is one order of magnitude higher than the thermal expansion in the longitudinal direction. The hygroexpansion results illustrated that the swelling of bamboo specimens increases with the relative humidity while the expansion of bamboo specimens decreases with reduction in relative humidity. In the radial direction, the data indicated that the hygroexpansion values from high to low were the external specimen, the middle specimen and the internal specimen. The hygroexpansion in the longitudinal direction is one order of magnitude lower than hygroexpansion in the radial and tangential directions. The thermal expansion and hygroexpansion results showed that the swelling or shrinkage which was by moisture variation is much higher than that caused by temperature variation*.

(*The content of this chapter is from a submitted manuscript of author. See self bibliography (Huang *et al.* 2016c))

Chapter 9 Heat and moisture transfer behaviour of Moso bamboo based panels

The content of this chapter has been submitted to a peer reviewed journal: *Construction and building materials*. See self bibliography (Huang *et al.* 2016d).

9.1 Research objectives

This chapter focuses on the heat and moisture transfer behaviours of the *Phyllostachys edulis* (Moso bamboo) panels in various temperature and relative humidity conditions. To prepare this study, a number of experiments have been conducted to acquire the data of density, specific heat capacity, thermal conductivity, water diffusivity, water vapour permeability and sorption isotherm curve of Moso bamboo. These experiments indicated that Moso bamboo demonstrated non-homogeneous hygrothermal properties in different directions. Especially in the radial direction, the ratio of vascular bundle tissue to the parenchymatous ground tissue varied significantly from the external side to the internal side (See Figure 9.1.1). To quantify the influence of the non-homogeneous hygrothermal properties on the temperature and relative humidity, both experimental studies and simulation prediction works are included in this chapter.

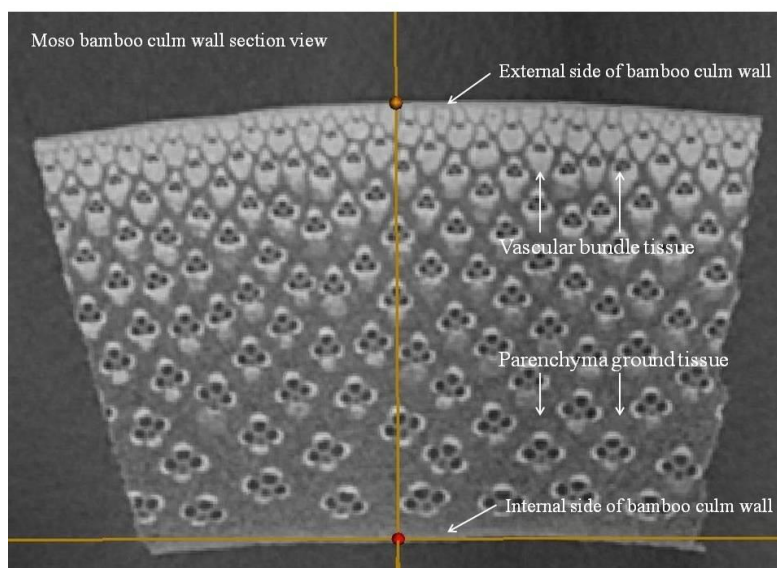


Figure 9.1.1 Section view of a Moso bamboo culm wall

9.2 Methodology

9.2.1 Heat and moisture transfer experiment design

Four Moso bamboo panels were prepared for heat and moisture transfer experiments. All panels were made from laminated Moso bamboo strips. The cutting position of the bamboo strips is illustrated by Fig 9.2.1. Panel 1 was laminated from the strips from the external surface of bamboo culm wall. Panel 2 was made by the strips from the internal surface. These two panels were utilised to study the cutting position caused variation of the hygrothermal performance. Panel 3 and panel 4 were laminated from three types of bamboo strips. Both two panels have the same middle layer. Panel 3 utilised the external strips as the outdoor surface while Panel 4 utilised the internal surface as the outdoor surface. These two panels were prepared to demonstrate the direction of lamination caused variation of the hygrothermal performance.

The panel manufacturing plan based on the following considerations: In the radial direction, bamboo culms demonstrated obvious non-homogeneous features in terms of hygrothermal performance. The minimum glue was used in this lamination method. The manufacture method is simple and it is easy for mass production.

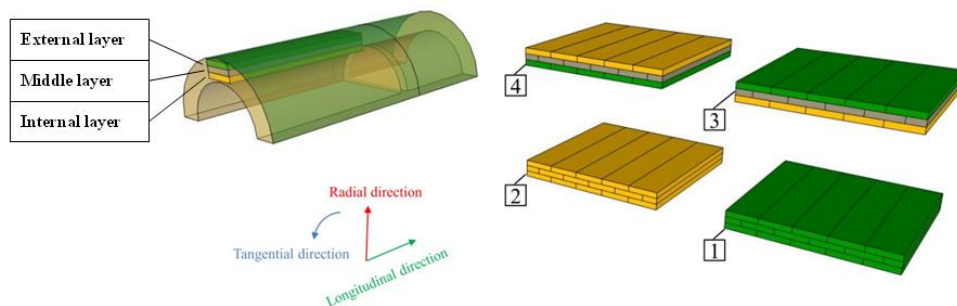


Figure 9.2.1 Four types of bamboo laminated panels

The dimensions of the panel are illustrated by Figure 9.2.2. Grooves were milled on the bamboo strips. The temperature and RH sensors were embedded in the middle point of every layer of the bamboo strip. The monitor points were nominated as No.1, No.2, and No.3 from left to right (See Figure 9.2.3). Two extra bamboo strips were utilised to fill the gap and to fix the sensors in-between two grooves. The side surfaces of the bamboo panel were insulated with wax to avoid undesired heat and moisture losses. Four panels were assembled using the same method. Each panel used three groups of temperature and RH sensors.

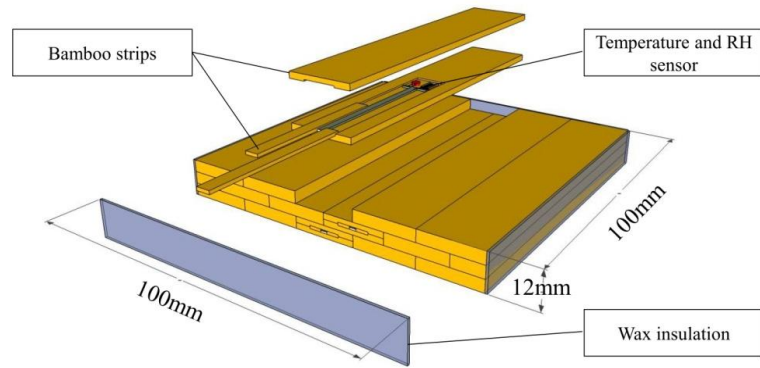


Figure 9.2.2 The assembling of the bamboo panel with the temperature and RH sensor

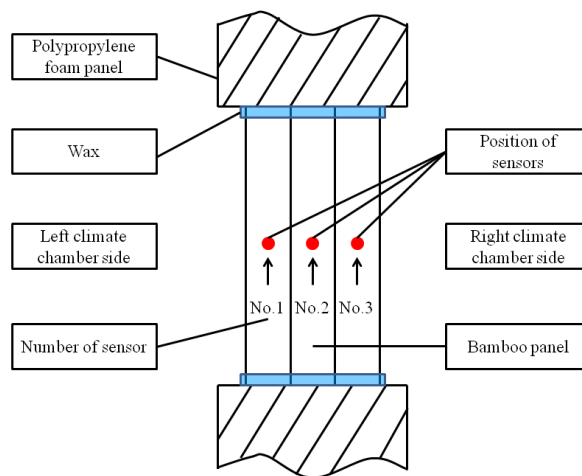


Figure 9.2.3 The edge section of bamboo panels with the temperature and RH sensors

The bamboo panels were fixed in a polypropylene foam panel. The external surface of the polypropylene foam panel was covered by the aluminium foil tapes. (See Figure 9.2.4) The polypropylene foam panel was placed between two climate chambers. The left climate chamber was utilised to simulate the outdoor temperature and RH conditions. The right climate chamber remained at constant temperature and RH values. The polypropylene foam and wax insulation aim to ensure that the heat and moisture flow are perpendicular to the surface with the largest area of bamboo panel.

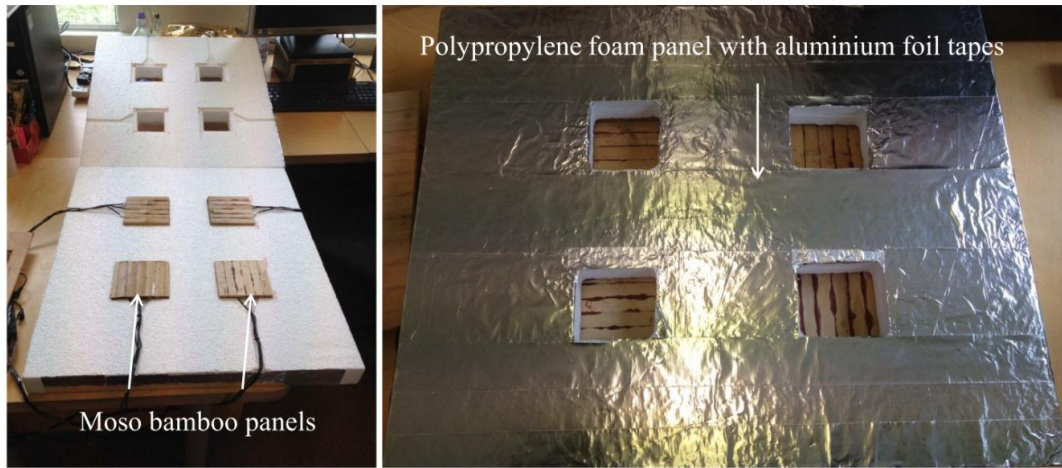


Figure 9.2.4. Bamboo panels in a special designed polypropylene foam panel

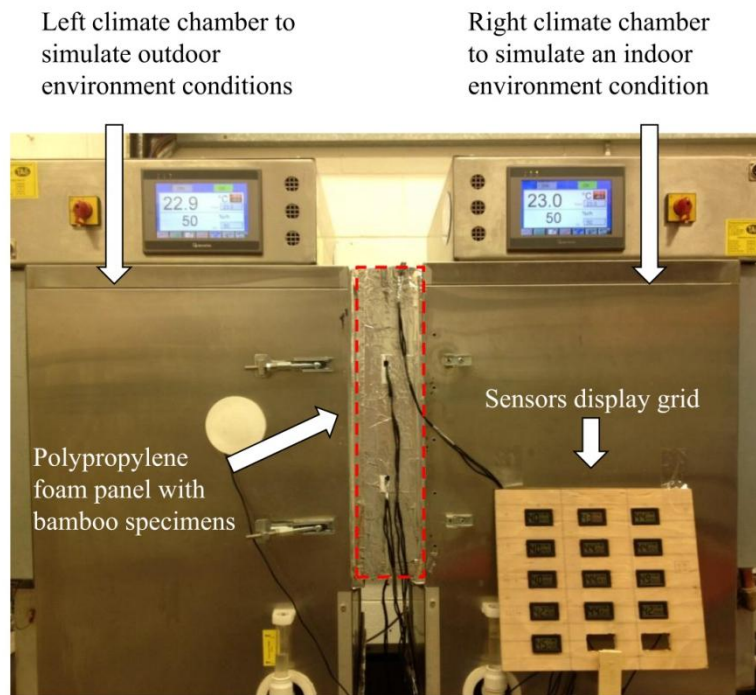


Figure 9.2.5 Twin climate chambers for heat and moisture transfer study

The temperature and RH condition plan is summarised by table 9.2.1.

Table 9.2.1 The temperature condition plan of two climate chambers

Step number	Time	Left climate chamber condition		Right climate chamber condition	
1	0-Day 1	25 °C	50% RH	25 °C	50% RH
2	Day 1 – Day 4	15 °C	90% RH		
3	Day 4 – Day 8	25 °C	50% RH		
4	Day 8 – Day 11	35 °C	10% RH		
5	Day 11 – Day 15	25 °C	50% RH		

All bamboo panels were stored in the right climate chamber until the temperature and RH became uniform. Then, the panels were sealed between two climate chambers with same initial conditions for 24 hours. A relatively cold and moist climate condition (15 ° and 90% RH) was set for the left climate chamber for 3 days at first. The temperature and RH condition of the left climate chamber were reset to the same initial condition with the right climate chamber for 4 days. The left climate chamber was set to provide a relatively hot and dry climate condition (35 ° and 10% RH) for 3 days. The experiments were terminated after both chambers had maintained same condition for 4 days. The temperature and RH data were recorded every 5 minutes.

9.2.2 Heat and moisture transfer simulation

The numerical modelling method of coupled heat and moisture transfer in this study is based on the following PDEs (See equation 9.2.1 and 9.2.2). The PDEs are also utilised in MOISTURE-EXPERT and WUFI software (Kunzel and Kiessl 1996, Delgado et al. 2012 and Nusser and Teibinger 2012). However, variables and conditional parameters were widely utilised in the inputs of this study. To satisfied these specific and flexible requirement, COMSOL Multiphysics and Matlab software were involved in this study.

$$\frac{\partial H}{\partial T} \frac{\partial T}{\partial t} = \nabla(\lambda \nabla T) + h_v \nabla[\delta_p \nabla(\varphi P_{sat})] \quad (9.2.1)$$

$$\frac{\partial w}{\partial \varphi} \frac{\partial \varphi}{\partial t} = \nabla[(D_l \nabla \varphi + \delta_p \nabla(\varphi P_{sat})] \quad (9.2.2)$$

$\frac{\partial H}{\partial T}$ Heat storage capacity (J/m³ K)

T Temperature (K)

t Time (s)

λ Thermal conductivity (W/m K)

h_v Evaporation enthalpy of water (J/kg)

δ_p Water vapour permeability (kg/m s Pa)

φ Relative humidity

P_{sat} Saturated pressure of water vapour (Pa)

W water content of the bamboo substance (kg/m³)

$\frac{\partial w}{\partial \varphi}$ Moisture capacity $\frac{\partial w}{\partial \varphi} = \xi$

D_l Liquid water diffusivity (m²/s)

∇ : Gradient operator $\nabla T = \frac{\partial T}{\partial x}$ in one dimension

To solve the PDEs, at least 6 input parameters, temperature and RH initial and boundary conditions need to be known. The data of 6 input parameters are summarised by table 9.2.2. Although some data of the whole Moso bamboo culms have been worked out before, the detailed data to reflect the gradient variation and non-homogenous hygrothermal properties of Moso bamboo were still insufficient. The data of table 9.2.2 were accumulated by the previous works of the authors for this paper.

Table 9.2.2 The essential parameters for heat and moisture transfer PDEs

Input parameters	External	Middle	Internal	Method of measurement
Density (kg/m ³)	1157	723	474	CT (Huang <i>et al.</i> 2015)
Thermal diffusivity (m ² /s)	6.36×10 ⁻⁷	1.74×10 ⁻⁷	1.28×10 ⁻⁷	Flash tube
Specific heat capacity	See fig 9.2.6			DSC
Thermal conductivity at 25 °C (W/m K)	1.12	0.19	0.09	Calculated by Equation 3
Water liquid diffusivity (m ² /s)	6.15×10 ⁻¹⁰	2.65×10 ⁻¹²	2.95×10 ⁻¹³	Partial immersion (BS 15148: 2002 +A1:2016)
Water vapour diffusion resistance factor	57	42	38	Dry cup
Sorption isotherm	See figure 9.2.7			Desiccator and DVS

The average density data of Moso bamboo were obtained by a computed tomography (CT) method. The thermal diffusivity values of Moso bamboo were measured by a flash tube method. The thermal diffusivity values can be used to calculate the thermal conductivity.

The thermal conductivity was calculated by equation 9.2.3.

$$\lambda_s = \alpha \rho C_p \quad (9.2.3)$$

λ_s Thermal conductivity of bamboo solid phase (W/m K)

α Thermal diffusivity (m²/s)

ρ Density (kg/m³)

C_p Specific heat capacity (J/kg K)

The average specific heat capacity of Moso bamboo was measured by the differential scanning calorimeter (DSC). The results are illustrated by the figure 9.2.6. The specific heat

capacity values vary as the function of temperature. Therefore, the thermal conductivity data, which are calculated by equation 3, are also the function of temperature.

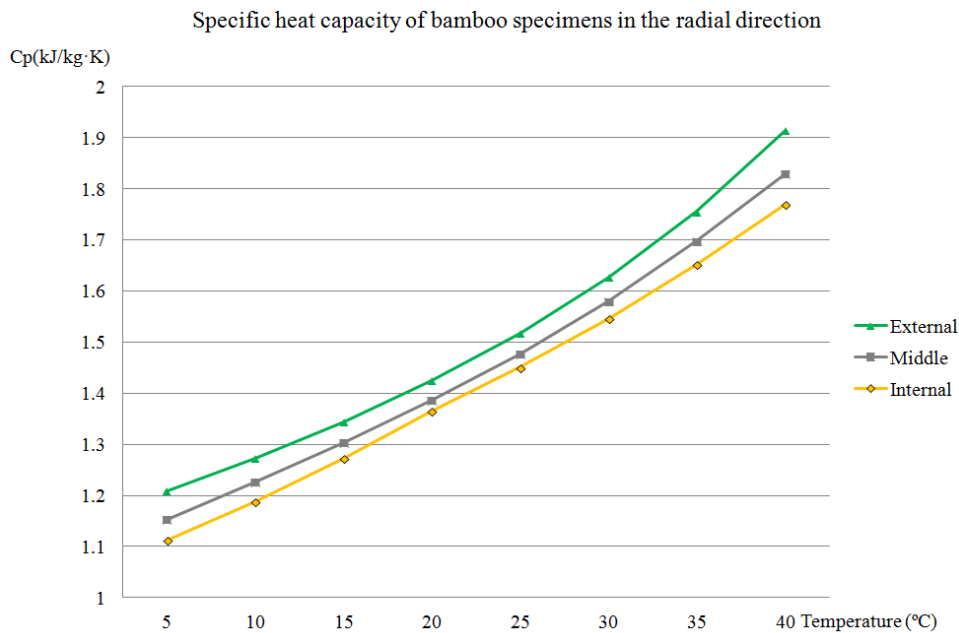


Figure 9.2.6 The average specific heat capacity results of bamboo specimens

The liquid water diffusivity of Moso bamboo was measured by a partial immersion method (BS 15148: 2002 +A1:2016). The water vapour permeability of Moso bamboo was measured by a dry cup method.

The water vapour permeable capability of a construction material is often expressed by the water vapour diffusion resistance factor. The water vapour diffusion resistance factor was calculated by equation 9.2.4.

$$\mu = \frac{\delta_{air}}{\delta_p} \quad (9.2.4)$$

μ Water vapour diffusion resistance factor, dimensionless

δ_{air} Water vapour permeability of air (kg/m s Pa)

δ_p Water vapour permeability of the specimen (kg/m s Pa)

The water vapour permeability of air can be calculated by equation 9.2.5.

$$\delta_{air} = \frac{2.306 \cdot 10^{-5} \cdot P_0}{R_v \cdot T \cdot P_a} \left(\frac{T}{273.13} \right)^{1.81} \quad 9.2.5$$

δ_{air} Water vapour permeability of air (kg/m s Pa)

P_0 Standard atmospheric pressure (101325 Pa)

R_v Gas constant for water (461.5 J/K kg)

T The temperature (K)

P_a Ambient air pressure (Pa)

The values of water vapour permeability of bamboo (δ_p) need to be inputted in the PDEs for calculation. These values vary with temperature because the water vapour permeability of the air (δ_{air}) is also a function of temperature.

The moisture capacity values of Moso bamboo were calculated by equation 9.2.6. To calculate the moisture capacity values, the sorption isotherm curves of bamboo specimens of three different layers are necessary. The sorption isotherm curves were measured by the desiccator method. The sorption curves were utilised for the step number 1, 2, and 5 whilst the esorption curves were utilised for step number 3 and 4 (See table 9.2.1).

$$\frac{\partial w}{\partial \phi} = \xi \quad (9.2.6)$$

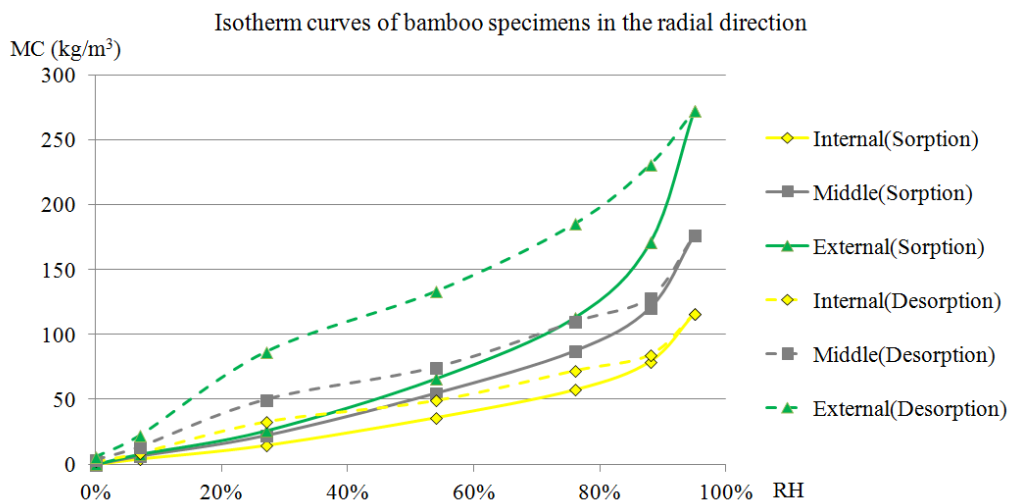


Figure 9.2.7 Sorption isotherm curves of the Moso bamboo in the radial direction

To study the influence of the moisture content on thermal properties, the equivalent thermal conductivity of a bamboo strip can be described by equation 9.2.7.

$$\lambda = \lambda_s + u''\lambda_w \quad (9.2.7)$$

λ Total or the equivalent thermal conductivity of a bamboo (W/m K)

λ_s Thermal conductivity of bamboo solid phase (W/m K)

u'' The ratio of water substance to dry wood substance, dimensionless

λ_w Thermal conductivity of water phase (W/m K)

Similarly, the heat storage capacity can be described by the equation 9.2.8:

$$\frac{\partial H}{\partial T} = (C_s + \frac{1}{\rho_s} C_w W) \rho_s \quad (9.2.8)$$

C_s Specific heat capacity of dry material (J/kg K)

ρ_s Bulk density of the dry material

C_w Specific heat capacity of water (J/kg K)

9.2.3 Boundary conditions

The heat boundary condition of this study is classified as the Robin condition. The two surfaces, which are exposed to the two climate chambers, are regarded as the convective surfaces. Therefore, the heat flux density and moisture flux density of two convective surfaces can be described by equation 9.2.9 and 9.2.10.

$$q = h(T_a - T_b) \quad (9.2.9)$$

q Heat flux density (W/m²)

h Heat transfer coefficient (W/m² K)

T_a Temperature of the ambient air (K)

T_b Temperature of the bamboo surface (K)

$$\dot{m} = h_m(\rho_a - \rho_b) \quad (9.2.10)$$

\dot{m} Water vapour flux density (kg/m² s)

h_m Water vapour transfer coefficient driven by the difference of water vapour density (m/s)

ρ_a Density of the water vapour in the ambient air (kg/m³)

ρ_b Density of the water vapour in the bamboo surface (kg/m³)

In this study, the water vapour flux density needs to be calculated by the relative humidity. Therefore, the equation 9.2.10 can be changed to equation 9.2.11.

$$\dot{m} = h_{mRH}(\varphi_a - \varphi_b) \quad (9.2.11)$$

\dot{m} Water vapour flux density (kg/m² s)

h_{mRH} Water vapour transfer coefficient driven by the difference of RH (kg/m² s)

φ_a RH of the water vapour in the ambient air (kg/m³)

φ_b RH of the water vapour in the bamboo surface (kg/m³)

The RH can be expressed by the ratio of the density of the water vapour in a medium to the saturated density of the water vapour (See equation 9.2.12 and equation 9.2.13).

$$\varphi_a = \frac{\rho_a}{\rho_{sat}} \quad (9.2.12)$$

$$\varphi_b = \frac{\rho_b}{\rho_{sat}} \quad (9.2.13)$$

ρ_a Density of the water vapour in the ambient air (kg/m³)

ρ_b Density of the water vapour in the bamboo surface (kg/m³)

ρ_{sat} Saturated density of the water vapour (kg/m³)

Therefore, the water vapour transfer coefficient in this study can be calculated by equation 9.2.14. This coefficient is a variable of temperature because the saturated density of the water vapour varies with temperature.

$$h_{mRH} = \rho_{sat} h_m \quad (9.2.14)$$

h_{mRH} Water vapour transfer coefficient driven by the difference of RH ($\text{kg/m}^2 \text{ s}$)

h_m Water vapour transfer coefficient driven by the difference of water vapour density (m/s)

ρ_{sat} Saturated density of the water vapour

9.2.4 Assumptions

The heat and moisture transfer behaviour of biological materials is fairly complex. This study examines the influence of basic hygrothermal properties on the heat and moisture transfer behaviour of Moso bamboo. A number of assumptions were made to simplify the numerical model:

- The temperature, RH, and velocity of the air in the climate chambers were regarded as constant parameters in this study.
- The heat and moisture loss from the wax insulation and polypropylene foam panel was neglected.
- The heat and moisture transfer of four bamboo panels was one dimensional.
- The expansion of bamboo panels is negligible in this study.

9.2.5 Model validation

The heat and moisture transfer models were solved by COMSOL Multiphysics™. This model was validated by the benchmark example in a British standard (BS EN 15026: 2007). The results are illustrated in figures 9.2.8 and 9.2.9. Solid lines describe the maximum and minimum values of the benchmark material. Dashed lines are the simulation results of the model applied in this study. Both temperature and moisture content results indicated that the model is reliable for the heat and moisture transfer simulation of the building material. Similar validation works has been done by other heat and moisture transfer researches on building materials. (Nusser and Teibinger 2012, and Portal *et al.* 2014)

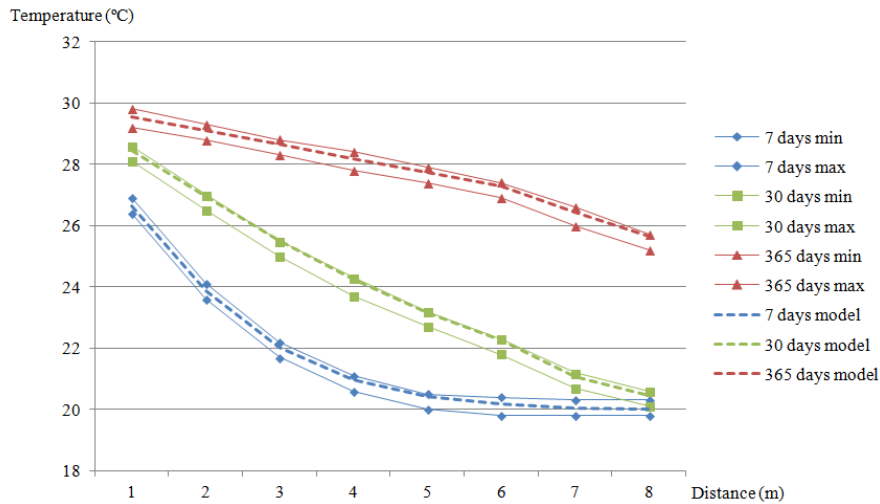


Figure 9.2.8 The benchmark validation results for temperature

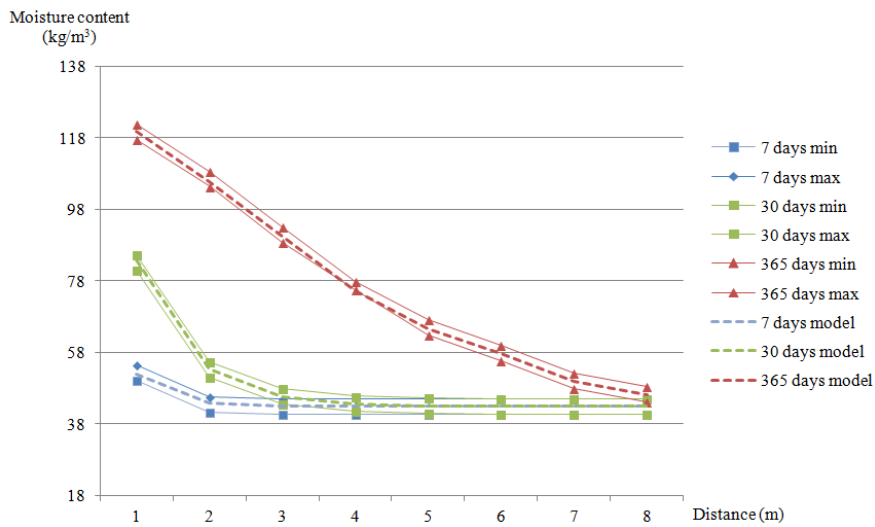


Figure 9.2.9 The benchmark validation results for moisture content

9.3. Results and discussion

9.3.1 Simulation and experimental results

The temperature results are illustrated by figure 9.3.1. The red dashed line represents the set temperature. The other dashed lines are the simulation results of three monitor points. The solid lines represent the results from experimental measurements.

It can be seen that the lowest difference among No.1, No.2, and No.3 was observed from the results of panel 1 while the highest difference among No.1, No.2 and No.3 was found from the results of panel 2. The temperature at No.3 of panel 2 is closer to the right climate chamber than the temperature at No.3 of panel 1. The results from panel 1 and panel 2 clearly indicated that bamboo internal strips have lower thermal conductivity than bamboo external strips when the heat transfer achieves equilibrium state. Similarly, the temperature at No.2

position is closer to the temperature at No.1 position for panel 3. The temperature at No.2 position is closes to the temperature at No.3 position for panel 4. The reason of this phenomenon is caused by the thermal conductivity difference of the first layers and last layers between the panel 3 and panel 4. The first layer of panel 3 is the bamboo external parts and the first layer of panel 4 is the bamboo internal parts. The results are consistent with the measured results from the thermal diffusivity and thermal conductivity calculation.

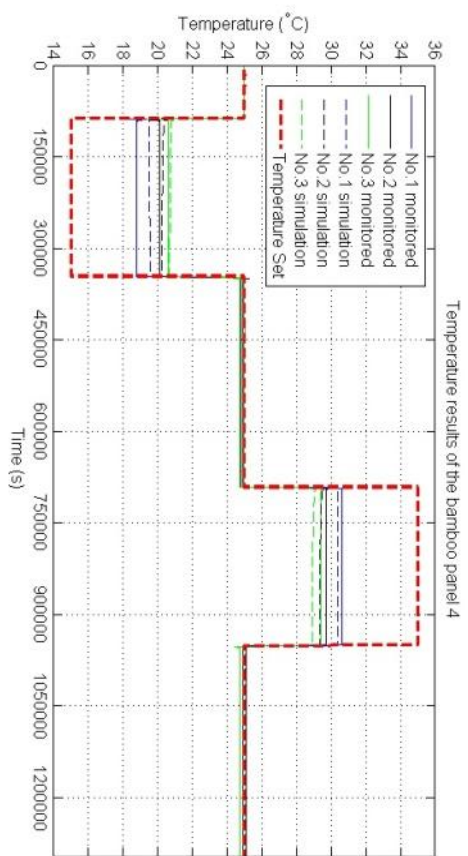
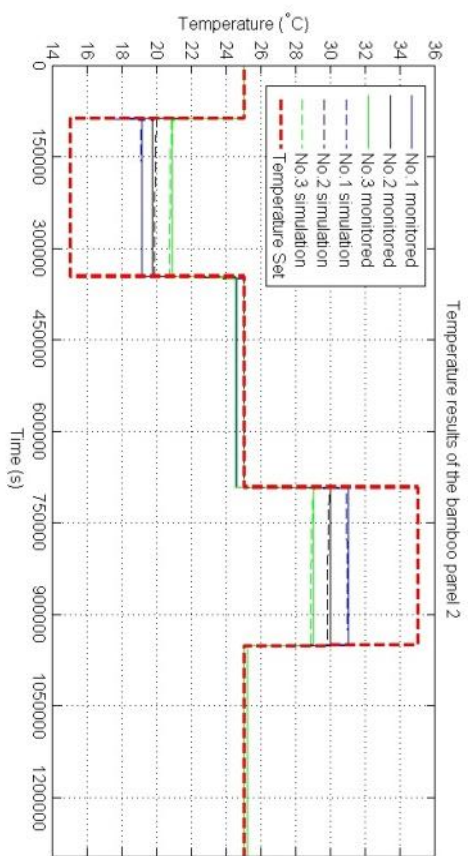
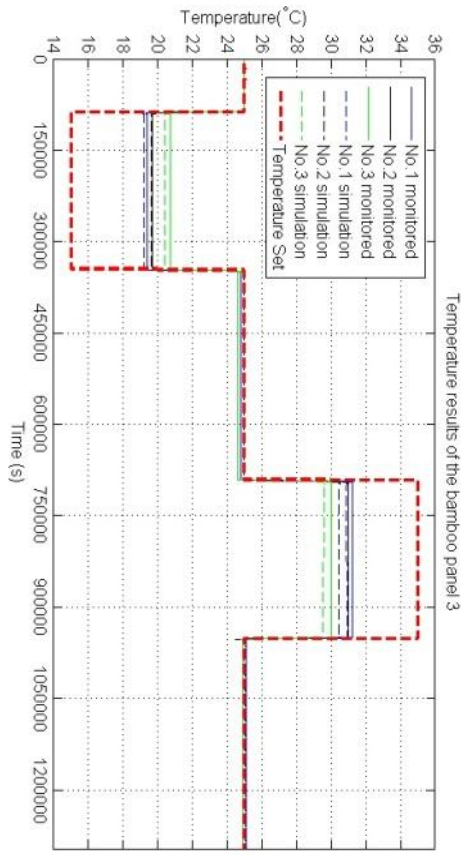
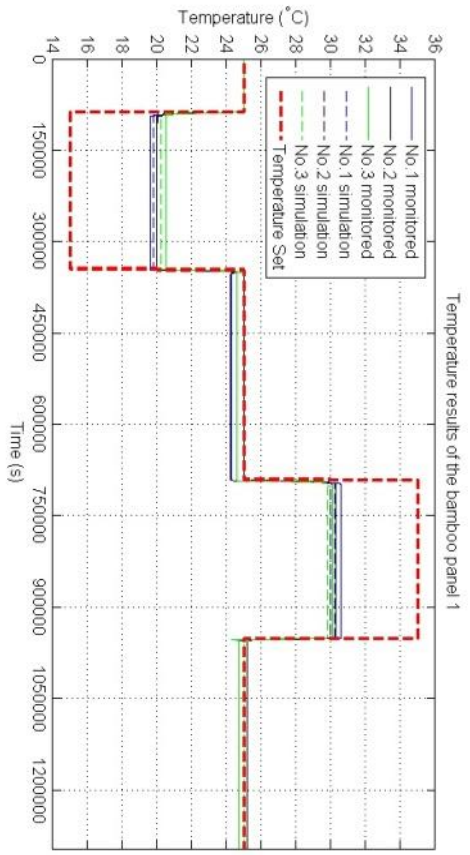


Figure 9.3.1 Temperature results for four panels

The relative humidity results are shown by figure 9.3.2. The results indicated that the RH values of the four panels needs much more time to approach equilibrium state than the temperature values. The lowest RH peak value and relatively slow RH response can be found from the results of panel 1. The highest peak RH value and relatively quick RH response can be found from the results of panel 2. The RH response speed of the panel 3 and panel 4 are intermediate between the results from panel 1 and panel 2. The results from the panel 3 are similar to the results of the panel 1. The results from the panel 4 are similar to the results of the panel 2. A high water vapour diffusion resistance factor and a high moisture capacity were found from the external bamboo culms. Internal bamboo culms demonstrated low water vapour diffusion resistance factor and low moisture capacity. These results also appear to be consistent with the results of sorption isotherm and water vapour diffusion resistance measurements.

The temperature and RH results indicated that although the layer of panel made from the internal part of bamboo culm wall can provide good insulation performance, its performance in resisting the high RH variation is inferior to the layer from the external part of bamboo culm wall. The external part of the bamboo culm wall can provide a barrier to the unsteady RH conditions. The internal part of the bamboo culm wall can be utilised to increase the thermal resistance of a panel.

The difference between simulation results and measured results of all panels is less than 0.5 °C in the equilibrium state. The difference of the RH between simulation results and monitored results from experimental measurements is higher than the difference of temperature results.

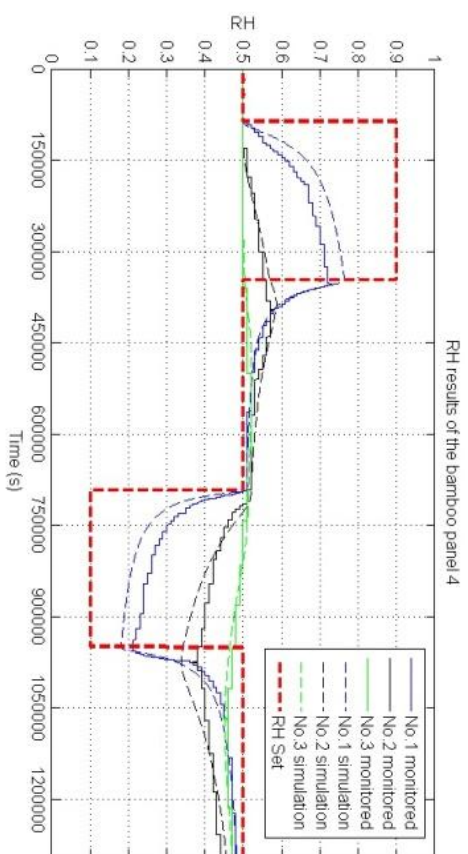
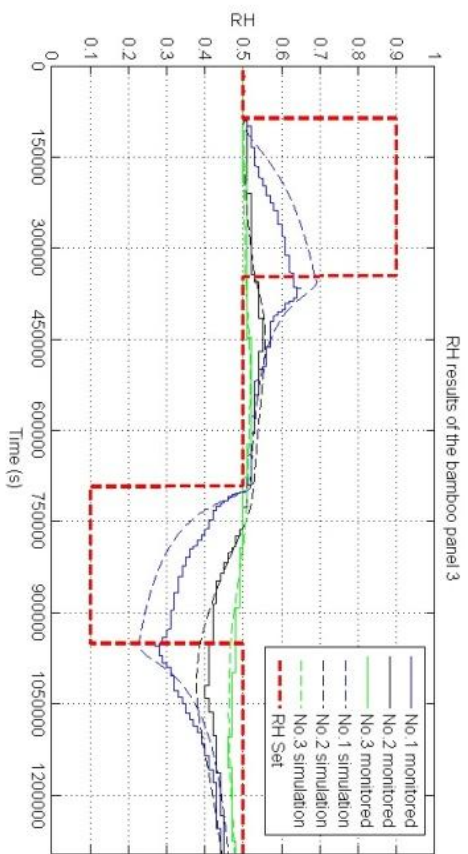
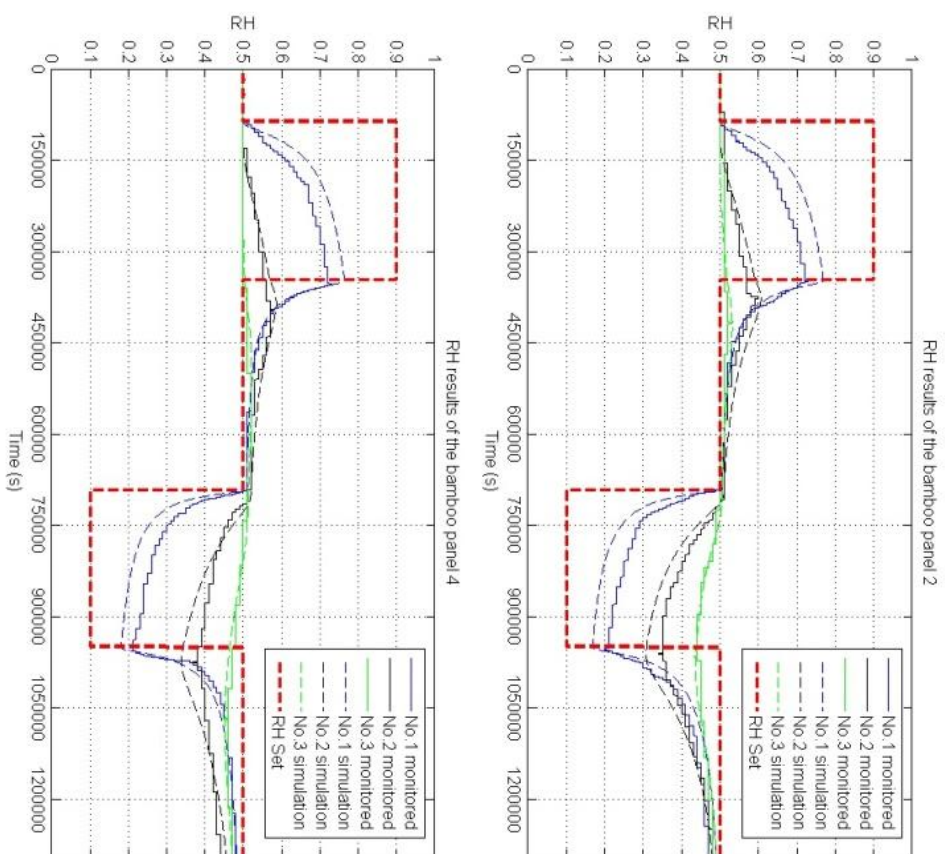
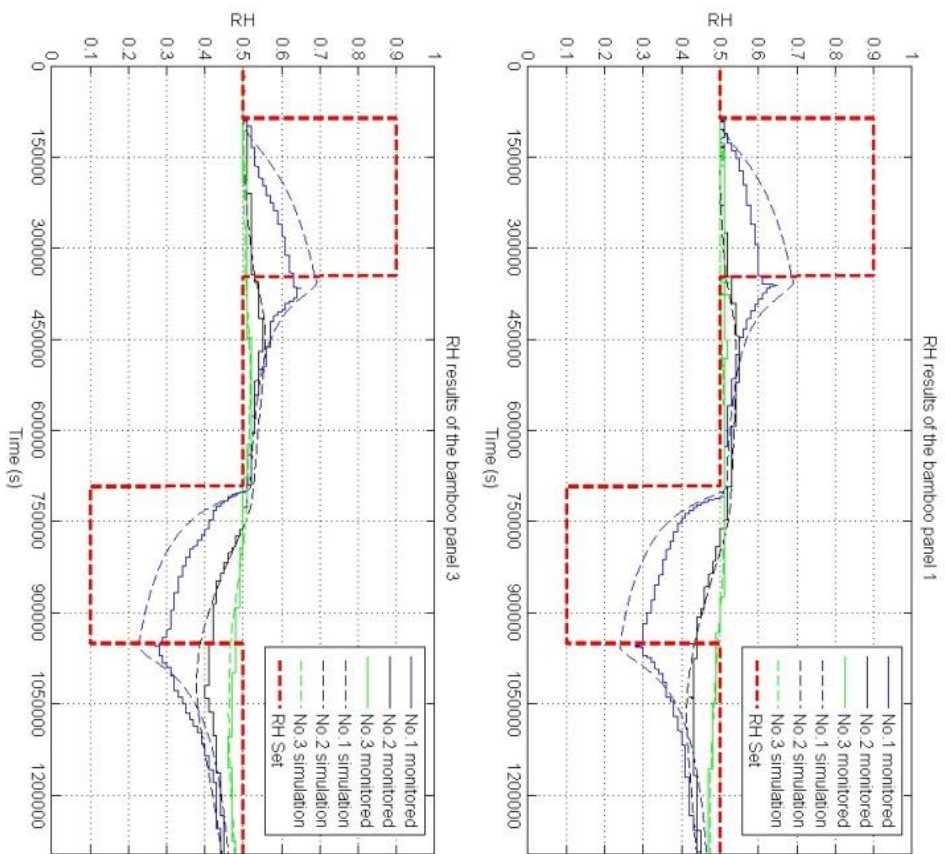


Figure 9.3.2 The RH results of four panels

9.3.2 Parametric studies

The parametric study aims to find the parameter which has the highest influence on the temperature or RH results. The value of each parameter was set to vary from 80% to 120% of the original simulation input. The increasing or decreasing pace is 20%. The reason of using this range is that the variation of the measured parameters is less than 20% at the same point of measurement. Furthermore, the variation needs to be from both positive and negative directions to make sure the results are also from two directions.

The temperature results of the parametric study are shown by Figure 9.3.3. The results indicated that variation of parameters in 20% causes little changes on the simulation results at the equilibrium stage. The duration of temperature change is less than 2 hours at the transient stage. Therefore, the temperature variation in this short time period is invisible in Fig. 9.3.3.

Figure 9.3.4 illustrates the transient temperature change of four panels within the 8 hours from the temperature change time point to a time of approaching the equilibrium stage. Although, the adjustments of each parameter demonstrate little changes on the simulation results, the influence of density can be found. The temperature variation caused by density adjustments are illustrated by the yellow solid line and yellow dash lines. These two lines deviate the most value from the original simulation results. Therefore, density can be regarded as the most sensitive parameters to influence the temperature simulation results. The results of panel 1 indicated that higher density input can lead to closer results to the experiment results. This trend is not obvious for other four panels.

- Temperature Set
- No. 1 monitored
- No. 2 monitored
- No. 3 monitored
- No. 1 simulation
- No. 2 simulation
- No. 3 simulation
- No. 1 thermal diffusivity +20%
- No. 2 thermal diffusivity +20%
- No. 3 thermal diffusivity +20%
- No. 1 thermal diffusivity -20%
- No. 2 thermal diffusivity -20%
- No. 3 thermal diffusivity -20%
- No. 1 specific heat capacity +20%
- No. 2 specific heat capacity +20%
- No. 3 specific heat capacity +20%
- No. 1 specific heat capacity -20%
- No. 2 specific heat capacity -20%
- No. 3 specific heat capacity -20%
- No. 1 density +20%
- No. 2 density +20%
- No. 3 density +20%
- No. 1 density -20%
- No. 2 density -20%
- No. 3 density -20%
- No. 1 liquid diffusivity +20%
- No. 2 liquid diffusivity +20%
- No. 3 liquid diffusivity +20%
- No. 1 liquid diffusivity -20%
- No. 2 liquid diffusivity -20%
- No. 3 liquid diffusivity -20%
- No. 1 vapour diffusion resistance factor +20%
- No. 2 vapour diffusion resistance factor +20%
- No. 3 vapour diffusion resistance factor +20%
- No. 1 vapour diffusion resistance factor -20%
- No. 2 vapour diffusion resistance factor -20%
- No. 3 vapour diffusion resistance factor -20%
- No. 1 isotherm moisture content +20%
- No. 2 isotherm moisture content +20%
- No. 3 isotherm moisture content +20%
- No. 1 isotherm moisture content -20%
- No. 2 isotherm moisture content -20%
- No. 3 isotherm moisture content -20%

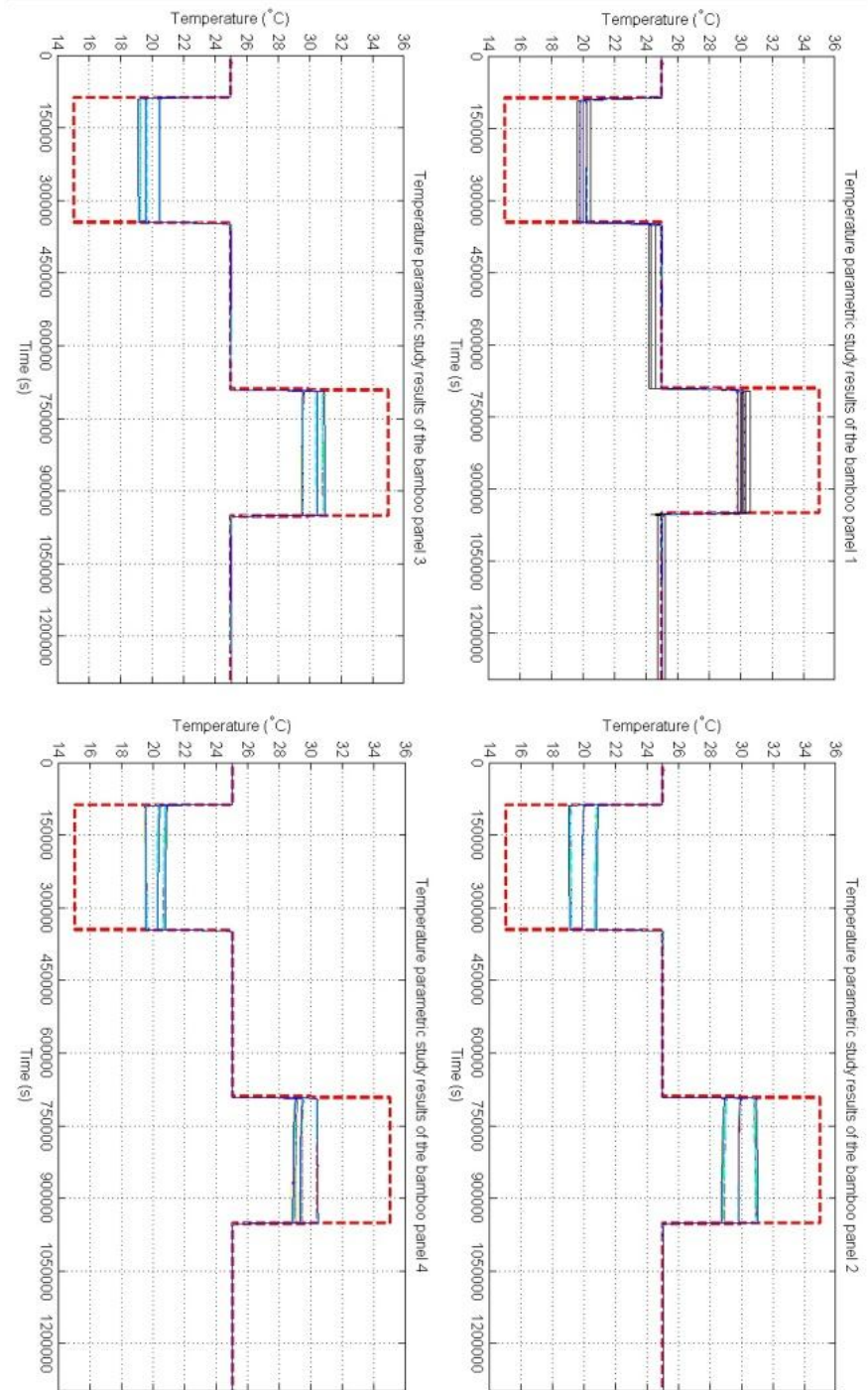


Figure 9.3.3 Parametric study results of temperature of four panels

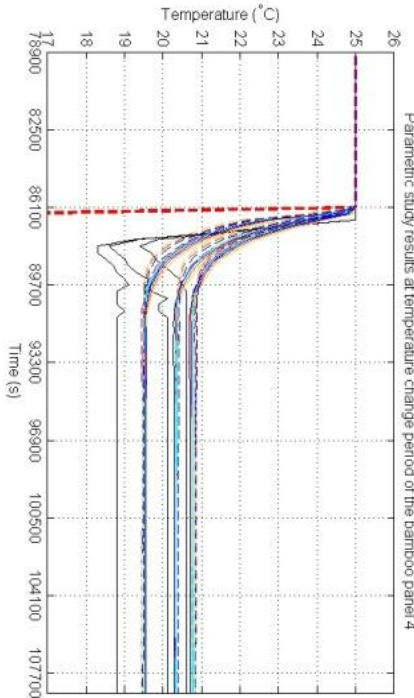
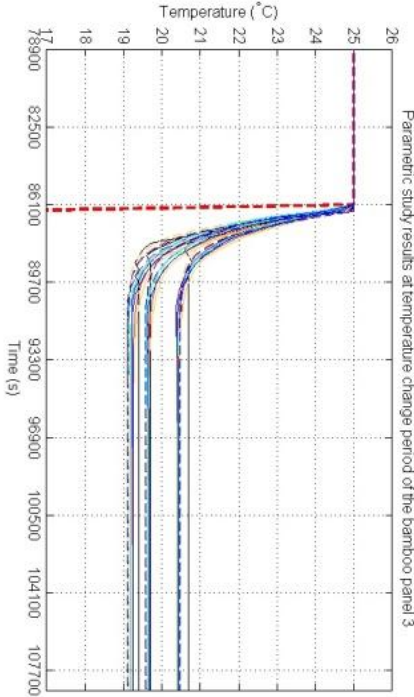
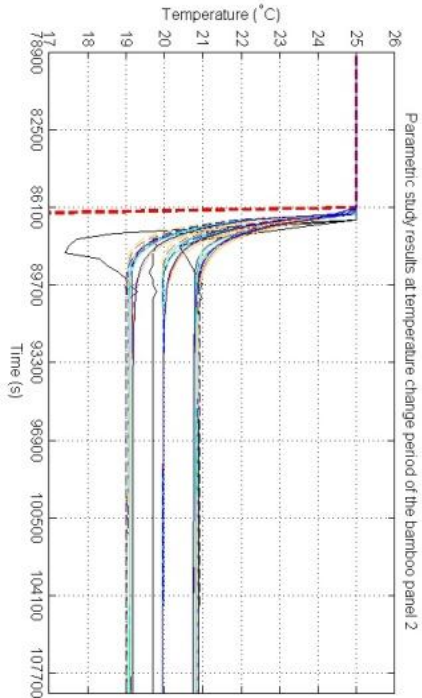
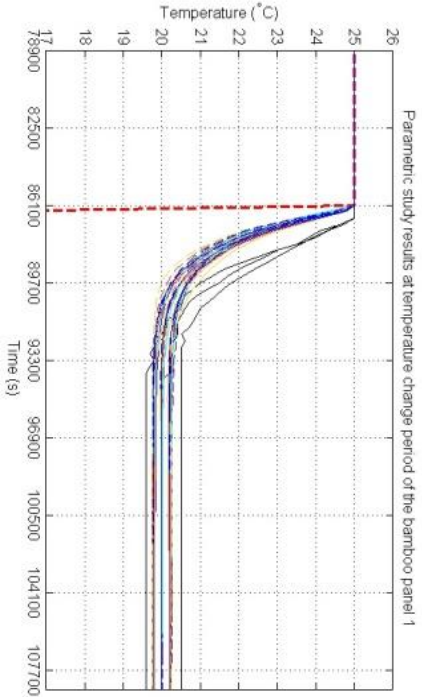
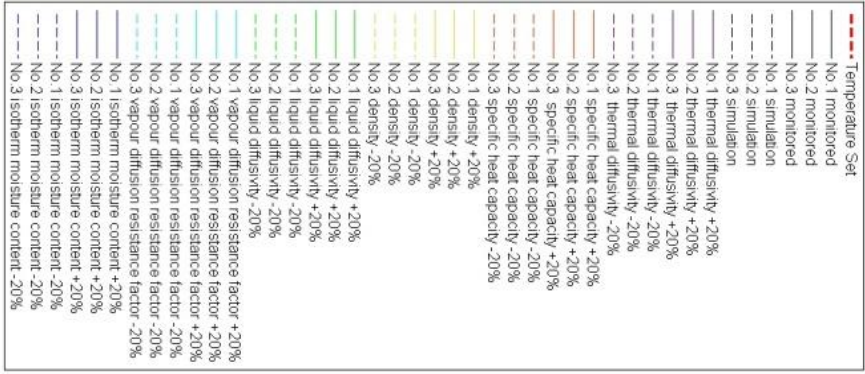


Figure 9.3.4 Parametric study results at a temperature change period

To enlarge the influence of density, a further parametric study was conducted. The results are shown in Figure 9.3.5. The input density values were set to increase 50% and 100% respectively. The results indicated that the simulation results at the transient stage are closer to the experiment results by increasing 100% density value for panel 1. However, for other panels, the original simulation results are more accurate. At the equilibrium stage, the original simulation results are closer to the experiment results.

In addition, the temperature results of all panels show a rebound trend after the lowest temperature point. The rebound trend is more obvious for panel 2 and panel 4 than for panel 1 and panel 3. The condensation of water can be regarded as a reason for this rebound trend. Low temperature may cause the water condensation. Water condensation can release heat. Panel 2 and panel 4 have a low density layer adjacent to the left climate chamber. This layer also demonstrates high vapour permeability and low moisture capacity. Higher content of water vapour can be passed but cannot be stored in this layer. Therefore, the extent of temperature rebound trend is higher for panel 2 and panel 4 than for panel 1 and panel 3.

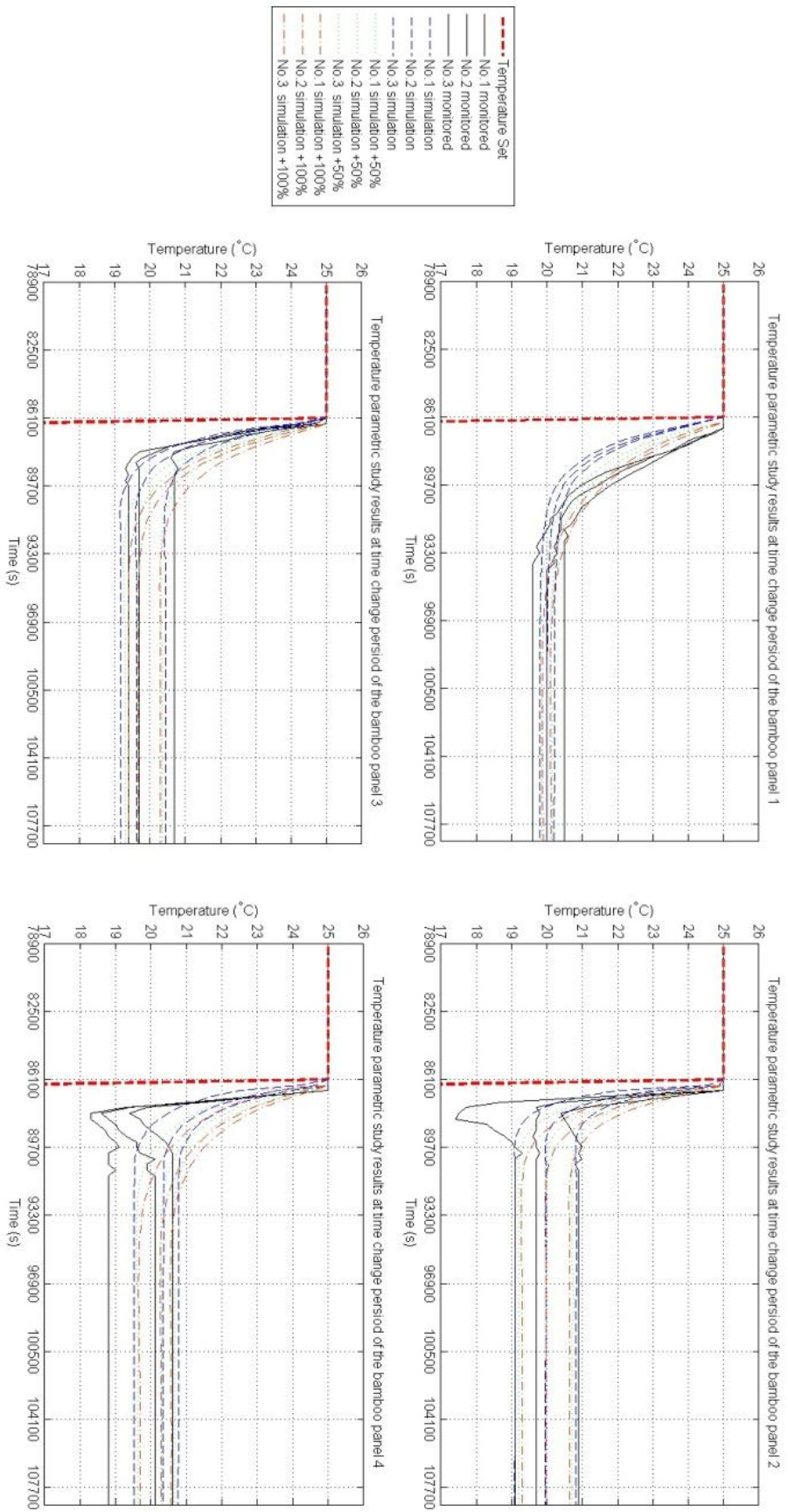


Figure 9.3.5 Parametric study results of enlarged density values at a temperature change period

The RH results of the parametric study are shown by Figure 9.3.6. The results indicated that variation at 20% for both vapour diffusion resistance and sorption isotherm cause relatively higher influence than other parameters. The 120% lines of these two parameters are closer to the experiment results at the No.1 monitor point. Two solid lines are highly overlapped.

The influence of the sorption isotherm and water vapour diffusion resistance factor were considered in a further parametric study. Here, the original values of the parametric study were set to increase to 50% and 100% for a new simulation. The results are shown by the Figure 9.3.7 and Figure 9.3.8.

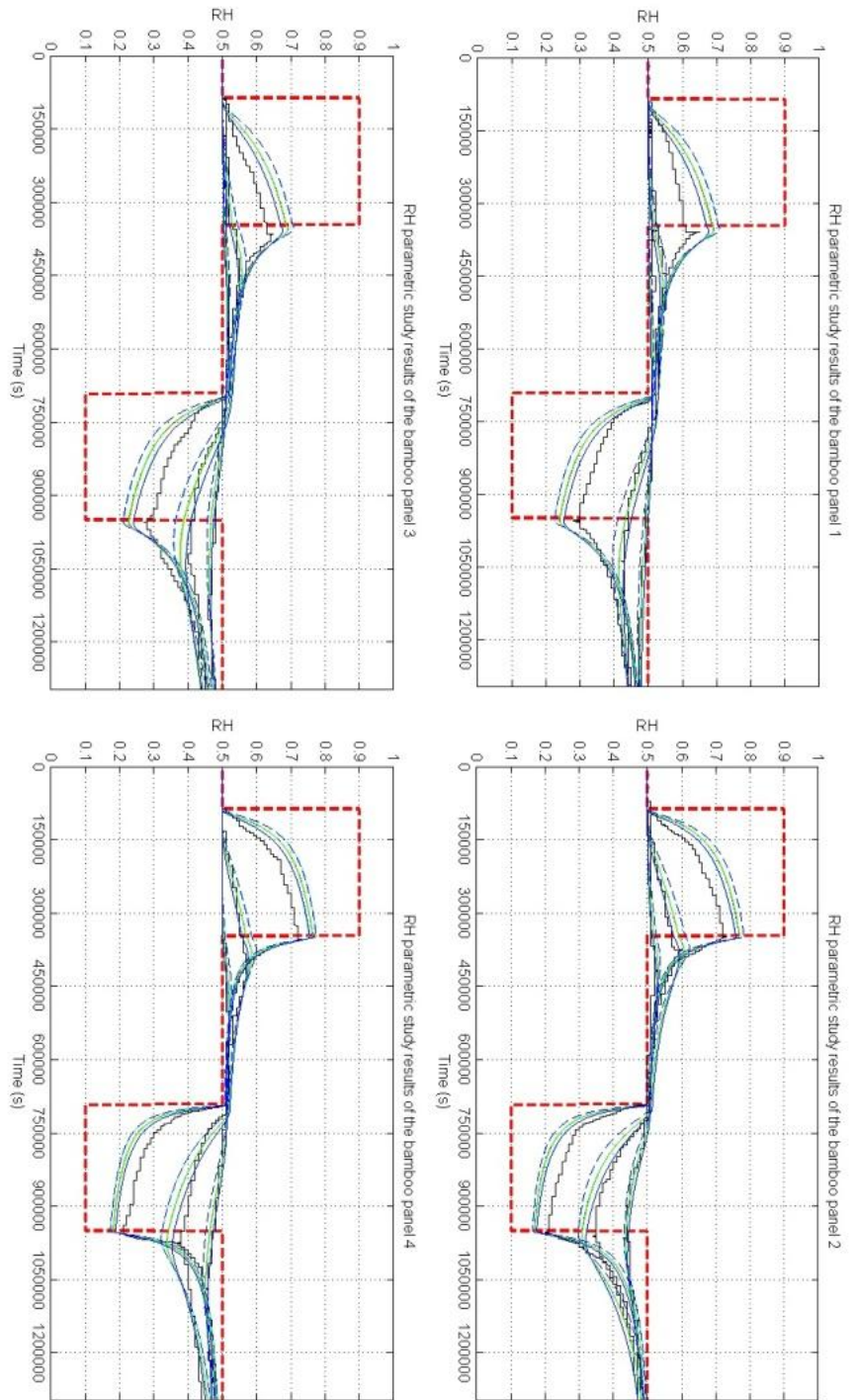
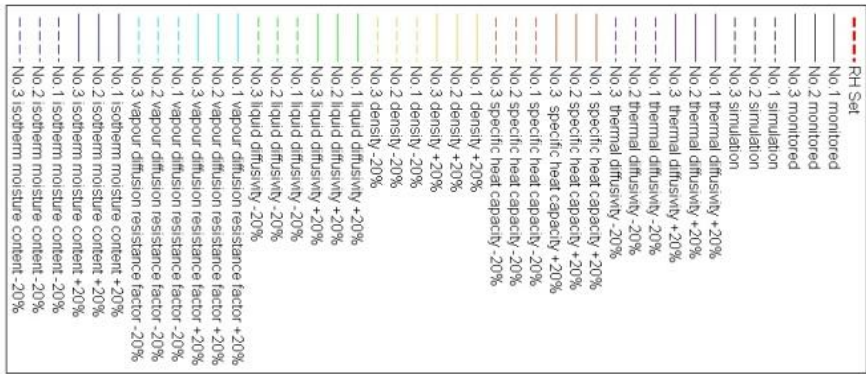


Figure 9.3.6 Parametric study results of RH of four panels

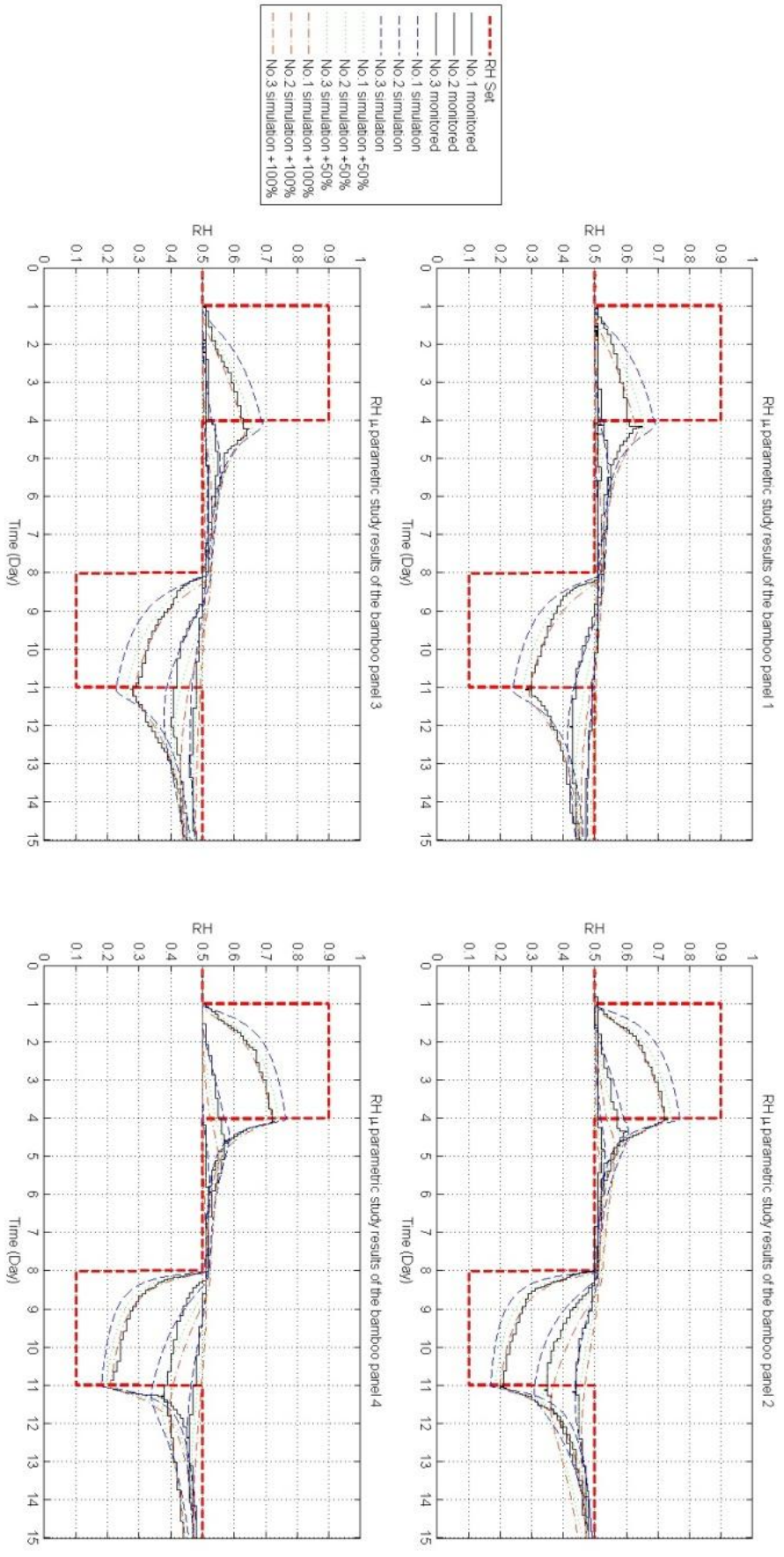


Figure 9.3.7 Parametric study results of the RH by increasing the μ

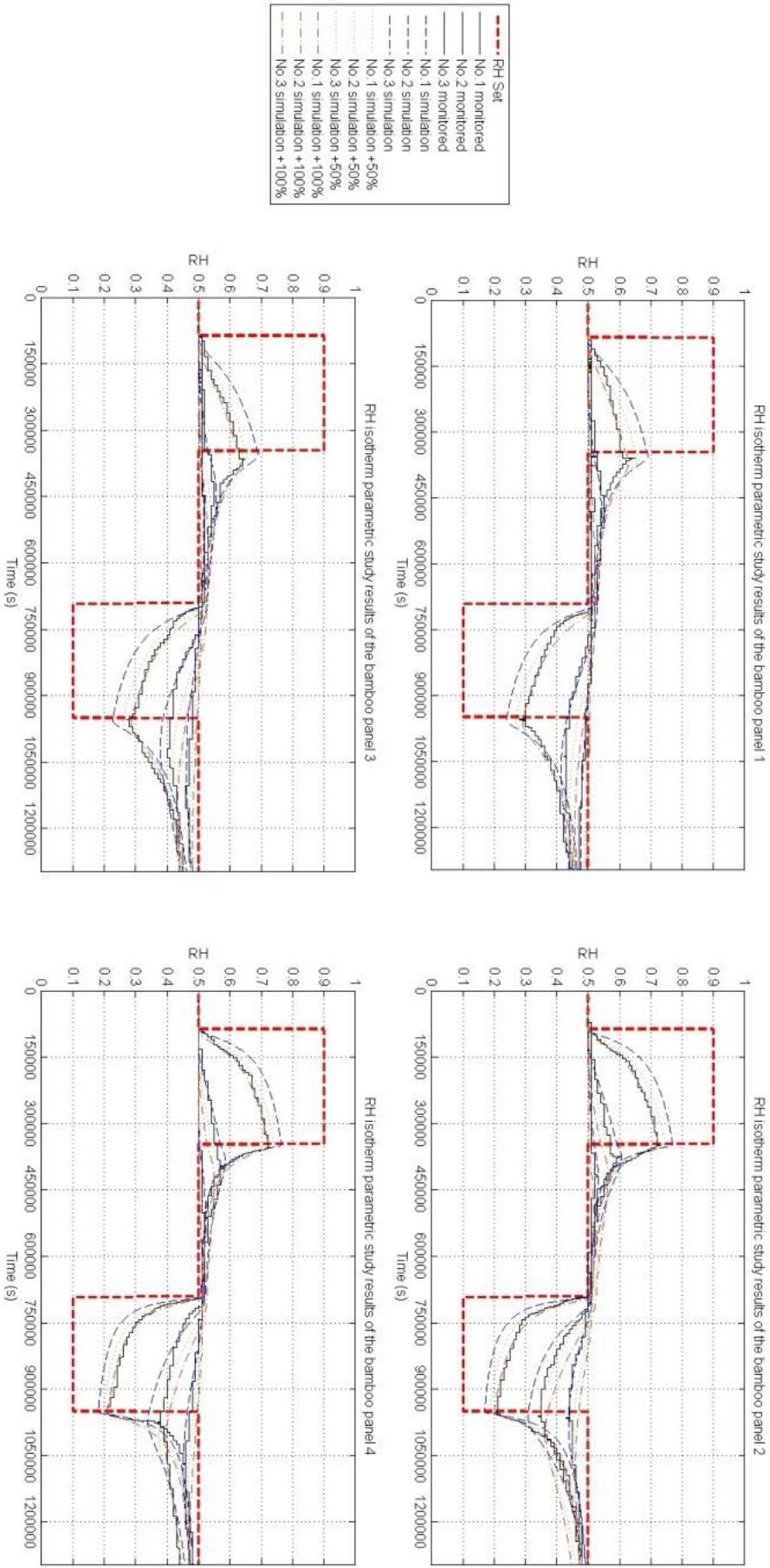


Figure 9.3.8 Parametric study results of the RH by increasing the moisture content of sorption isotherm

The results indicated that better fitting can be found in the No.1 position of all panels after the parametric adjustment. However, the original simulation results of No.2 and No.3 demonstrated better fitting trends than the results of parametric study. Therefore, the parametric study can further focus on the individual adjustment for each layer.

The further parametric study firstly increased the water vapour diffusion resistance factor of the No.1 position for all panels. The effect is obvious on results of the No.1 position. However, concomitant values increasing can also be found at No.2 and No.3 positions. To neutralise the undesired increasing values from these two positions, the water vapour diffusion resistance factors of the No.2 position were set to decrease by a trial range. Another method was to increase the water vapour diffusion resistance factors of both No.1 and No.2 positions. This method is not as sensitive as the initial method. After a number of trials, an acceptable adjustment scheme was utilised on the individual adjustment for each layer. See table 9.3.1.

Table 9.3.1 The adjustment of water vapour diffusion resistance factors for individual layer

	No.1	No.2	No.3
Panel 1	+50%	-50%	0%
Panel 2	+50%	-20%	0%
Panel 3	+50%	-20%	0%
Panel 4	+50%	-20%	0%

The results are shown by Figure 9.3.9. The adjustment of water vapour diffusion resistance factors can lead to a relatively closer simulation results compared to the original simulation results.

Same scheme in table 9.3.1 was utilised for sorption isotherm adjustment, the results of the sorption isotherm adjustment are compared with the results of μ adjustment in Figure 9.3.10. The comparison indicated that results of μ adjustment are closer to the experimental results. That means, in this scheme, the water vapour diffusion resistance factor can be regarded as a more sensitive factor than the sorption isotherm. Sorption isotherm adjustment may need further variation to approach the same results.

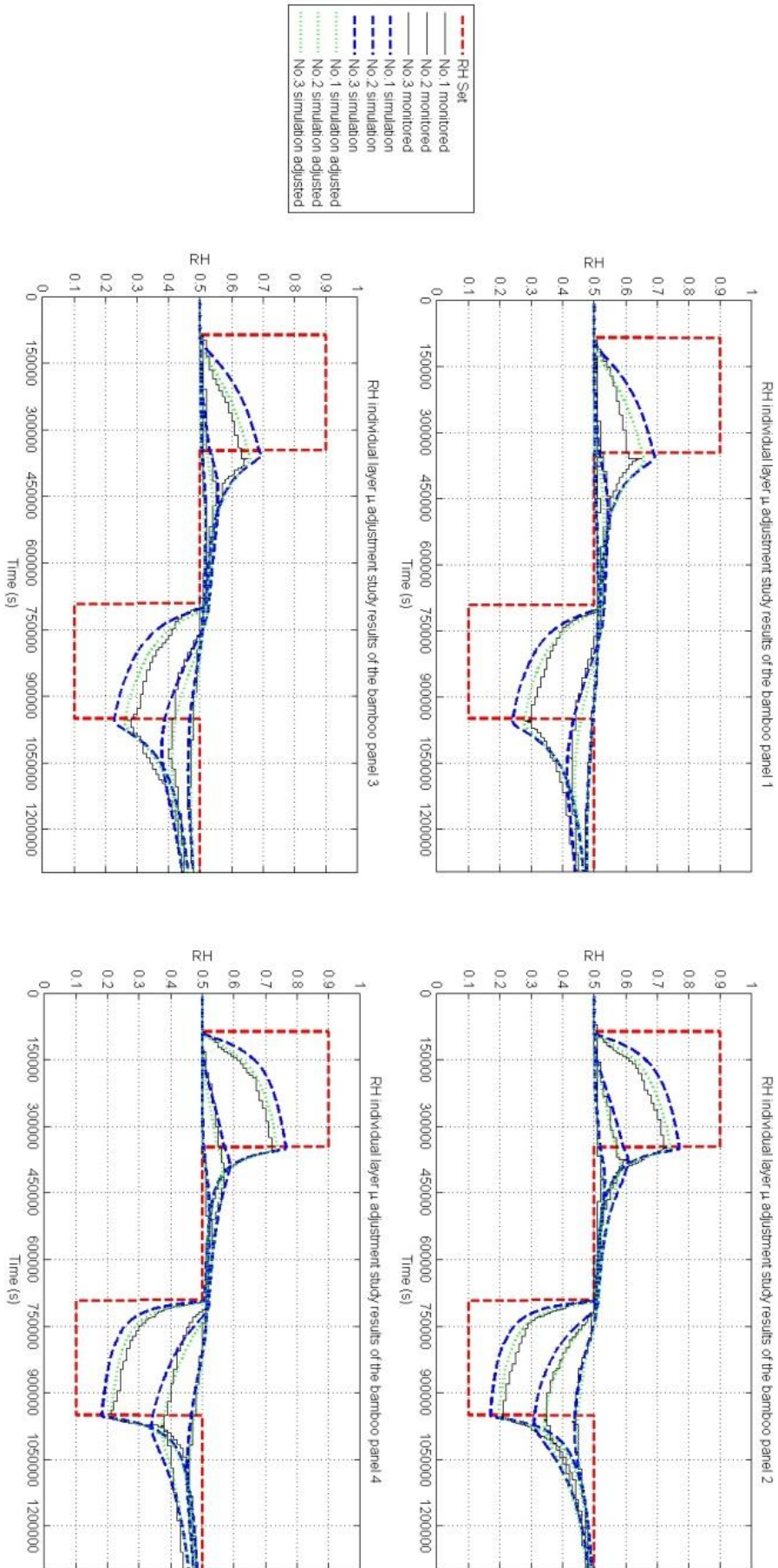


Figure 9.3.9 The RH results of individual layer μ adjustment

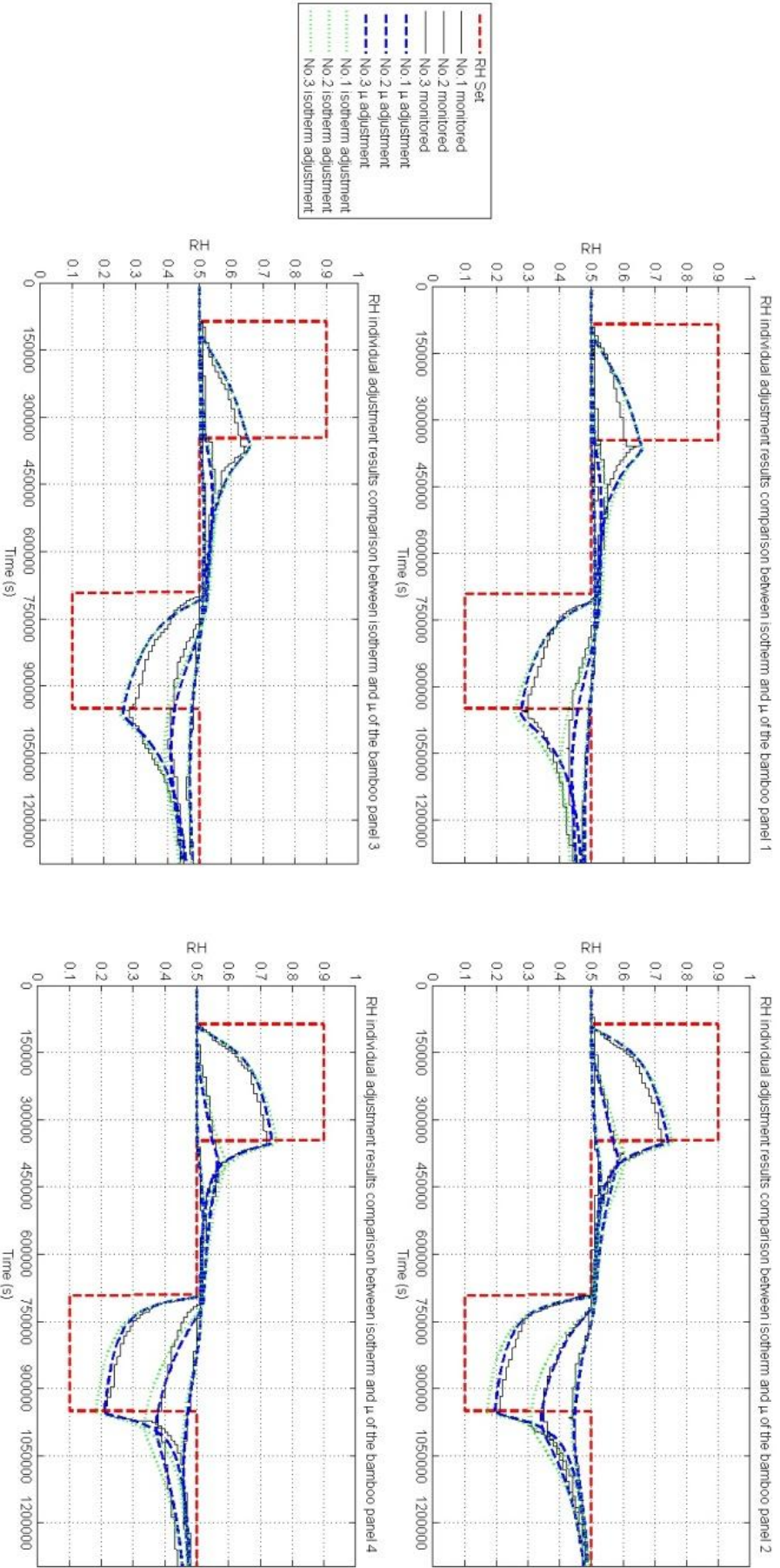


Figure 9.3.10 The RH results of individual layer μ adjustment and sorption isotherm adjustment

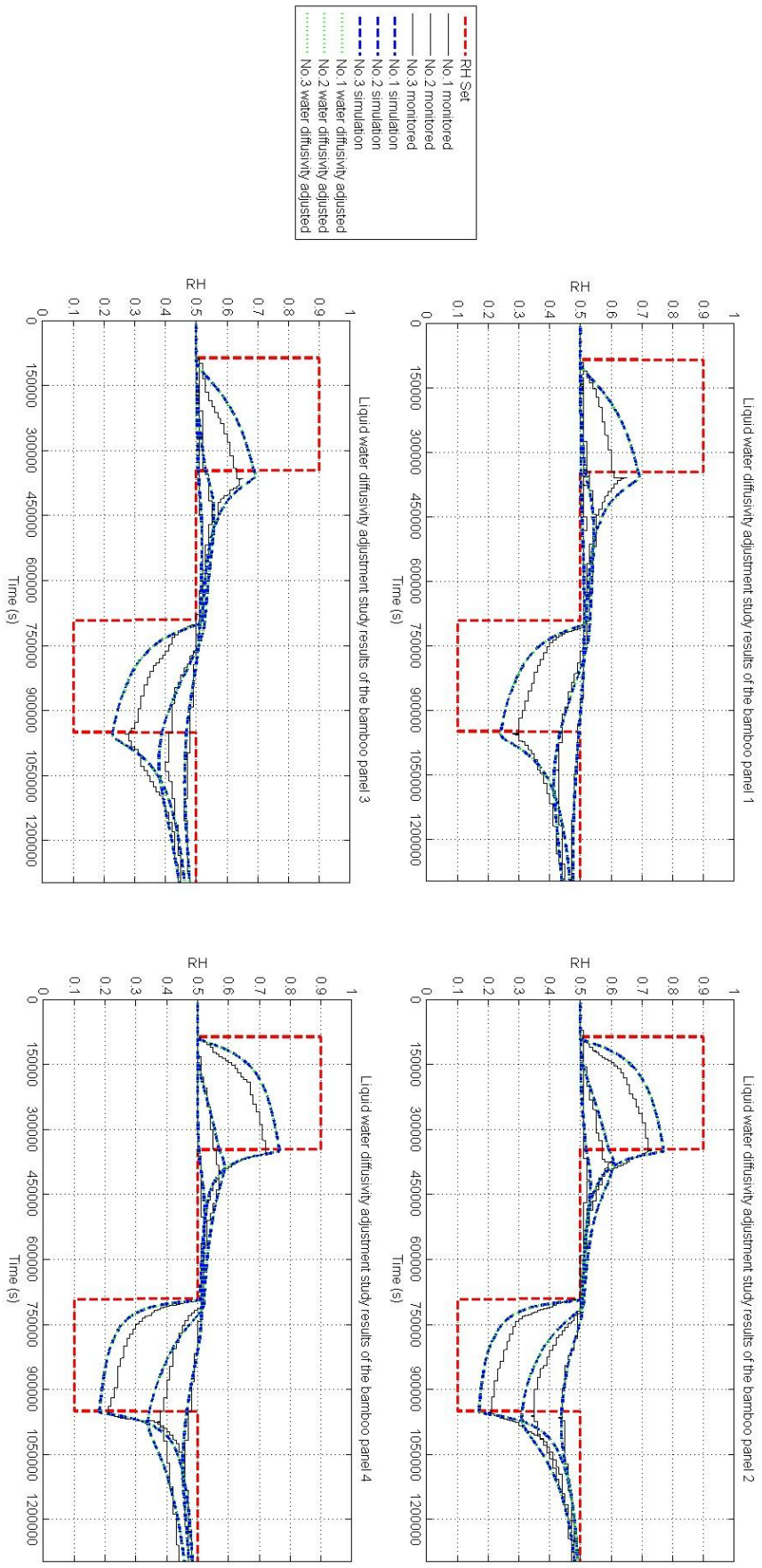


Figure 9.3.11 The liquid water diffusivity adjustment results

The liquid water diffusivity was estimated in chapter 7. In this study, the impact of the existence of liquid water diffusivity in the simulation results was evaluated. The Figure 9.3.11 shows that the RH difference between the simulation results with liquid water diffusivity and the simulation results without liquid water diffusivity is ignorable. After the simulation, the highest difference is 0.2% at panel 3. Therefore, simply ignoring the liquid water diffusivity value is acceptable in this study.

An extreme case, which was considered in the parametric study, is the existence of moisture caused influence on the temperature results. Figure 9.3.12 compares the results for the experiments, the initial simulation, and a simulation without involving any moisture. The results indicated that the simulation with moisture is more accurate than the simulation without moisture in both equilibrium and transient state. The results also imply that the existence of moisture could increase the heat capacity and reduce the thermal conductivity. The slower response in the transient state is obvious for panel 1, and narrower temperature distribution can be found at panel 2.

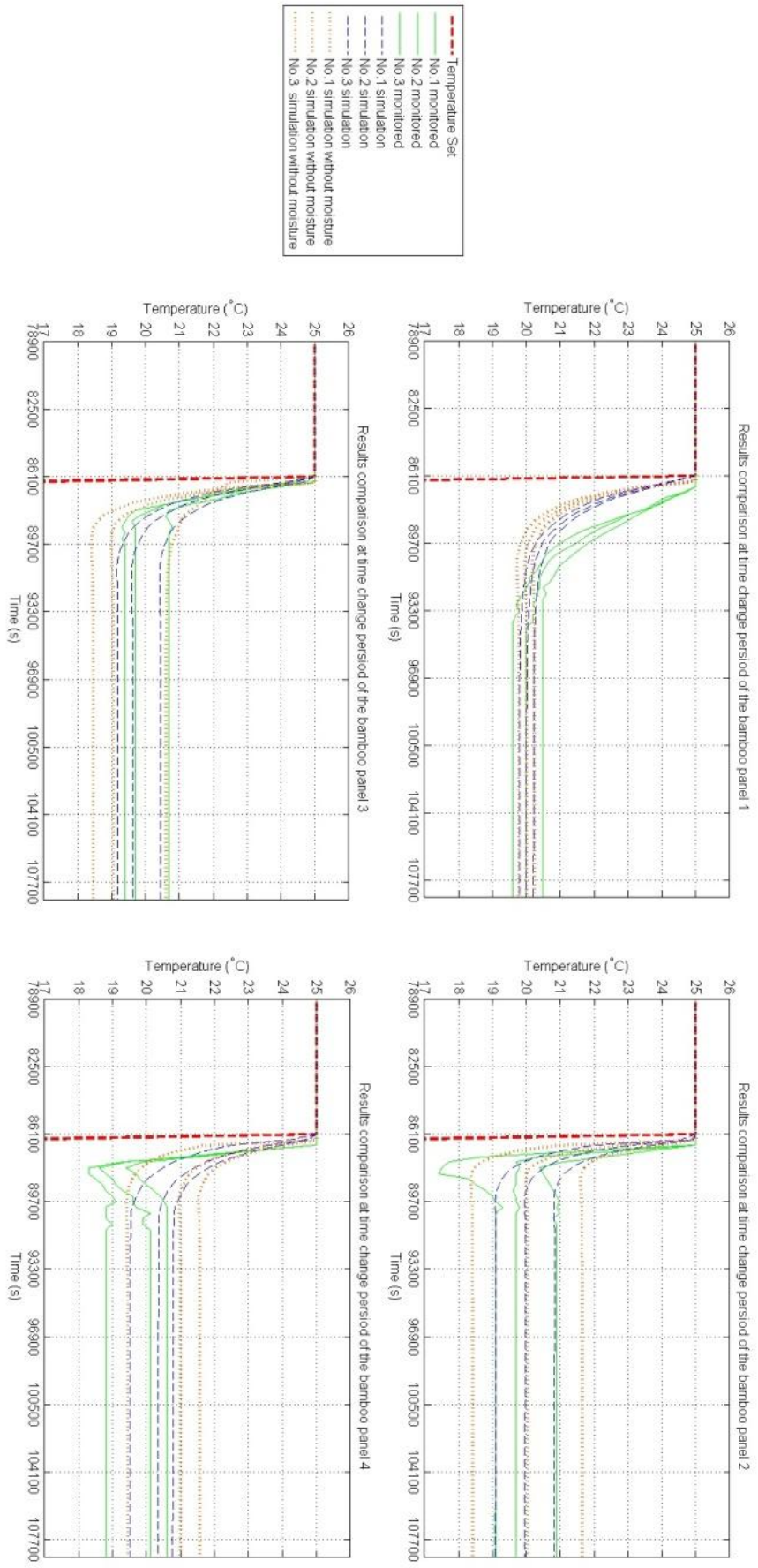


Figure 9.3.12 The results of the simulation with and without moisture content

9.4 Conclusions

This chapter focuses on the heat and moisture transfer behaviour in *Phyllostachys edulis* (Moso bamboo) panels at various temperature and relative humidity conditions. Four Moso bamboo panels with different lamination methods were prepared for heat and moisture transfer experiments. The numerical modelling of coupled heat and moisture transfer was conducted by COMSOL Multiphysics and Matlab software. The model was validated by the benchmark example in a British standard (BS EN 15026: 2007).

Both experiment and simulation results appear to be consistent with the results of measurements of the basic hygrothermal parameters. The temperature and RH results indicates that although the layer of panel made by the internal part of bamboo culm wall can provide good insulation performance, its ability to resist the high RH variation is inferior to the layer from the external part of bamboo culm wall. The difference of the RH between simulation results and monitored results from experiment measurements is higher than the difference of temperature results.

The parametric study found that density can be regarded as the most sensitive parameter to influence the temperature simulation results in the transient state. The water vapour diffusion resistance factor can be regarded as the most sensitive parameter to influence the RH simulation results. The parametric study results indicated that the simulation with moisture is more accurate than the simulation without moisture in both equilibrium and transient state. The results also imply that the existence of moisture could increase the heat capacity and reduce the thermal conductivity.

The results of this study recommend that the external part of the bamboo culm wall can be utilised to minimise the RH variation of the panel while the internal part of bamboo culm wall is suitable for increasing the thermal insulation performance of the panel.

It should be noticed that the laboratory experiment cannot be replaced by the modelling study. The modelling study was utilised to predict the temperature and RH results. The boundary condition and initial condition are expressed by theoretical values. In laboratory experiments, these conditions are not strictly the same as the theoretical values. In addition, a modelling study can only predict part of the real phenomenon. The temperature rebound phenomenon is a response which is not predicted by the modelling study. Furthermore, the highly corresponding result from the parametric scheme in this study is just one possible performance of the real situation. In laboratory experiments, the hygrothermal response may be caused by the effects of multiple factors.

Chapter 10 Conclusions and future work

10.1 Conclusions

This thesis has systematically studied the hygrothermal performance of Moso bamboo. The literature review established that there is a lack of published data on the basic hygrothermal properties of Moso bamboo which can be applied to buildings constructed from bamboo. To overcome this barrier, a series of experimental investigations were conducted to obtain the density, porosity, specific heat capacity, thermal conductivity (or thermal diffusivity), water vapour permeability (or water vapour resistance factor) and isothermal properties of Moso bamboo.

Density

The density of both the internode parts and node parts of the Moso bamboo decreases from the external surface to the internal surface of the culm wall in the radial direction. The different proportions of the vascular bundle tissues and the parenchyma ground tissues dominate the density variation of the Moso bamboo in the radial direction. A high proportion of the vascular bundles' tissues are of higher density than the surrounding material, while a high proportion of parenchyma ground tissues is of low density. In the longitudinal direction, internode parts of Moso bamboo retain relatively uniform density due to the straight vascular bundles but the density distribution for node parts is irregular. In the tangential direction, the density fluctuation of internode parts is more significant than in the longitudinal direction. This fluctuation is caused by the distribution of vascular bundles and ground tissue in the transverse section. For node parts, the density of the Moso bamboo fluctuates irregularly because the vascular bundles are organised in different directions at the node parts.

Although the bulk density of the bamboo ranges from 601kg/m^3 to 640kg/m^3 , Moso Bamboo has a relatively wide density distribution at different measurement points. The minimum and maximum densities are 237kg/m^3 and 1412kg/m^3 respectively. High density parts of Moso bamboo are concentrated on the external side of the bamboo culm wall for both internode and node parts. Low density parts of Moso bamboo appear on the internal side of the bamboo culm wall of internode parts.

The density results indicate that obvious variations exist in different orientations of the Moso bamboo culm. To enhance the reliability of the simulation models in thermal and mechanical fields, variation of the density must be considered.

Porosity

Computed Tomography (CT) and Back-Scattered Electron (BSE) imaging are the two effective technologies to measure the actual morphological porosity distribution from the external side to the internal side of the bamboo culm wall. The CT scanning results show similar trends to the BSE results. The correlation relationship between BSE and CT results lies between the moderate correlation level and the strong correlation level. The average porosity of internode specimens is from 43.9% to 58.8% by BSE measurement and from 44.9% to 63.4% by CT measurement. The average porosity of node specimens is from 37.4% to 56.6% by using BSE measurement and from 32.1% to 62.2% by CT measurement. Typical porosity results from 400 sampling points and 10 portions indicated that the BSE porosity results are lower than the CT results. The reason is that the BSE results are based on the image of the cross section. If the pores are beneath the plane of the cross section, they will not be included in the cross section image but these pores can be included in the three dimensional CT measurement. The porosity fluctuation of node specimens demonstrated larger variation in each CT scan than internode specimens. The similarity between the BSE and CT results is lower in the node specimens than the internode specimens. The porosity increases in proportion to the distance from the external side of the bamboo culm wall.

Specific heat capacity

The specific heat capacity of the Moso bamboo specimens was measured by DSC. The measurements were conducted in all directions of the cylindrical coordinate system for both the internode parts and the node parts. All results demonstrated that the specific heat capacity of the bamboo specimens increased with the temperature. Relatively small pits, holes and tightly arranged cells resulted in higher specific heat capacity. In the radial direction, the results for both internode and node parts indicate that the specific heat capacity decreases from the external surface to the internal surface. In tangential and longitudinal directions, average specific heat capacity values present an irregular trend. No specific gradient in the specific heat capacity was found in these two directions.

Thermal diffusivity

The thermal diffusivity of the Moso bamboo specimens was measured by a flash tube system. The specimens were measured in all directions of the cylindrical coordinates system for both the internode parts and the node parts. Obvious differences in thermal diffusivity were found in the radial direction. The significant differences in porosity and complexity of the heat propagation zone in the radial direction are regarded as factors which influence the thermal diffusivity. Higher thermal diffusivity values were measured in the longitudinal direction

rather than the specimens in the tangential direction and the specimens from middle and internal positions in the radial direction. These phenomena can be attributed to the vertically grown fibres and permeable vascular bundle vessels in the longitudinal direction.

Water vapour diffusion resistance factor

The water vapour diffusion resistance factor of the Moso bamboo specimens was measured by a dry cup method. The specimens were measured in all directions of the cylindrical coordinates system in both the internode parts and the node parts. The water vapour diffusion resistance factor results for Moso bamboo specimens demonstrated a decreasing trend from the external surface to the internal surface in the radial direction. This trend may be attributed to the more densified fibre cells and low quantity of pits at the external surface. The water vapour diffusion resistance factor of bamboo specimens is significantly lower in the longitudinal direction than in the radial and tangential directions. The large diameter, high interconnectivity and straight structure of the vascular bundle vessels are the factors which determine the lower water vapour diffusion resistance factor in the longitudinal direction. The majority of the node specimens demonstrated lower water vapour diffusion resistance factor values than internode specimens in the radial and tangential directions due to the irregularly growing vascular bundle vessels which are oriented in different directions.

Sorption isotherm curves for sorption and desorption

The sorption isotherm curves of the Moso bamboo specimens were measured by a saturated salt solutions method. The specimens were measured in all directions of the cylindrical coordinates system for both the internode parts and the node parts. Both sorption and desorption process were included in this study. The evidence from density and microstructure indicates that a hygroscopic gradient exists in both the sorption and desorption processes in the radial direction. External specimens absorb less water in the sorption procedure and desorb less water in the desorption procedure than internal specimens. The hygroscopic difference of specimens at internodes is less significant than specimens at nodes due to the distribution of vascular bundles. Considerable interconnectivity in the longitudinal direction can explain why the moisture content difference between sorption and desorption curves of specimens in the longitudinal direction at the majority of RHs is less than specimens in other directions.

This study made an assumption that the liquid water diffusivity of bamboo is similar to the liquid water diffusivity of wood because the values cannot be measured for the small size of the specimens in this study. The simulation results indicated that ignoring the liquid water diffusivity of bamboo led to negligible differences in the RH results in this study.

Thermal expansion and hygroexpansion

The thermal expansion and hygroexpansion of Moso bamboo specimens have been measured whilst increasing and then decreasing temperature and moisture respectively. The thermal expansion measurements were conducted with a dilatometer. The hygroexpansion of bamboo specimens was measured with a micrometer for specimens placed in desiccators using different saturated solutions. The thermal expansion of the bamboo specimen in the radial and the tangential direction is one order of magnitude higher than the thermal expansion in the longitudinal direction. The hygroexpansion results illustrated that the swelling of bamboo specimens increases with the relative humidity while the expansion of bamboo specimens decreases with reduction in relative humidity. In the radial direction, the data indicated that the hygroexpansion values were highest for the external specimen, intermediate for the middle specimen and lowest for the internal specimen. The hygroexpansion in the longitudinal direction was one order of magnitude lower than hygroexpansion in the radial and tangential directions. The thermal expansion and hygroexpansion results showed that the swelling or shrinkage which was by moisture variation is much higher than that caused by temperature variation.

Coupled heat and moisture transfer

The simulation and experimental studies were conducted to understand the temperature and RH response of Moso bamboo in different climatic conditions. Four Moso bamboo panels with different lamination constructions were prepared for heat and moisture transfer experiments. The numerical modelling of coupled heat and moisture transfer was conducted by COMSOL Multiphysics and Matlab software. The model was validated by the benchmark example in a British standard (BS EN 15026: 2007).

Both experimental and simulation results appear to be consistent with the results of measurements of the basic hygrothermal parameters. The temperature and RH results indicated that although the layer of panel made by the internal part of bamboo culm wall can provide good insulation performance, its ability to resist the high RH variation is inferior to the layer from the external part of bamboo culm wall. The difference of the RH between simulation results and monitored results from experiment measurements is higher than the difference of temperature results.

The parametric study found that density can be regarded as the most sensitive parameter to influence the temperature simulation results in the transient state. The water vapour diffusion resistance factor can be regarded as the most critical parameter to influence the RH simulation results. The parametric study results indicated that the simulation with moisture is more

accurate than the simulation without moisture in both equilibrium and transient state. The results also imply that the existence of moisture could increase the heat capacity and reduce the thermal conductivity.

The results of this study recommend that the external part of bamboo culm wall can be utilised to minimise the RH variation of the panel while the internal part of bamboo culm wall is suitable to increase the thermal insulation performance of the panel. To avoid hygroexpansion caused by structural instability, the implementation of the external part of bamboo culm wall needs to be minimised.

Therefore, for outdoor climates with large temperature and RH variation, insulation panels can be made from a thin layer of the external side of bamboo culm wall laminated with a thick layer of the internal side of bamboo culm wall. The external side of bamboo culm wall needs to face the outdoor environment.

Major outcomes of the thesis

- This study accumulated large amounts of new data on the density, porosity, thermal conductivity, specific heat capacity, water vapour permeability, water diffusion coefficient and isothermal sorption and desorption of Moso bamboo. The non-homogenous characteristics of these properties are recorded in this study.
- A numerical simulation of coupled transient heat and moisture transfer at the material level has been conducted. Non-homogeneous hygrothermal properties of bamboo replaced the average values reported in the literature as the simulation inputs. As a result, an original and probably more accurate simulation has been achieved.
- The temperature and relative humidity results derived from the heat and moisture transfer experiments carried out in this study have resulted in a comprehensive database for understanding the temperature and relative humidity response of Moso bamboo in different indoor and outdoor hygrothermal conditions which is not available in the literature.
- The results of this study provide guidance for the manufacture of bamboo panels with optimised hygrothermal properties.

10.2 Future work

There is insufficient density and porosity data for Moso bamboo in the literature. The results of chapter 3 have expanded the data available, but the data could be more universal and refined by considering the specimens in different locations within the bamboo culm and using higher resolution for CT scanning and BSE capture.

The data for density, porosity, specific heat capacity, thermal diffusivity, water vapour diffusion resistance factor, sorption isotherm, and hygrothermal expansion data of Moso bamboo would be more representative if the number of the Moso bamboo specimens were to be increased in the future.

The majority of the experiments for measuring the hygrothermal properties of Moso bamboo consume a considerable amount of time. The research into hygrothermal properties could be closer to the real life situation if multiple cycle experiments were to be conducted in the future.

Anatomically, Moso bamboo showed obvious micro-structural variations in the radial direction. Therefore, this study preferentially investigated the hygrothermal performance in the radial direction when the experimental resources were not available for more specimens. The size of the climate chamber restricted the number of specimens for the dynamic heat and moisture experiments. In future, the study could be expanded with more specimens and more measurement directions if large climate chambers were to be available. The accumulated hygrothermal properties of Moso bamboo in this study are sufficient for both simulation and experimental work in the tangential and longitudinal directions. Especially, the low water vapour diffusion factor of Moso bamboo in the longitudinal directions would have valuable further research potential in terms of reducing moisture content in buildings.

The dynamic heat and moisture experiments only investigated the hygrothermal response of Moso bamboo panel exposed to a cold moist outdoor environment and a warm dry outdoor environment when the indoor environment remains constant. If larger equipment and more time can be utilised in the future, the moisture buffer performance of Moso bamboo can be investigated.

With the evolution of software and hardware, more details of the anatomical structures and more accurate hygrothermal properties of Moso bamboo will be obtained and faster data processing and calculation will be achievable. More complex equivalent models of hygrothermal properties will be established. More precise two-dimensional and three dimensional hygrothermal research on Moso bamboo will be possible.

Nevertheless, this thesis has laid a foundation for hygrothermal research on Moso bamboo as a building material. This thesis has not provided a complete picture of the hygrothermal performance of Moso bamboo. However, significant advances have been made in characterizing this important structural material.

References

- Almeida, G. and Hernández, R. E. 2006. Changes in physical properties of tropical and temperate hardwoods below and above the fiber saturation point. *Wood Science and Technology*, 40 (7), pp.599-613.
- Ansell, M. P., 2015. Wood composites. Woodhead Publishing Ltd.. (Woodhead Publishing Series in Composites Science and Engineering; 54)
- Baetens, R., Jelle, B. P., Thue, J. V., Tenpierik, M. J., Grynning, S., Uvsløkk, S. and Gustavsen, A. 2010. Vacuum insulation panels for building applications: A review and beyond. *Energy and Buildings*, 42 (2), pp.147-172.
- Banerjee, S. and Tyagi, A. 2011. *Functional materials: preparation, processing and applications*, London: Elsevier.
- Barber, N. and Meylan, B. 1964. The anisotropic shrinkage of wood. A theoretical model. *Holzforschung*. 18 (5), pp.146-156.
- Fourier, J. B. J. 1878. *The analytical theory of heat*, The University Press.
- Beall, F. C. 1968. *Specific heat of wood : further research required to obtain meaningful data*, Madison, U.S.D.A.
- Benson-Cooper, D. M. 1982. *Computed tomographic scanning for the detection of defects within logs*, Forest Service, Forest Research Institute.
- Bergman, T. L., Incropera, F. P. and Lavine, A. S. 2011. *Fundamentals of heat and mass transfer*, John Wiley & Sons.
- Blok, K., Greene, D.L., Jaszay, T., Kashiwagi, T., Levine, M., McFarland, M., Sims, R., Zhou, F. & Zhou, P. 2001. Technological and economic potential of greenhouse gas emissions reduction. *Climate Change*, pp.167-299.
- Blumm, J. and Lindemann, A. 2003. Characterization of the thermophysical properties of molten polymers and liquids using the flash technique. *High Temperatures-High Pressures*, 35 (36), pp.6.
- Boden, S., Schinker, M. G., Duncker, P. and Spiecker, H. 2012. Resolution abilities and measuring depth of High-Frequency densitometry on wood samples. *Measurement*, 45 (7), pp.1913-1921.

- Bribian, I.Z., Capilla, A.V. & Uson, A.A. 2011. Life cycle assessment of building materials: Comparative analysis of energy and environmental impacts and evaluation of the eco-efficiency improvement potential. *Build. Environ.*, 46(5), pp.1133-1140.
- BS EN 12086:2013 *Thermal insulating products for building applications-Determination of water vapour transmission properties*. BSI.
- BS EN 12524:2000 *Building materials and products-Hygrothermal properties-Tabulated design values*. BSI.
- BS EN 15026: 2007 *Hygrothermal performance of building components and building elements-Assessment of moisture transfer by numerical simulation*. BSI.
- BS EN ISO 12571:2013 *Hygrothermal performance of building materials and products. Determination of hygroscopic sorption properties*. BSI.
- BS EN ISO 15148:2002+A1:2016 *Hygrothermal performance of building materials and products. Determination of water absorption coefficient by partial immersion*. BSI.
- BS EN ISO 17828:2015 *Solid biofuels — Determination of bulk density*. BSI.
- Bucur, V. 2003. Techniques for high resolution imaging of wood structure: A review. *Measurement Science and Technology*, 14 (12), pp.R91-R98.
- Burgess, S. S. O., Adams, M. A., Turner, N. C., Beverly, C. R., Ong, C. K., Khan, A. A. H. and Bleby, T. M. 2001. An improved heat pulse method to measure low and reverse rates of sap flow in woody plants. *Tree Physiology*, 21 (9), pp.589-598.
- Casalegno, V., Vavassori, P., Valle, M., Ferraris, M., Salvo, M. and Pintsuk, G. 2010. Measurement of thermal properties of a ceramic/metal joint by laser flash method. *Journal of Nuclear Materials*, 407 (2), pp.83-87.
- Castleton, H. F., Stovin, V., Beck, S. B. M. and Davison, J. B. 2010. Green roofs; building energy savings and the potential for retrofit. *Energy and Buildings*, 42 (10), pp.1582-1591.
- Carmeliet, J. and Derome, D., 2008. Influence of the microstructure on the vapour transport in wood. *Proceedings of the 8th Symposium on Building Physics in the Nordic Countries (NSB2008)*. 16-18 June 2008, Copenhagen. Lyngby: Department of Civil Engineering, Technical University of Denmark pp.983-990.
- Cao, J., Long, Y. and Shanks, R. A. 1997. Experimental investigation into the heat capacity measurement using a modulated DSC. *Journal of Thermal Analysis*, 50 (3), pp.365-373.

- Chapman, A. J. 1987. *Fundamentals of heat transfer*, New York. London, New York: Macmillan., London : Collier Macmillan.
- Chinga-Carrasco, G. 2002. Microscopy and computerized image analysis of wood pulp fibres multi-scale structures. *Microscopy: Science, Technology, Applications and Education, Formatex, Badajoz*, pp.2182-2189.
- Chomcharn, A. and Skaar, C. 1983. Dynamic sorption and hygroexpansion of wood wafers exposed to sinusoidally varying humidity. *Journal of the International Academy of Wood Science*, 17(4), pp.259-277.
- Cook, R. A. and Hover, K. C. 1993. Mercury porosimetry of cement-based materials and associated correction factors. *Construction and Building Materials*, 7 (4), pp.231-240.
- Cverna, F. 2002. *ASM ready reference: thermal properties of metals*, ASM International.
- Dancey, C., and Reidy, J. (2004). *Statistics without Maths for Psychology: using SPSS for Windows*, London: Prentice Hall.
- Davis, J. and Wells, P. 1992. Computed tomography measurements on wood. *Industrial Metrology*, 2 (3-4), pp.195-218.
- Delgado, J., Barreira, E., Ramos, N. M. and De Freitas, V. P. 2012. *Hygrothermal numerical simulation tools applied to building physics*, Springer Science & Business Media.
- DCLG and Ellison 2015. 2010 to 2015 government policy: energy efficiency in buildings. London: DCLG. [online] available from: <https://www.gov.uk/government/publications/2010-to-2015-government-policy-energy-efficiency-in-buildings/2010-to-2015-government-policy-energy-efficiency-in-buildings> [Accessed 26 July 2016].
- Derome, D., Zillig, W. and Carmeliet, J. 2012. Variation of measured cross-sectional cell dimensions and calculated water vapor permeability across a single growth ring of spruce wood. *Wood Science and Technology*, 46 (5), pp.827-840.
- Ding, W.-D., Koubaa, A., Chaala, A., Belem, T. and Krause, C. 2008. Relationship between wood porosity, wood density and methyl methacrylate impregnation rate. *Wood Material Science & Engineering*, 3 (1-2), pp.62-70.
- Dong, Q. and Xiong, Y. 2014. Kinetics study on conventional and microwave pyrolysis of moso bamboo. *Bioresource Technology*, 171, pp.127-131.

- Du, L., Li, Y., Lee, S. and Wu, Q. 2014. Water Absorption Properties of Heat-Treated Bamboo Fiber and High Density Polyethylene Composites. *BioResources*, 9(1), pp.1189-1200.
- Dupleix, A., Kusiak, A., Hughes, M. and Rossi, F. 2013. Measuring the thermal properties of green wood by the transient plane source (TPS) technique. *Holzforschung*, 67 (4), pp.437-445.
- EPBD, 2010. Directive 2010/31/EU of the European Parliament and of the Council of 19 May 2010 on the energy performance of buildings (recast). *Official Journal of the European Union*, 18 (06), pp.2010.
- Fangueiro, R. 2011. Fibrous and composite materials for civil engineering applications, Elsevier.
- Fasina, O. and Sokhansanj, S. 1996. Estimation of Moisture diffusivity coefficient and thermal properties of alfalfa Pellets. *Journal of Agricultural Engineering Research*, 63 (4), pp.333-343.
- Fei, Y. 1995. Thermal expansion. *Mineral physics and crystallography: a handbook of physical constants*, 2, pp.29-44.
- Flander, K. D. and Rovers, R. 2009. One laminated bamboo-frame house per hectare per year. *Construction and Building Materials*, 23 (1), pp.210-218.
- Fleischer, H.O. 1971. The impact of utilization research on the complete use of the forest. *Wood Science and Technology*, 5(4), pp.247-254.
- Freyburger, C., Longuetaud, F., Mothe, F., Constant, T. and Leban, J.-M. 2009. Measuring wood density by means of X-ray computer tomography. *Annals of Forest Science*, 66 (8), pp.804-804.
- Fourier, J. B. J. 1878. *The analytical theory of heat*, The University Press.
- Furuta, Y., Kojiro, K., Miki, T. and Kanayama, K. 2012. The Behaviors of Endothermic and Exothermic of Wood and Wood Components between 100 °C and 200 °C. *Journal of the Society of Materials Science, Japan*, 61 (4), pp.323-328.
- Giesche, H. 2006. Mercury Porosimetry: A General (Practical) Overview. *Particle & Particle Systems Characterization*, 23 (1), pp.9-19.
- Granta Design LTD. CES Edupack 2013. Cambridge, 2013.

- Griffith, B., Türler, D. and Arasteh, D. 1993. Optimizing the effective conductivity and cost of gas-filled panel thermal insulations. *Thermal conductivity*, 22(1993), pp.413-413.
- Grosser, D. and Liese, W. 1971. On the anatomy of Asian bamboos, with special reference to their vascular bundles. *Wood Science and Technology*, 5 (4), pp.290-312.
- Grundberg, S., Grönlund, A. and Grönlund, U. 1995. *The Swedish Stem Bank: A Database for Different Silvicultural and Wood Properties*.
- Guo, W., Lim, C. J., Bi, X., Sokhansanj, S. and Melin, S. 2013. Determination of effective thermal conductivity and specific heat capacity of wood pellets. *Fuel*, 103 (0), pp.347-355.
- Gupta, M., Yang, J. and Roy, C. 2003. Specific heat and thermal conductivity of softwood bark and softwood char particles. *Fuel*, 82 (8), pp.919-927.
- Hagentoft, C.-E., Kalagasidis, A. S., Adl-Zarrabi, B., Roels, S., Carmeliet, J., Hens, H., Grunewald, J., Funk, M., Becker, R. and Shamir, D. 2004. Assessment method of numerical prediction models for combined heat, air and moisture transfer in building components: benchmarks for one-dimensional cases. *Journal of thermal envelope and building science*, 27 (4), pp.327-352.
- Hammond, G. P. and Jones, C. I., 2008. Embodied energy and carbon in construction materials. *Proceedings of the Institution of Civil Engineers - Energy*, 161 (2), pp. 87-98.
- Harada, T., Hata, T. and Ishihara, S. 1998. Thermal constants of wood during the heating process measured with the laser flash method. *Journal of Wood Science*, 44 (6), pp.425-431.
- Hass, P., Wittel, F. K., McDonald, S. A., Marone, F., Stampanoni, M., Herrmann, H. J. and Niemz, P. 2010. Pore space analysis of beech wood: the vessel network. *Holzforschung*, 64 (5), pp.639-644.
- Hendershot, O. P. 1924. Thermal expansion of wood. *Science*, 60 456-457.
- Hens, H. 2007. *Building Physics—Heat, Air and Moisture, Fundamentals and Engineering Methods with Examples and Exercises*, Ernst & Sohn A Wiley. ISBN 978-3-433-01841-5.
- Hill, C. A. and Papadopoulos, A. N. 2001. A review of methods used to determine the size of the cell wall microvoids of wood. *Journal of the institute of wood science*, 15 (6; ISSU 90), pp.337-345.
- Hori, R. and Wada, M. 2005. The thermal expansion of wood cellulose crystals. *Cellulose*, 12(5), pp.479-484.

- Huang, R., Zhang, Y., Xu, X., Zhou, D. and Wu, Q. 2012. Effect of hybrid mineral and bamboo fillers on thermal expansion behavior of bamboo fiber and recycled polypropylene–polyethylene composites. *BioResources*, 7(4), pp.4563-4574.
- Hurtado, P. L., Rouilly, A., Vandebossche, V. and Raynaud, C. 2016. A review on the properties of cellulose fibre insulation. *Building and Environment*, 96(2016), pp.170-177.
- Iassonov, P., Gebrenegus, T. and Tuller, M. 2009. Segmentation of X-ray computed tomography images of porous materials: A crucial step for characterization and quantitative analysis of pore structures. *Water Resources Research*, 45 (9), pp.1 -12.
- Incropera, F. P. 1981. *Fundamentals of heat transfer*, New York Chichester : Wiley.
- Isagi, Y., Kawahara, T., Kamo, K. & Ito, H. 1997. Net production and carbon cycling in a bamboo phyllostachys pubescens stand. *Plant Ecology*, 130(1), pp.41-52.
- James, D. 1968. The thermal diffusivity of ice and water between -40 °C and +60 °C. *Journal of Materials Science*, 3 (5), pp.540-543.
- Jelle, B. P. 2011. Traditional, state-of-the-art and future thermal building insulation materials and solutions–Properties, requirements and possibilities. *Energy and Buildings*, 43 (10), pp.2549-2563.
- Jiang, Z., Wang, H., Yu, Y., Tian, G. and Liu, X. 2006. Hygroscopic behaviour of bamboo and its blocking units. *Journal of Nanjing Forestry University*, 36 (2), pp.11-14.
- Jiang, Z., Yu, W.J. and Yu, Y.L. 2006. Analysis of chemical components of bamboo wood and characteristic of surface performance. *Journal of Northeast Forestry University*, 34(4), pp. 1-6.
- Jiang, Z., Zou, Y., Ruan, X., W, J. and Liu, Y. 2000. A study on the ultrastructure of bamboo cell wall by X-ray. *Scientia Silvae Sinicae*. 36 (3), pp.122-125.
- Johansson, J., Hagman, O. and Oja, J. 2003. Predicting moisture content and density of Scots pine by microwave scanning of sawn timber. *Computers and Electronics in Agriculture*, 41 (1–3), pp.85-90.
- Kang, W. and Chung, W. Y. 2009. Liquid water diffusivity of wood from the capillary pressure-moisture relation. *Journal of Wood Science*, 55 (2), pp.91-99.

- Kavgic, M., Mavrogianni, A., Mumovic, D., Summerfield, A., Stevanovic, Z. and Djurovic-Petrovic, M. 2010. A review of bottom-up building stock models for energy consumption in the residential sector. *Building and Environment*, 45 (7), pp.1683-1697.
- Kellogg, R. Wangaard, F. 1969. Variation in the cell-wall density of wood. *Wood Fiber Sci* 1: pp.180–204.
- Kristijan, R., Igor, Đ. and Stjepan, P. 2014. Specific Heat Capacity of Wood. *Drvna Industrija*, 65 (2), pp.151.
- Koch, Peter 1968. Specific heat of oven-dry spruce pine wood and bark. *Wood Science*, 1(4): pp.203-214.
- Kunzel, H. M. and Kiessl, K. 1996. Calculation of heat and moisture transfer in exposed building components. *International Journal of Heat and Mass Transfer*, 40 (1), pp.159-167.
- Kymäläinen, H. R. and Sjöberg, A. M. 2008. Flax and hemp fibres as raw materials for thermal insulations. *Building and Environment*, 43 (7), pp.1261-1269.
- Kymäläinen, M., Rautkari, L. and Hill, C. a. S. 2015. Sorption behaviour of torrefied wood and charcoal determined by dynamic vapour sorption. *Journal of Materials Science*, 50 (23), pp.7673-7680.
- Lawrence, M., Heath, A. and Walker, P., 2009. Determining moisture levels in straw bale construction. *Construction and Building Materials*, 23 (8), pp. 2763-2768.
- Li, N.P., Long, J.B., Su, L., Wang, L. and Zhong, S. 2012. Experimental and theoretical study on thermal and moisture characteristics of new-type bamboo structure wall. *Journal of Central South University*, 19(2012), pp.600-608.
- Li, S., Wu, S., and Shen, X. 2011. A prediction model of neural networks for *Phyllostachys pubescens*' thermal conductivity. *Chinese agricultural science bulletin*. 27(31), pp.53-57.
- Li, W., He, Y. and Chen, P. 2006. The Factors Influencing the Characteristic of Bamboo Pyrolysis, a Hot Analytic Approach. *Journal of bamboo research*, 25(2), pp.31-34.
- Liese, W., 1985. Anatomy and properties of bamboo. In: *Proceedings of the International Bamboo Workshop*, Oct, 1985. Hangzhou: International Development Research Centre (IDRC), pp.6-14.
- Lindgren, L.O., 1991. The accuracy of medical CAT-scan images for non-destructive density measurements in small volume elements within solid wood. *Wood Sci. Technol.* 25: 425–432.

- Lo, T. Y., Cui, H. Z. and Leung, H. C. 2004. The effect of fiber density on strength capacity of bamboo. *Materials Letters*, 58 (21), pp.2595-2598.
- Lobovikov, M. 2003. Bamboo housing: market potential for low-income groups. *Journal of Bamboo and Rattan*, 2 (4), pp.381-396.
- Luikov, A. 1966. *Heat and mass transfer in capillary-porous bodies*. Pergamon Press, Oxford.
- Ma, E.-N., Zhao, G.-J. and Cao, J.-Z. 2005. Hygroexpansion of wood during moisture adsorption and desorption processes. *Forestry Studies in China*, 7(2), pp.43-46.
- Majumdar, A., Mukhopadhyay, S. and Yadav, R. 2010. Thermal properties of knitted fabrics made from cotton and regenerated bamboo cellulosic fibres. *International Journal of Thermal Sciences*, 49 (10), pp.2042-2048.
- Maxwell, J. C. 1871. *Theory of Heat*. Dover Publications.
- Miki, T., Sugimoto, H., Kojiro, K., Furuta, Y. and Kanayama, K. 2012. Thermal behaviors and transitions of wood detected by temperature-modulated differential scanning calorimetry. *Journal of Wood Science*, 58 (4), pp.300-308.
- Mounika, M., Anusha, P., Ramanaiah, K., Ratnaprasad, A. V. and Reddy, K. H. C. 2014. Thermal properties of bamboo fiber reinforced polyester composite. *International journal of engineering research and science & technology*. 3(4), pp. 87-93
- Mull, R. T. 1984. Mass estimates by computed tomography: physical density from CT numbers. *American journal of roentgenology*, 143 (5), pp.1101-1104.
- Nusser, B. and Teibinger, M. 2012. Coupled Heat and Moisture Transfer in Building Components-Implementing WUFI Approaches in COMSOL Multiphysics. In: Proceedings of the COMSOL Users Conference 2012 Milan, 2012.
- Ohmae, Y. and Nakano, T. 2009. Water adsorption properties of bamboo in the longitudinal direction. *Wood Science and Technology*, 43 (5-6), pp.415-422.
- Pan, S. and Kudo, M. 2011. Segmentation of pores in wood microscopic images based on mathematical morphology with a variable structuring element. *Computers and Electronics in Agriculture*, 75 (2), pp.250-260.

- Parker, W., Jenkins, R., Butler, C. and Abbott, G. 1961. Flash method of determining thermal diffusivity, heat capacity, and thermal conductivity. *Journal of Applied Physics*, 32 (9), pp.1679-1684.
- Paudel, S. and Lobovikov, M. 2003. Bamboo housing: market potential for low-income groups. *Journal of Bamboo and Rattan*, 2 (4), pp.381-396.
- Peng, G. Y., Jiang, Z. H., Qin, D. C., Ren, H. Q., Fei, B. H., and Shao, L. M. 2009. Study on density detection of bamboo with computed tomography. *Wood Processing Machinery*, 20(6), pp.16-19.
- Pentoney, R. E. 1953. Mechanisms affecting tangential vs. radial shrinkage. *Journal of Forest Product Research Society*, 3(2), pp.27–32.
- Pizzo, B., Rizzo, G., Lavischi, P., Megna, B. and Berti, S. 2002. Comparison of thermal expansion of wood and epoxy adhesives. *Holz als Roh-und Werkstoff*, 60(4), pp.285-290.
- Plumb, O. A., Spolek, G. A. and Olmstead, B. A. 1985. Heat and mass transfer in wood during drying. *International Journal of Heat and Mass Transfer*, 28 (9), pp.1669-1678.
- Popescu, C.-M., Hill, C. a. S., Anthony, R., Ormondroyd, G. and Curling, S. 2015. Equilibrium and dynamic vapour water sorption properties of biochar derived from apple wood. *Polymer Degradation and Stability*, 111, pp.263-268.
- Portal, N. W. 2011. Evaluation of heat and moisture induced stress and strain of historic building materials and artefacts.
- Portal, N. W., Van Schijndel, A. W. M. and Kalagasidis, A. S. 2014. The multiphysics modeling of heat and moisture induced stress and strain of historic building materials and artefacts. *Building Simulation*, 7 (3), pp.217-227.
- Prakash, C., Ramakrishnan, G. and Koushik, C. V. 2011. A study of the thermal properties of single jersey fabrics of cotton, bamboo and cotton/bamboo blended-yarn vis-a-vis bamboo fibre presence and yarn count. *Journal of Thermal Analysis and Calorimetry*, 110 (3), pp.1173-1177.
- Rafsanjani, A., Stiefel, M., Jefimovs, K., Mokso, R., Derome, D. and Carmeliet, J. 2014. Hygroscopic swelling and shrinkage of latewood cell wall micropillars reveal ultrastructural anisotropy. *Journal of The Royal Society Interface*, 11(95), 20140126.
- Reeves, T., Mah, P. and Mcdavid, W. 2012. Deriving Hounsfield units using grey levels in cone beam CT: a clinical application. *Dentomaxillofacial Radiology*, 41 (6), pp.500-508.

- Ritzen, M. J., Haagen, T., Rovers, R., Vroon, Z. a. E. P. and Geurts, C. P. W. 2016. Environmental impact evaluation of energy saving and energy generation: Case study for two Dutch dwelling types. *Building and Environment*.
- Roels, S., Elsen, J., Carmeliet, J. and Hens, H. 2001. Characterisation of pore structure by combining mercury porosimetry and micrography. *Materials and Structures*, 34 (2), pp.76-82.
- Sanabria, S. J., Hilbers, U., Neuenschwander, J., Niemz, P., Sennhauser, U., Thömen, H. and Wenker, J. L. 2013. Modeling and prediction of density distribution and microstructure in particleboards from acoustic properties by correlation of non-contact high-resolution pulsed air-coupled ultrasound and X-ray images. *Ultrasonics*, 53 (1), pp.157-170.
- Schirmer, R. 1938. Die Diffusionszahl von Wasserdampf-Luft-Gemischen und die Verdampfungsgeschwindigkeit, *Beiheft VDI-Zeitschrift, Verfahrenstechnik* (6), pp.170-177.
- Shah, D. U., Bock, M. C., Mulligan, H. and Ramage, M. H. 2016. Thermal conductivity of engineered bamboo composites. *Journal of Materials Science*, 51 (6), pp.2991-3002.
- Shamaeva, A., Tolstyakov, D. and Fedorova, F. 1987. Water-content dependence of the thermal conductivity for a phenolic foam plastic composite. *Measurement Techniques*, 30 (5), pp.464-465.
- Shinzato, K. and Baba, T. 2001. A laser flash apparatus for thermal diffusivity and specific heat capacity measurements. *Journal of Thermal Analysis and Calorimetry*, 64 (1), pp.413-422.
- Siau, J. 1984. Wood structure and chemical composition. *Transport processes in wood*. Springer Berlin Heidelberg.
- Simpson, W., Tenwolde, A., 1999. Physical properties and moisture relations of wood. Chapter. 3. In: Forest Products Laboratory. Wood Handbook-wood as an engineering material. Gen. Tech. Rep. FPL-GTR-113. United States Department of Agriculture, Forest Service, Forest Products Laboratory, Madison, Wisconsin, USA. pp.463.
- Skaar, C. 1988. *Wood water relations*. Berlin: Springer Verlag.
- Spink, C. and Wadsö, I. 1976. Calorimetry as an analytical tool in biochemistry and biology. *Methods Biochem. Anal*, 23 (1), pp.1-160.
- Solomonov, I., Talmi-Frank, D., Milstein, Y., Addadi, S., Aloschin, A. and Sagi, I. 2014. Introduction of correlative light and air SEM TM microscopy imaging for tissue research under ambient conditions. *Sci. Rep.*, 4.5987.

- Stamm, A.J. 1928. Density of wood substance, adsorption by wood, and permeability of wood. *The Journal of Physical Chemistry*, 33(3), pp.398-414.
- Stamm, A.J, Hansen L.A. 1937. The bonding force of cellulosic materials for water (from specific volume and thermal data). *J Phys Chem* 41, pp.1007–1016
- Stamm, A. J. 1964. *Wood and cellulose science*. New York: Ronald Press.
- Steppe, K., Cnudde, V., Girard, C., Lemeur, R., Cnudde, J.-P. and Jacobs, P. 2004. Use of X-ray computed microtomography for non-invasive determination of wood anatomical characteristics. *Journal of Structural Biology*, 148 (1), pp.11-21.
- Stevens, W. 1960. The thermal expansion of wood. *Wood*, 25(8), pp.328-9.
- Stone, J. 1964. The porous structure of wood and fibres. *Pulp and Paper Magazine of Canada*, 1 T3.
- Sun, Z., Tian, Y. and An, S. 2006. Status of study on bamboo timber drying technology. *World forestry research*, 19(6), pp.41-44.
- Taud, H., Martinez-Angeles, R., Parrot, J. F. and Hernandez-Escobedo, L. 2005. Porosity estimation method by X-ray computed tomography. *Journal of Petroleum Science and Engineering*, 47 (3–4), pp.209-217.
- Thomson, J. 2010. Observations of thermal diffusivity and a relation to the porosity of tidal flat sediments. *Journal of Geophysical Research: Oceans (1978–2012)*, 115 (C5), pp.1-6.
- Thormak, C. 2002. A low energy building in a life cycle—its embodied energy, energy need for operation and recycling potential. *Building and Environment*, 37 (4), pp.429–435.
- Time, B. 1998. *Hygroscopic moisture transport in wood*, Norwegian University of Science and Technology. Thesis (PhD). 1998.
- Trujillo, D. J. A., Ramage, M. and Chang, W.-S., 2013. Lightly modified bamboo for structural applications. *Proceedings of the Institution of Civil Engineers: Construction Materials*, 166 (4), pp. 238-247.
- Tu, D. and Xu, B. 2008. Character of hygrothermal and expansion effects of bamboo. *Journal of Anhui Agricultural University*. 35(2), pp.178-180.
- Ukrainczyk, N. 2009. Thermal diffusivity estimation using numerical inverse solution for 1D heat conduction. *International Journal of Heat and Mass Transfer*, 52 (25–26), pp.5675-5681.

- UNEP, 2014. Buildings and climate change, Greening the Buildings Supply Chain. Nairobi: UNEP.
- Van Der Lugt, P., Van Den Dobbelsteen, A. a. J. F. and Janssen, J. J. A. 2006. An environmental, economic and practical assessment of bamboo as a building material for supporting structures. *Construction and Building Materials*, 20 (9), pp.648-656.
- Vololonirina, O., Coutand, M. and Perrin, B. 2014. Characterization of hygrothermal properties of wood-based products – Impact of moisture content and temperature. *Construction and Building Materials*, 63(2014), pp.223-233.
- Wadsö L. 1993. *Studies of water vapor transport and sorption in wood*. Lund University. Thesis (PhD). 1993.
- Wang, C. and Mandelis, A. 1999. Measurement of thermal diffusivity of air using photopyroelectric interferometry. *Review of Scientific Instruments*, 70 (5), pp.2372-2378.
- Wang, H., 2010. *Study of the mechanism of moisture affecting the bamboo fibre cell walls and macroscopic mechanical behavior*. Thesis (MSc). Central South University of Forestry and Technology, Changsha.
- Weatherwax, R. C. and Stamm, A. J. 1956. The coefficients of thermal expansion of wood and wood products, US. Forest products laboratory Rep. No. 1487.
- Wu, S., Yu, S., Han, J. and Wu, Y. 2004. Testing and analysis of the thermodynamics parameters of *Phyllostachys edulis*. *Journal of central south forestry university*. 24(5), pp.70-75.
- Wilson, J. 2007. Thermal diffusivity. *Electronic cooling*, pp.1-3.
- Wu, s., Yu, s., Han, J. and Wu, Y. 2004. Testing and Analysis of the Thermodynamics Parameters of *Phyllostachys edulis*. *Journal of central south forestry university*, 24 (5), pp.70-75.
- Wu, X., Ma, H., Chen, X., Li, Z. and Li, J. 2013. Thermal Conductivity and Microstructure Properties of Porous SiC Ceramic Derived from Silicon Carbide Powder. *New Journal of Glass and Ceramics*, 3 (15), pp.43-47.
- Xie, Y., Hill, C. a. S., Xiao, Z., Mai, C. and Militz, H. 2011. Dynamic water vapour sorption properties of wood treated with glutaraldehyde. *Wood Science and Technology*, 45 (1), pp.49-61.

- Younsi, R., Kocaefe, D. and Kocaefe, Y. 2006. Three-dimensional simulation of heat and moisture transfer in wood. *Applied Thermal Engineering*, 26 (11–12), pp.1274-1285.
- Yu, Y., Wang, G., Qin, D. and Zhang, B. 2007. Variation in microfibril angle of bamboo by X-ray diffraction. *Journal of northeast forestry university*. 35(8), pp.28-29.
- Zach, J., Hroudová, J., Brožovský, J., Krejza, Z. and Gailius, A. 2013. Development of thermal insulating materials on natural base for thermal insulation systems. *Procedia Engineering*, 57(2013), pp.1288-1294.
- Zalameda, J. N. and Winfree, W. P. 1990. Thermal diffusivity measurements on composite porosity samples. *Review of Progress in Quantitative Nondestructive Evaluation*. Springer. pp.1541-1548.
- Zanoni, B., Peri, C. and Gianotti, R. 1995. Determination of the thermal diffusivity of bread as a function of porosity. *Journal of Food Engineering*, 26 (4), pp.497-510.
- Zauer, M., Pfriem, A. and Wagenführ, A. 2013. Toward improved understanding of the cell-wall density and porosity of wood determined by gas pycnometry. *Wood Science and Technology*, 47 (6), pp.1197-1211.
- Zauer, M., Kretschmar, J., Großmann, L., Pfriem, A. and Wagenführ, A. 2014. Analysis of the pore-size distribution and fiber saturation point of native and thermally modified wood using differential scanning calorimetry. *Wood Science and Technology*, 48 (1), pp.177-193.
- Zillig, W., Janssen, H., Carmeliet, J. and Derome, D. 2006. Liquid water transport in wood: towards a mesoscopic approach. *Research in Building Physics and Building Engineering*. London: Taylor and Francis Group.

Self bibliography and published work

Huang, P., Chang, W.S., Shea, A., Ansell, M. and Lawrence, M. 2014a. Non-homogeneous Thermal Properties of Bamboo. In: Aicher, s., Reinhardt, H. W. and Garrecht, H. (eds.) *Materials and Joints in Timber Structures*. Springer Netherlands.

Huang, P., Chang, W.S., Shea, A., Ansell, M. John Y.M.C., Shea, A., Zeidler, A. and Pickering, S. 2014b. Heat transfer simulation and experimental studies of bamboo in radial direction. In: *Forest Products Society (FPS) 68th International Convention*, August 10-13, Quebec, Canada.

Huang, P., Chang, W.-S., Ansell, M., Chew, Y.M.J., and Shea, A. 2015. Density distribution profile for internodes and nodes of *Phyllostachys edulis* (Moso bamboo) by computed tomography scanning. *Construction and Building Materials*, 93 (2015), pp.197-204.

Huang, P., Zeidler, A., Chang, W.-S., Ansell, M., Chew, J. and Shea, A., 2016a. Specific heat capacity measurement of *Phyllostachys edulis* (Moso bamboo) by differential scanning calorimetry. *Construction and Building Materials*, 125, pp.821-831.

Huang, P., Chang, W.-S., Ansell, M. P., John, C. Y. M. and Shea, A. 2017a. Porosity estimation of *Phyllostachys edulis* (Moso bamboo) by computed tomography and backscattered electron imaging. *Wood Science and Technology*, 51 (1), pp.11-27.

Huang, P., Pickering Simon, G., Chang, W.-S., Ansell Martin, P., Chew John, Y. M. and Shea, A. 2017b. Thermal diffusivity measurement of *Phyllostachys edulis* (Moso bamboo) by the flash method. *Holzforschung*. [Ahead of print]

Huang, P., Latif, E., Chang, W.-S., Ansell, M. P. and Lawrence, M. 2017c. Water vapour diffusion resistance factor of *Phyllostachys edulis* (Moso bamboo). *Construction and Building Materials*, 141(15), pp.216-221.

Huang, P., Chang, W.-S., Ansell, M., Latif, E. and Lawrence, M. 2016b. Moisture sorption and desorption properties of *Phyllostachys edulis* (Moso bamboo). *Construction and Building Materials*, [In progress]. Bath: University of Bath. *Pure* [Online]. Available from: <https://purehost.bath.ac.uk/admin/workspace.xhtml?uid=5> [Accessed 18/09/2016].

Huang, P., Chang, W.-S., Ansell, M., Bowen, C., Chew, J. and Adamaki, V. 2016c. Thermal and hygroscopic expansion characteristics of bamboo. *Proceedings of the Institution of Civil Engineers, Structures and Buildings*, [In progress]. Bath: University of Bath. *Pure* [Online].

Available from: <https://purehost.bath.ac.uk/admin/workspace.xhtml?uid=5> [Accessed 18/09/2016].

Huang, P., Chew, J., Chang, W.-S., Ansell, M., Lawrence, M., Latif, E., Curling, S., and Ormondroyd, G. 2016d. Heat and moisture transfer behaviour in *Phyllostachys edulis* (Moso bamboo) based panels. *Construction and Building Materials*, [In progress]. Bath: University of Bath. *Pure* [Online]. Available from:

<https://purehost.bath.ac.uk/admin/workspace.xhtml?uid=5> [Accessed 18/09/2016].